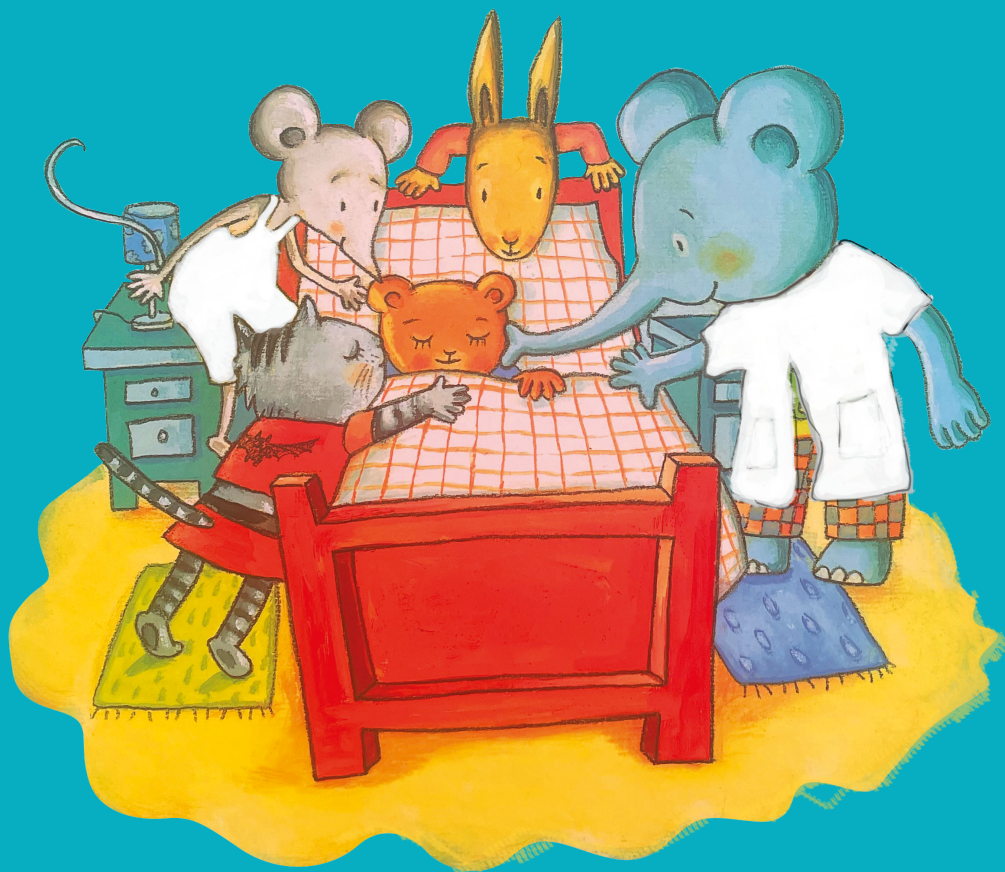


# TOWARDS UNRAVELING THE PUZZLE OF *KMT2A*-REARRANGED INFANT ACUTE LYMPHOBLASTIC LEUKEMIA

novel insights into the relapse mechanisms,  
pathobiology, and therapeutic vulnerabilities



Pauline Schneider



**TOWARDS UNRAVELING THE PUZZLE  
OF *KMT2A*-REARRANGED INFANT ACUTE  
LYMPHOBLASTIC LEUKEMIA**

**novel insights into the relapse mechanisms,  
pathobiology, and therapeutic vulnerabilities**

**Pauline Schneider**

**Cover & lay-out design**

Maaïke Disco, proefschriftopmaak.nl

*Omslagafbeelding origineel: Danila Kulot*

**Printed by** Ridderprint

**ISBN** 978-94-6483-562-5

© 2023, Pauline Schneider, the Netherlands. All rights reserved.

No part of this thesis may be reproduced or transmitted in any form or by any means without the prior permission of the copyright owner.

**towards Unraveling the Puzzle  
of *KMT2A*-rearranged Infant  
Acute Lymphoblastic Leukemia**

novel insights into the relapse mechanisms,  
pathobiology, and therapeutic vulnerabilities

**Op weg naar het ontrafelen van het raadsel van  
*KMT2A*-herschikte acute lymfatische leukemie bij zuigelingen**

nieuwe inzichten in de mechanismen die verband houden met  
recidiveren, de pathobiologie en therapeutische kwetsbaarheden  
(met een samenvatting in het Nederlands)

**Proefschrift**

ter verkrijging van de graad van doctor aan de  
Universiteit Utrecht  
op gezag van de  
rector magnificus, prof. dr. H.R.B.M. Kummeling,  
ingevolge het besluit van het college voor promoties  
in het openbaar te verdedigen op

donderdag 1 februari 2024 des ochtends te 10.15 uur

door

**Pauline Schneider**

geboren op 16 augustus 1977  
te Alkmaar

**Promotor**

Prof. dr. R. Pieters

**Copromotor**

Dr. R.W. Stam

**Beoordelingscommissie**

Prof. dr. M.L. den Boer

Prof. dr. O.T. Heidenreich

Dr. E. Hulleman

Prof. dr. G.J. Kaspers

Prof. dr. R.P. Kuiper (voorzitter)







# TABLE OF CONTENTS

<b>Chapter 1</b>	General introduction and scope of this thesis	<b>9</b>
<b>Chapter 2</b>	Decitabine mildly attenuates <i>MLL</i> -rearranged acute lymphoblastic leukemia in vivo, and represents a poor chemo-sensitizer	<b>21</b>
<b>Chapter 3</b>	Modelling acquired resistance to DOT1L inhibition exhibits the adaptive potential of <i>KMT2A</i> -rearranged acute lymphoblastic leukemia	<b>41</b>
<b>Chapter 4</b>	CRISPR-Cas9 library screening identifies novel molecular vulnerabilities in <i>KMT2A</i> -rearranged acute lymphoblastic leukemia	<b>71</b>
<b>Chapter 5</b>	Identification and characterization of relapse-initiating cells in <i>MLL</i> -rearranged infant ALL by single-cell transcriptomics	<b>101</b>
<b>Chapter 6</b>	General discussion and implications	<b>127</b>
<b>Chapter 7</b>	Nederlandse wetenschappelijke samenvatting	<b>139</b>
<b>About the author</b>		
	Curriculum Vitae	<b>148</b>
	List of Publications	<b>150</b>
	Dankwoord/Acknowledgments	<b>152</b>
<b>Appendix</b>	Supplementals	<b>159</b>



# CHAPTER 1

## General introduction and scope of this thesis



## Cancer

The first recorded description of human cancer dates back to 3000 BC in the Edwin Smith Papyrus, an ancient Egyptian medical text (1). It includes an illustration of a breast tumor, providing evidence of the existence of cancer in ancient times. Around 460 BC, the renowned Greek physician Hippocrates began using the Greek word “Karakinos”, meaning crab, to describe tumor masses with irregular projections that resembled the claws of a crab (1). The term “cancer” originated from this Greek word and has been used to describe the disease ever since. However, cancer existed long before. Paleontological findings suggest cancer existed on Earth even before the emergence of humans (2). Fossil evidence suggests that various animal species, including dinosaurs, also experienced cancerous growths. In fact, the earliest known occurrence of cancer dates back to approximately 70 million years ago, as revealed by fossilized dinosaur bones (3). These ancient remains provide evidence of the existence of tumors in prehistoric times. The identification of tumors in dinosaur fossils also suggests that cancer is not solely a modern disease but has affected living organisms for millions of years.

Cancer has been one of the most challenging and complex diseases to understand and treat, and despite the immense progress that has been made in research and treatment over centuries, cancer continues to be a leading cause of death worldwide. According to the World Health Organization (WHO), cancer accounts for approximately 9.6 million deaths annually, which is around one in six deaths globally. The incidence of cancer is expected to increase by more than 50% in the next two decades, with a projected 24 million new cases annually by 2035 (4).

The term cancer refers to a disease that results from the uncontrolled growth of abnormal cells and their ability to invade and colonize areas that are normally reserved for other cells (5, 6). Although there is a huge variety of cancer cell types, they can be collectively defined by a set of biological capabilities acquired by normal human cells to develop into malignant tumors, known as the hallmarks of cancer. As our knowledge of cancer has advanced, the hallmarks of cancer have evolved into a set of eight functional capabilities of cancer cells. These hallmarks include sustaining proliferative signaling, evading growth suppressors, resisting cell death, enabling replicative immortality, inducing or accessing vasculature, activating invasion and metastasis, reprogramming energy metabolism, and evading immune destruction (7, 8). In addition to these hallmarks, there are underlying enabling capabilities such as genome instability and mutation, which generate genetic diversity that drives tumor progression, and inflammation of the microenvironment, which promotes multiple hallmark functions (8). Recently, gained insights have led to the addition of four new hallmarks. These include unlocking phenotypic plasticity by disrupting the differentiation of tumor cells, non-mutational epigenetic reprogramming as a disruptive

mechanism independent from genome instability and gene mutation, polymorphic microbiomes that are implicated in modulating tumor phenotype, and senescent cells, which originate from cancer of stromal cells and are implicated in modulating hallmark capabilities (8). Overall, the hallmarks of cancer provide a framework for understanding the key functional capabilities of cancer cells and the underlying mechanisms that drive tumor progression. This understanding has been crucial in developing new treatments and therapies for cancer patients (7-9).

### **Pediatric cancer**

With an estimated 400.000 cancer patients between 0-19 years of age annually, pediatric cancer is a rare disease. Nonetheless, like for adults, cancer remains the leading cause of death from illness in both children and adolescents. The most common types of childhood cancers include leukemias, brain cancers, lymphomas, and solid tumors such as neuroblastoma (arising from nerve cells) and Wilms tumors (a kidney cancer primarily affecting children) (10, 11).

Despite being a rare disease compared to cancer in adults, childhood cancer demands attention and specialized care. The unique nature of pediatric cancers sets them apart from their adult counterparts. Pediatric cancers exhibit a lower frequency of genetic mutations, with significantly fewer somatic mutations compared to many adult cancers. Furthermore, only a small percentage of 8,5% of children with cancer have identifiable germline mutations in cancer-predisposing genes (12). In contrast to many cancers in adults, childhood cancers are not strongly linked to lifestyle or environmental risk factors (12). These differences necessitate a distinct approach in the treatment of pediatric cancer. Furthermore, when treating childhood cancer, it is crucial to consider the potential long-term effects on children. Unlike adults, where the focus is often on balancing short-term complications with treatment benefits, the long-term consequences of therapies and interventions in children must be carefully considered (13).

### **Childhood acute lymphoblastic leukemia**

Leukemia, and acute lymphoblastic leukemia (ALL) specifically, represents the most common type of cancer diagnosed in children. ALL accounts for approximately 30% of all pediatric cancer cases, with around 125 new cases reported annually in the Netherlands. ALL can originate from B and T lymphocytes and as such are divided into two subtypes known as B-cell precursor ALL (or BCP-ALL) and T-ALL. BCP-ALL represents the most prevalent subtype, accounting for approximately 80% of all cases.

Leukemia is a type of blood cancer that originates in the bone marrow. It occurs when abnormal white blood cells, lymphoblasts, accumulate and proliferate in the bone marrow

(14). In healthy blood cell formation, also known as hematopoiesis, functional blood cells are formed in the bone marrow and upon differentiation the more mature blood cells are released to the blood stream to exert their functions. In leukemia, however, rapid and uncontrollably growing immature lymphoblasts outcompete and suppress the formation of normal blood cells. The presence of large numbers of non-functional lymphoblasts in the bone marrow and their subsequent release into the peripheral blood circulation contribute to the characteristic features and complications of leukemia. These may include bone marrow failure, compromised immune function, anemia, and infiltration of vital organs such as the spleen, brain, liver, and others. The infiltration of cancer cells into organs can result in organ dysfunction and various clinical manifestations, depending on the specific sites affected (14). Understanding the mechanisms and consequences of abnormal lymphoblast proliferation and infiltration is crucial for the diagnosis, treatment, and management of leukemia in children.

Over the past few decades, significant improvements have been made in the treatment of pediatric ALL, leading to remarkable improvements in patient outcomes. In the 1960s, the 5-year overall survival rate for pediatric ALL was less than 10 percent. However, due to advancements in understanding the disease, the development of more effective treatment strategies, and the establishment of comprehensive protocols, the 5-year overall survival rate currently exceeds 90 percent (15).

### **ALL in infants**

ALL diagnosed in infants, i.e., children less than 1 year of age, constitutes approximately 5% of all pediatric leukemias, and represents a challenging subgroup of patients to treat effectively with current treatment protocols (16). Despite advances in treatment, the overall survival rate for infants with ALL remains around 50% when treated according to the international INTERFANT treatment protocols (17, 18). Infants diagnosed with ALL often exhibit more aggressive disease characteristics compared to older children. They frequently present with high tumor burdens, evident as elevated white blood cell (WBC) counts, which can pose significant challenges in treatment. Furthermore, infants with ALL are at high risk of experiencing central nervous system (CNS) involvement, i.e., the presence of leukemic cells in the brain and spinal cord. Leukemic CNS infiltration further complicates treatment and necessitates additional therapeutic approaches to target leukemia cells in this particular disease reservoir (19). Additionally, infants with ALL have high rates of relapse often while still on treatment, indicating the need for more effective treatment strategies to prevent disease recurrence (17, 18).

### **Unique biology of infant ALL**

Infant ALL is distinguished by a high frequency of chromosomal translocations of the

*Lysine Methyltransferase 2A (KMT2A)* gene, formerly known as the *Mixed Lineage Leukemia (MLL)* gene. Among infant ALL patients, *KMT2A* translocations occur in around 80% of the cases. In contrast, the frequency of these translocations in older children with ALL is only ~5% (16). *KMT2A* translocations lead to fusion of the N-terminus of *KMT2A* on chromosome 11q23 with the C-terminus of one of its translocation partners. The most recurrent *KMT2A* translocation partners in infant ALL are *AFF1 (AF4)* on chromosome 4 in 49% of cases, *MLLT1 (ENL)* on chromosome 19 in 22%, and *MLLT3 (AF9)* on chromosome 9 in 16% of cases (20). Unfortunately, *KMT2A*-rearranged infant ALL (*KMT2A-r iALL*) represents a very aggressive type of childhood leukemia with a unique biology that is characterized by chemotherapy resistance and high relapse rates, resulting in a poor prognosis. *KMT2A-r iALL* patients treated according to INTERFANT treatment protocols have 6-year event-free survival (EFS) rate of ~20-40%, compared to nearly 75% for infant ALL without *KMT2A* translocations (germline *KMT2A*) (17, 18). *KMT2A-r iALL* is associated with a highly immature B-cell precursor immunophenotype, resembling that of CD34-positive, CD19-positive, CD10-negative (CD34+/CD19+/CD10-) pro-B cells. In contrast, in the absence of *KMT2A* translocations, childhood ALL displays slightly more mature immunophenotypes such as that of common B-cells (CD19+/CD10+/IgM-) or pre-B (CD19+/CD10+/IgM+) cells (21). Furthermore, *KMT2A-r iALL* cells often co-express myeloid surface markers, such as CD13, CD15, and CD33 (22).

*KMT2A-r iALL* displays a mutational landscape that is remarkably silent, suggesting that the *KMT2A* translocation may be the only oncogenic event responsible for dysregulating epigenetic and transcriptional programs in this type of leukemia (23, 24). The wild-type *KMT2A* protein plays a crucial role in hematopoiesis by epigenetically regulating gene expression through its C-terminal Su(Var)3-9, Enhancer-of-zeste, Trithorax (SET) domain, which has histone 3 lysine 4 (H3K4) methyltransferase activity (20, 25). In the case of *KMT2A* rearrangements, *KMT2A* fusion proteins lose their SET domain and instead recruit the DOT1 Like Histone Lysine Methyltransferase (DOT1L) through binding motifs encoded by the C-terminal portions of translocation partner genes (26-28). DOT1L is the only known histone 3 lysine 79 (H3K79) methyltransferase, and binding of DOT1L to *KMT2A* fusion proteins causes inappropriate H3K79 hypermethylation at *KMT2A* target genes, leading to an altered transcriptomic landscape that strongly favors leukemia development (6-9).

The most common *KMT2A* fusion gene partners in infant ALL, i.e., *AFF1 (AF4)*, *MLLT3 (AF9)*, and *MLLT1 (ENL)*, encode proteins that are part of complexes responsible for regulating epigenetic mechanisms (20). These proteins disrupt and redirect the activities of these regulatory complexes, causing promoter overactivation, abnormal histone modifications landscape, changes in the gene expression profiles, and the reemergence of stem cell characteristics (29, 30). Consequently, *KMT2A-r iALL* is characterized by an abnormal

epigenome, reflected by aberrant DNA methylation patterns (31-33) and histone modification signatures (34), which alter the epigenetic and transcriptomic landscape of the cell. Consequently, the use of epigenetic-based drug classes, such as DNA demethylating agents, as well as DOT1L histone methyltransferase, BET protein, histone deacetylases (HDAC), and MENIN inhibitors, have been anticipated to represent attractive therapeutics to improve treatment of *KMT2A*-rearranged ALL (31, 32, 35-38).

### Scope of this thesis

As we and others previously demonstrated, *KMT2A*-r iALL is characterized by aberrant DNA methylation patterns, which led to the evaluation of DNA methyltransferase inhibitors, such as decitabine and zebularine (31, 32, 39). While cytotoxicity against *KMT2A*-r ALL cells has been observed *in vitro* (31, 32), data on the *in vivo* efficacy of DNA demethylating agents was largely missing. Therefore, in **chapter 2** of this thesis we assessed the *in vivo* anti-leukemic potential of low and clinically relevant dosages of decitabine in a xenograft mouse model of human *KMT2A*-r ALL. Moreover, we explored whether prolonged exposure to low-dose decitabine could chemo-sensitize *KMT2A*-r ALL cells toward conventional chemotherapy as well as other known epigenetic-based and anti-neoplastic compounds.

In **chapter 3** of this thesis, we focused on DOT1L inhibition. The first-in-class DOT1L inhibitor pinometostat showed efficacy against *KMT2A*-rearranged leukemias *in vitro* as well as *in vivo* in animal models (35, 40). In clinical trials for adult *KMT2A*-rearranged leukemia patients, disease progression due to acquired pinometostat-related resistance appeared unavoidable (41, 42). Understanding the mechanisms underlying acquired resistance to pinometostat may reveal how to circumvent or counter this, or may unveil alternative mechanisms through which *KMT2A* fusion proteins exert their oncogenic functions in a DOT1L-independent manner. Therefore, we set out to explore the mechanisms of acquired pinometostat resistance by establishing and comprehensively characterizing a model of acquired resistance to DOT1L inhibition in *KMT2A*-r ALL. Interestingly, this model provided important insights in the adaptive potential of this type of leukemia upon losing dependency on one of its main oncogenic properties.

Next, we asked whether other and yet unknown epigenetic vulnerabilities exist that are specifically essential to *KMT2A*-r ALL cells. To answer this question, we utilized *in vitro* RNA-guided 'clustered regularly interspaced short palindromic repeats - Cas9 knockout (CRISPR KO) screens using single guide RNA (sgRNA) libraries directed against the human Epigenome and Kinome. This indeed led to the identification of novel molecular dependencies and potential therapeutic targets, including the epigenetic regulators ARID4B and MBD3, as well as the receptor kinase BMPR2 (**chapter 4**).



While it is of high interest to fully understand how *KMT2A*-r ALL cells exploit the epigenetic machinery to drive leukemogenesis and identify therapeutic strategies to counter that, it is equally as important to understand the mechanisms underlying leukemia relapse during currently available treatment regimes. Therefore, in **chapter 5**, we performed single-cell RNA sequencing (scRNA-seq) on diagnostic *KMT2A*-r iALL samples derived from patients who experienced early relapses or who remained event-free for over 7 years, to unravel the intricate biology of relapse occurrence. This allowed us to classify individual leukemic cells predicted to be either resistant or sensitive to treatment and showed that the quantification of subpopulations of the most therapy-resistant cells at diagnosis can be used to accurately predict the occurrence of future relapse in individual patients. The identification and characterization of these relapse-predictive cells represents a crucial step towards our understanding of leukemia reemergence during treatment, and how to prevent it.

### **Nomenclature**

Until recently, the *KMT2A* gene was predominantly known as the *Mixed Lineage Leukemia (MLL)* gene, referring to the fact that chromosomal translocations involving this gene occur in both ALL and in acute myeloid leukemia (AML). The new and current nomenclature reflects the gene's function as a lysine methyltransferase 2A (*KMT2A*) that catalyzes the methylation of lysine 4 on the histone H3 tail at critical regulatory regions in the genome, inducing gene transcription (43). Due to the long-standing use of *KMT2A*'s previous name *MLL*, both names appear in this thesis. Similarly, different names refer to the same translocation partner for *KMT2A* fusion. For example, according to the old nomenclature, translocation t(4;11) generates the *MLL-AF4* fusion gene which now officially is termed *KMT2A::AFF1*. Likewise, translocation t(9;11) and t(11;19), leading to the assembly of the fusion genes *MLL-AF9* and *MLL-ENL*, are now known as *KMT2A::MLLT3* and *KMT2A::MLLT1*, respectively.

## REFERENCES

1. Papavramidou N, Papavramidis T, Demetriou T. Ancient Greek and Greco–Roman Methods in Modern Surgical Treatment of Cancer. *Annals of Surgical Oncology*. 2010;17(3):665-7.
2. Di Lonardo A, Nasi S, Pulciani S. Cancer: we should not forget the past. *J Cancer*. 2015;6(1):29-39.
3. Rothschild BM, Tanke DH, Helbling M, 2nd, Martin LD. Epidemiologic study of tumors in dinosaurs. *Naturwissenschaften*. 2003;90(11):495-500.
4. Global Burden of Disease Cancer C, Kocarnik JM, Compton K, Dean FE, Fu W, Gaw BL, et al. Cancer Incidence, Mortality, Years of Life Lost, Years Lived With Disability, and Disability-Adjusted Life Years for 29 Cancer Groups From 2010 to 2019: A Systematic Analysis for the Global Burden of Disease Study 2019. *JAMA Oncol*. 2022;8(3):420-44.
5. Alberts B. *Molecular biology of the cell*. 3rd ed. New York: Garland Pub.; 1994. xliii, 1294, 67 p. p.
6. Alberts B. *Molecular biology of the cell*. Seventh edition. ed. New York: W. W. Norton & Company; 2022. pages cm p.
7. Hanahan D, Weinberg RA. The hallmarks of cancer. *Cell*. 2000;100(1):57-70.
8. Hanahan D, Weinberg RA. Hallmarks of cancer: the next generation. *Cell*. 2011;144(5):646-74.
9. Hanahan D. Hallmarks of Cancer: New Dimensions. *Cancer Discov*. 2022;12(1):31-46.
10. Steliarova-Foucher E, Colombet M, Ries LAG, Moreno F, Dolya A, Bray F, et al. International incidence of childhood cancer, 2001-10: a population-based registry study. *Lancet Oncol*. 2017;18(6):719-31.
11. Kaatsch P. Epidemiology of childhood cancer. *Cancer Treat Rev*. 2010;36(4):277-85.
12. Ma X, Liu Y, Liu Y, Alexandrov LB, Edmonson MN, Gawad C, et al. Pan-cancer genome and transcriptome analyses of 1,699 paediatric leukaemias and solid tumours. *Nature*. 2018;555(7696):371-6.
13. Kattner P, Strobel H, Khoshnevis N, Grunert M, Bartholomae S, Pruss M, et al. Compare and contrast: pediatric cancer versus adult malignancies. *Cancer Metastasis Rev*. 2019;38(4):673-82.
14. Hoffbrand AV, Moss PAH. *Essential haematology*. 6th ed. ed. Chichester: Wiley-Blackwell; 2011.
15. Hunger SP, Mullighan CG. Acute Lymphoblastic Leukemia in Children. *N Engl J Med*. 2015;373(16):1541-52.
16. Moorman AV, Ensor HM, Richards SM, Chilton L, Schwab C, Kinsey SE, et al. Prognostic effect of chromosomal abnormalities in childhood B-cell precursor acute lymphoblastic leukaemia: results from the UK Medical Research Council ALL97/99 randomised trial. *Lancet Oncol*. 2010;11(5):429-38.
17. Pieters R, De Lorenzo P, Ancliffe P, Aversa LA, Brethon B, Biondi A, et al. Outcome of Infants Younger Than 1 Year With Acute Lymphoblastic Leukemia Treated With the Interfant-06 Protocol: Results From an International Phase III Randomized Study. *J Clin Oncol*. 2019;37(25):2246-56.
18. Pieters R, Schrappe M, De Lorenzo P, Hann I, De Rossi G, Felice M, et al. A treatment protocol for infants younger than 1 year with acute lymphoblastic leukaemia (Interfant-99): an observational study and a multicentre randomised trial. *Lancet*. 2007;370(9583):240-50.
19. Hilden JM, Dinndorf PA, Meerbaum SO, Sather H, Villaluna D, Heerema NA, et al. Analysis of prognostic factors of acute lymphoblastic leukemia in infants: report on CCG 1953 from the Children's Oncology Group. *Blood*. 2006;108(2):441-51.
20. Meyer C, Burmeister T, Groger D, Tsaour G, Fechina L, Renneville A, et al. The MLL recombinome

- of acute leukemias in 2017. *Leukemia*. 2018;32(2):273-84.
21. Jansen MW, Corral L, van der Velden VH, Panzer-Grumayer R, Schrappe M, Schrauder A, et al. Immunobiological diversity in infant acute lymphoblastic leukemia is related to the occurrence and type of MLL gene rearrangement. *Leukemia*. 2007;21(4):633-41.
  22. Basso G, Rondelli R, Covezzoli A, Putti M. The role of immunophenotype in acute lymphoblastic leukemia of infant age. *Leuk Lymphoma*. 1994;15(1-2):51-60.
  23. Agraz-Doblas A, Bueno C, Bashford-Rogers R, Roy A, Schneider P, Bardini M, et al. Unraveling the cellular origin and clinical prognostic markers of infant B-cell acute lymphoblastic leukemia using genome-wide analysis. *Haematologica*. 2019;104(6):1176-88.
  24. Andersson AK, Ma J, Wang J, Chen X, Gedman AL, Dang J, et al. The landscape of somatic mutations in infant MLL-rearranged acute lymphoblastic leukemias. *Nat Genet*. 2015;47(4):330-7.
  25. Ernst P, Wang J, Korsmeyer SJ. The role of MLL in hematopoiesis and leukemia. *Curr Opin Hematol*. 2002;9(4):282-7.
  26. Bernt KM, Armstrong SA. A role for DOT1L in MLL-rearranged leukemias. *Epigenomics*. 2011;3(6):667-70.
  27. Okada Y, Feng Q, Lin Y, Jiang Q, Li Y, Coffield VM, et al. hDOT1L links histone methylation to leukemogenesis. *Cell*. 2005;121(2):167-78.
  28. Bernt KM, Zhu N, Sinha AU, Vempati S, Faber J, Krivtsov AV, et al. MLL-rearranged leukemia is dependent on aberrant H3K79 methylation by DOT1L. *Cancer Cell*. 2011;20(1):66-78.
  29. Sanjuan-Pla A, Bueno C, Prieto C, Acha P, Stam RW, Marschalek R, et al. Revisiting the biology of infant t(4;11)/MLL-AF4+ B-cell acute lymphoblastic leukemia. *Blood*. 2015;126(25):2676-85.
  30. Zhang Y, Chen A, Yan XM, Huang G. Disordered epigenetic regulation in MLL-related leukemia. *Int J Hematol*. 2012;96(4):428-37.
  31. Stumpel DJ, Schneider P, van Roon EH, Boer JM, de Lorenzo P, Valsecchi MG, et al. Specific promoter methylation identifies different subgroups of MLL-rearranged infant acute lymphoblastic leukemia, influences clinical outcome, and provides therapeutic options. *Blood*. 2009;114(27):5490-8.
  32. Stumpel DJ, Schneider P, van Roon EH, Pieters R, Stam RW. Absence of global hypomethylation in promoter hypermethylated Mixed Lineage Leukaemia-rearranged infant acute lymphoblastic leukaemia. *Eur J Cancer*. 2013;49(1):175-84.
  33. Schafer E, Irizarry R, Negi S, McIntyre E, Small D, Figueroa ME, et al. Promoter hypermethylation in MLL-r infant acute lymphoblastic leukemia: biology and therapeutic targeting. *Blood*. 2010;115(23):4798-809.
  34. Krivtsov AV, Armstrong SA. MLL translocations, histone modifications and leukaemia stem-cell development. *Nat Rev Cancer*. 2007;7(11):823-33.
  35. Daigle SR, Olhava EJ, Therkelsen CA, Majer CR, Sneeringer CJ, Song J, et al. Selective killing of mixed lineage leukemia cells by a potent small-molecule DOT1L inhibitor. *Cancer Cell*. 2011;20(1):53-65.
  36. Bardini M, Trentin L, Rizzo F, Vieri M, Savino AM, Garrido Castro P, et al. Antileukemic Efficacy of BET Inhibitor in a Preclinical Mouse Model of MLL-AF4(+) Infant ALL. *Mol Cancer Ther*. 2018;17(8):1705-16.
  37. Garrido Castro P, van Roon EHJ, Pinhancos SS, Trentin L, Schneider P, Kerstjens M, et al. The HDAC inhibitor panobinostat (LBH589) exerts in vivo anti-leukaemic activity against MLL-rearranged

- acute lymphoblastic leukaemia and involves the RNF20/RNF40/WAC-H2B ubiquitination axis. *Leukemia*. 2018;32(2):323-31.
38. Krivtsov AV, Evans K, Gadrey JY, Eschle BK, Hatton C, Uckelmann HJ, et al. A Menin-MLL Inhibitor Induces Specific Chromatin Changes and Eradicates Disease in Models of MLL-Rearranged Leukemia. *Cancer Cell*. 2019;36(6):660-73 e11.
  39. Stumpel DJ, Schotte D, Lange-Turenhout EA, Schneider P, Seslija L, de Menezes RX, et al. Hypermethylation of specific microRNA genes in MLL-rearranged infant acute lymphoblastic leukemia: major matters at a micro scale. *Leukemia*. 2011;25(3):429-39.
  40. Daigle SR, Olhava EJ, Therkelsen CA, Basavapathruni A, Jin L, Boriack-Sjodin PA, et al. Potent inhibition of DOT1L as treatment of MLL-fusion leukemia. *Blood*. 2013;122(6):1017-25.
  41. Stein EM, Garcia-Manero G, Rizzieri DA, Tibes R, Berdeja JG, Savona MR, et al. The DOT1L inhibitor pinometostat reduces H3K79 methylation and has modest clinical activity in adult acute leukemia. *Blood*. 2018;131(24):2661-9.
  42. Waters NJ. Preclinical Pharmacokinetics and Pharmacodynamics of Pinometostat (EPZ-5676), a First-in-Class, Small Molecule S-Adenosyl Methionine Competitive Inhibitor of DOT1L. *Eur J Drug Metab Pharmacokinet*. 2017;42(6):891-901.
  43. Rao RC, Dou Y. Hijacked in cancer: the KMT2 (MLL) family of methyltransferases. *Nat Rev Cancer*. 2015;15(6):334-46.





# CHAPTER 2

## Decitabine mildly attenuates *MLL*-rearranged acute lymphoblastic leukaemia *in vivo*, and represents a poor chemo-sensitizer



Pauline Schneider<sup>1\*</sup>, Patricia Garrido Castro<sup>1\*</sup>, Sandra M. Pinhanços<sup>1</sup>, Mark Kerstjens<sup>2</sup>, Eddy H. van Roon<sup>2</sup>, Anke H.W. Essing<sup>1</sup>, M. Emmy M. Dolman<sup>1</sup>, Jan J. Molenaar<sup>1</sup>, Rob Pieters<sup>1</sup>, Ronald W. Stam<sup>1</sup>

<sup>1</sup>Princess Máxima Center for Pediatric Oncology, Heidelberglaan 25, 3584 CS Utrecht, the Netherlands

<sup>2</sup>Dept. of Pediatric Hematology/Oncology, Erasmus MC - Sophia Children's Hospital, Wytemaweg 80, 3015 CN Rotterdam, Netherlands

\*Both authors contributed equally

## ABSTRACT

*MLL*-rearranged acute lymphoblastic leukaemia (ALL) represents a highly aggressive ALL subtype, characterized by aberrant DNA methylation patterns. DNA methyltransferase inhibitors, such as decitabine have previously been demonstrated to be effective in eradicating *MLL*-rearranged ALL cells *in vitro*.

Here we assessed the *in vivo* anti-leukaemic potential of low-dose DNA methyltransferase inhibitor decitabine using a xenograft mouse model of human *MLL*-rearranged ALL. Furthermore we explored whether prolonged exposure to low-dose decitabine could chemo-sensitize *MLL*-rearranged ALL cells towards conventional chemotherapy as well as other known epigenetic-based and anti-neoplastic compounds.

Our data reveals that decitabine prolonged survival in xenograft mice of *MLL*-rearranged ALL by 8,5 days ( $p=0.0181$ ), but eventually was insufficient to prevent leukaemia out-growth, based on the examination of the MLLAF4 cell line SEM. Furthermore, we observe that prolonged pre-treatment of low-dose decitabine mildly sensitized towards the conventional drugs prednisolone, vincristine, daunorubicin, asparaginase, and cytarabine in a panel of *MLL*-rearranged cell lines. Additionally, we assessed synergistic effects of decitabine with other epigenetic-based or anti-cancer drugs using high-throughput drug library screens. Validation of the top hits, including histone deacetylase inhibitor panobinostat, BCL2 inhibitor Venetoclax, MEK inhibitor pimasertib, and receptor tyrosine kinase foretinib, revealed additive and moderate synergistic effects for the combination of each drug together with decitabine in a cell line-dependent manner.



## INTRODUCTION

Rearrangement of the *Mixed Lineage Leukaemia* (*MLL*, or *KMT2A*) gene is a cytogenetic aberration highly prevalent in infants (<1 year of age) diagnosed with acute lymphoblastic leukaemia (ALL), where it constitutes ~80% of the cases. *MLL* rearrangements mark a very aggressive ALL subtype. Despite highly intensified treatment protocols, event-free survival (EFS) chances for *MLL*-rearranged infant ALL only reach 35-40%, falling well short of survival rates of infants and older children with ALL carrying other cytogenetic aberrations (70-90%)<sup>1-3</sup>. Hence, novel treatment strategies based on the specific molecular pathobiology are crucial.

The main oncogenic hit of *MLL*-rearranged ALL is the in frame fusion of the *MLL* gene with one of multiple fusion partner genes, generating *MLL* fusion genes that encode chimeric proteins that drive leukaemogenicity and disease maintenance<sup>4-6</sup>. *MLL* itself functions as a histone methyltransferase, and the most recurrent fusion partner genes, *AF4* (*AFF1*), *ENL* (*MLLT1*) and *AF9* (*MLLT3*), all encode proteins which are part of complexes regulating epigenetic mechanisms. As truncated parts of the *MLL* fusions these proteins interfere with and mistarget the regulating complexes, hijacking their activities<sup>7</sup>. As a result, *MLL*-rearranged acute leukaemia typically presents with a highly abnormal epigenome, reflected by aberrant DNA methylation patterns<sup>8-10</sup> and histone modification signatures<sup>11</sup>, which alter the epigenetic and transcriptomic landscape of the cell. Consequently, several epigenetic drug classes, including DOT1L histone methyltransferase, BET protein and histone deacetylases (HDAC) inhibitors, have shown promising results in *MLL*-rearranged ALL animal models<sup>12-16</sup>, providing pre-clinical rationales for their implementation in current and future clinical trials<sup>17</sup>.

However, despite their known cytotoxicity against *MLL*-rearranged ALL cells *in vitro*<sup>7,9,17,18</sup>, pre-clinical *in vivo* activity studies of another pivotal class of epigenetic drugs, i.e. the DNA methyltransferase inhibitors (DNMTi), such as decitabine and 5-azacytidine, are limited. Therefore we assessed the *in vivo* anti-leukemic potential of low and clinically relevant dosages of decitabine for a prolonged timespan in a *MLL*-rearranged ALL xenograft mouse model. Furthermore, using high-throughput combinatorial drug library screens, we explored whether prolonged low-dose decitabine would epigenetically prime and chemo-sensitize *MLL*-rearranged ALL cells towards standard chemotherapy, as well as towards an array of other, mostly FDA-approved compounds.

## METHODS

### Animal Models

Animal experiments were performed under compliance of Dutch legislation after approval of the institutional Animal Ethics Committee at the Erasmus MC, Rotterdam, The Netherlands. Immunodeficient NOD.Cg-Prkdc<sup>scid</sup>Il2rg<sup>tm1Wjl</sup>/SzJ (NSG) mice (n=26) were transplanted intrafemorally (i.f.) with the luciferase-expressing *MLL*-rearranged ALL reporter cell line SEM-SLIEW (10<sup>5</sup> cells per mouse). Mice were kept in individually ventilated cages with food and water *ad libitum*. Bioluminescence measurements were performed under isoflurane narcotization to confirm engraftment three days post-injection and to monitor disease progression every other week; Rediject D-Luciferin (PerkinElmer) substrate was administered intraperitoneally and bioluminescence signals were visualized and whole-body photon flux (photons/sec) quantified on an IVIS Spectrum system using Living Image software (PerkinElmer). To overcome the therapeutic limitations of the short physiological half-life of decitabine *in vivo*, the cytidine deaminase inhibitor tetrahyourine (THU, Sigma-Aldrich, 4mg/kg in saline) was administered i.p. in parallel, on the opposite abdominal quadrant. The control group was treated with the corresponding vehicle (10% DMSO in saline).

Mice showing overt clinical signs of leukaemia and reaching humane end points as indicated by Animal Ethical Committee statutes and in compliance with ARRIVE guidelines (lethargy, acute weight loss >15%, severe behavioral abnormalities, hind limb paralysis, etc.) were humanely culled, and systemic leukemic burden was determined using multi-color flow cytometry, as described before <sup>15</sup>. Statistical significance was determined by log-rank testing.

### Cell culture

The *MLL*-rearranged B-cell precursor acute lymphoblastic leukaemia (pre-B ALL) cell lines SEM (MLL-AF4<sup>+</sup>) and KOPN-8 (MLL-ENL<sup>+</sup>) were purchased from DSMZ (Braunschweig, Germany), while the *MLL*-rearranged ALL cell line ALLPO (MLL-AF4<sup>+</sup>) was a kind gift from the lab of Dr. Cazzaniga, University of Milano-Bicocca, Italy. SEM-SLIEW is derived from MLL-AF4<sup>+</sup> cell line SEM and was modified to express the luciferase reporter gene <sup>15</sup>.

All cell lines were cultured in Gibco™ RPMI-1640 with GlutaMAX™, supplemented with 10% Fetal Calf Serum, 100 IU/mL penicillin, 100 IU/mL streptomycin and 0.125 µg/mL amphotericin B (Thermo Fisher Scientific, Waltham, USA) at 37°C under 5% CO<sub>2</sub> atmosphere. Cell line integrity was regularly checked by DNA fingerprinting as well as mycoplasma free status by mycoplasma testing.

## High-throughput drug screening

The *MLL*-rearranged ALL cell lines SEM was pre-treated for 14 days with 10nM decitabine (5-Aza-2'-deoxycytidine, Merck, Sigma-Aldrich, St. Louis, USA) or equal amount of DMSO (vehicle), compound-containing medium was refreshed every two days and cells passaged every four days. Subsequently the pre-treated cells were tested on a drug library containing all 43 compounds of the Enzo SCREEN-WELL® epigenetics library (Enzo Life Sciences, Farmingdale, USA), all 59 compounds of the Cayman epigenetic library (Cayman chemicals, Ann Arbor, USA), all 157 compounds of the Sequoia anti-neoplastic drug library (Sequoia Research Products, Pangbourne, UK), 84 FDA approved compounds of interest (Spectrum, MicroSource, Gaylordsville, USA), as well as 26 additional compounds of interest (Sigma-Aldrich, Selleckchem. All compounds tested are listed in table S1.

The decitabine or vehicle pre-treated cell lines were seeded in 384-well plates at 10000 cells/well and treated with 10, 100 or 1000 nM of the compounds using the Sciclone ALH 3000 liquid handling robot (Perkin Elmer). Control samples were treated with DMSO (maximum concentration 0.5% v/v). The cell viability was assessed by a 4-day thiazolyl blue tetrazolium bromide (MTT; Sigma) assay as previously described<sup>19</sup>. The cell viability was normalized to the DMSO controls. This normalized cell viability of the three concentrations of each compound was used to calculate the area under the curve (AUC) for the compound using GraphPrism. The top hits were defined as drugs with a reduction of more than 30% AUC in the decitabine pre-treated SEM cells compared to vehicle-treated cells.

## Drug exposures and synergy determination

For the validation of the top hits from the high-throughput drug screen and synergy studies, expanded dose response curves were made using the Tecan D300 Digital Dispenser (Tecan, Switzerland) to dispense the drug. Again the drug response on the cell viability was assessed by a MTT assay. MTT data was normalized to DMSO control, tolerating a maximum concentration of ≤0.5% (v/v). Experiments performed in triplicate for ALLPO and SEM, in duplo for KOPN8, with three technical replicates each.

Drug synergy between decitabine and the combined compounds was determined using BLISS independence model calculations<sup>20</sup>, with the equation  $E_{\text{combi}} = E_A + E_B - E_A * E_B$ , where  $E_A$  and  $E_B$  represent the fraction of inhibition by drug A and drug B alone, respectively. The excess over Bliss (EOB) is the difference between the Bliss expectation and the observed growth inhibition of the combination of A and B ( $E_{\text{combi}}$ ) at a given dosage. The percentage excess over Bliss (%EOB) was calculated by multiplying the EOB by 100%. A positive %EOB indicates an additive or synergistic effect, while a negative score indicates an antagonistic effect. Synergy was

defined if the inhibition of the combination ( $E_{\text{combi}}$ ) showed an excess over BLISS of > 10%, while antagonism was defined if the  $E_{\text{combi}}$  showed an excess over BLISS of < -10%.

### **Western blotting**

Cell pellets of the cell lines pre-treated with decitabine or vehicle were collected at several time points and lysed with RIPA buffer supplemented with protease inhibitors (Thermo Fisher Scientific, Waltham, USA). Western blot analysis was performed for two independent drug exposure experiments. 25  $\mu\text{g}$  of whole cell protein lysates were resolved on 10% polyacrylamide Mini-PROTEAN® TGX™ Precast Gels (Bio-Rad, Hercules, USA), and subsequently transferred to nitrocellulose membranes using the Transblot Turbo Transfer System (Bio-Rad, Hercules, USA). Membranes were blocked with 5% skim milk in TBS and probed with primary antibodies against rabbit polyclonal anti-DNMT1 (1/1000 dilution, #M0231S, New England Biolabs, Ipswich, MA, USA). Anti-GAPDH rabbit monoclonal antibodies (1/1000 dilution, # 2118, Cell Signaling Technology Inc., Danvers, USA) were used to detect GAPDH and confirm equal loading in all lanes. The membranes were then probed with infrared-labelled secondary antibodies IRDye 800CW goat-anti-rabbit antibody (1/2000 dilution, #926-32211, LI-COR, Lincoln, USA) and IRDye 680 goat-anti-mouse antibody (1/2000 dilution, #926-32220, LI-COR, Lincoln, USA). Images were acquired using an Odyssey Infrared Imaging System (LI-COR, Leusden, The Netherlands) and protein expression was quantified using the Odyssey software Image Studio Lite ver 4.0.

## **RESULTS**

### **Decitabine monotherapy mildly attenuates leukaemia progression in *MLL*-rearranged ALL xenografts**

Xenograft mouse models still represent the standard for *in vivo* anti-leukemic drug efficacy testing in *MLL*-rearranged ALL, as to date *bona fide* genetic mouse models have not yet been reliably established for this type of leukaemia. In order to generate xenografts, we used a previously described reporter cell line, SEM-SLIEW, which is derived from the *MLL*-AF4-positive B-cell precursor ALL cell line SEM. SEM-SLIEW was modified to express the luciferase reporter gene, allowing for longitudinal *in vivo* disease monitoring by bioluminescence<sup>15</sup>. Decitabine dose response curves showed comparable sensitivity of SEM-SLIEW and its parental cell line SEM to the drug *in vitro* (Supplementary Figure 1). Xenografts were established by injecting  $10^5$  SEM-SLIEW cells intrafemorally into the bone marrow of immunodeficient NSG mice, creating an orthotopic model. Successful engraftment was confirmed by bioluminescence post-transplantation, and mice were divided into a control (n=13) and treatment group (n=13). The treatment group was intraperitoneally injected with a low dose of decitabine (0.1 mg/kg), three times a week.

The control group was injected with the corresponding vehicle (10% DMSO in saline) (Figure 1A). One of the therapeutic limitations of decitabine *in vivo* is its short physiological half-life due to metabolization by liver cytidine deaminases<sup>21</sup>. As previous animal studies have shown that co-administration of tetrahydourine (THU), a cytidine deaminase inhibitor, elevates decitabine plasma levels 10-fold, while revealing no anti-leukaemic efficacy in monotherapy, we co-injected decitabine with THU (4 mg/kg in saline)<sup>22-27</sup>.

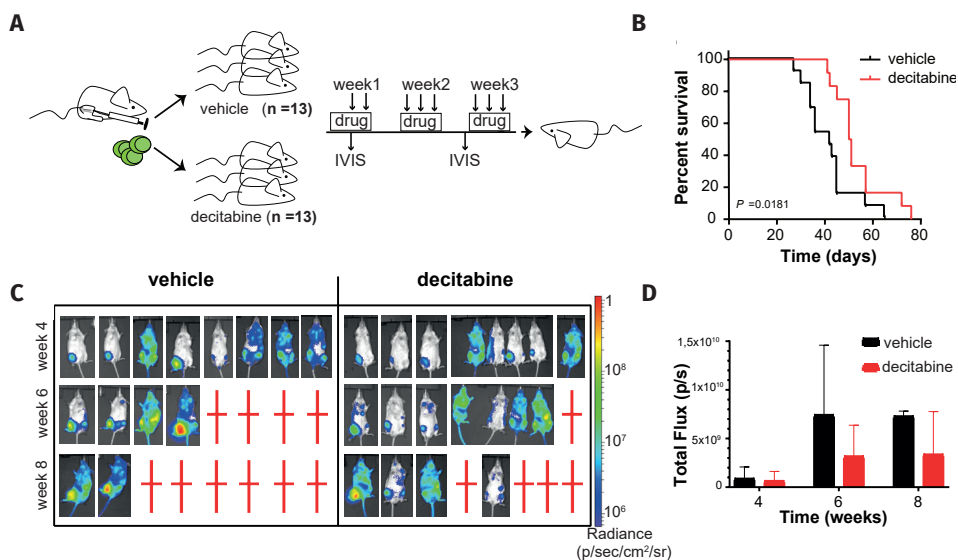


**Figure 1. Decitabine mildly attenuates *MLL*-rearranged ALL disease progression in xenograft mouse models.**

Experimental design: NSG mice (n = 26) were injected with  $10^5$  SEM-SLIEW cells. Three days post-transplantation, mice were imaged and randomly allocated to different treatment arms; treated with either 0,1 mg/kg decitabine + 4 mg/kg THU or vehicle, 10% DMSO in saline (A). Kaplan-Meier plots illustrate a significantly extended median survival in the decitabine-treated group (n = 13, 50.5 days) compared to controls (n = 13, 42 days). Statistical significance was determined by log-rank testing (B). Longitudinal intra-vital bioluminescence imaging of a representative panel of mice showed confirmed an overall reduced systemic disease burden in decitabine-treated mice compared to controls. Red crosses represent deceased mice (C). Quantification of intra-vital imaging data of each individual mouse from the vehicle and decitabine groups (black and red, respectively), as measured on weeks 4, 6, and 8. Data are presented as mean photonic flux with standard deviation (ie, the number of emitted photons per second) with (D)

Leukaemia progression was assessed by bioluminescence imaging every other week, and mice displaying overt signs of leukaemia were sacrificed. The median survival times were 50,5 days in the decitabine-treated mice and 42 days in the control mice revealing a prolonged survival in the treated mice of 8,5 days (p=0.0181, Figure 1B).The disease

burden was reduced as illustrated by whole body luminescence measurements (Figure 1C-D). Although decitabine prolonged survival in the xenograft mouse model of *MLL* rearranged ALL, decitabine was insufficient to prevent leukaemia out-growth.

Previous reports hinted on the use of decitabine as a chemo-sensitizer in a variety of cancer types<sup>28-30</sup>. Hence, to elucidate whether decitabine would exert chemo-sensitizing effects in *MLL*-rearranged ALL, we next performed high-throughput combinatorial drug screens.

### **Chemo-sensitizing effect of decitabine towards conventional chemotherapeutics in *MLL*-rearranged ALL**

The chemo-sensitizing capability of decitabine was assessed by performing a combinatorial screen of decitabine with prednisone, asparaginase, cytarabine, daunorubicin, or vincristine, which represent cornerstone drugs in current *MLL*-rearranged infant ALL treatment<sup>1,2</sup>. Prior to synergy testing, the *MLL*-rearranged ALL cell lines SEM, ALLPO and KOPN8 were first pre-treated with a low dose of 5 nM decitabine or corresponding vehicle (controls). Since high concentrations of decitabine cause DNA damage by the formation of DNA double strand breaks<sup>31,32</sup>, we used a low-dose decitabine similar to others<sup>33</sup> to solely evaluate the demethylating effect of decitabine. The low dose of decitabine is clinically relevant, since in pediatric patients with Acute Myeloid Leukemia a dosage of 20mg/m<sup>2</sup> decitabine is safely achievable<sup>34,35</sup>, leading to overall maximal plasma levels of 100ng/ml or 0.4 $\mu$ M, which will decrease substantially within 1 hour. As DNMT inhibitors typically require several cell divisions to fully exert their demethylating activity, decitabine pre-treatment was performed using a prolonged period of exposure of 14 days<sup>36</sup>. Due to the short half-life of decitabine, the drug was refreshed every other day, and passaging of the cells was performed every 4 days for optimal cell growth conditions (Figure 2A).

The demethylating effect of decitabine during 14 days of pre-treatment was assessed by monitoring DNMT1 protein expression. Decitabine represents a deoxycytidine analogue that, like normal deoxycytidines, becomes incorporated into the DNA during replication. Once incorporated, decitabine covalently binds and traps *DNA methyltransferases* (DNMTs), thereby depleting subsequent daughter cells from functional DNMTs in consecutive cell cycles<sup>37</sup>. Depletion of *DNMT1* is commonly used as a reliable read-out for DNA demethylation, and we confirmed that expression of DNMT1 was completely lost after the 14-day pre-treatment with low-dose decitabine in all cell lines tested (Figure 2B). In KOPN8 reduction of DNMT1 expression is seen after 4 days and further reduced in the later timepoints until a total loss after 14 days. In SEM and ALLPO inhibition of DNMT1 expression is evident after 4 days and completely lost after 8 days. In these cell lines the band for DNMT1 reappears after 12 days, probably due to decay of decitabine.

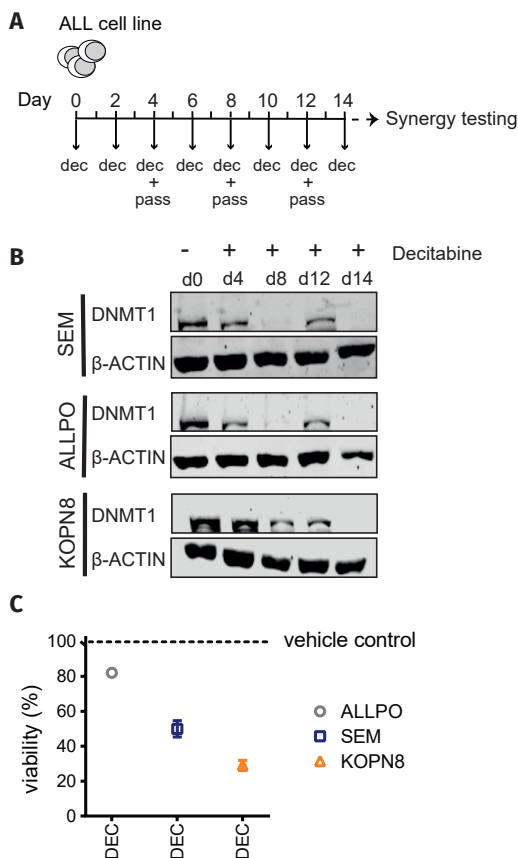


**Figure 2. Setup of combinatorial synergy screening and effect of decitabine monotherapy on cell lines. Schematic setup *in vitro* synergy testing of decitabine:**

the *MLL*-rearranged ALL cell lines SEM, ALLPO, and KOPN8 were pre-treated for 14 days with 5 nM decitabine or vehicle and subsequently exposed to synergy testing (A), the effect on DNMT1 protein expression was determined using western blotting with β-ACTIN as a loading control (B). Mean percentage of cell viability effects of 14 days of 5 nM decitabine (DEC) pretreatment or vehicle control in *MLL*-rearranged ALL cell lines SEM, ALLPO, and KOPN8 with standard deviation. Viability was determined using MTT assays. Data has been corrected for the effect of vehicle (C)

Interestingly, all three *MLL*-rearranged ALL cell lines displayed different responses in viability to the 14-day low-dose decitabine pre-treatment. The low concentration of 5 nM of decitabine corresponded to the  $IC_{80}$ ,  $IC_{50}$ , and  $IC_{30}$  values in ALL-PO, SEM and KOPN8, respectively (Figure 2C).

After the 14-day period of decitabine pre-treatment, the leukemic cells were subjected to synergy testing, using 5 nM decitabine in combination with prednisone, asparaginase, cytarabine, daunorubicin, or vincristine, which are currently used in the treatment of *MLL*-rearranged infant ALL. The *in vitro* efficacy of each drug combination was assessed by 4-day dose-response curves (MTT assays), normalized to the effects of decitabine as a single agent and analyzed for synergistic, additive, or antagonistic effects by means of the Bliss Independence model<sup>20</sup>. For all three tested cell lines a mild chemo-sensitizing effect was observed towards asparaginase in the decitabine treated cells (Figure 3). The combination of decitabine and 15,6 nM cytarabine appeared to have a synergistic effect

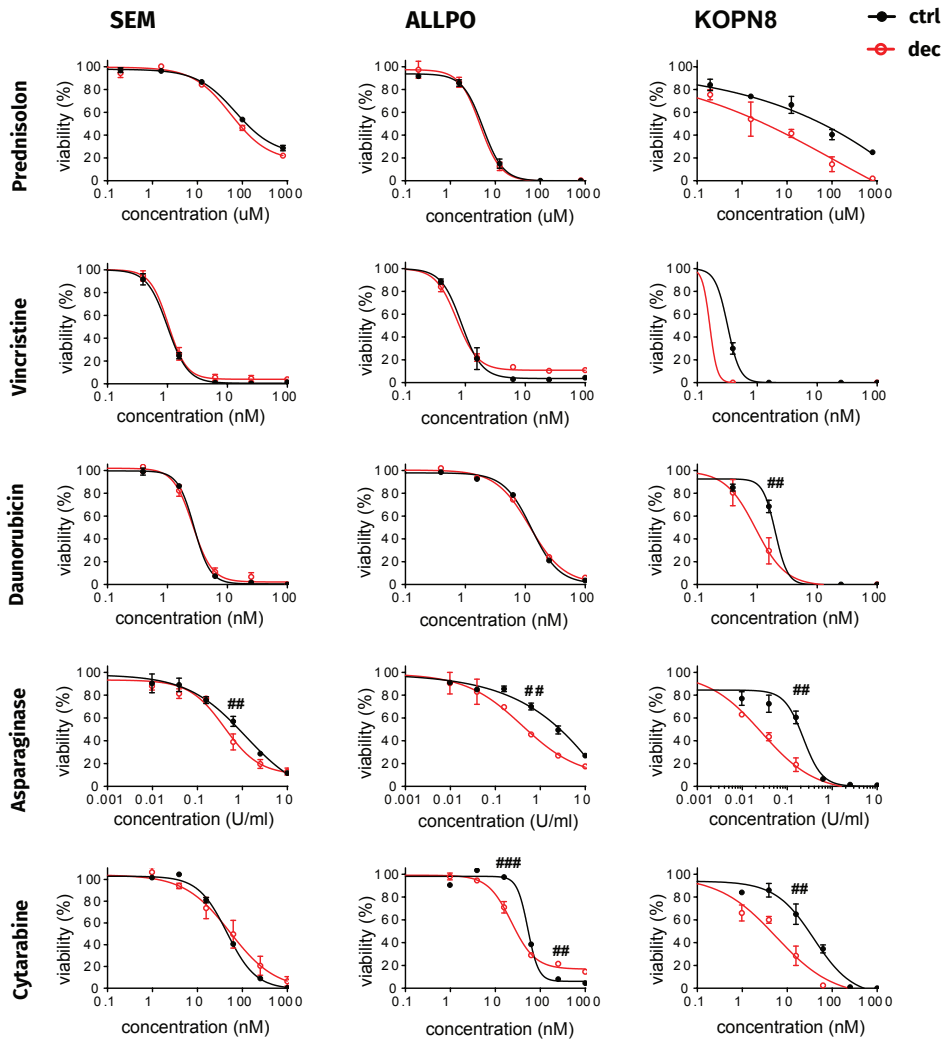


**Figure 3. Long-term low-dose decitabine treatment acts as a poor chemo-sensitizer in *MLL*-rearranged ALL cells.**

Chemo-sensitizing effect of decitabine pre-treatment (dec) on current chemotherapeutics. Decitabine pretreated cells were subsequently cultured with additional compounds in the presence or absence (ctrl) of the hypomethylating agent for 4 additional days. Synergy is determined using Bliss independence model. Percentage excess over Bliss (EoB) is indicated: ##EoB > 10%; ###EoB > 20%. Error bars represent the standard error of the mean (SEM). Graphs represent the average of n = 3 independent experiments (n = 2 for KOPN8)

in ALLPO, while showing an antagonistic effect for the combination of decitabine and 250 nM of cytarabine. Enhanced sensitivity towards all the conventional drugs was evident in KOPN8, although this is not considered as synergy by the Bliss independence model



due to the increased effect of decitabine alone reducing cell viability by 70% (Figure 2C). Taken together we observe decitabine chemo-sensitizes towards the conventional drugs prednisolone, vincristine, daunorubicin, asparaginase, and cytarabine for inhibition of cell survival of *MLL* rearranged ALL in a limited range of concentrations. Additionally, the observed synergy was not consistent in all of the cell lines tested. These results indicate prolonged exposure to low-dose decitabine is sufficient to completely deplete *MLL*-rearranged ALL cells from DNTM1, however only mildly sensitizes *MLL*-rearranged ALL cells towards conventional chemotherapeutics.

### **Combinatorial high-throughput screening of decitabine with other drug classes**

Next we assessed whether a prolonged pre-treatment of low-dose decitabine could sensitize *MLL*-rearranged ALL cells to other epigenetic-based or anti-cancer drugs. For this, SEM cells were exposed to a slightly higher concentration of 10 nM decitabine (or vehicle) compared to earlier experiments, for a period of 14 days. Subsequently, the sensitivity of these cells towards 369 different compounds, derived from an epigenetic-based drug library and an anti-neoplasm drug library, was tested using 4-day MTT assays with drug concentrations of 10, 100 or 1000 nM. Results of all inhibitors tested is listed in table S2. Drug synergy was based on area under the curve (AUC) calculations. A cut-off of  $\geq 30\%$  difference in AUC of drugs in the decitabine pre-treated SEM cells compared to vehicle-treated cells was applied to determine the top hits, which could be mainly categorized as either histone deacetylase (HDAC) inhibitors, receptor tyrosine kinase (RTK) inhibitors, MEK inhibitors and BCL2 protein family inhibitors (Figure 4A). As HDAC, MEK and BCL2 inhibitors have shown promising pre-clinical efficacy against *MLL*-rearranged ALL<sup>15,38-40</sup>, these drug classes are of particular interest. Hence, we proceeded to validate a potential synergistic combinatorial effect of these compounds with decitabine in an extended *MLL*-rearranged ALL cell line panel.

For all three cell lines tested, a chemo-sensitizing effect was observed towards the HDAC inhibitor panobinostat, yet only for the combination of 3,3 nM panobinostat with decitabine (Figure 4B), potentially due to the steep dose-response curve panobinostat elicits on its own. The combination of the BCL-2 inhibitor venetoclax and decitabine enhanced the efficacy of venetoclax in KOPN8 cells.

MEK inhibitors have previously been shown to be effective for the treatment of *MLL*-rearranged infant ALL cells harboring *RAS*-mutations<sup>38</sup>. The effect of *RAS* mutations is represented here by the cell line KOPN8, while both cell lines ALLPO and SEM are *RAS*-wildtype. Interestingly, in the *RAS*-wildtype cell line SEM treated with decitabine the MEK inhibitor pimasertib revealed a mild chemo-sensitizing effect, while showing a more pronounced chemo-sensitizing effect in decitabine treated *RAS*-mutant KOPN8 cells.

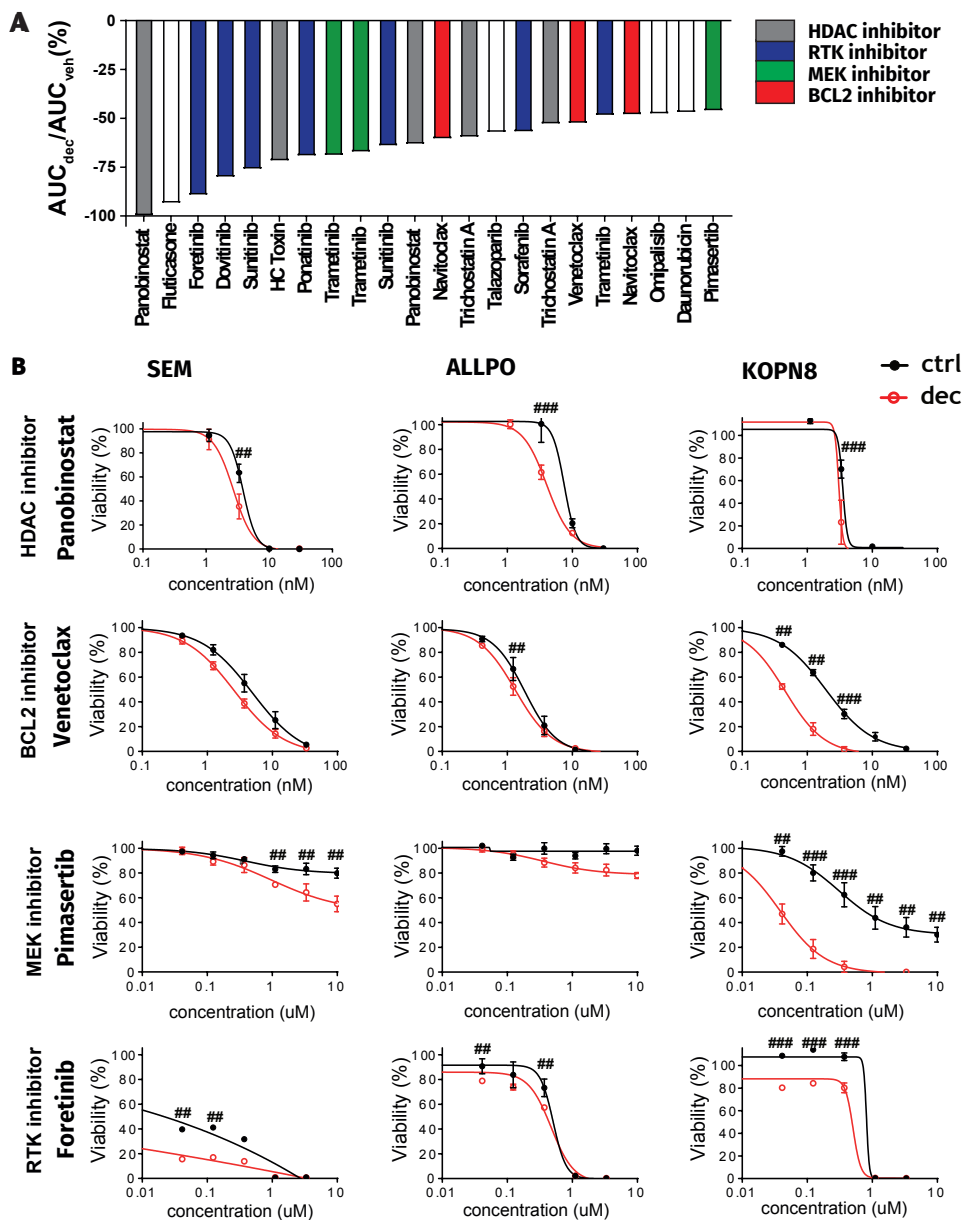


**Figure 4. Long-term low-dose decitabine treatment fails to sensitize *MLL*-rearranged ALL cells to epigenetic-based or anti-neoplastic agents**

(A). Validation the drug screening top hits with an extended concentration range in the *MLL*-rearranged leukemic cell lines SEM, ALLPO, and KOPN8. Decitabine pretreatment mildly sensitizes to the HDAC inhibitor Panobinostat, the BCL2 inhibitor Venetoclax, the MEK inhibitor Pimasertib, and the RTK inhibitor Foretinib.

Synergy is determined using Bliss independence model. Percentage excess over Bliss (EoB) is indicated: ##EoB > 10%; ###EoB > 20% (B). Error bars represent the standard error of the mean (SEM). Graphs represent the average of n = 3 independent experiments (n = 2 for KOPN8)

---

The combination of the RTK inhibitor foretinib and decitabine decreased cell viability more potently than either drug alone and indicated moderate synergy according to the Bliss independence model in all three cell lines tested.

Taken together we showed drug synergy by means of the Bliss Independence model appeared moderate and was evident at limited drug concentrations (Figure 4B). Therefore, these data show that prolonged DNA demethylation by decitabine hardly sensitizes *MLL*-rearranged ALL cells to known epigenetic-based or anti-cancer drugs.

## DISCUSSION

We previously demonstrated the efficacy of DNA demethylating agents, such as decitabine and zebularine, in eradicating *MLL*-rearranged ALL cells *in vitro*<sup>8,9</sup>. However, not much research has demonstrated the efficacy of DNA demethylating agents against *MLL*-rearranged ALL *in vivo*, while clinical trials have already been conducted for other types of leukaemia. For instance, decitabine shows promising results against acute myeloid leukaemia (AML) in both children and adults<sup>29,41</sup>.

Recently, Roelf *et al.*, reported that decitabine induced a significant delay of leukemic progression *in vivo* in mouse xenografts of the *MLL*-rearranged ALL cell lines SEM and RS4;11, but could not eradicate the leukaemia<sup>42</sup>. In line with that study, our present data also shows a significant delay in leukaemia progression induced by decitabine in xenografts of the *MLL*-rearranged ALL cell line SEM, albeit modestly. There are, however, clear differences in the experimental design of both studies. Roelf and co-workers treated their mice with 0.4 mg/kg decitabine daily for only four consecutive days, 7 days after leukaemia injection. In contrast, we treated our mice with only 0,1 mg/kg decitabine three times a week over a period of 3 weeks, starting treatment 3 days after tumor injection. Moreover, THU was co-administered in the mice, which is known to elevate decitabine plasma levels up to 10-fold<sup>22-26</sup>. We deliberately choose to use 0.1 mg/kg of decitabine, as low-dose decitabine is sufficient to deplete *MLL*-rearranged ALL cells from DNMT1 (and thus to induce DNA demethylation), and prevents aspecific drug effects such as diminished DNA polymerase functioning<sup>37</sup>. Yet, it seems evident that the promising inhibitory effects of DNA demethylating agents against *MLL*-rearranged ALL cells *in vitro*, were not indicative for similarly promising results in *in vivo* mouse models. Possibly, the typical experimental set-up of *in vitro* drug response assays, in which tumor cells are

cultured for a fixed period of time in the presence of increasing drug concentrations, provides a plausible explanation. If, as we show here, low concentrations of decitabine are sufficient to completely deplete *MLL*-rearranged ALL cells from functional DNMT1, higher concentrations of decitabine should not provide any additional effects, other than aspecific drug effects that are not related to DNA demethylation. Thus, increasing concentrations of decitabine may eradicate most *MLL*-rearranged ALL cells in *in vitro* drug response curves, this might not be solely due to DNA demethylation. If so, this may suggest that *MLL*-rearranged ALL cells are not necessarily depending very heavily on their aberrant promotor DNA methylation patterns to maintain leukaemogenic potential as observed previously<sup>8,10</sup>.

Additionally, we investigated whether prolonged low-dose decitabine pre-treatment could chemo-sensitize *MLL*-rearranged ALL cells towards chemotherapeutics currently used in the treatment of this type of leukaemia, as well as towards various other epigenetic or anti-neoplastic compounds. Earlier findings revealed that short-term exposure to high-dose decitabine could synergize with cytarabine to eradicate *MLL*-rearranged ALL cells *in vitro*<sup>42</sup>, as well as with L-asparaginase to enhance cytotoxicity in the pediatric T-ALL<sup>28</sup>. Here we demonstrate that prolonged exposure to low-dose decitabine occasionally sensitizes *MLL*-rearranged ALL cells to some of the current chemotherapeutics at certain concentrations in some of the cell lines tested. These observations were most notable for L-asparaginase and cytarabine, thereby confirming the results reported by others<sup>28,42</sup>.

Interestingly, the combination of decitabine and the MEK inhibitor pimasertib strongly decreased cell viability in *RAS*-mutant KOPN8 cells than either drug alone. Previously, we showed that MEK inhibitors are effective for the treatment of *RAS*-mutant *MLL*-rearranged infant ALL cells<sup>38,39</sup>. *RAS* mutations are found in 14-24% of infant ALL patients and these *RAS* mutations decrease the survival chances even further<sup>5</sup>. Here, the MEK inhibitor pimasertib revealed a mild chemo-sensitizing effect in the *RAS*-wildtype cell line SEM, while showing a more pronounced chemo-sensitizing effect in decitabine treated *RAS*-mutant KOPN8 cells. Therefore there might be a benefit for the treatment of *MLL*-rearranged infant ALL harboring *RAS* mutations by combining decitabine and MEK inhibitors.

However, the *in vitro* chemo-sensitizing effects of decitabine are modest and therefore clinical relevance may be rather limited. Additionally, since synergy was observed for limited concentration ranges, reaching and maintaining these exact concentration ranges in patients would be challenging due the many factors influencing the pharmacokinetics of the drugs<sup>43-46</sup>.

Furthermore, a recent study in relapsed pediatric ALL, all above 1 year of age, revealed that the combination of decitabine and HDAC inhibitor vorinostat in the current intensive chemotherapy protocol was determined not feasible due to the high incidence of infectious toxicities, despite encouraging response rates and pharmacodynamics <sup>47</sup>. Current clinical trials will shed more light on the feasibility and efficacy of demethylating agents for the treatment of *MLL*-rearranged infant ALL.

Ch1

Ch2

In conclusion, our present study demonstrates that prolonged exposure to a clinically relevant low-dose of the DNA methyltransferase inhibitor decitabine significantly, but mildly delays leukaemia progression in *MLL*-rearranged ALL xenograft mouse models. Moreover, long-term pre-treatment with low-dose decitabine moderately sensitizes *MLL*-rearranged ALL cells towards conventional chemotherapeutics as well as towards known epigenetic-based compounds and anti-neoplastic agents, *in vitro*.

For a better understanding of the potential of demethylating agents in the treatment of *MLL*-rearranged ALL, agents with increased stability and bioavailability could be further evaluated. Ongoing clinical trials should shed more light on the efficacy of demethylating agents for the treatment of *MLL*-rearranged infant ALL.

## REFERENCES

1. Pieters R, De Lorenzo P, Ancliffe P, et al. Outcome of Infants Younger Than 1 Year With Acute Lymphoblastic Leukemia Treated With the Interfant-06 Protocol: Results From an International Phase III Randomized Study. *J Clin Oncol*. 2019;JCO1900261.
2. Pieters R, Schrappe M, De Lorenzo P, et al. A treatment protocol for infants younger than 1 year with acute lymphoblastic leukaemia (Interfant-99): an observational study and a multicentre randomised trial. *Lancet*. 2007;370(9583):240-250.
3. Hunger SP, Mullighan CG. Acute Lymphoblastic Leukemia in Children. *N Engl J Med*. 2015;373(16):1541-1552.
4. Andersson AK, Ma J, Wang J, et al. The landscape of somatic mutations in infant MLL-rearranged acute lymphoblastic leukemias. *Nat Genet*. 2015;47(4):330-337.
5. Driessen EM, van Roon EH, Spijkers-Hagelstein JA, et al. Frequencies and prognostic impact of RAS mutations in MLL-rearranged acute lymphoblastic leukemia in infants. *Haematologica*. 2013;98(6):937-944.
6. Agraz-Doblas A, Bueno C, Bashford-Rogers R, et al. Unravelling the cellular origin and clinical prognostic markers of infant B-cell acute lymphoblastic leukemia using genome-wide analysis. *Haematologica*. 2019.
7. Zhang Y, Chen A, Yan XM, Huang G. Disordered epigenetic regulation in MLL-related leukemia. *Int J Hematol*. 2012;96(4):428-437.
8. Stumpel DJ, Schneider P, van Roon EH, et al. Specific promoter methylation identifies different subgroups of MLL-rearranged infant acute lymphoblastic leukemia, influences clinical outcome, and provides therapeutic options. *Blood*. 2009;114(27):5490-5498.
9. Stumpel DJ, Schneider P, van Roon EH, Pieters R, Stam RW. Absence of global hypomethylation in promoter hypermethylated Mixed Lineage Leukaemia-rearranged infant acute lymphoblastic leukaemia. *Eur J Cancer*. 2013;49(1):175-184.
10. Schafer E, Irizarry R, Negi S, et al. Promoter hypermethylation in MLL-r infant acute lymphoblastic leukemia: biology and therapeutic targeting. *Blood*. 2010;115(23):4798-4809.
11. Krivtsov AV, Feng Z, Lemieux ME, et al. H3K79 methylation profiles define murine and human MLL-AF4 leukemias. *Cancer Cell*. 2008;14(5):355-368.
12. Bernt KM, Zhu N, Sinha AU, et al. MLL-rearranged leukemia is dependent on aberrant H3K79 methylation by DOT1L. *Cancer Cell*. 2011;20(1):66-78.
13. Daigle SR, Olhava EJ, Therkelsen CA, et al. Selective killing of mixed lineage leukemia cells by a potent small-molecule DOT1L inhibitor. *Cancer Cell*. 2011;20(1):53-65.
14. Wang X, Chen CW, Armstrong SA. The role of DOT1L in the maintenance of leukemia gene expression. *Curr Opin Genet Dev*. 2016;36:68-72.
15. Garrido Castro P, van Roon EHJ, Pinhancos SS, et al. The HDAC inhibitor panobinostat (LBH589) exerts in vivo anti-leukaemic activity against MLL-rearranged acute lymphoblastic leukaemia and involves the RNF20/RNF40/WAC-H2B ubiquitination axis. *Leukemia*. 2018;32(2):323-331.
16. Bardini M, Trentin L, Rizzo F, et al. Antileukemic Efficacy of BET Inhibitor in a Preclinical Mouse Model of MLL-AF4(+) Infant ALL. *Mol Cancer Ther*. 2018;17(8):1705-1716.
17. Brown P, Pieters R, Biondi A. How I treat infant leukemia. *Blood*. 2019;133(3):205-214.
18. Stumpel DJ, Schotte D, Lange-Turenhout EA, et al. Hypermethylation of specific microRNA genes in MLL-rearranged infant acute lymphoblastic leukemia: major matters at a micro scale.

- Leukemia. 2011;25(3):429-439.
19. Pieters R, Loonen AH, Huismans DR, et al. In vitro drug sensitivity of cells from children with leukemia using the MTT assay with improved culture conditions. *Blood*. 1990;76(11):2327-2336.
  20. Fouquier J, Guedj M. Analysis of drug combinations: current methodological landscape. *Pharmacol Res Perspect*. 2015;3(3):e00149.
  21. Ebrahim Q, Mahfouz RZ, Ng KP, Saunthararajah Y. High cytidine deaminase expression in the liver provides sanctuary for cancer cells from decitabine treatment effects. *Oncotarget*. 2012;3(10):1137-1145.
  22. Holleran JL, Beumer JH, McCormick DL, et al. Oral and intravenous pharmacokinetics of 5-fluoro-2'-deoxycytidine and THU in cynomolgus monkeys and humans. *Cancer Chemother Pharmacol*. 2015;76(4):803-811.
  23. Lavelle D, Vaitkus K, Ling Y, et al. Effects of tetrahydrouridine on pharmacokinetics and pharmacodynamics of oral decitabine. *Blood*. 2012;119(5):1240-1247.
  24. Molokie R, Lavelle D, Gowhari M, et al. Oral tetrahydrouridine and decitabine for non-cytotoxic epigenetic gene regulation in sickle cell disease: A randomized phase 1 study. *PLoS Med*. 2017;14(9):e1002382.
  25. Morfouace M, Nimmervoll B, Boulos N, et al. Preclinical studies of 5-fluoro-2'-deoxycytidine and tetrahydrouridine in pediatric brain tumors. *J Neurooncol*. 2016;126(2):225-234.
  26. Newman EM, Morgan RJ, Kummar S, et al. A phase I, pharmacokinetic, and pharmacodynamic evaluation of the DNA methyltransferase inhibitor 5-fluoro-2'-deoxycytidine, administered with tetrahydrouridine. *Cancer Chemother Pharmacol*. 2015;75(3):537-546.
  27. Neil GL, Moxley TE, Manak RC. Enhancement by tetrahydrouridine of 1-beta-D-arabinofuranosylcytosine (cytarabine) oral activity in L1210 leukemic mice. *Cancer Res*. 1970;30(8):2166-2172.
  28. Serravalle S, Bertuccio SN, Astolfi A, Melchionda F, Pession A. Synergistic Cytotoxic Effect of L-Asparaginase Combined with Decitabine as a Demethylating Agent in Pediatric T-ALL, with Specific Epigenetic Signature. *Biomed Res Int*. 2016;2016:1985750.
  29. Gore L, Triche TJ, Jr., Farrar JE, et al. A multicenter, randomized study of decitabine as epigenetic priming with induction chemotherapy in children with AML. *Clin Epigenetics*. 2017;9:108.
  30. Fang F, Zuo Q, Pilrose J, et al. Decitabine reactivated pathways in platinum resistant ovarian cancer. *Oncotarget*. 2014;5(11):3579-3589.
  31. Karpf AR, Moore BC, Ririe TO, Jones DA. Activation of the p53 DNA damage response pathway after inhibition of DNA methyltransferase by 5-aza-2'-deoxycytidine. *Mol Pharmacol*. 2001;59(4):751-757.
  32. Pali SS, Van Emburgh BO, Sankpal UT, Brown KD, Robertson KD. DNA methylation inhibitor 5-Aza-2'-deoxycytidine induces reversible genome-wide DNA damage that is distinctly influenced by DNA methyltransferases 1 and 3B. *Mol Cell Biol*. 2008;28(2):752-771.
  33. Tsai HC, Li H, Van Neste L, et al. Transient low doses of DNA-demethylating agents exert durable antitumor effects on hematological and epithelial tumor cells. *Cancer Cell*. 2012;21(3):430-446.
  34. Zhou W, Parasrampur DA, Nemat S, et al. Population Pharmacokinetic Analysis of Decitabine in Pediatric Patients With Acute Myeloid Leukemia. *J Clin Pharmacol*. 2019;59(5):668-676.
  35. Kearns P, Zwaan CM, Reinhardt D, et al. Phase 1-2 safety, efficacy and pharmacokinetic study of decitabine in sequential administration with cytarabine in children with relapsed or refractory acute myeloid leukaemia. *Br J Haematol*. 2019;186(3):e7-e11.
  36. Issa JP, Garcia-Manero G, Giles FJ, et al. Phase 1 study of low-dose prolonged exposure

Ch1

Ch2

- schedules of the hypomethylating agent 5-aza-2'-deoxycytidine (decitabine) in hematopoietic malignancies. *Blood*. 2004;103(5):1635-1640.
37. Seelan RS, Mukhopadhyay P, Pisano MM, Greene RM. Effects of 5-Aza-2'-deoxycytidine (decitabine) on gene expression. *Drug Metab Rev*. 2018;50(2):193-207.
  38. Kerstjens M, Driessen EM, Willekes M, et al. MEK inhibition is a promising therapeutic strategy for MLL-rearranged infant acute lymphoblastic leukemia patients carrying RAS mutations. *Oncotarget*. 2017;8(9):14835-14846.
  39. Kerstjens M, Pinhancos SS, Castro PG, et al. Trametinib inhibits RAS-mutant MLL-rearranged acute lymphoblastic leukemia at specific niche sites and reduces ERK phosphorylation in vivo. *Haematologica*. 2018;103(4):e147-e150.
  40. Khaw SL, Suryani S, Evans K, et al. Venetoclax responses of pediatric ALL xenografts reveal sensitivity of MLL-rearranged leukemia. *Blood*. 2016;128(10):1382-1395.
  41. Fili C, Candoni A, Zannier ME, et al. Efficacy and toxicity of Decitabine in patients with acute myeloid leukemia (AML): A multicenter real-world experience. *Leuk Res*. 2019;76:33-38.
  42. Roof C, Richter A, Konkolefski C, et al. Decitabine demonstrates antileukemic activity in B cell precursor acute lymphoblastic leukemia with MLL rearrangements. *J Hematol Oncol*. 2018;11(1):62.
  43. Gerber W, Steyn JD, Kotze AF, Hamman JH. Beneficial Pharmacokinetic Drug Interactions: A Tool to Improve the Bioavailability of Poorly Permeable Drugs. *Pharmaceutics*. 2018;10(3).
  44. Wang R, Zhong C, Zhang C, Hua M, Ma D. Insight to Pharmacokinetics of TKIs: Optimizing Practical Guidelines for Individualized Therapy. *Curr Drug Metab*. 2017;18(3):199-206.
  45. Srinivas NR. Clinical pharmacokinetics of panobinostat, a novel histone deacetylase (HDAC) inhibitor: review and perspectives. *Xenobiotica*. 2017;47(4):354-368.
  46. Salem AH, Agarwal SK, Dunbar M, Enschede SL, Humerickhouse RA, Wong SL. Pharmacokinetics of Venetoclax, a Novel BCL-2 Inhibitor, in Patients With Relapsed or Refractory Chronic Lymphocytic Leukemia or Non-Hodgkin Lymphoma. *J Clin Pharmacol*. 2017;57(4):484-492.
  47. Burke MJ, Kostadinov R, Sposto R, et al. Decitabine and Vorinostat with Chemotherapy in Relapsed Pediatric Acute Lymphoblastic Leukemia: A TACL Pilot Study. *Clin Cancer Res*. 2020.



Decitabine mildly attenuates *MLL*-rearranged acute lymphoblastic leukaemia in vivo, and represents a poor chemo-sensitizer

Ch1

Ch2



# CHAPTER 3

## Modelling acquired resistance to DOT1L inhibition exhibits the adaptive potential of *KMT2A*-rearranged Acute Lymphoblastic Leukemia



Pauline Schneider<sup>1</sup>, Nicholas T. Crump<sup>2,3</sup>, Susan T.C.J.M. Arentsen-Peters<sup>1</sup>, Alastair L. Smith<sup>2</sup>, Rico Hagelaar<sup>1,4</sup>, Fabienne R.S. Adriaanse<sup>1</sup>, Romy S. Bos<sup>1</sup>, Anja de Jong<sup>1</sup>, Stefan Nierkens<sup>1</sup>, Bianca Koopmans<sup>1</sup>, Thomas A. Milne<sup>2</sup>, Rob Pieters<sup>1</sup>, Ronald W. Stam<sup>1</sup>

<sup>1</sup>Princess Máxima Center for Pediatric Oncology, Utrecht, The Netherlands

<sup>2</sup>MRC Molecular Haematology Unit, MRC Weatherall Institute of Molecular Medicine, Radcliffe Department of Medicine, University of Oxford, Oxford, United Kingdom

<sup>3</sup>Hugh and Josseline Langmuir Centre for Myeloma Research, Centre for Haematology, Department of Immunology and Inflammation, Imperial College London, UK

<sup>4</sup>Oncode Institute, Utrecht, The Netherlands

## ABSTRACT

In *KMT2A*-rearranged acute lymphoblastic leukemia (ALL), an aggressive malignancy, oncogenic *KMT2A*-fusion proteins inappropriately recruit DOT1L to promote leukemogenesis, highlighting DOT1L as an attractive therapeutic target. Unfortunately, treatment with the first-in-class DOT1L inhibitor pinometostat eventually leads to non-responsiveness. To understand this we established acquired pinometostat resistance in pediatric *KMT2A::AFF1*<sup>+</sup> B-ALL cells. Interestingly, these cells became mostly independent of DOT1L-mediated H3K79 methylation, but still relied on the physical presence of DOT1L, HOXA9 and the *KMT2A::AFF1* fusion. Moreover, these cells selectively lost the epigenetic regulation and expression of various *KMT2A*-fusion target genes such as *PROM1/CD133*, while other *KMT2A::AFF1* target genes, including *HOXA9* and *CDK6* remained unaffected. Concomitantly, these pinometostat-resistant cells showed upregulation of several myeloid-associated genes, including *CD33* and *LILRB4/CD85k*. Taken together, this model comprehensively shows the adaptive potential of *KMT2A*-rearranged ALL cells upon losing dependency on one of its main oncogenic properties.

## Background

Chromosomal translocations involving the *KMT2A* (*MLL*) gene constitute the cytogenetic hallmark of acute lymphoblastic leukemia (ALL) diagnosed in infants (<1 year of age), giving rise to an aggressive malignancy with high relapse rates and low event-free survival (EFS) chances of 30-40%.<sup>1,2</sup> Hence, currently available treatment regimens for *KMT2A*-rearranged infant ALL are inadequate and require more effective therapeutic options to improve clinical outcome.

*KMT2A* translocations result in the fusion of *KMT2A* to one of its many translocation partner genes,<sup>3</sup> generating chimeric transcripts encoding highly oncogenic *KMT2A* fusion proteins. Among infant ALL patients, *KMT2A* is most recurrently fused to either *AFF1* (*AF4*), *MLLT1* (*ENL*), or *MLLT3* (*AF9*).<sup>3</sup> Functionally, wild-type *KMT2A* plays an essential role in definitive hematopoiesis<sup>4</sup> regulating gene expression through histone 3 lysine 4 (H3K4) methyltransferase activity, mediated by its Su(Var)<sub>3-9</sub>, Enhancer-of-zeste, Trithorax (SET) domain.<sup>5</sup> In contrast, *KMT2A* fusion proteins lose their SET domain, but instead recruit the histone 3 lysine 79 (H3K79) methyltransferase DOT1L through binding motifs encoded by the translocation partner genes.<sup>6-8</sup> Binding of DOT1L to *KMT2A* fusion proteins causes inappropriate H3K79 hypermethylation at *KMT2A* target genes, leading to an altered transcriptomic landscape that strongly favors leukemia development.<sup>6-9</sup>

Interestingly, the mutational landscape of *KMT2A*-rearranged infant ALL is remarkably silent, with only 1.3 – 2.5 leukemia-specific, non-silent mutations in the dominant clone per patient,<sup>10,11</sup> suggesting that the *KMT2A* translocation may well be the sole oncogenic

lesion driving this aggressive type of leukemia.<sup>12</sup> Therefore, targeting DOT1L, through which *KMT2A* fusion proteins exert their oncogenic effects, represents an attractive therapeutic strategy. Accordingly, the development of the DOT1L inhibitor EPZ004777 and its successor EPZ5676 (pinometostat)<sup>13,14</sup> were expected to become key to successful treatment of *KMT2A*-rearranged acute leukemias. However, despite promising preclinical results, subsequent clinical trials revealed that good initial responses in patients treated with pinometostat readily led to non-responsiveness due to acquired resistance and poor pharmacokinetics (PK).<sup>15,16</sup> Previously, it was reported that acquired resistance to pinometostat in *KMT2A*-rearranged acute leukemic cell lines is associated with enhanced drug efflux mediated by the elevated expression of the multidrug resistance transporters ABCB1 and ABCG2.<sup>17</sup>

Ch1

Ch2

Ch3

Despite this, targeting DOT1L remains a promising avenue for treating *KMT2A* rearranged leukemias, and novel small-molecule DOT1L inhibitors with improved PK profiles have already been identified.<sup>18,19</sup> For future drug development, more needs to be understood about exactly how DOT1L contributes to leukemogenesis, the role of its enzymatic methyltransferase activity, and how leukemias might develop resistance. Understanding these issues could not only impact the development of novel DOT1L inhibitors but could also be essential for better understanding the activity of novel compounds designed to target similar pathways. Therefore, following up on the study by Campbell and colleagues,<sup>17</sup> we here established and extensively characterized a model of acquired resistance to DOT1L inhibition in *KMT2A*-rearranged ALL cells.

## METHODS

### Cell line models

The *KMT2A::AFF1*<sup>+</sup> B-cell precursor ALL cell lines used are SEM, (DSMZ, cat.nr. ACC 546), and RS4;11, (ATCC; cat.nr. CRL-1873). Culture conditions are described in detail in the supplemental methods.

### Establishment of acquired pinometostat resistance in SEM and RS4;11 cells.

SEM and RS4;11 cells were cultured in the presence of gradually increasing concentrations (ranging from 1 to 100  $\mu$ M) of the DOT1L inhibitor pinometostat (EPZ5676, Selleckchem), for 14 weeks. For assessment of the *in vitro* response to pinometostat, cells were cultured in the absence of pinometostat for a few passages before exposing the cells to six concentrations (ranging from 0  $\mu$ M to 100  $\mu$ M), of pinometostat for 14 days. Trypan blue exclusion counts were used to calculate the inhibitory pinometostat concentration to 50% of the leukemic cells (i.e., IC<sub>50</sub> value). *p* values were determined by ratio paired t-test using four biological replicates, mean with range.

### **Immunoblotting**

The presence of histone modifications and the levels of protein expression were determined by immunoblot analysis, as described in the supplemental methods.

### **RNA sequencing (RNA-seq) and Chromatin Immunoprecipitation sequencing (ChIP-seq)**

RNA- and ChIP-sequencing was performed on a NextSeq® 500 System (Illumina®). Experimental procedures and analyses are described in the supplemental methods.

### **Assay for Transposase-Accessible Chromatin sequencing (ATAC-seq)**

ATAC sequencing was outsourced to Active Motif (ATACseq Service: <https://www.activemotif.com/catalog/1233/atac-seq-service>) to identify regions that have open or accessible chromatin states, as described in the supplemental methods.

### **Flow cytometry (FACS) analysis**

Details of FACS analysis are described in the supplemental methods.

### **RNA interference**

To transiently induce mRNA knockdowns, leukemic cells were electroporated in the presence of 500 nM of small-interfering RNAs (siRNAs) directed against the mRNA of selected target genes, as described previously<sup>20</sup>, and as described in the supplemental methods.

### **Quantitative reverse-transcription PCR analysis**

RNA, isolated using the RNeasy Mini Kit (QIAGEN), was reverse transcribed and the obtained cDNA was used for quantitative reverse-transcription PCR (qRT-PCR) analysis as described previously<sup>21</sup>, and as described in the supplemental methods.

### **Cell viability assays and High-throughput drug screening**

Cell viability assays were performed using flow cytometry and 7-AAD viability dye (BioLegend) to discriminate between viable and dead cells. Further details on the cell viability assays and high-throughput drug screens are described in the supplemental methods.

### **Statistical analysis**

Statistical significance of independent experimental replicates in graphs were determined by two-sided Student's t-tests. All statistical analyses were conducted using GraphPad Prism8, version 8.3.4.  $p < 0.05$  was considered statistically significant.

## RESULTS

Ch1

### Establishment of acquired resistance to DOT1L inhibition in *KMT2A*-rearranged ALL cells

Ch2

To induce acquired resistance to DOT1L inhibition, the *KMT2A::AFF1*<sup>+</sup> ALL cell line SEM<sup>22</sup> was exposed to increasing concentrations of the first-in-class DOT1L inhibitor pinometostat for 14 weeks (Figure 1A). Next, cells were cultured in the absence of drug before evaluating potential changes in pinometostat-induced cytotoxicity. Exposure of maternal SEM cells to 50  $\mu$ M pinometostat for 1 week reduced the percentage of viable cells to ~35%.

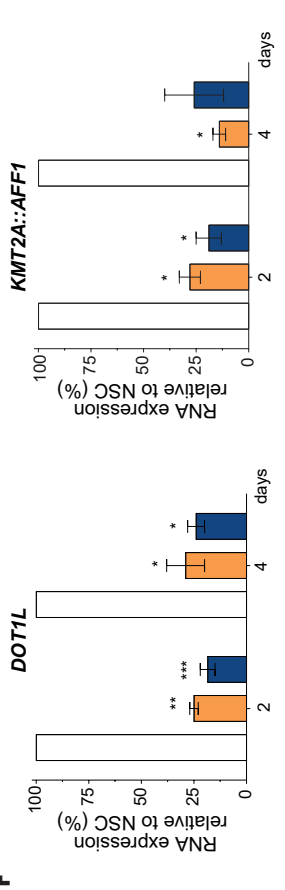
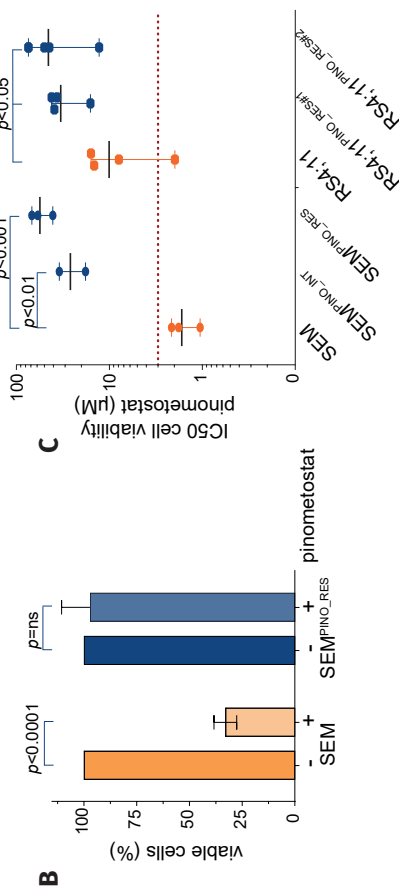
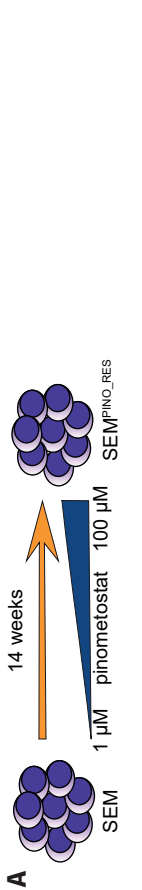
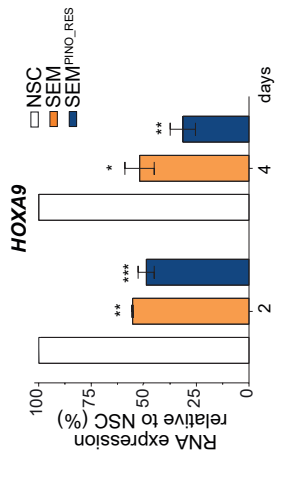
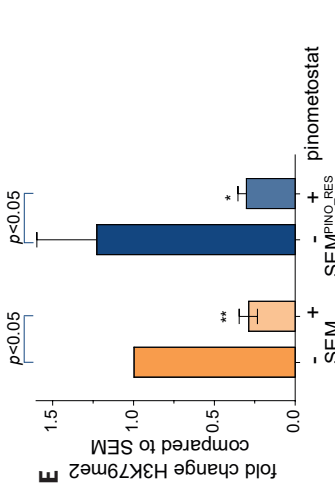
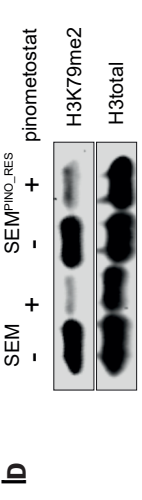
Ch3

In contrast the viability of SEM cells that underwent prolonged exposure to increasing pinometostat concentrations was hardly affected (Figure 1B). This pinometostat-resistant daughter line, designated as SEM<sup>PINO\_RES</sup>, revealed a 34-fold higher 14-day-IC<sub>50</sub> value as compared to maternal SEM cells (Figure 1C), indicating that SEM<sup>PINO\_RES</sup> became highly resistant. An additional model of intermediate resistance was established in SEM cells (i.e., SEM<sup>PINO\_INT</sup>) by prolonged exposure to 4.5  $\mu$ M pinometostat for 7 weeks, leading to a 16-fold higher IC<sub>50</sub> (Figure 1C).

Similar to SEM<sup>PINO\_RES</sup>, we also induced pinometostat resistance in the *KMT2A::AFF1*<sup>+</sup> ALL cell line RS4;11. With a mean 14-day-IC<sub>50</sub> value of ~10  $\mu$ M, representing pinometostat concentrations well above maximum achievable plasma levels in pinometostat-treated patients,<sup>15,16,23</sup> maternal RS4;11 is more resistant than SEM (Figure 1C). Two emerging pinometostat-resistant RS4;11 daughter lines, i.e., RS4;11<sup>PINO\_RES#1</sup> and RS4;11<sup>PINO\_RES#2</sup>, showed IC<sub>50</sub> values of 33 – 45  $\mu$ M (Figure 1C).

To assess the inhibitory effects of pinometostat on DOT1L-mediated methyltransferase activity, the levels of H3K79 di-methylation (H3K79me2) were determined by immunoblot analysis. Interestingly, the levels of H3K79me2 in SEM and SEM<sup>PINO\_RES</sup> were comparable and pinometostat was able to substantially reduce the levels of H3K79me2 equally in both cell lines (Figure 1D-E). Hence, despite persistent inhibition of DOT1L-mediated H3K79 methylation, cell viability in SEM<sup>PINO\_RES</sup> is no longer affected, suggesting that these cells became largely independent of H3K79 methylation induced by DOT1L.

Next, we assessed whether changes in global histone modifications had occurred between SEM and SEM<sup>PINO\_RES</sup>. For this we used Mod Spec<sup>®</sup>, a mass spectrometry-based measurement for the relative abundance of over 80 distinct histone marks. This analysis confirmed no differences in the levels of H3K79 mono-, di-, and tri-methylation (i.e., H3K79me1, H3K79me2, and H3K79me3, respectively) between SEM and SEM<sup>PINO\_RES</sup>, and showed equal reduction of these histone marks upon pinometostat exposure (Supplementary Figure 1). Moreover, these data demonstrated that the global landscape of histone modifications between SEM cells and SEM<sup>PINO\_RES</sup> largely remained similar. The only histone modification





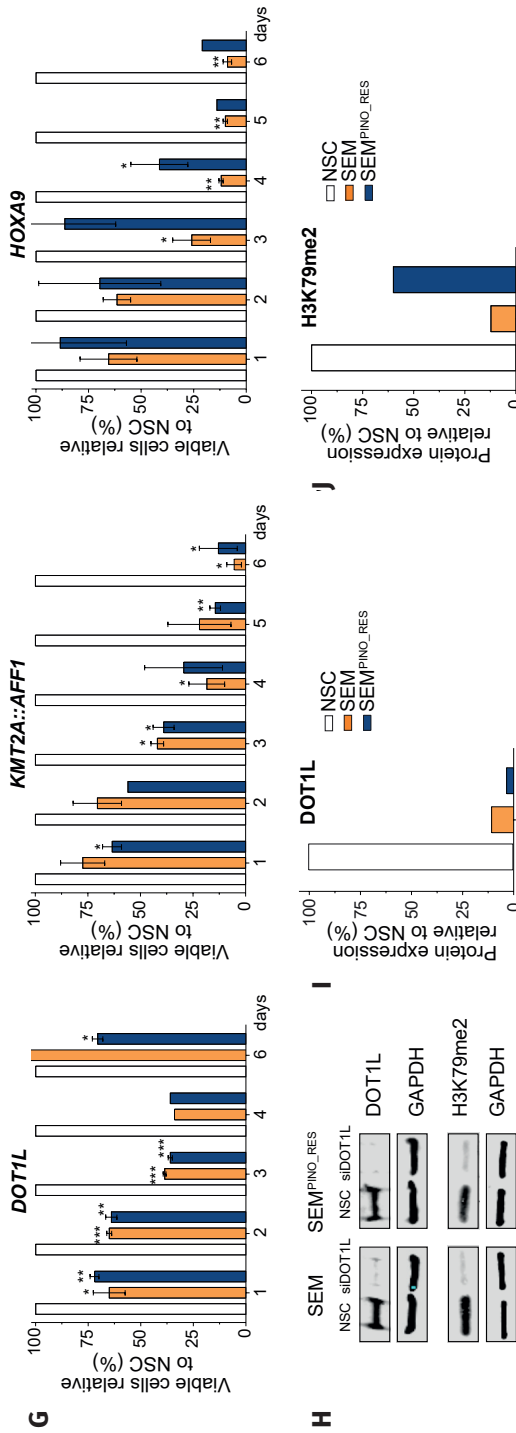


**Figure 1. Establishment of acquired resistance to DOT1L inhibition in KMT2A-rearranged ALL cells**

**A.** Graphic overview of acquired resistance induction to DOT1L inhibition in KMT2A::AFF1+ B-cell ALL (SEM) leading to pinometostat-resistant cells (SEM<sup>PINO\_RES</sup>). **B.** Viable cell percentage of SEM and SEM<sup>PINO\_RES</sup> cells in the absence (-) or presence (+) of 50µM pinometostat for 7 days, normalized to cells cultured without pinometostat. Data present the mean +/- the standard deviation (SD) derived from 2 biological replicates **C.** IC50 values of viable cells of the indicated cell line models determined using six drug concentrations (0-100 µM) for 14 days. The data illustrates the mean +/- SD from 4 biological replicates, each comprising 3 technical replicates. **D.** Immunoblot images of H3K79me2 and total histone H3 in SEM and SEM<sup>PINO\_RES</sup> cells cultured with or without 50 µM pinometostat for 7 days. **E.** Quantification of H3K79me2 protein expression using densitometry analysis normalized against total histone H3 expression. Data represent fold-changes normalized against untreated SEM cells for 2 biological replicates **F.** mRNA expression of DOT1L, KMT2A::AFF1, and HOXA9 determined by qRT-PCR analysis, and **G.** viable cell percentage in SEM and SEM<sup>PINO\_RES</sup> at day 2 and day 4 after siRNA-mediated knockdown (KD) relative to non-silencing controls (NSCs). Data of 2 biological replicates ± SD, \*p<0.05, \*\*p<0.005, \*\*\*p<0.0005, \*\*\*\*p<0.0001. **H.** Immunoblot images of DOT1L, H3K79me2, and GAPDH protein expression in SEM and SEM<sup>PINO\_RES</sup> cells at day 4 following siRNA-mediated KD of DOT1L, and corresponding quantification of **I.** DOT1L or **J.** H3K79me2 protein expression relative to GAPDH using densitometry analysis. Differences were statistically evaluated using unpaired t-tests.

that is downregulated in response to pinometostat exposure appeared to be H3K79 methylation, demonstrating the specificity of this agent.

In *KMT2A*-rearranged acute leukemias, the *KMT2A* fusion protein is considered to be the main oncogenic driver and loss of *DOT1L* was shown to specifically decrease *KMT2A* fusion-driven transcriptional programs, including the expression of *HOXA9*.<sup>7</sup> Therefore, we asked whether acquired resistance to *DOT1L* inhibition was accompanied by an altered dependency on *DOT1L*, *KMT2A::AFF1* and/or *HOXA9*. Therefore SEM and SEM<sup>PINO\_RES</sup> cells were subjected to siRNA-mediated knockdown of these genes, resulting in significant reductions in mRNA expression of ~75-80% for *DOT1L* and *KMT2A::AFF1*, and ~50-65% for *HOXA9*, relative to non-silencing controls (NSCs) (Figure 1F). Validation on the protein level confirmed a reduction of *DOT1L* of ~90% in SEM and of >90% in SEM<sup>PINO\_RES</sup> (Figure 1H,I). Knockdown of *DOT1L* was accompanied by a reduction of H3K79me2 of ~90% in SEM, and of ~40% SEM<sup>PINO\_RES</sup> (Figure 1H, J). Surprisingly, knockdown of *DOT1L* and *KMT2A::AFF1* resulted in similar reductions in cell viability in both SEM and SEM<sup>PINO\_RES</sup>. For *HOXA9* suppression the effects on cell viability in SEM<sup>PINO\_RES</sup> appeared to be somewhat delayed (Figure 1G). This suggests that although SEM<sup>PINO\_RES</sup> cells became less sensitive to inhibition of H3K79 methylation in terms of leukemic cell survival, these cells remained dependent on the physical presence of proteins known to be important in *KMT2A*-mediated leukemogenesis, including *DOT1L*.

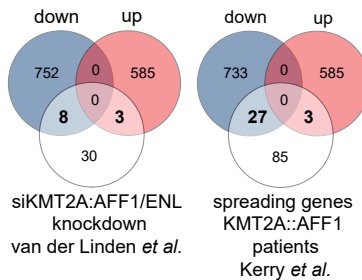
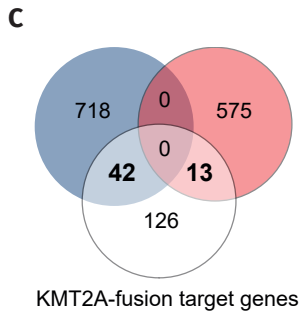
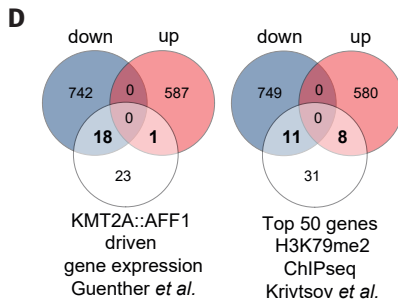
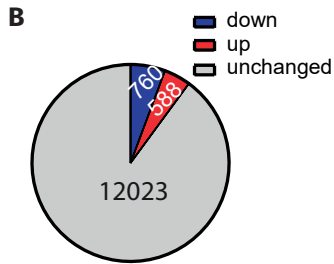
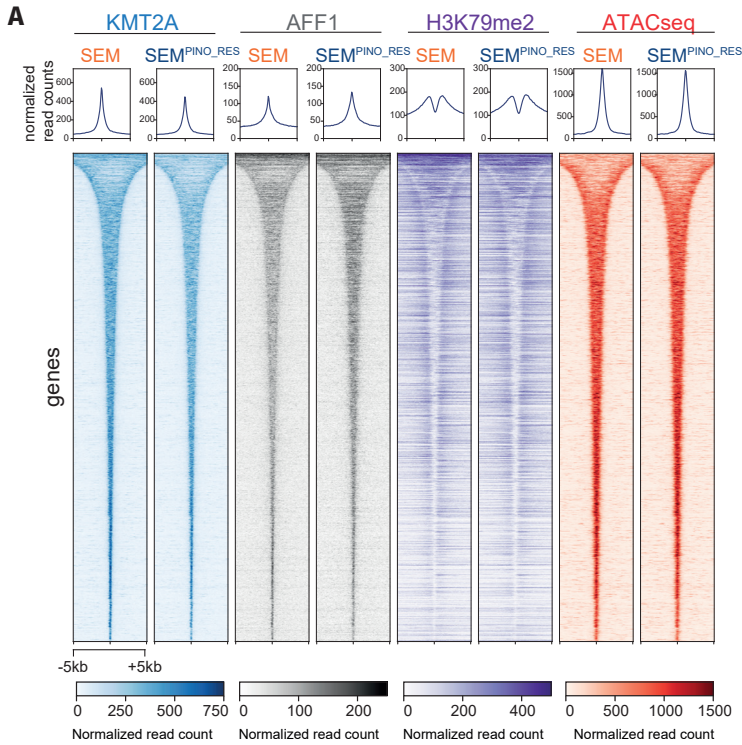
### **Acquired resistance to *DOT1L* inhibition leads to selective loss of *KMT2A*-fusion driven gene expression**

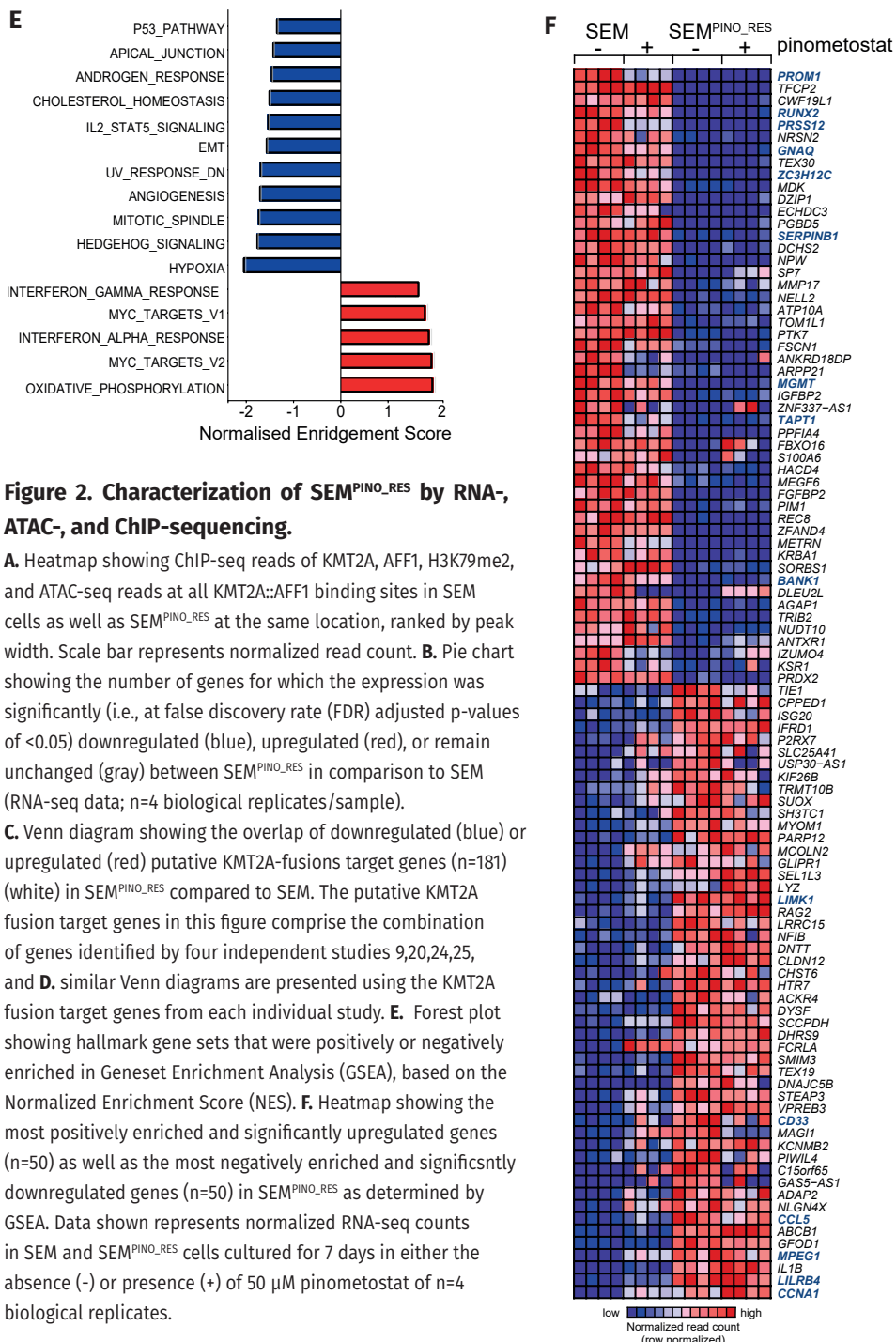
Next, we performed RNA- and ChIP-seq for *KMT2A*, *AFF1*, H3K4me3, H3K79me2, and H3K27ac, as well as ATAC-seq on SEM and SEM<sup>PINO\_RES</sup> cells cultured in both the absence and presence of 50  $\mu$ M pinometostat for 7 days. Interestingly, as assessed by ChIP-seq, there are very few observable differences in the global profiles of *KMT2A*, *AFF1* or H3K79me2 as well as ATACseq profiles between SEM or SEM<sup>PINO\_RES</sup> (Figure 2A) suggesting that acquired pinometostat resistance does not lead to obvious global changes in open chromatin (Figure 2A). Upon analyzing gene expression profiles, it became apparent that in the absence of pinometostat, there was a noteworthy decrease in the expression of 760 out of the 13371 genes expressed (5.7%), while 588 genes (4.4%) exhibited an increase in expression in SEM<sup>PINO\_RES</sup> cells in comparison to SEM cells (Figure 2B, Supplementary Table 1). The differences in gene expression patterns triggered by pinometostat were relatively less prominent between the two cell line models (Figure 2, Supplementary Table 2, Supplementary Table 1). In the presence of pinometostat in the original SEM cells, 670 genes (5.0%) revealed a significant decrease in expression, and 596 genes (4.5%) demonstrated a notable increase in expression, when compared to untreated SEM cells. Conversely, in the presence of pinometostat in SEM<sup>PINO\_RES</sup> cells, 208 genes

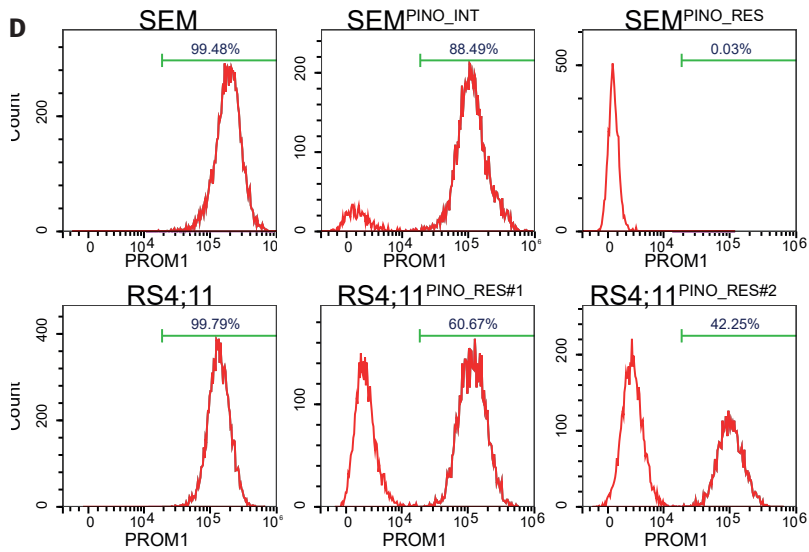
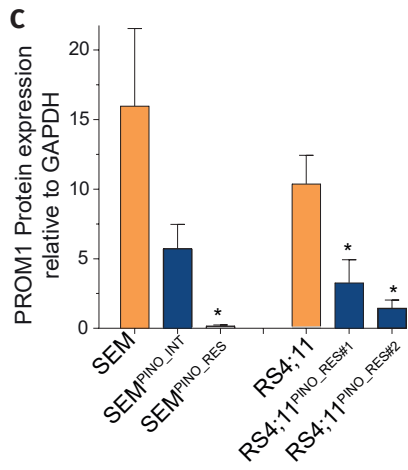
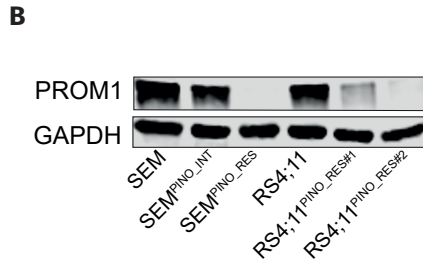
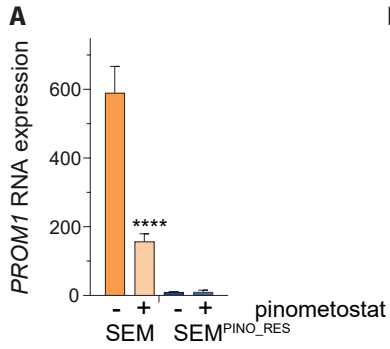
(1.6%) were significantly downregulated, while 388 genes (2.9%) were significantly upregulated compared to untreated SEM<sup>PINO\_RES</sup> cells. Interestingly, a considerable number of genes reported to represent potential target genes of *KMT2A* fusion proteins<sup>9,20,24,25</sup> were significantly downregulated in SEM<sup>PINO\_RES</sup> cells (Figure 2C, Supplementary Table 1). Approximately half of the *KMT2A::AFF1* target genes identified by Guenther *et al.*<sup>24</sup> were downregulated in SEM<sup>PINO\_RES</sup> (Figure 2D, Supplementary Table 1), as well as a quarter of the top 50 genes associated with H3K79 methylation in *KMT2A*-rearranged acute leukemia patient samples as identified by Krivtsov *et al.*<sup>9</sup>

Likewise, ~25% of the genes we previously reported to be differentially expressed in response to siRNA-mediated repression of *KMT2A::AFF1* and *KMT2A::MLL1* in *KMT2A*-rearranged ALL cells,<sup>20</sup> as well as a fourth of the genes reported to display binding of *KMT2A::AFF1* that spreads beyond the gene promoter and well into the gene body as recently identified in SEM cells by Kerry *et al.*,<sup>25</sup> were downregulated in SEM<sup>PINO\_RES</sup> (Figure 2D, Supplementary Table 1). Thus, acquired resistance to DOT1L inhibition leads to selective (or partial) loss of *KMT2A*-fusion driven gene expression. To explore biological pathways potentially affected by acquired resistance to DOT1L inhibition, we performed Gene Set Enrichment Analysis (GSEA) on all RNA-seq data, and identified various hallmark gene sets to be significantly (nominal *p*-value <0.05) modulated in SEM<sup>PINO\_RES</sup>. These included the upregulated gene sets 'MYC targets v1 and v2' and 'Oxidative Phosphorylation', as well as downregulated gene sets such as 'p53 pathway' (i.e., DNA damage response genes), 'epithelial-to-mesenchymal transition (EMT)' and 'hypoxia' (Figure 2E).

Examination of the genes most prominently enriched (n=50) and the genes most notably under-represented (n=50) in our GSEA data revealed *PROM1* to be the most downregulated gene (GSEA score of -4,83) and *CCNA1* the most positively enriched gene (GSEA score of 3,66) in SEM<sup>PINO\_RES</sup> cells (Figure 2F). Both genes represent putative *KMT2A* fusion targets epigenetically marked by H3K79 methylation and have shown to be highly and specifically expressed in *KMT2A*-rearranged ALL<sup>9</sup>. *PROM1* encodes a transmembrane glycoprotein (i.e., CD133) commonly regarded as a cancer stem cell marker<sup>26-28</sup> and reported to be an important target of *KMT2A::AFF1*<sup>24,29,30</sup>. *PROM1* is robustly expressed in SEM cells but readily downregulated during pinometostat exposure, whereas *PROM1* expression was nearly absent in SEM<sup>PINO\_RES</sup> (Figure 3A). Analysis at protein level by immunoblot and FACS confirmed the complete loss of PROM1/CD133 in SEM<sup>PINO\_RES</sup>, while in SEM<sup>PINO\_INT</sup> PROM1/CD133 was still present in in ~88% of the cells (Figure 3B-E). This indicates that PROM1/CD133 expression is gradually lost from the population after prolonged pinometostat exposure. Similarly, RS4;11 cells firmly express PROM1/CD133, which was markedly reduced in both RS4;11<sup>PINO\_RES#1</sup> and RS4;11<sup>PINO\_RES#2</sup> (Figure 3B-E).







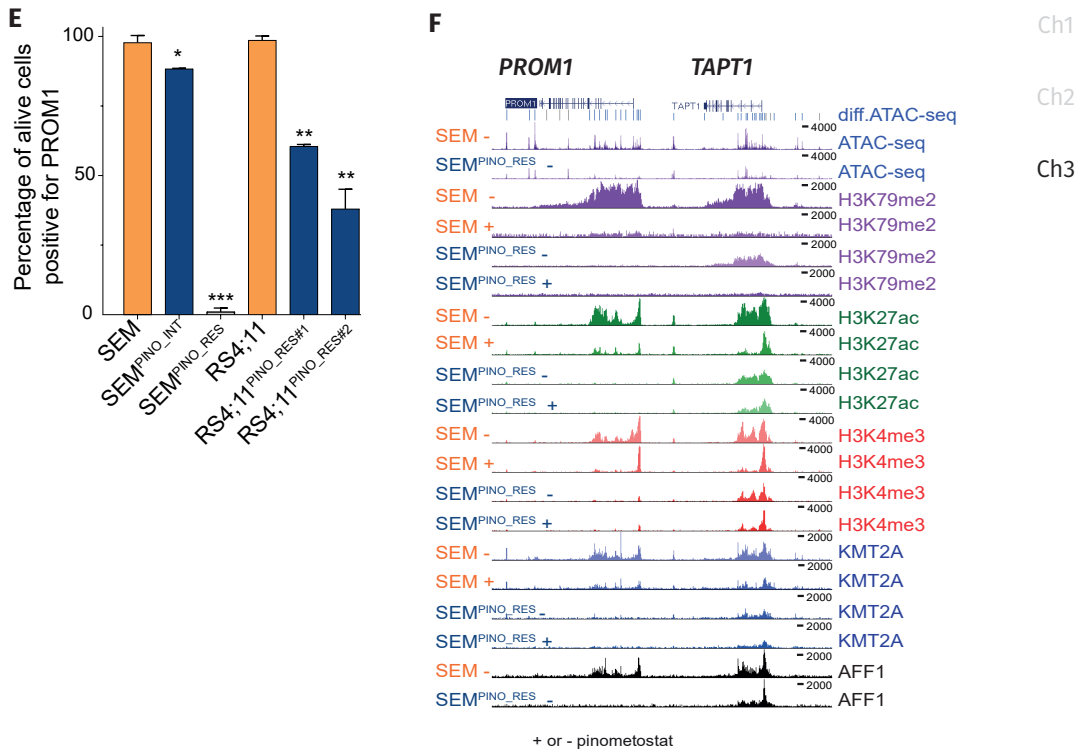


**Figure 3. Acquired resistance to DOT1L inhibition leads to selective loss of *KMT2A*-fusion driven *PROM1* expression.**

**A.** *PROM1* mRNA expression in SEM and SEM<sup>PINO\_RES</sup> cells cultured for 7 days in the absence (-) or presence (+) of 50  $\mu$ M pinometostat, as determined by RNA-seq. Values indicate normalized counts with SD derived from four biological replicates for each cell line and condition. \*\*\*\* $p < 0.0001$ . **B.** Western blot images of *PROM1* and *GAPDH* protein levels in indicated cell line models, and **C.** quantification of *PROM1* expression relative to *GAPDH* by densitometry analysis. Values indicate mean  $\pm$  SD *PROM1* protein expression as determined in two biological replicates. \* $p < 0.05$ . **D.** Histograms showing the counts of viable cells positive for *PROM1*/CD133 of indicated cell line models, as determined by flow cytometry (FACS) analysis, and **E.** Quantification of *PROM1*/CD133 expression presented as the mean  $\pm$  SD as determined by two independent FACS experiments. \* $p < 0.05$ , \*\* $p < 0.005$ . **F.** Differences in chromatin accessibility at the *PROM1* and *TAPT1* gene locus between SEM<sup>PINO\_RES</sup> and SEM cells as determined by ATAC-sequencing of two biological replicates (on top). Vertical blue lines indicate significant decreases of chromatin accessibility in SEM<sup>PINO\_RES</sup> cells, whereas grey lines indicate equal chromatin accessibility in both SEM<sup>PINO\_RES</sup> and SEM. The ATAC-sequencing results are followed by ChIP-sequencing tracks of the same locus showing the distribution of H3K79Me2, H3K27Ac, H3K4Me3, KMT2A in SEM and SEM<sup>PINO\_RES</sup> cells cultured for 7 days in either the absence (-) or presence (+) of 50  $\mu$ M pinometostat.

Differences were statistically evaluated using unpaired t-tests

ChIP-sequencing data for KMT2A, AFF1, H3K4me3, H3K79me2, and H3K27ac showed that upon pinometostat exposure, SEM cells display a clear reduction of KMT2A binding in *PROM1*, which was accompanied by strong reductions of the levels of H3K79me2, H3K4me3, and H3K27ac at the *PROM1* gene as well as at its enhancer *TAPT1*<sup>30</sup> (Figure 3F). In untreated SEM<sup>PINO-RES</sup> cells the *PROM1* locus is completely devoid of KMT2A, AFF1, H3K79me2, H3K4me3, and H3K27ac, suggesting that this gene is no longer being regulated by KMT2A::AFF1 and subsequent DOT1L-mediated H3K79 methylation. Also, ATAC-sequencing clearly revealed decreased chromatin accessibility at the promoter and enhancer of *PROM1* in SEM<sup>PINO-RES</sup> (Figure 3F). Interestingly, at the *TAPT1* locus in these same SEM<sup>PINO-RES</sup> cells KMT2A and AFF1 binding as well as the levels of H3K4me3, H3K79me2, and H3K27ac to some extent remained intact (Figure 3F).

In addition to *PROM1*, the expression of other putative KMT2A::AFF1 target genes, including *RUNX2*, *PRSS12*, *ZC3H12*, *SERPINB1*, *GNAQ* and *BANK1* were severely downregulated in SEM<sup>PINO-RES</sup> with a logFC of >3-fold (Figure 2F and Supplementary Figure 13A) and exhibited similar patterns of RNA-, ChIP-, and ATAC-seq as observed for *PROM1* (Supplementary Figure 3B), indicating their dependence on KMT2A::AFF1-mediated epigenetic control. In contrast, at *SERPINB1* only moderate levels of H3K79me2 were observed, accompanied by rather weak binding of KMT2A and absence of AFF1, suggesting that this gene may not necessarily be regulated KMT2A fusion proteins and DOT1L (Supplementary Figure 3A, B).

Collectively, these data demonstrate that a selection of known KMT2A::AFF1 target genes that are responsive to pinometostat-mediated DOT1L inhibition in SEM cells are relieved from the epigenetic control of KMT2A::AFF1 and become transcriptionally silenced in SEM<sup>PINO-RES</sup> cells.

Following previous evidence on the role of DOT1L in *HOXA* gene expression in KMT2A::AFF1<sup>+</sup> ALL cells,<sup>9,24</sup> we examined the *HOXA* locus and found that *HOXA9* and *HOXA10* were expressed at comparable levels in both SEM and SEM<sup>PINO-RES</sup> (Figure 4A). Inhibition of DOT1L-mediated H3K79 methylation by pinometostat resulted in moderately decreased expression of *HOXA9*, *HOXA7*, and *HOXA10*, while the levels of H3K27ac, H3K4me3, KMT2A, and AFF1 remained unchanged in both cell lines (Figure 4A,B). Similar patterns were found for other KMT2A-fusion target genes, including *CDK6*, involved in cell proliferation in KMT2A rearranged ALL<sup>20</sup> (Figure 4A,B and Supplementary Figure 4A-C). The expression of *MEIS1*, which encodes a required co-factor of HOXA9-driven leukemogenesis,<sup>9,24,31,32</sup> remained unaltered upon pinometostat exposure despite reductions in the levels of H3K79me2 in both SEM and SEM<sup>PINO-RES</sup> (Figure 4A,B and Supplementary Figure 4A,B,C). Collectively, this indicates that a subset of KMT2A-fusion target genes continued to be regulated by DOT1L in pinometostat-resistant ALL cells, while a separate group of genes showed no transcriptional response to the inhibition of DOT1L-mediated H3K79 methylation.



Intriguingly, we also found the expression of some putative *KMT2A*-fusion target genes to be upregulated in *SEM*<sup>PINO\_RES</sup> in the absence of pinometostat (Supplementary Figure 4D), including *HOXA7*, *NLGN4X*, *CCNA1*, *FCRLA*, *IL7R*, *LYN* and *FUT4* (Figure 4A,B and Supplementary Figure 4D,E)

Ch1

Ch2

Ch3

### **Upregulation of myeloid-associated gene expression in *KMT2A*-rearranged ALL cells upon acquired resistance to DOT1L inhibition**

Apart from differential gene expression of putative *KMT2A*::*AFF1* target genes, our data also revealed changes in expression of genes not associated with *KMT2A* fusions and/or H3K79 methylation (Figure 2F). One of the most enriched and upregulated genes upon acquired pinometostat-resistance according to our GSEA is *LILRB4* (Figure 2F and Figure 5A), encoding the monocytic differentiation marker CD85k<sup>33-35</sup>. *LILRB4* is hardly expressed in SEM cells but is moderately upregulated during pinometostat exposure and substantially expressed in *SEM*<sup>PINO\_RES</sup> cells (Figure 5A). In SEM cells, pinometostat induced an increase of chromatin accessibility as well as an increase in the levels of H3K27ac and *KMT2A* binding at the *LILRB4* locus, yet no H3K79me2 or binding of *AFF1* was detected, suggesting that upregulation of *LILRB4* expression is not dependent on DOT1L or *KMT2A*::*AFF1* (Figure 5B).

FACS analysis confirmed an increased population of ~60% in *LILRB4*/CD85k positive cells in *SEM*<sup>PINO\_RES</sup> compared to only ~7% in SEM (Figure 5C,E). Counterintuitively, instead of an expected moderate increase in *LILRB4*/CD85k-positive cells, we found *SEM*<sup>PINO\_INT</sup> to have lost *LILRB4*/CD85k expression almost completely (Figure 5C,E). In RS4;11 already 25% of the cells were positive for *LILRB4*/CD85k, which tremendously increased to approximately 90% of the cells in both RS4;11<sup>PINO\_RES</sup> daughter lines (Figure 5C,E). Interestingly, apart from *LILRB4*/CD85k, we found additional myeloid-associated genes to be upregulated in *SEM*<sup>PINO\_RES</sup>, including *CD33*, *CCL5*, *LIMK1*, and *MPEG1*, revealing similar patterns of RNA-, ChIP- and ATAC-seq as *LILRB4*, although less prominent (Figure 2F, Supplementary Figure 5A,S5B). *CD33*, commonly expressed in a subpopulation in *KMT2A*-rearranged infant ALL<sup>36-38</sup>, serves as an important immunophenotypic marker for the characterization of pediatric acute myeloid leukemia (AML) by EuroFlow<sup>39-42</sup> and has been exploited as a therapeutic target for AML. In SEM a subpopulation of 20% of CD33-positive cells was identified, which was increased in *SEM*<sup>PINO\_RES</sup> to about 40%, yet CD33-positive cells again were largely absent in *SEM*<sup>PINO\_INT</sup> (Figure 5D,F). Similarly, in RS4;11 a CD33-positive subpopulation of 9% was increased upon pinometostat resistance to 14% in RS4;11<sup>PINO\_RES#1</sup> and up to 50% in RS4;11<sup>PINO\_RES#2</sup> (Figure 5D,F).

Together these data indicate that under prolonged pressure of DOT1L inhibition, *KMT2A*-rearranged ALL cells seem to initiate a reprogramming process that involves the acquisition (or selection) of myeloid-like characteristics.

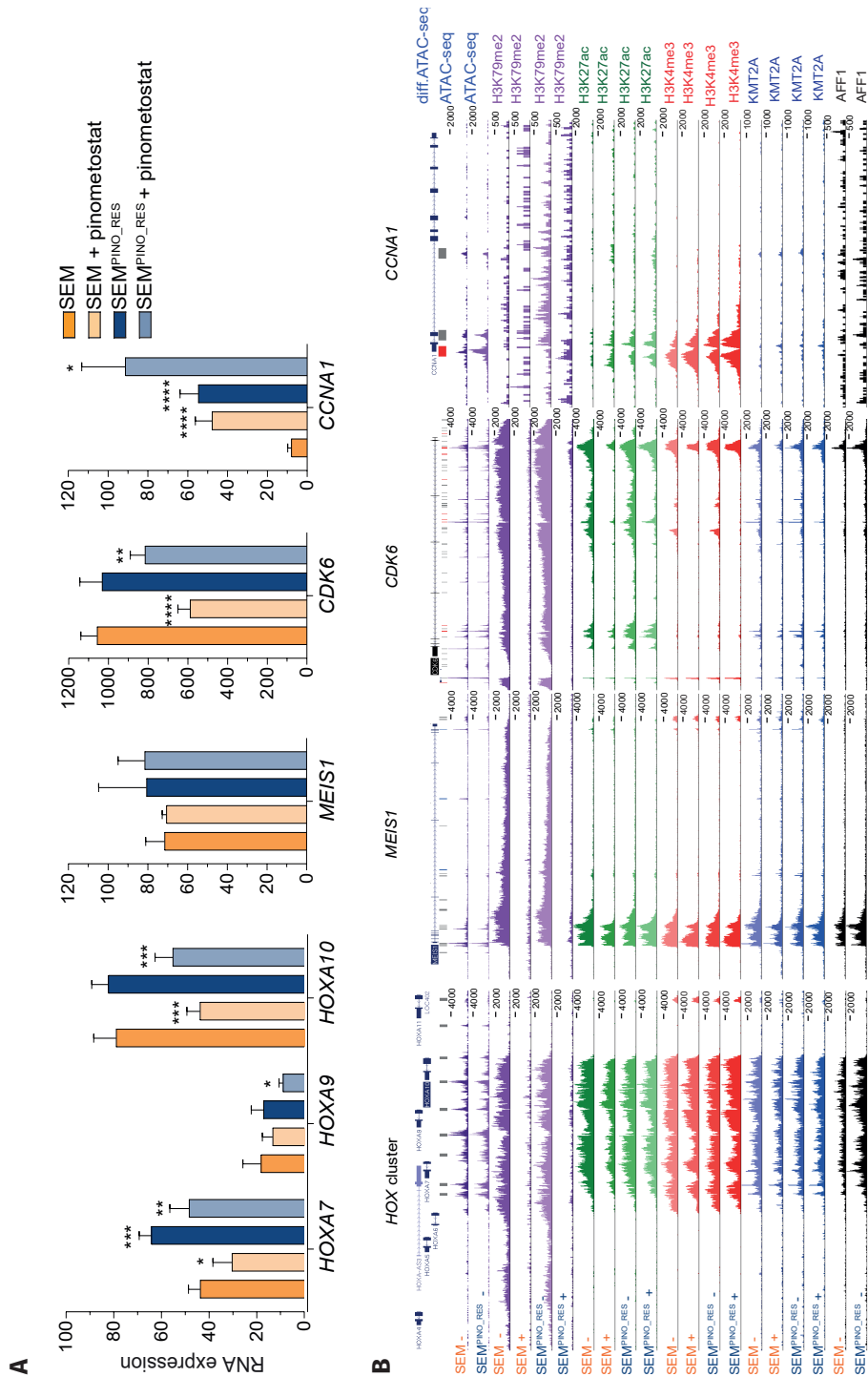


**Figure 4.**

**Figure 4. Unaltered or upregulated gene expression of *KMT2A*-fusion targets after acquired resistance to DOT1L inhibition.**

**A.** *HOXA7*, *HOXA9*, *HOXA10*, *MEIS1*, *CKD6*, and *CCNA1* mRNA expression SEM and SEM<sup>PINO\_RES</sup> cells cultured for 7 days in the absence (-) or presence (+) of 50  $\mu$ M pinometostat, as determined by RNA-seq. Values indicate normalized counts with standard deviation (SD) derived from four biological replicates for each cell line and condition. Differences in expression were statistically evaluated using unpaired t-tests; \*  $p < 0.05$ , \*\*  $p < 0.005$ , \*\*\*  $p < 0.0005$ , \*\*\*\*  $p < 0.0001$ . Differences in chromatin accessibility at the *HOXA*, *MEIS1*, *CKD6*, and *CCNA1* gene loci between SEM<sup>PINO\_RES</sup> and SEM cells as determined by ATAC-sequencing by two biological replicates (on top). Vertical blue lines indicate significant decreases of chromatin accessibility in SEM<sup>PINO\_RES</sup> cells, whereas grey lines indicate equal chromatin accessibility in both SEM<sup>PINO\_RES</sup> and SEM. Red lines indicate significant increases in chromatin accessibility in SEM<sup>PINO\_RES</sup>. Below the ATAC-sequencing data, ChIPseq tracks showing the presence of H3K79Me2, H3K27Ac, H3K4Me3, *KMT2A*, and *AFF1* at the corresponding gene loci in SEM and SEM<sup>PINO\_RES</sup> cells cultured for 7 days in the absence (-) or presence (+) of 50  $\mu$ M pinometostat.

Ch1

Ch2

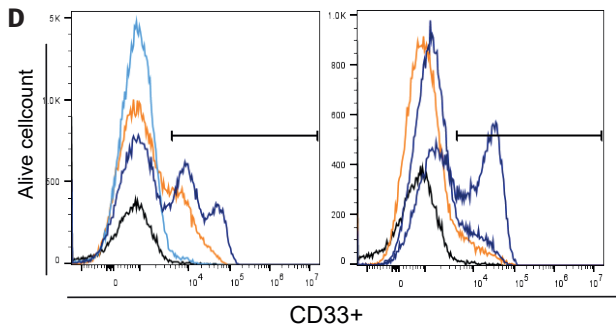
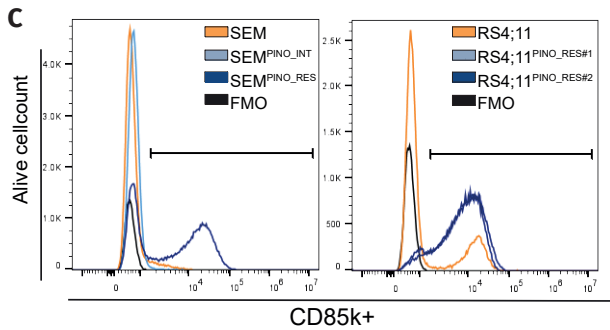
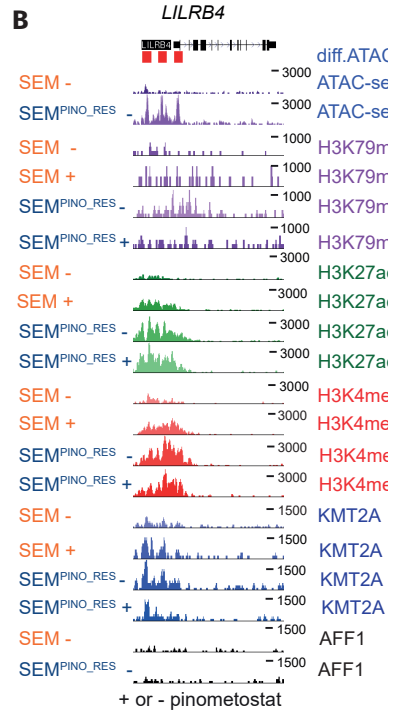
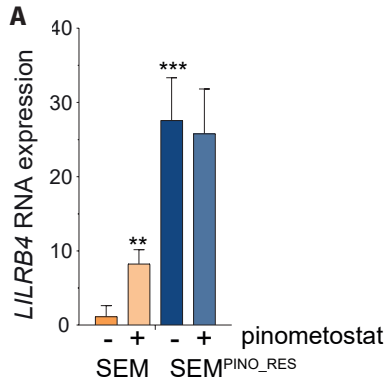
Ch3

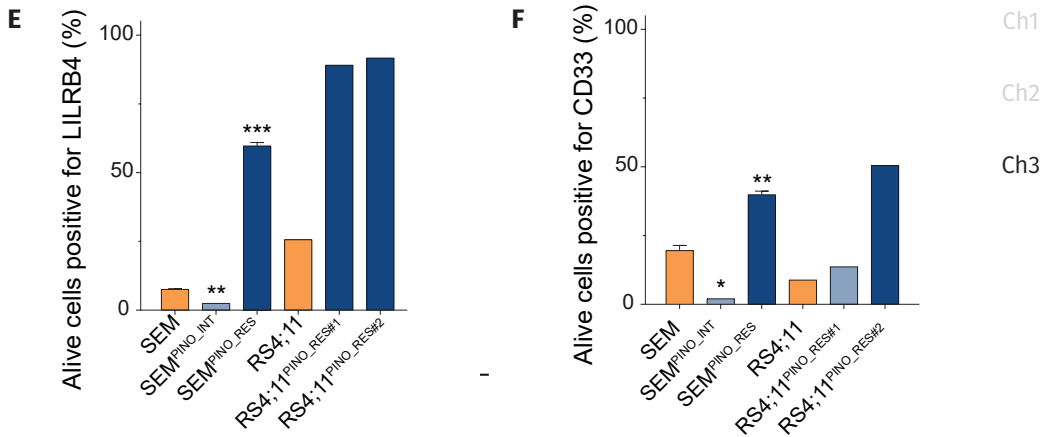
**Drug screens reveal minimal cross resistance, and sensitization towards venetoclax after acquired pinometostat resistance**

Finally, acquired pinometostat resistance led to the upregulation of the multidrug efflux pump ABCB1 (Figure 2F and Supplementary Figure 6A,B), associated with multidrug resistance and previously reported as the mechanism of pinometostat resistance in *KMT2A*-rearranged acute leukemia cell lines<sup>17</sup>. However, our data challenges the concept that elevated ABCB1 expression alone is the mechanism of resistance to DOT1L inhibition as reported previously.<sup>17</sup> Despite significant ABCB1 upregulation, we still observe comparable inhibition of H3K79 methylation in SEM and SEM<sup>PINO\_RES</sup> (Figure 1D and 1E), indicating that the amount of pinometostat and/or its retention in SEM<sup>PINO\_RES</sup> cells is sufficient to effectively reduce H3K79me2 levels, overriding the impact of ABCB1 upregulation.

Since multidrug efflux pumps are associated with multidrug resistance<sup>43,44</sup>, we assessed whether SEM<sup>PINO\_RES</sup> cells had become more resistant to current chemotherapeutics for *KMT2A*-rearranged infant ALL<sup>12</sup> and whether we could identify agents to which SEM<sup>PINO\_RES</sup> cells had become more sensitive by performing drug library screens (Supplementary Figure 2, Figure 6A,B).

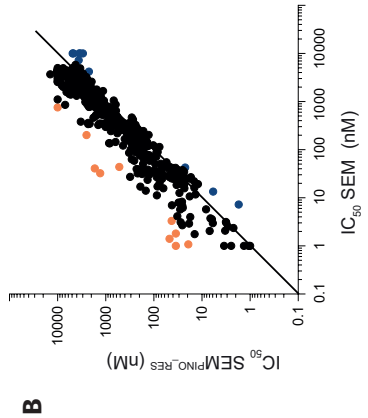
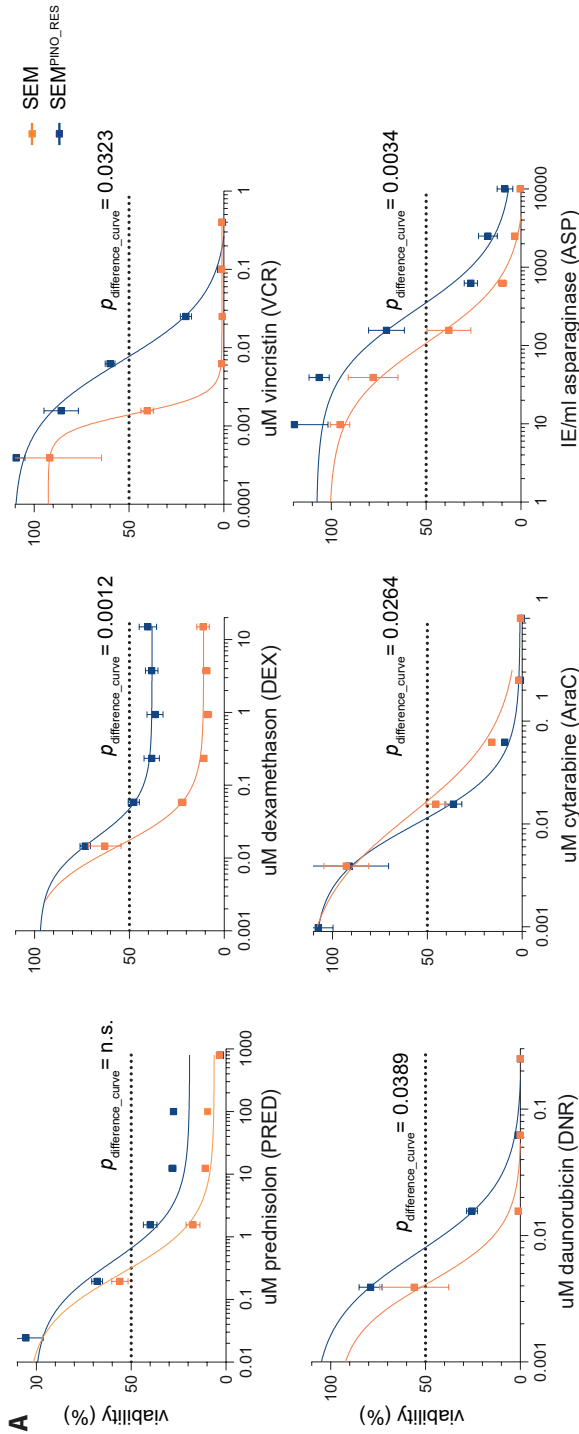
This revealed an increased resistance to the glucocorticoids dexamethasone and prednisolone (the liver-activated form of prednisone), vincristine, daunorubicin, and L-asparaginase, and increased sensitivity to cytarabine and for instance to the BCL-2 inhibitor venetoclax (Figure 6A-E). Interestingly, cytarabine typically represents a drug commonly used in the treatment of myeloid leukemias, and the combination of venetoclax and cytarabine<sup>45-47</sup> has successfully been tested in AML patients<sup>45-47</sup>.





**Figure 5. Upregulation of myeloid-associated CD85k/LILRB4 and CD33 expression during the acquirement of resistance to DOT1L inhibition.**

**A** *LILRB4* mRNA expression in SEM and SEM<sup>PINO\_RES</sup> cells cultured for 7 days in the absence (-) or presence (+) of 50  $\mu$ M pinometostat, as determined by RNA-seq. Values indicate normalized counts with SD derived from four biological replicates for each cell line and condition. Differences in expression were statistically evaluated using unpaired t-tests; \*\* $p < 0.005$ , \*\*\* $p < 0.0005$ . **B.** Differences in chromatin accessibility at the *LILRB4* gene locus between SEM<sup>PINO\_RES</sup> and SEM cells as determined by ATAC-sequencing by 2 biological replicates (on top). Red boxes indicate locations within the *LILRB4* gene locus of significantly increased chromatin accessibility in SEM<sup>PINO\_RES</sup> as compared to SEM cells. In addition, ChIPseq tracks are presented showing the presence of H3K79Me2, H3K27Ac, H3K4Me3, KMT2A, and AFF1 at the same locus in and indicated cell line models cultured for 7 days in the absence (-) or presence (+) of 50  $\mu$ M pinometostat. **C.** Histograms showing the counts of viable cells positive for CD85k/LILRB4 and **D.** CD33 protein surface expression of indicated cell line models, as determined by flow cytometry (FACS) analysis. Fluorescence Minus One (FMO) controls were used to determine the cut-off point for the positive cell population. **E.** Quantification of CD85k/LILRB4 and **F.** CD33 expression represented as the mean  $\pm$  SD, determined through either one (RS4;11 cells) or two (SEM cells) independent FACS experiments, each involving biological replicates. Differences in expression were statistically evaluated using unpaired t-tests; \* $p < 0.05$ , \*\* $p < 0.005$ , \*\*\* $p < 0.0005$ .



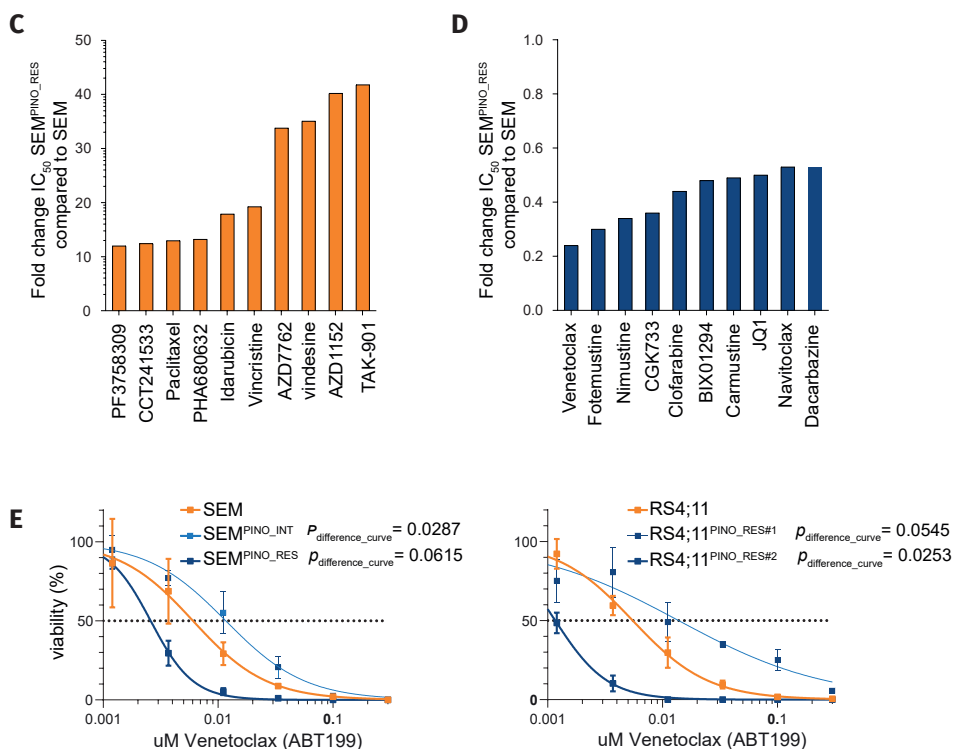


**Figure 6. Moderate levels of cross-resistance and substantial sensitization towards venetoclax in pinometostat-resistant *KMT2A*-rearranged ALL cells.**

**A.** Drug response curves for prednisolone, dexamethasone, vincristine, daunorubicin, cladribine, cytarabine, and L-asparaginase as determined by 4-day MTT assays in SEM and SEM<sup>PINO-RES</sup> cells with n=4 biological replicates, each comprising n=3 technical replicates, and presented as the mean  $\pm$  standard error of the mean (SEM). **B.** Comparison of the  $IC_{50}$  in SEM and SEM<sup>PINO-RES</sup> cells for a total of 679 compounds tested in drug library screens. **C.** Showing the top 10 agents with the highest fold-changes in  $IC_{50}$  values in SEM<sup>PINO-RES</sup> as compared to SEM, indicating enhanced resistance in SEM<sup>PINO-RES</sup> cells. **D.** The top 10 drugs with the lowest fold-changes in  $IC_{50}$  values in SEM<sup>PINO-RES</sup> as compared to SEM, indicating enhanced sensitivity in SEM<sup>PINO-RES</sup> cells. **E.** Drug response curves for venetoclax as determined by 4-day MTT assays in indicated cell lines models (in duplicate), presented as the mean  $\pm$  standard error of the mean (SEM).

## DISCUSSION

The currently accepted dogma of *KMT2A*-fusion driven leukemogenesis dictates the requirement of DOT1L-mediated activation of *KMT2A* target genes through H3K79 methylation.<sup>6,9,48,49</sup> Therefore, targeting DOT1L<sup>13,18,19</sup> represents an attractive therapeutic option for patients diagnosed with *KMT2A*-rearranged acute leukemia, despite the first-in-class DOT1L inhibitor pinometostat showing dissatisfying results in adult patients<sup>15</sup>. While next generation DOT1L inhibitors with improved pharmacokinetic profiles are in development,<sup>18,19</sup> we reasoned that the mechanisms by which *KMT2A*-rearranged acute leukemia cells evade DOT1L inhibition may provide novel insights into the biology of these unique malignancies. Therefore, and in a similar fashion as published by Campbell and colleagues<sup>17</sup>, we efficiently induced acquired pinometostat resistance in various cell line models, demonstrating how readily *KMT2A*-rearranged acute leukemia cells become resistant to DOT1L inhibition. The study of Campbell *et al.*, mainly focused on examples of possible mechanisms of pinometostat resistance including increased expression of drug efflux transporters and activation of the PI3K/AKT and RAS/RAF/MEK/ERK pathways<sup>17</sup>. In contrast, we here specifically focused on the behavior and epigenetic regulation of DOT1L-associated *KMT2A* fusion-driven target genes and on how the transcriptomic landscape changes in *KMT2A*-rearranged ALL cells that are able to evade leukemic cell death during prolonged inhibition of DOT1L-mediated H3K79 methylation.

In concordance with the previous finding by Campbell *et al.*, we found increased expression of the multi-drug efflux pump *ABCB1* in our pinometostat-resistant SEM<sup>PINO\_RES</sup> cells. However, despite the elevated levels of *ABCB1* expression, pinometostat continued to inhibit H3K79 methylation in SEM<sup>PINO\_RES</sup>. This strongly indicates that the increased levels of *ABCB1* are insufficient to prevent pinometostat from exerting its inhibitory effects, and therefore cannot be the sole mechanism of acquired pinometostat resistance.

Interestingly, while cell viability of SEM<sup>PINO\_RES</sup> cells was no longer affected by pinometostat-induced inhibition of DOT1L-mediated H3K79 methylation, these cells remained dependent on the physical presence of DOT1L protein. This may indicate that recently described biological functions of DOT1L that are independent of H3K79 methylation<sup>50-52</sup> are also important for *KMT2A*-rearranged acute leukemia cells. Thus, in addition to its enzymatic methyltransferase activity, DOT1L clearly has a scaffold function in assembling transcriptionally competent complexes. Therefore, therapeutic degradation of DOT1L instead of solely inhibiting its catalytic activities might be beneficial in the treatment of *KMT2A*-rearranged acute leukemia.

Another intriguing aspect of our model of acquired pinometostat resistance is the observation that SEM<sup>PINO\_RES</sup> cells remained vulnerable to knockdown of the *KMT2A::AFF1*



fusion gene. This may suggest that inappropriate recruitment of DOT1L to loci otherwise not associated with H3K79me2 may not represent the sole *KMT2A* fusion-mediated attribute driving leukemogenesis and/or leukemia maintenance. If so, the identification of such DOT1L-independent oncogenic properties may well uncover important therapeutic targets and more effective treatment options for *KMT2A*-rearranged acute leukemias.

Ch1

Ch2

Ch3

As shown, acquired resistance to pinometostat led to marked transcriptional downregulation of putative *KMT2A*-fusion target genes, which was accompanied by reductions in H3K79me2, as well as loss of binding of *KMT2A* and *AFF1*, and chromatin condensation at the corresponding loci. The complete loss of *PROM1/CD133*, which was shown to be transcriptionally regulated via *KMT2A::AFF1*-mediated H3K79me2/3 enhancer-promoter interactions,<sup>30</sup> in SEM<sup>PINO\_RES</sup> is highly remarkable, since the expression of *PROM1/CD133* was reported to be essential for leukemic cell growth in *KMT2A*-rearranged ALL.<sup>29,30</sup> Consequently, targeting *PROM1/CD133*-positive cells has been proposed as a therapeutic option for *KMT2A*-rearranged ALL, although the expression of *PROM1/CD133* on both fetal and adult hematopoietic stem cells (HSCs) may compromise the specificity of such an approach<sup>29,30,53,54</sup>. Moreover, *PROM1/CD133* is expressed in most, but not all, *KMT2A*-rearranged acute leukemia patients, and its presence seems to reflect the immunophenotype and/or cell of origin of the leukemia, as HSCs and early progenitors typically express *PROM1/CD133*, while more differentiated B-cell progenitors do not.<sup>30,54,55</sup> As acquiring resistance to DOT1L inhibition was accompanied by a complete loss of *PROM1/CD133* expression, this may suggest that prolonged exposure to pinometostat triggered the differentiation towards (or selection of) a more mature immunophenotype. On the other hand, our data revealed that prolonged exposure of *KMT2A*-rearranged ALL cells to pinometostat seems to initiate a reprogramming process that involves the acquirement (or selection) of myeloid-like characteristics. Co-expression of myeloid CD markers, including *CD33*,<sup>36</sup> represents a familiar phenomenon in *KMT2A*-rearranged infant ALL with prognostic relevance.<sup>37,38</sup> Moreover, a recent single-cell multiomics study by Chen and co-workers revealed the presence of pre-existing lymphomyeloid primed progenitors and myeloid blasts in diagnostic samples derived from *KMT2A*-rearranged B-ALL patients<sup>56</sup>. From this perspective, prolonged inhibition of DOT1L seems to favor *KMT2A*-rearranged leukemia cells that completely lack *PROM1/CD133* but do display *LILRB4/CD85k* and *CD33* expression. Interestingly, both *LILRB4/CD85k* and *CD33* are therapeutic targets in AML<sup>57-63</sup> and have shown potential as therapeutic vulnerabilities in *KMT2A*-rearranged ALL. Targeting *LILRB4/CD85k* with antibody-conjugates<sup>57</sup> or anti-*LILRB4* CAR-T cell,<sup>54,65</sup> and/or *CD33* with gemtuzumab ozogamicin, could prevent resistance to DOT1L inhibitors in *KMT2A*-rearranged ALL. Moreover, combining BCL-2 inhibition by venetoclax with agents targeting DOT1L, *LILRB4/CD85k*, and/or *CD33* may enhance the efficacy of these drug combinations. Venetoclax was found to synergize with DOT1L inhibitors<sup>25,66</sup> and is being

evaluated in clinical trials for pediatric *KMT2A*-rearranged leukemias.<sup>67,68</sup>

Taken together, we present an *in vitro* model of acquired resistance to DOT1L inhibition in *KMT2A*-rearranged ALL, revealing selective loss of epigenetic regulation and gene expression of *KMT2A*-fusion target genes, accompanied by upregulation of myeloid-like characteristics. This study may not only impact the development of novel DOT1L inhibitors, but also reveal key characteristics of *KMT2A*-rearranged ALL cells that are able to evade therapy, providing therapeutic targets to prevent that.

## REFERENCES

1. Pieters R, De Lorenzo P, Ancliffe P, et al. Outcome of Infants Younger Than 1 Year With Acute Lymphoblastic Leukemia Treated With the Interfant-06 Protocol: Results From an International Phase III Randomized Study. *J Clin Oncol*. 2019;37(25):2246-2256.
2. Pieters R, Schrappe M, De Lorenzo P, et al. A treatment protocol for infants younger than 1 year with acute lymphoblastic leukaemia (Interfant-99): an observational study and a multicentre randomised trial. *Lancet*. 2007;370(9583):240-250.
3. Meyer C, Burmeister T, Groger D, et al. The MLL recombinome of acute leukemias in 2017. *Leukemia*. 2018;32(2):273-284.
4. Ernst P, Wang J, Korsmeyer SJ. The role of MLL in hematopoiesis and leukemia. *Curr Opin Hematol*. 2002;9(4):282-287.
5. Krivtsov AV, Armstrong SA. MLL translocations, histone modifications and leukaemia stem-cell development. *Nat Rev Cancer*. 2007;7(11):823-833.
6. Bernt KM, Armstrong SA. A role for DOT1L in MLL-rearranged leukemias. *Epigenomics*. 2011;3(6):667-670.
7. Bernt KM, Zhu N, Sinha AU, et al. MLL-rearranged leukemia is dependent on aberrant H3K79 methylation by DOT1L. *Cancer Cell*. 2011;20(1):66-78.
8. Okada Y, Feng Q, Lin Y, et al. hDOT1L links histone methylation to leukemogenesis. *Cell*. 2005;121(2):167-178.
9. Krivtsov AV, Feng Z, Lemieux ME, et al. H3K79 methylation profiles define murine and human MLL-AF4 leukemias. *Cancer Cell*. 2008;14(5):355-368.
10. Agraz-Doblas A, Bueno C, Bashford-Rogers R, et al. Unraveling the cellular origin and clinical prognostic markers of infant B-cell acute lymphoblastic leukemia using genome-wide analysis. *Haematologica*. 2019;104(6):1176-1188.
11. Andersson AK, Ma J, Wang J, et al. The landscape of somatic mutations in infant MLL-rearranged acute lymphoblastic leukemias. *Nat Genet*. 2015;47(4):330-337.
12. Sanjuan-Pla A, Bueno C, Prieto C, et al. Revisiting the biology of infant t(4;11)/MLL-AF4+ B-cell acute lymphoblastic leukemia. *Blood*. 2015;126(25):2676-2685.
13. Daigle SR, Olhava EJ, Therkelsen CA, et al. Selective killing of mixed lineage leukemia cells by a potent small-molecule DOT1L inhibitor. *Cancer Cell*. 2011;20(1):53-65.
14. Daigle SR, Olhava EJ, Therkelsen CA, et al. Potent inhibition of DOT1L as treatment of MLL-fusion leukemia. *Blood*. 2013;122(6):1017-1025.
15. Stein EM, Garcia-Manero G, Rizzieri DA, et al. The DOT1L inhibitor pinometostat reduces H3K79 methylation and has modest clinical activity in adult acute leukemia. *Blood*. 2018;131(24):2661-2669.
16. Stein EM, Tallman MS. Mixed lineage rearranged leukaemia: pathogenesis and targeting DOT1L. *Curr Opin Hematol*. 2015;22(2):92-96.
17. Campbell CT, Haladyna JN, Drubin DA, et al. Mechanisms of Pinometostat (EPZ-5676) Treatment-Emergent Resistance in MLL-Rearranged Leukemia. *Mol Cancer Ther*. 2017;16(8):1669-1679.
18. Perner F, Gadrey JY, Xiong Y, et al. Novel inhibitors of the histone methyltransferase DOT1L show potent antileukemic activity in patient-derived xenografts. *Blood*. 2020;136(17):1983-1988.
19. Chen C, Zhu H, Stauffer F, et al. Discovery of Novel Dot1L Inhibitors through a Structure-Based Fragmentation Approach. *ACS Med Chem Lett*. 2016;7(8):735-740.

Ch1

Ch2

Ch3

20. van der Linden MH, Willekes M, van Roon E, et al. MLL fusion-driven activation of CDK6 potentiates proliferation in MLL-rearranged infant ALL. *Cell Cycle*. 2014;13(5):834-844.
21. Spijkers-Hagelstein JA, Pinhancos SS, Schneider P, Pieters R, Stam RW. Chemical genomic screening identifies LY294002 as a modulator of glucocorticoid resistance in MLL-rearranged infant ALL. *Leukemia*. 2014;28(4):761-769.
22. Greil J, Gramatzki M, Burger R, et al. The acute lymphoblastic leukaemia cell line SEM with t(4;11) chromosomal rearrangement is biphenotypic and responsive to interleukin-7. *Br J Haematol*. 1994;86(2):275-283.
23. Waters NJ. Preclinical Pharmacokinetics and Pharmacodynamics of Pinometostat (EPZ-5676), a First-in-Class, Small Molecule S-Adenosyl Methionine Competitive Inhibitor of DOT1L. *Eur J Drug Metab Pharmacokinet*. 2017;42(6):891-901.
24. Guenther MG, Lawton LN, Rozovskaia T, et al. Aberrant chromatin at genes encoding stem cell regulators in human mixed-lineage leukemia. *Genes Dev*. 2008;22(24):3403-3408.
25. Kerry J, Godfrey L, Repapi E, et al. MLL-AF4 Spreading Identifies Binding Sites that Are Distinct from Super-Enhancers and that Govern Sensitivity to DOT1L Inhibition in Leukemia. *Cell Rep*. 2017;18(2):482-495.
26. Barzegar Behrooz A, Syahir A, Ahmad S. CD133: beyond a cancer stem cell biomarker. *J Drug Target*. 2019;27(3):257-269.
27. Wu Y, Wu PY. CD133 as a marker for cancer stem cells: progresses and concerns. *Stem Cells Dev*. 2009;18(8):1127-1134.
28. Zhang Q, Shi S, Yen Y, Brown J, Ta JQ, Le AD. A subpopulation of CD133(+) cancer stem-like cells characterized in human oral squamous cell carcinoma confer resistance to chemotherapy. *Cancer Lett*. 2010;289(2):151-160.
29. Mak AB, Nixon AM, Moffat J. The mixed lineage leukemia (MLL) fusion-associated gene AF4 promotes CD133 transcription. *Cancer Res*. 2012;72(8):1929-1934.
30. Godfrey L, Crump NT, O'Byrne S, et al. H3K79me2/3 controls enhancer-promoter interactions and activation of the pan-cancer stem cell marker PROM1/CD133 in MLL-AF4 leukemia cells. *Leukemia*. 2021;35(1):90-106.
31. Adamaki M, Lambrou GI, Athanasiadou A, Vlahopoulos S, Papavassiliou AG, Moschovi M. HOXA9 and MEIS1 gene overexpression in the diagnosis of childhood acute leukemias: Significant correlation with relapse and overall survival. *Leuk Res*. 2015;39(8):874-882.
32. Hu YL, Fong S, Ferrell C, Largman C, Shen WF. HOXA9 modulates its oncogenic partner Meis1 to influence normal hematopoiesis. *Mol Cell Biol*. 2009;29(18):5181-5192.
33. Dobrowolska H, Gill KZ, Serban G, et al. Expression of immune inhibitory receptor ILT3 in acute myeloid leukemia with monocytic differentiation. *Cytometry B Clin Cytom*. 2013;84(1):21-29.
34. Costa AFO, Menezes DL, Pinheiro LHS, et al. Role of new Immunophenotypic Markers on Prognostic and Overall Survival of Acute Myeloid Leukemia: a Systematic Review and Meta-Analysis. *Sci Rep*. 2017;7(1):4138.
35. Churchill HRO, Fuda FS, Xu J, et al. Leukocyte immunoglobulin-like receptor B1 and B4 (LILRB1 and LILRB4): Highly sensitive and specific markers of acute myeloid leukemia with monocytic differentiation. *Cytometry B Clin Cytom*. 2021;100(4):476-487.
36. Hara J, Hosoi G, Okamura T, et al. CD33+ B-cell precursor acute lymphoblastic leukemia in children: a distinct subgroup of B-cell precursor acute lymphoblastic leukemia. *Int J Hematol*. 1995;61(2):77-84.

37. Stutterheim J, de Lorenzo P, van der Sluis IM, et al. Minimal residual disease and outcome characteristics in infant KMT2A-germline acute lymphoblastic leukaemia treated on the Interfant-06 protocol. *Eur J Cancer*. 2022;160:72-79. Ch1
38. Stutterheim J, van der Sluis IM, de Lorenzo P, et al. Clinical Implications of Minimal Residual Disease Detection in Infants With KMT2A-Rearranged Acute Lymphoblastic Leukemia Treated on the Interfant-06 Protocol. *J Clin Oncol*. 2021;39(6):652-662. Ch2
39. Laszlo GS, Estey EH, Walter RB. The past and future of CD33 as therapeutic target in acute myeloid leukemia. *Blood Rev*. 2014;28(4):143-153. Ch3
40. van Dongen JJ, Orfao A, EuroFlow C. EuroFlow: Resetting leukemia and lymphoma immunophenotyping. Basis for companion diagnostics and personalized medicine. *Leukemia*. 2012;26(9):1899-1907.
41. van Dongen JJ, Lhermitte L, Bottcher S, et al. EuroFlow antibody panels for standardized n-dimensional flow cytometric immunophenotyping of normal, reactive and malignant leukocytes. *Leukemia*. 2012;26(9):1908-1975.
42. Kalina T, Flores-Montero J, van der Velden VH, et al. EuroFlow standardization of flow cytometer instrument settings and immunophenotyping protocols. *Leukemia*. 2012;26(9):1986-2010.
43. Baguley BC. Multiple drug resistance mechanisms in cancer. *Mol Biotechnol*. 2010;46(3):308-316.
44. Szakacs G, Paterson JK, Ludwig JA, Booth-Genthe C, Gottesman MM. Targeting multidrug resistance in cancer. *Nat Rev Drug Discov*. 2006;5(3):219-234.
45. Dillon R, Maycock S, Jackson A, et al. Venetoclax combined with low dose cytarabine compared to standard of care intensive chemotherapy for the treatment of favourable risk adult acute myeloid leukaemia (VICTOR): Study protocol for an international, open-label, multicentre, molecularly-guided randomised, phase II trial. *BMC Cancer*. 2022;22(1):1174.
46. Kadia TM, Reville PK, Wang X, et al. Phase II Study of Venetoclax Added to Cladribine Plus Low-Dose Cytarabine Alternating With 5-Azacididine in Older Patients With Newly Diagnosed Acute Myeloid Leukemia. *J Clin Oncol*. 2022;40(33):3848-3857.
47. Wei AH, Strickland SA, Jr., Hou JZ, et al. Venetoclax Combined With Low-Dose Cytarabine for Previously Untreated Patients With Acute Myeloid Leukemia: Results From a Phase Ib/II Study. *J Clin Oncol*. 2019;37(15):1277-1284.
48. Nguyen AT, He J, Taranova O, Zhang Y. Essential role of DOT1L in maintaining normal adult hematopoiesis. *Cell Res*. 2011;21(9):1370-1373.
49. Kuntimaddi A, Achille NJ, Thorpe J, et al. Degree of recruitment of DOT1L to MLL-AF9 defines level of H3K79 Di- and tri-methylation on target genes and transformation potential. *Cell Rep*. 2015;11(5):808-820.
50. Cao K, Ugarenko M, Ozark PA, et al. DOT1L-controlled cell-fate determination and transcription elongation are independent of H3K79 methylation. *Proc Natl Acad Sci U S A*. 2020;117(44):27365-27373.
51. Wu A, Zhi J, Tian T, et al. DOT1L complex regulates transcriptional initiation in human erythroleukemic cells. *Proc Natl Acad Sci U S A*. 2021;118(27).
52. Yi Y, Ge S. Targeting the histone H3 lysine 79 methyltransferase DOT1L in MLL-rearranged leukemias. *J Hematol Oncol*. 2022;15(1):35.
53. Li D, Hu Y, Jin Z, et al. TanCAR T cells targeting CD19 and CD133 efficiently eliminate MLL leukemic cells. *Leukemia*. 2018;32(9):2012-2016.

54. Bueno C, Velasco-Hernandez T, Gutierrez-Aguera F, et al. CD133-directed CAR T-cells for MLL leukemia: on-target, off-tumor myeloablative toxicity. *Leukemia*. 2019;33(8):2090-2125.
55. O'Byrne S, Elliott N, Rice S, et al. Discovery of a CD10-negative B-progenitor in human fetal life identifies unique ontogeny-related developmental programs. *Blood*. 2019;134(13):1059-1071.
56. Chen C, Yu W, Alikarami F, et al. Single-cell multiomics reveals increased plasticity, resistant populations, and stem-cell-like blasts in KMT2A-rearranged leukemia. *Blood*. 2022;139(14):2198-2211.
57. Anami Y, Deng M, Gui X, et al. LILRB4-targeting Antibody-Drug Conjugates for the Treatment of Acute Myeloid Leukemia. *Mol Cancer Ther*. 2020;19(11):2330-2339.
58. Gui X, Deng M, Song H, et al. Disrupting LILRB4/APOE Interaction by an Efficacious Humanized Antibody Reverses T-cell Suppression and Blocks AML Development. *Cancer Immunol Res*. 2019;7(8):1244-1257.
59. Deng M, Chen H, Liu X, et al. Leukocyte immunoglobulin-like receptor subfamily B: therapeutic targets in cancer. *Antib Ther*. 2021;4(1):16-33.
60. Dhunpath C, Strullu M, Petit A, et al. Single-dose (4.5 mg/m<sup>2</sup>) gemtuzumab ozogamicin in combination with fludarabine, cytarabine and anthracycline as reinduction therapy in relapsed or refractory paediatric acute myeloid leukaemia. *Br J Haematol*. 2022.
61. de Rooij JD, Zwaan CM, van den Heuvel-Eibrink M. Pediatric AML: From Biology to Clinical Management. *J Clin Med*. 2015;4(1):127-149.
62. Abuasab T, Rowe J, Tvtio A. Emerging Monoclonal Antibody Therapy for the Treatment of Acute Lymphoblastic Leukemia. *Biologics*. 2021;15:419-431.
63. Percival MM, Estey EH. Current treatment strategies for measurable residual disease in patients with acute myeloid leukemia. *Cancer*. 2019;125(18):3121-3130.
64. John S, Chen H, Deng M, et al. A Novel Anti-LILRB4 CAR-T Cell for the Treatment of Monocytic AML. *Mol Ther*. 2018;26(10):2487-2495.
65. Smith C HR, Xie J, Liu X, He Y, Ludwig K, Klesse L, Zhang C, John S. LILRB4 Is a Novel Target for KMT2A Rearranged Acute Leukemia. *Blood*; 2022.
66. Benito JM, Godfrey L, Kojima K, et al. MLL-Rearranged Acute Lymphoblastic Leukemias Activate BCL-2 through H3K79 Methylation and Are Sensitive to the BCL-2-Specific Antagonist ABT-199. *Cell Rep*. 2015;13(12):2715-2727.
67. Gibson A, Trabal A, McCall D, et al. Venetoclax for Children and Adolescents with Acute Lymphoblastic Leukemia and Lymphoblastic Lymphoma. *Cancers (Basel)*. 2021;14(1).
68. Winters AC, Maloney KW, Treece AL, Gore L, Franklin AK. Single-center pediatric experience with venetoclax and azacitidine as treatment for myelodysplastic syndrome and acute myeloid leukemia. *Pediatr Blood Cancer*. 2020;67(10):e28398.

Ch1

Ch2

Ch3





# CHAPTER 4

## CRISPR-Cas9 library screening identifies novel molecular vulnerabilities in *KMT2A*-rearranged acute lymphoblastic leukemia



Pauline Schneider<sup>1</sup>, Priscilla Wander<sup>1</sup>, Susan T.C.J.M. Arentsen-Peters<sup>1</sup>, Kirsten S. Vrenken<sup>1</sup>, Dedeke Rockx-Brouwer<sup>1</sup>, Fabienne R.S. Adriaanse<sup>1</sup>, Veerle Hoeve<sup>1</sup>, Irene Paassen<sup>1,2</sup>, Jarno Drost<sup>1,2</sup>, Rob Pieters<sup>1</sup>, Ronald W. Stam<sup>1</sup>

<sup>1</sup> *Princess Máxima Center for Pediatric Oncology, Utrecht, the Netherlands*

<sup>2</sup> *Oncode Institute, Utrecht, the Netherlands*

## ABSTRACT

In acute lymphoblastic leukemia (ALL), chromosomal translocations involving the *KMT2A* gene represent highly unfavorable prognostic factors and most commonly occur in patients less than 1 year of age. Rearrangements of the *KMT2A* gene drive epigenetic changes that lead to aberrant gene expression profiles that strongly favor leukemia development. Apart from this genetic lesion, the mutational landscape of *KMT2A*-rearranged ALL is remarkably silent, providing limited insights for the development of targeted therapy. Consequently, identifying potential therapeutic targets often relies on differential gene expression, yet the inhibition of these genes has rarely translated into successful therapeutic strategies. Therefore, we performed CRISPR-Cas9 knock-out screens to search for genetic dependencies in *KMT2A*-rearranged ALL. We utilized small-guide RNA libraries directed against the entire human epigenome and kinome in various *KMT2A*-rearranged ALL as well as wild-type *KMT2A* ALL cell line models. This screening approach led to the discovery of the epigenetic regulators *ARID4B* and *MBD3*, as well as the receptor kinase *BMP2R* as novel molecular vulnerabilities and attractive therapeutic targets in *KMT2A*-rearranged ALL.

## INTRODUCTION

Acute lymphoblastic leukemia (ALL) represents the most common type of cancer diagnosed in children and is currently curable in ~90% of patients [1]. Unfortunately, the survival chances for infants with ALL, patients <1 year of age, are significantly worse. Overall, the event-free survival (EFS) chances for infants diagnosed with ALL are ~50% [2,3]. Approximately 80% of the cases infant ALL is characterized by chromosomal translocations involving the Lysine Methyltransferase 2A (*KMT2A*) gene at chromosome 11q23, in which the N-terminus of *KMT2A* fuses with the C-terminus of one of its translocation partner genes, such as *AFF1* (*AF4*; in ~49% of cases), *MLL1* (*ENL*; ~22%) or *MLLT3* (*AF9*; ~16%) [4]. Strikingly, the 6-year EFS chances for *KMT2A*-rearranged infant ALL patients are at best 40% [2,3]. Hence, currently available treatment regimens clearly do not suffice and finding more effective therapeutic strategies still represents an unmet but urgent clinical need.

Functionally, wild-type *KMT2A* plays an essential role in regulating gene expression during early development and hematopoiesis[5] regulating gene transcription through histone 3 lysine 4 (H3K4) methyltransferase activity mediated by its C-terminal Su(Var)3-9, Enhancer-of-zeste, Trithorax (SET) domain[6-8]. In contrast, oncogenic *KMT2A* fusion proteins lose the SET domain, but instead recruit the histone methyltransferase DOT1L which catalyzes the dimethylation of histone H3 on lysine 79 (H3K79me2)[6,9,10], leading to aberrant gene expression profiles that strongly favor leukemogenesis [11,12].

In addition to the use of immunotherapeutic approaches such as blinatumomab [13], treatment of *KMT2A*-rearranged ALL (*KMT2A*-r ALL) may be improved by using epigenetic-based drugs targeting epigenetic vulnerabilities that are specifically essential to this type of leukemia. For instance, we recently showed that *KMT2A*-r ALL responds remarkably well to histone deacetylase (HDAC) inhibition [14,15]. Interestingly, small-molecule kinase inhibitors often exhibit synergistic anticancer effects in combination with HDAC inhibition, which led to the development of a rapidly expanding repertoire of chimeric HDAC/kinase dual inhibitors [16,17]. Moreover, *FLT3*, a receptor tyrosine kinase, has been previously identified as a vulnerability in *KMT2A*-r ALL. A recent clinical trial with the *FLT3* inhibitor lestaurtinib revealed that patients whose leukemia blasts exhibited sensitivity to *FLT3* inhibition *ex vivo* experienced benefits from the addition of the *FLT3* inhibitor to chemotherapy [18]. Given that kinases represent the largest group of druggable targets in the human genome [19], and that *KMT2A*-r ALL is an epigenetically driven malignancy, combinations of epigenetic-based drugs and kinase inhibitors may well represent effective treatments for this elusive type of leukemia.

Therefore, we set out to identify novel epigenetic regulators and kinases specifically essential to *KMT2A*-r ALL cells by applying in vitro clustered regularly interspaced

Ch1

Ch2

Ch3

Ch4

short palindromic repeats (CRISPR)-associated protein 9 (Cas9) knockout screens using synthetically designed single guide RNA (sgRNA) libraries [20,21] directed against the entire human epigenome and kinome [22,23]. CRISPR-Cas9 technology has had a major impact on drug (target) discovery and development due to its ability to efficiently altering genomic information in mammalian cells [24]. In the present study this approach led to the identification of known as well as novel molecular vulnerabilities and potential therapeutic targets in *KMT2A-r* ALL.

## RESULTS

### *CRISPR-Cas9 knockout screens in KMT2A-rearranged and wild-type KMT2A ALL cells*

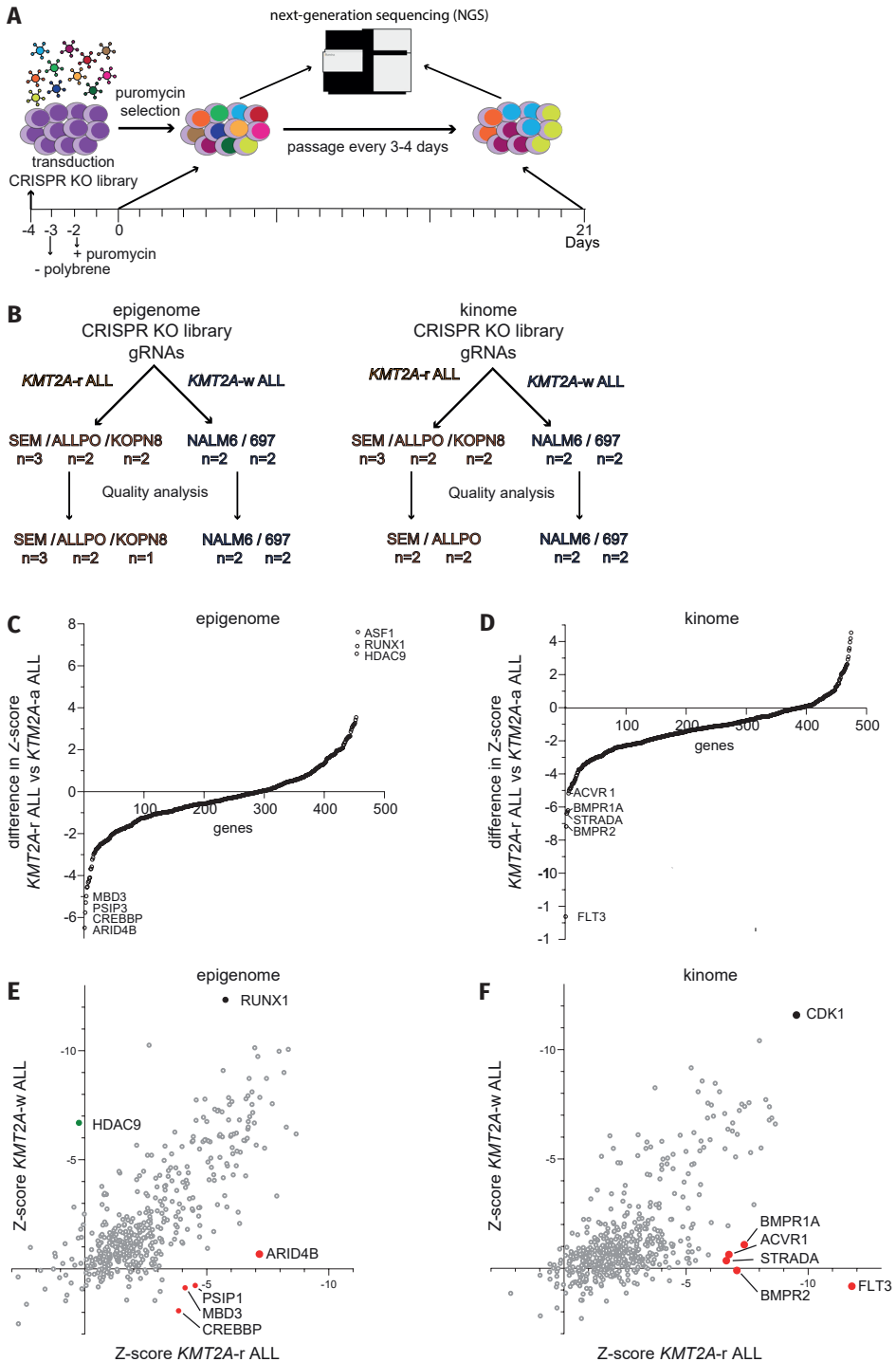
To identify epigenetic regulators and kinases essential for leukemia proliferation, maintenance, and survival, we conducted CRISPR-Cas9 knockout screens using sgRNA libraries targeting the human epigenome (446 genes) and kinome (504 genes). To distinguish between genes that are specifically essential to *KMT2A-r* ALL and those essential for ALL in general, we performed screens in *KMT2A-r* ALL cell lines (i.e., SEM, ALL-PO, and KOPN-8) as well as wild-type *KMT2A* (*KMT2A-w*) B-cell precursor (BCP) ALL cell lines (i.e., NALM-6 and 697). The experimental outline (Figure 1A) is based on a study by Shalem et al., in which sgRNAs were delivered into leukemia cells through lentiviral transduction, and non-transduced cells were eliminated through puromycin selection [21]. Samples drawn on day 0 provide the baseline representation of the sgRNA libraries, and samples drawn on day 21 were used to determine which of the sgRNAs were lost from the leukemic cell populations as a result of targeting genes essential to the proliferation and/or viability of the cells. For all cell line models, we obtained high-quality data for at least two independent replicates, except for KOPN-8, for which only a single sample provided reliable data in the epigenome screen (Figure 1B).

Approximately 67% or 76% of the sequenced reads at baseline (day 0) could be mapped to the epigenome or kinome sgRNA library, respectively. Read counts for non-targeting

---

**Figure 1. Epigenome and kinome CRISPR knockout screen identifies epigenetic genes and druggable targets essential for *KMT2A*-rearranged ALL cells** **A.** Graphic overview of the CRISPR-Cas9 knockout (KO) screen. **B.** Schematic overview of the CRISPR KO screen samples. **C-D.** Graph showing the difference in Z-scores, calculated by the MLE module of MAGeCK, for genes targeted in the epigenome CRISPR KO screen (**C**) and the kinome CRISPR KO screen (**D**) between *KMT2A-r* ALL cell lines and *KMT2A-w* ALL cell lines. **E-F.** Graphs showing the average Z scores of genes targeted in the epigenome (**E**) and the kinome CRISPR KO screen (**F**) for the *KMT2A-r* ALL cell lines and *KMT2A-w* ALL cell lines plotted against each other.

*Identification of novel epigenetic regulators and kinases specifically essential to *KMT2A-r* ALL*

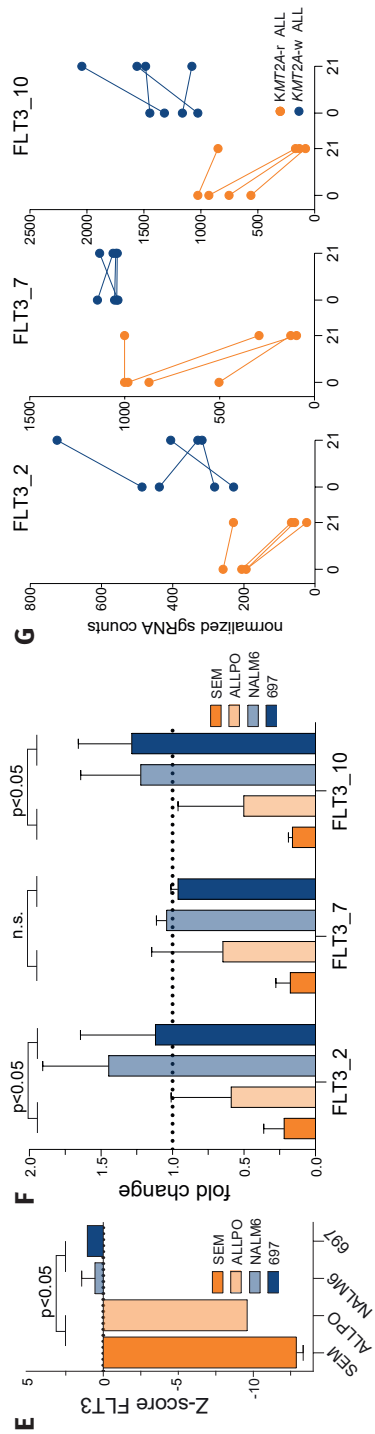
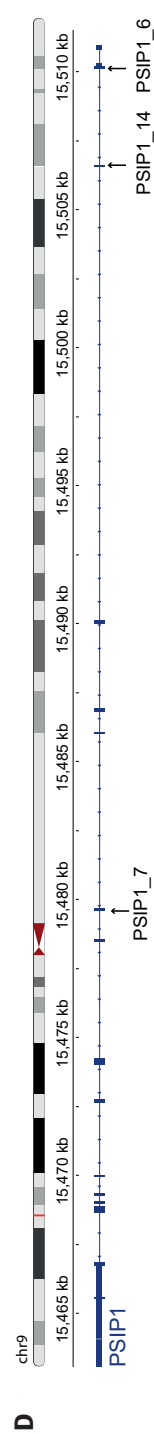
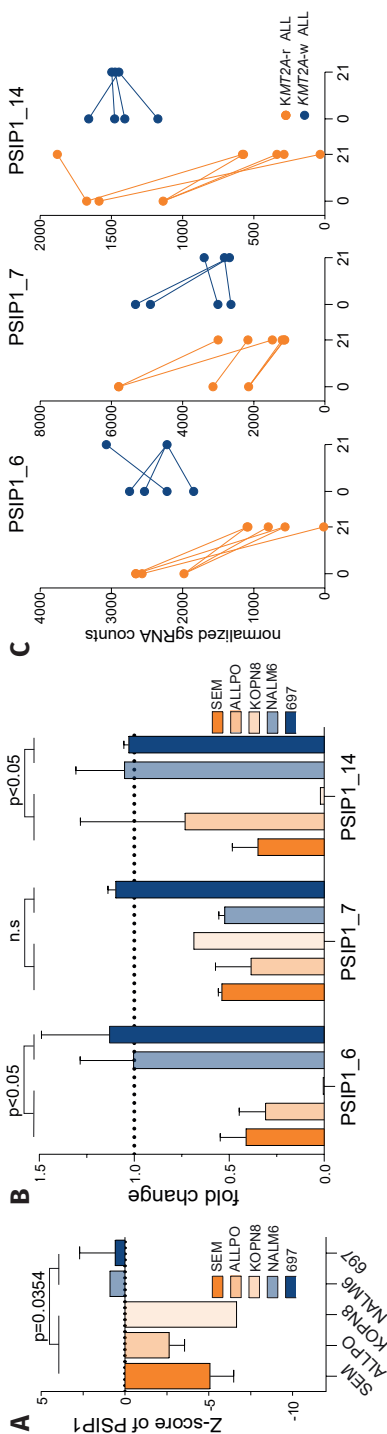


Ch1

Ch2

Ch3

Ch4



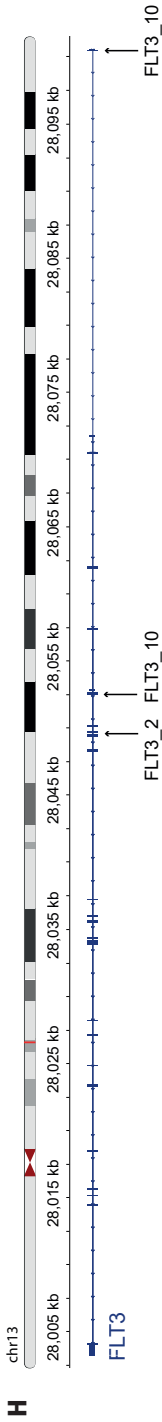


**Figure 2. Evaluation of the known *KMT2A*-rearranged ALL vulnerability genes *PSIP1* and *FLT3*** **A.** The z-scores of individual cell lines for *PSIP1* knockout. **B.** The fold change of normalized read counts at day 21 compared to baseline (day 0) for sgRNAs *PSIP1\_6*, *PSIP1\_7*, and *PSIP1\_14* derived from our original screening libraries. The mean value with the standard error of the mean (SEM) is depicted from two independent experiments. **C.** The normalized read counts at day 0 and day 21 of these sgRNAs. **D.** Overview of the target locations on the *PSIP1* gene for the sgRNAs presented in A en B. **E.** The z-scores of individual cell lines for *FLT3* knockout. **F.** The fold change of normalized read counts at day 21 compared to baseline (day 0) for sgRNAs *FLT3\_2*, *FLT3\_7* and *FLT3\_10* derived from our original screening libraries depicted for two independent experiments +/- SEM. **G.** The normalized read counts at day 0 and day 21 of these sgRNAs are presented by the mean +/- SEM of two independent experiments. **H.** Overview of the target locations of the sgRNAs presented in F en G on the *FLT3* gene. All differences in the figure were statistically evaluated using unpaired t-tests

control sgRNAs remained stable between day 0 and day 21, indicating that the transduction of non-targeting sgRNAs did not affect cell viability or proliferation (Supplementary Figure 1). Read counts for sgRNAs directed against genes known to be essential to human cells in general (i.e., positive control sgRNAs) markedly decreased over time (Figure S1) indicating that sgRNAs directed against essential genes indeed disappear from the leukemic cell populations.

First, we determined the difference in z-scores between *KMT2A-r* ALL cell lines against those of *KMT2A-w* ALL cell lines (Figure 1C and 1D). We identified *ARID4B*, *CREBBP*, *PSIP1* and *MBD3* as epigenetic regulator genes more essential to *KMT2A-r* ALL, and *ASF1*, *RUNX1* and *HDAC9* as more essential to *KMT2A-w* ALL (Figure 1C). In addition, we found *FLT3*, *BMPR2*, *STRADA*, *BMPR1A*, and *ACVR1* to represent kinases most essential to *KMT2A-r* ALL cells (Figure 1D). Next, we plotted the average z-scores of the *KMT2A-r* ALL cell line models against those of the *KMT2A-w* ALL cell lines (Figure 1E and 1F). This revealed that *RUNX1* is an essential epigenetic regulator in both *KMT2A-r* and *KMT2A-w* BCP-ALL, which is consistent with previously published data [25-32]. Among the genes specifically essential for the survival and proliferation of *KMT2A-r* ALL cells we found *PSIP1*, *CREBBP* (Figure 1E), as well as *FLT3* (Figure 1F), representing known vulnerabilities in *KMT2A-r* ALL [33-42]. *PSIP1*, also known as LEDGF/p75, plays a vital role in chromatin organization and transcriptional regulation [33,34]. *CREBBP*, a transcriptional coactivator, is involved in acetylating histones and regulating gene expression [35]. *FLT3*, a receptor tyrosine kinase, has previously been identified as a vulnerability in *KMT2A-r* ALL [38,39]. For all three genes, the z-scores were significantly lower in *KMT2A-r* ALL cell lines as compared with *KMT2A-w* BCP-ALL cell lines (Figure 2A and 2E, Supplementary Figure 2A) as were the read counts for individual sgRNA sequences at day 21 (Figure 2B-D and 2F-H, Supplementary Figure 2B-D). These results underscored the known importance of *PSIP1*, *CREBBP*, and *FLT3*, as the knockout of these genes resulted in impaired cell growth and survival specifically in *KMT2A-r* ALL cells, indicating their crucial roles. These observations clearly emphasize the validity of our screens and the newly identified genetic dependencies in *KMT2A-r* ALL, including the epigenetic regulators *MBD3* and *ARID4B* (Figure 1C and 1E), and the kinases *BMPR2*, *ACVR1*, *BMPR1A*, and *STRADA* (Figure 1D and 1F). Considering that *BMPR2*, *BMPR1A*, and *ACVR1* are all receptors for bone morphogenetic proteins (BMPs), we have selected the receptor that exhibits the most differential response between *KMT2A-r* and *KMT2A-w* ALL cells for further validation, i.e., *BMPR2*.

### **Validation of *ARID4B* and *MBD3* as epigenetic dependencies in *KMT2A-r* ALL cells**

For both *ARID4B* and *MBD3*, the z-scores were consistently and significantly lower in all *KMT2A-r* ALL cell line models (Figure 3A and 4A), as were the read counts of individual sgRNA sequences (Figure 3B-D and 4B-D). To validate whether *ARID4B* and *MBD3*



truly represent novel molecular vulnerabilities in *KMT2A*-r ALL, we used a GFP-based competition assay, recently described as a powerful screening methodology to identify novel therapeutic targets[43,44]. This assay involves the mixing of cells transduced with doxycycline (Dox)-inducible sgRNA/GFP expression vectors with non-transduced cells in equal proportions and monitoring the levels of GFP<sup>+</sup> cells over time using flow cytometry (Figure 3E). These competition assays were performed in the *KMT2A*-r ALL cell lines SEM and in the *KMT2A*-w BCP-ALL cell lines 697, using both sgRNAs derived from our original screening libraries as well as with commercially available sgRNAs with high efficiency and low off-target effects (i.e., *ARID4B\_IDT\_1AA*, *MBD3\_AB*, and *MBD3\_AC*). The location of these sgRNA sequences in *ARID4B* and *MBD3*, respectively, are indicated in Figure 3D and 4D. For all tested sgRNAs directed against either *ARID4B* or *MBD3*, the number of GFP<sup>+</sup> leukemic cells was progressively and significantly reduced over time in *KMT2A*-r ALL cells line SEM, but not in *KMT2A*-w ALL cell line 697 (Figure 3F and 4E).

To determine whether the observed decreases in the GFP<sup>+</sup> leukemic cell population was due to an effect on cell viability or cell proliferation, we evaluated the efficiency of CRISPR editing by measuring the percentage of cells within the GFP<sup>+</sup> cells that exhibited insertions or deletions at day 21 as determined by sequence analysis. This measurement allowed us to determine a CRISPR Knockout Score (KO Score) using the Synthego ICE Analysis tool. When genes that are essential for cell viability are targeted, knockout leads to cell death accompanied by the loss of the sgRNA sequence from the cell pool. In case of *ARID4B*, all tested sgRNAs showed low KO scores ranging from 1% to 35% in the *KMT2A*-r ALL cell line SEM, with the commercially available sgRNA (i.e., *ARID4B\_IDT\_1AA*) producing the lowest score (Figure 3G). In contrast, the scores in the *KMT2A*-w BCP-ALL cell line 697 remained consistently high for all sgRNAs. Taken together, this suggests that *ARID4B* is essential for leukemic cell survival in *KMT2A*-r ALL but not in *KMT2A*-w BCP-ALL.

Interestingly, the scores for *MBD3* remained high in both SEM and 697 cells, indicating that the sgRNA sequences directed against *MBD3* were still present in both cell line models (Figure 4F). These findings suggest that the significant decrease in the percentage of GFP<sup>+</sup> SEM cells could not have been the result of leukemic cell death, but instead is more likely due to inhibition of cell proliferation.

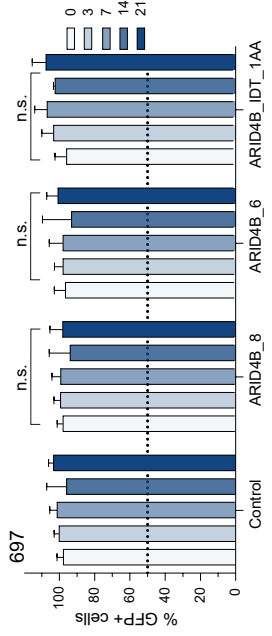
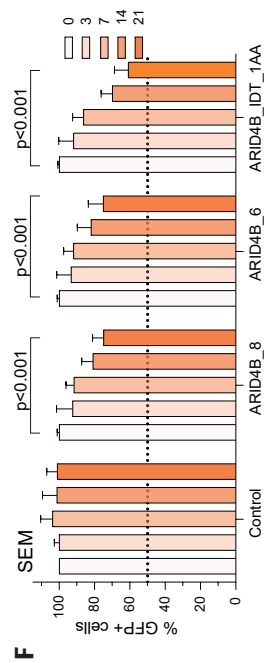
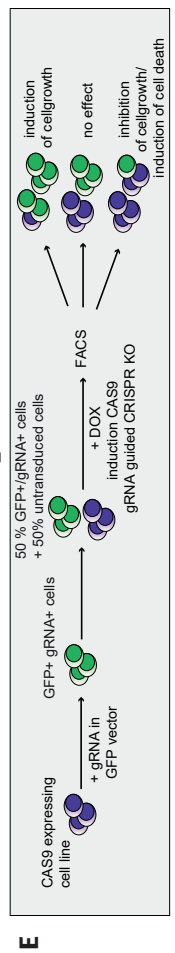
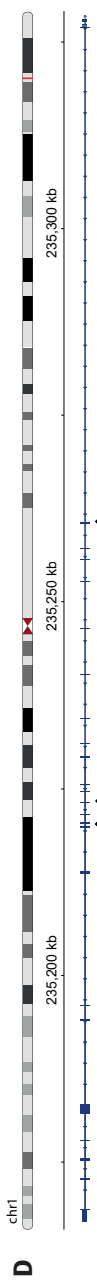
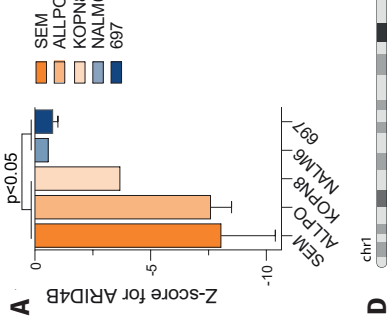
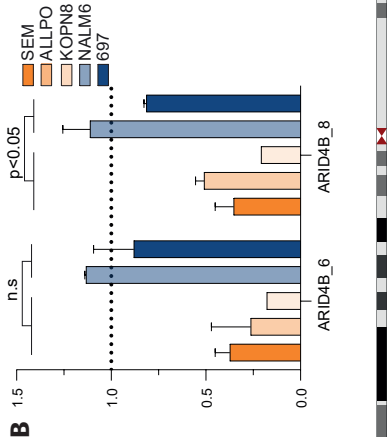
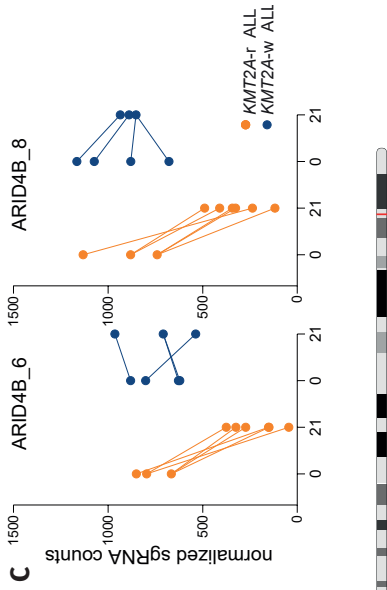
Since *ARID4B* overexpression was found to be of prognostic value in other types of cancer [45-47], we explored the protein expression of *ARID4B* in all cell lines used in our CRISPR-Cas9 knockout screens, and found no significant differences (Figure 3H and 3I). Comparison of transcriptional levels of patient samples diagnosed with either *KMT2A*-r ALL or *KMT2A*-w ALL, as well as healthy bone marrow samples, retrieved from previously performed expression arrays [12], also revealed no differences in expression between leukemia types, although the overall expression of *ARID4B* in pediatric ALL is significantly

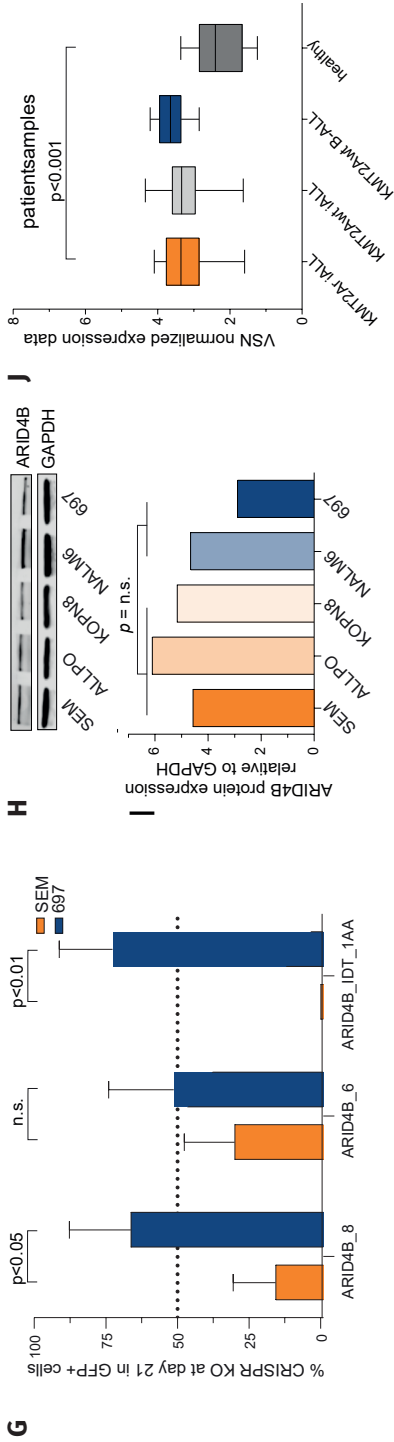
Ch1

Ch2

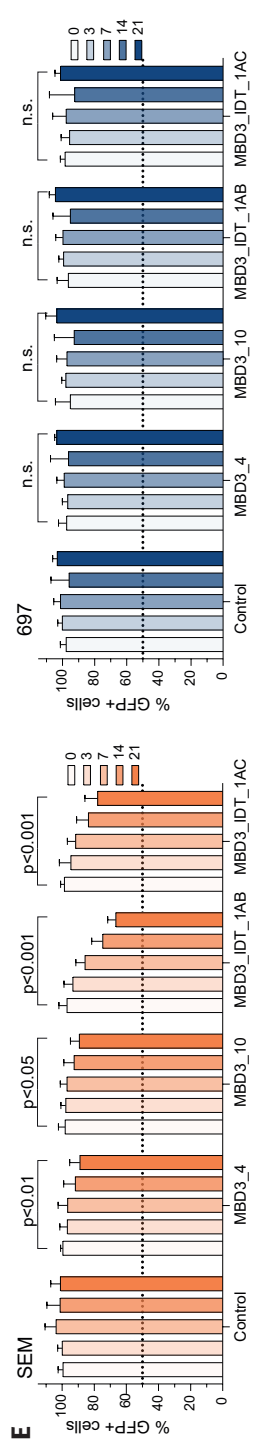
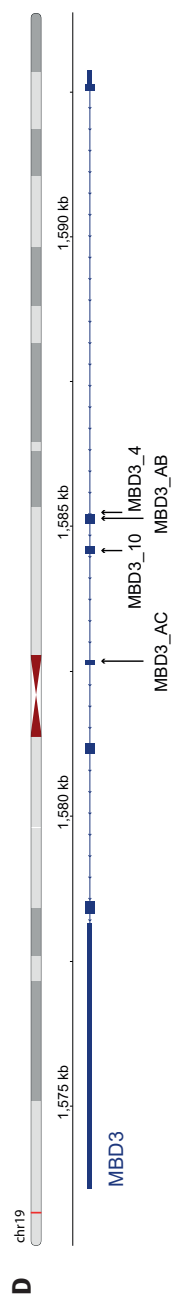
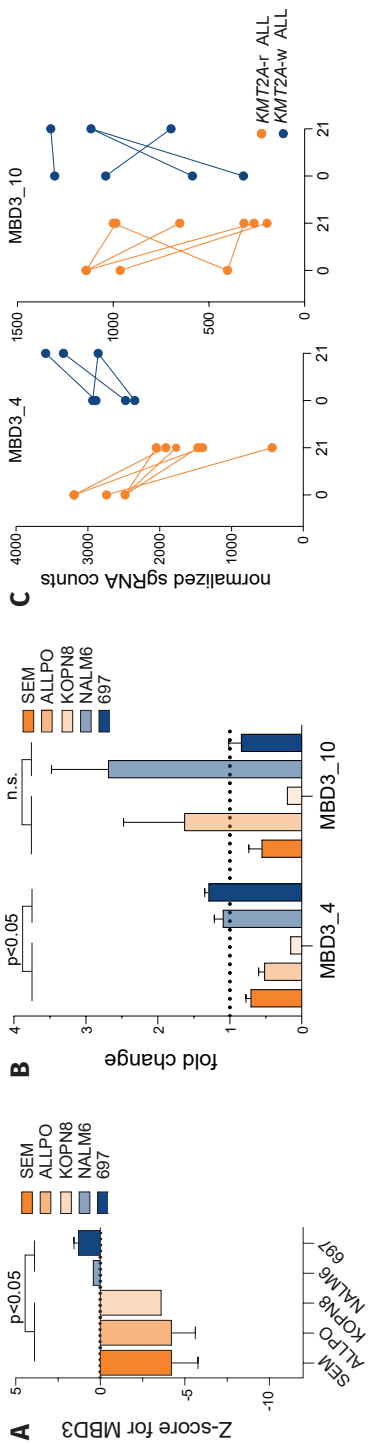
Ch3

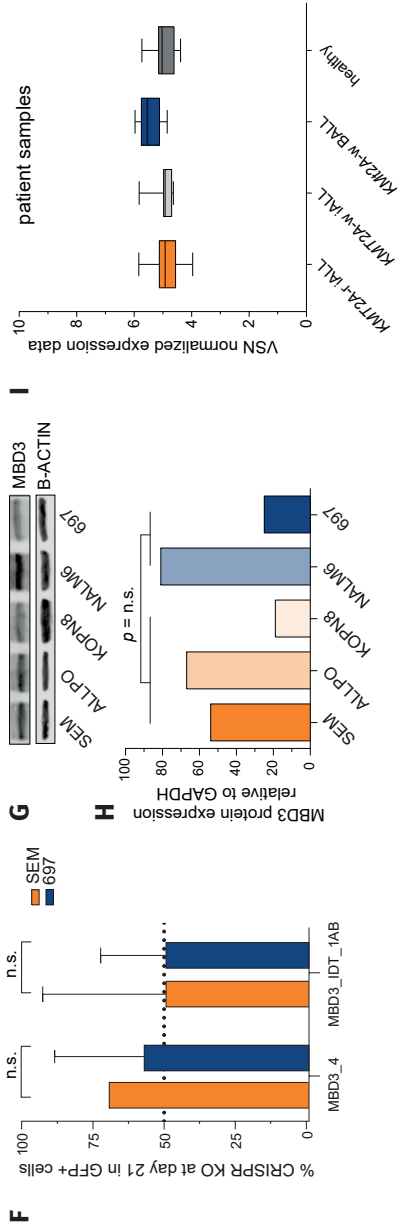
Ch4



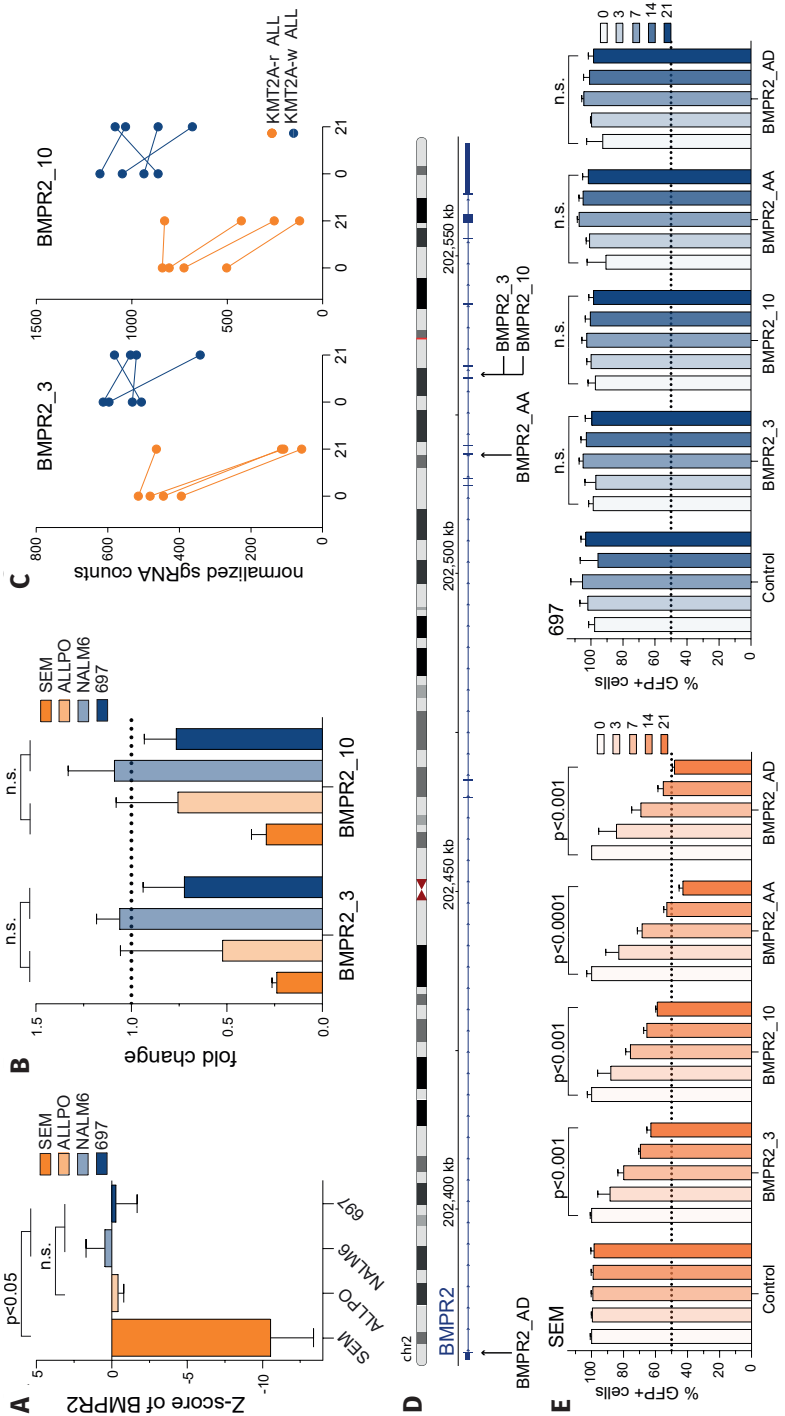


**Figure 3. Validation of novel identified epigenetic regulator ARID4B implicated in *KMT2A*-r ALL.** **A.** The z-scores of individual cell lines for *ARID4B* knockout. Differences were statistically evaluated using unpaired t-tests. **B.** The fold change of normalized read counts at day 21 compared to baseline (day 0) for sgRNAs ARID4B\_6 and ARID4B\_8 derived from our original screening libraries. The mean value +/- the SEM is depicted from two independent experiments from the CRISPR KO screen. Differences were statistically evaluated using unpaired t-tests. **C.** The normalized read counts at day 0 and day 21 of these sgRNAs. **D.** Overview of the target locations on the *ARID4B* gene of the sgRNAs used for validation experiments. **E.** Graphic overview of the green fluorescent protein (GFP) competition assay. **F.** The percentages of GFP positive cells in the GFP competition assay for sgRNAs targeting *ARID4B* in *KMT2A*-r ALL cell line SEM and *KMT2A*-w ALL cell line 697 were measured by flow cytometry. The proportion of GFP positive cells was normalized to the GFP positive cells at baseline (day 0). The data represents the mean +/- SEM of two independent experiments and the differences were statistically evaluated using multiple t-test. **G.** Percentages of CRISPR KO score as determined by sequencing data analysis using the Synthego ICE Analysis tool for sgRNAs targeting *ARID4B* in *KMT2A*-r ALL cell line SEM and *KMT2A*-w ALL cell line 697. The data represents the mean of two or three sequencing analysis +/- the SEM. **H.** Immunoblot images of ARID4B and GAPDH protein levels in *KMT2A*-r ALL cell lines SEM, ALL-PO, KOPN8, and *KMT2A*-w ALL cell lines NALM6 and 697. **I.** Protein expression quantification of immunoblot (H) by densitometry analysis of ARID4B compared to GAPDH. **J.** VSN normalised microarray data (Affymetrix HU133plus2.0 GeneChips) showing the expression of *ARID4B* (probeset 224322\_at), in infant ALL patients carrying *KMT2A* translocations (i.e. *KMT2A*-r ALL, n=59), infant ALL patients without *KMT2A* translocations (i.e. *KMT2A*wt ALL, n=14) and childhood ALL patients older than 1 year of age without *KMT2A* translocations (i.e. *KMT2A*wt BALL, n=16) and healthy bone marrow samples (i.e. healthy, n=13). Data depicted in box and whiskers plots with minimum and maximum values.





**Figure 4. Validation of novel identified epigenetic regulator MBD3 implicated in *KMT2A*-r ALL.** **A.** The z-scores of the individual cell lines for *MBD3* knockout. Differences were statistically evaluated using unpaired t-tests. **B.** The fold change of normalized read counts at day 21 compared to baseline (day 0) for sgRNAs *MBD3\_4* and *MBD3\_10* derived from our original screening libraries. The mean value +/- the SEM is depicted from two independent experiments from the CRISPR KO screen. Differences were statistically evaluated using unpaired t-tests. **C.** The normalized read counts at day 0 and day 21 of these sgRNAs. **D.** Overview of the target locations on the *MBD3* gene of the sgRNAs used for validation experiments. **E.** The percentages of GFP positive cells in the GFP competition assay for sgRNAs targeting *MBD3* in *KMT2A*-r ALL cell line SEM and *KMT2A*-w ALL cell line 697 were measured by flow cytometry. The proportion of GFP positive cells was normalized to the GFP positive cells at baseline (day 0). The data represents the mean +/- of two independent experiments and the differences were statistically evaluated using multiple t-test. **F.** Percentages of CRISPR KO score as determined by sequencing data analysis using the Synthego ICE Analysis tool for sgRNAs targeting *MBD3* in *KMT2A*-r ALL cell line SEM and *KMT2A*-w ALL cell line 697. The data represents the mean of two or three sequencing analysis +/- the SEM. **G.** Immunoblot images of *MBD3* and B-ACTIN protein levels in *KMT2A*-r ALL cell line SEM and *KMT2A*-w ALL cell line 697. The data represents the mean of two or three sequencing analysis +/- the SEM. **H.** Protein expression quantification of immunoblot (H) by densitometry analysis of *MBD3* compared to B-ACTIN. **I.** VSN normalised microarray data (Affymetrix HU133plus2.0 GeneChips) showing the expression of *MBD3* (probe set 41160\_at), in infant ALL patients carrying *KMT2A* translocations (i.e. *KMT2A*-r iALL, n=59), infant ALL patients without *KMT2A* translocations (i.e. *KMT2A*wt iALL, n=14) and childhood ALL patients older than 1 year of age without *KMT2A* translocations (i.e. *KMT2A*wt BALL, n=16) and healthy bone marrow samples (i.e. healthy, n=13). Data depicted in box and whiskers plots with minimum and maximum values.



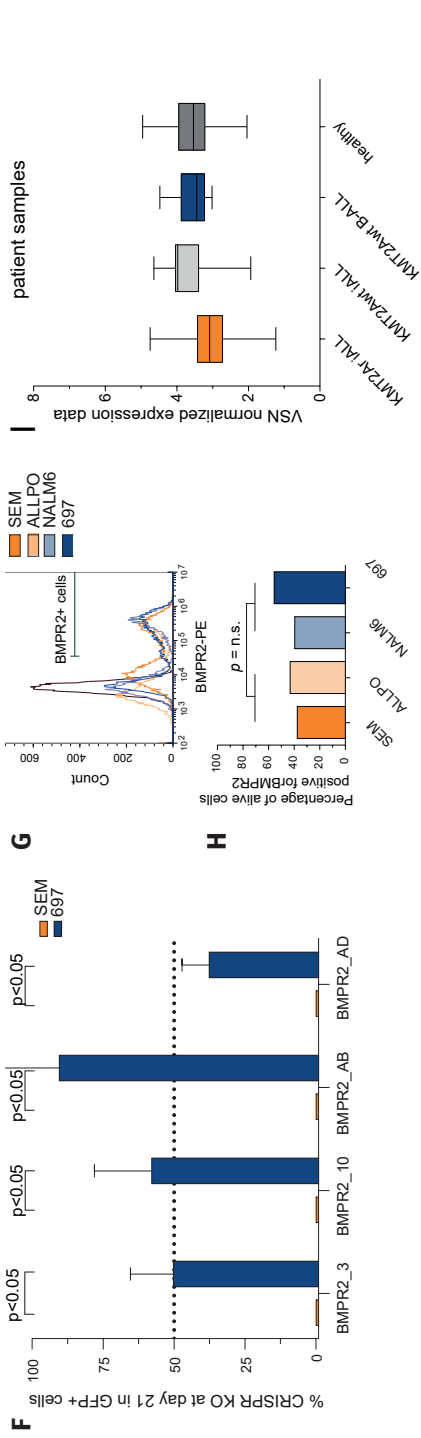


**Figure 5. Validation of novel identified kinase BMPR2 essential for KMT2A-rearranged ALL cells** **A.** The z-scores of the individual cell lines for *BMPR2* knockout. **B.** The fold change of normalized read counts at day 21 compared to baseline (day 0) for sgRNAs BMPR2\_3 and BMPR2\_10 derived from our original screening libraries. The mean value with the standard error of the mean (SEM) is depicted from two independent experiments from the CRISPR KO screen. Differences were statistically evaluated using unpaired t-tests. **C.** The normalized read counts at day 0 and day 21 of these sgRNAs. **D.** Overview of the target locations on the *BMPR2* gene of the sgRNAs used for validation experiments. **E.** The percentages of GFP positive cells in the GFP competition assay for sgRNAs targeting *BMPR2* in *KMT2A-r*-ALL cell line SEM and *KMT2A-w*-ALL cell line 697 were measured by flow cytometry. The proportion of GFP positive cells was normalized to the GFP positive cells at baseline (day 0). The data represents the mean with SEM of two independent experiments and the differences were statistically evaluated using multiple t-test. **F.** Percentages of CRISPR KO score as determined by sequencing data analysis using the Synthego ICE Analysis tool for sgRNAs targeting *BMPR2* in *KMT2A-r*-ALL cell line SEM and *KMT2A-w*-ALL cell line 697. The data represents the mean of two or three sequencing analysis with the SEM. **G.** Flow cytometry analysis of live cells positive for *BMPR2* in *KMT2A-r*-ALL cell lines SEM and ALL-PO, and *KMT2A-w*-ALL cell line NALM6 and 697. **H.** Quantification of Flow cytometry analysis of *BMPR2* positive cells. The data represents the mean of two Flow cytometry experiments with the SEM. **I.** VSN normalised microarray data (Affymetrix HU133plus2.0 GeneChips) showing the expression of *BMPR2* (probeset 225144\_at), in infant ALL patients carrying *KMT2A* translocations (i.e. *KMT2Ar* iALL, n=59), infant ALL patients without *KMT2A* translocations (i.e. *KMT2Aw* iALL, n=14) and childhood ALL patients older than 1 year of age without *KMT2A* translocations (i.e. *KMT2Aw* BALL, n=16) and healthy bone marrow samples (i.e. healthy, n=13). Data depicted in box and whiskers plots with minimum and maximum values.

higher than in healthy bone marrow cells (Figure 3J). Likewise, there were no notable differences in *MBD3* expression between *KMT2A-r* ALL and *KMT2A-w* BCP-ALL (Figure 4G-I). Hence the specific dependency of *KMT2A-r* ALL cells on *ARID4B* and *MBD3* is not caused by increased levels of expression.

### **Validation of receptor kinase *BMPR2* as a molecular vulnerability in *KMT2A-r* ALL cells**

Our CRISPR-Cas9 knockout screens using the sgRNA library directed against the human kinome identified the *BMPR2* as an essential gene to *KMT2A-r* ALL cells. However, our z-score analysis showed that the *KMT2A-r* ALL cell line SEM, but not ALL-PO, had a significantly decreased z-score (Figure 5A). Read count analysis for individual sgRNA sequences directed against *BMPR2* revealed that for the ALL-PO cell line, one of the duplicates clearly showed decreased expression of the sgRNA sequence, while the expression in the other duplicate remained stable over time (Figure 5B-D).

Validation experiments using the competition assay (see above) revealed a significant loss of GFP signal in the *KMT2A-r* ALL cell line SEM, but not in the *KMT2A-w* BCP-ALL cell line 697 (Figure 5E). Moreover, the CRISPR KO scores clearly demonstrate that all sgRNA tested disappeared from the leukemic cell population in *KMT2A-r* ALL SEM cells, while clearly remaining present in *KMT2A-w* BCP-ALL 697 cells (Figure 5F). Hence, knockout of *BMPR2* appears to be lethal to *KMT2A-r* ALL cells, while *KMT2A-w* BCP-ALL cells remain viable upon losing *BMPR2*. Again, the remarkable dependency of *KMT2A-r* ALL cells on *BMPR2* does not seem to be a consequence of differential *BMPR2* expression as we observed no differences in neither the protein nor the mRNA expression levels between *KMT2A-r* ALL and *KMT2A-w* BCP-ALL (Figure 5G-I).

## **DISCUSSION**

In this study we used CRISPR-Cas9 drop-out screens using sgRNA libraries against the human epigenome and kinome in various cell line models to identify novel molecular vulnerabilities in *KMT2A-r* ALL. These efforts and additional validation experiments revealed *PSIP1*, *CREBBP* and kinase *FLT3* representing known vulnerabilities in *KMT2A-r*, as well as *ARID4B*, *MBD3*, and *BMPR2* as potential candidates to be considered as novel therapeutic targets in this aggressive type of leukemia. While the selected cell lines may not be a complete representation of *KMT2A-r* and *KMT2A-w* ALL, it's important to note that this approach successfully pinpointed well-established vulnerabilities specific to *KMT2A-r* ALL, such as *CREBBP*, *PSIP1*, and *FLT3*. These findings align with existing knowledge about the involvement of these genes in *KMT2A-r* ALL, supporting the reliability of our approach in detecting relevant targets.



As shown, loss of *ARID4B*, encoding AT-Rich Interaction Domain 4B (a member of the ARID family of chromatin remodeling proteins), is specifically lethal to *KMT2A*-r ALL cells. *ARID4B* plays a role in various cellular processes including embryonic development, cell proliferation, differentiation, and apoptosis[48-51]. Apart from this, several studies demonstrated that *ARID4B* plays a significant role in cancer development, metastasis and cancer-related signaling pathways in different types of human cancers, including breast cancer, ovarian cancer, and hepatocellular carcinoma [45-47,52,53]. It functions as a component of the SIN3A transcriptional corepressor complex, which is dependent on histone deacetylase activity and is involved in regulating gene expression [54,55]. With its AT-rich domain, *ARID4B* has the capability to interact with DNA sequences rich in AT base pairs, enabling it to recruit the SIN3A complex to specific regions of the genome. Once recruited, the SIN3A complex interacts with histone deacetylases (HDACs), resulting in the deacetylation of histones at the corresponding DNA locus, leading to chromatin condensation and transcriptional repression. Although we here show that *ARID4B* is essential to *KMT2A*-r ALL cells, the exact mechanistic role of *ARID4B* in this aggressive type of leukemia remains to be elucidated and further explored in the context of *KMT2A*-r ALL patient samples. From a therapeutic perspective, it would obviously be of interest to evaluate small molecule inhibitors of *ARID4B* in patient samples *in vitro* and *in vivo* using patient-derived xenograft (PDX) mouse models. To date, however, *ARID4B* inhibitors are not available.

Ch1

Ch2

Ch3

Ch4

In contrast to *ARID4B*, loss of *MBD3* was not necessarily lethal to *KMT2A*-r ALL cells, but rather inhibited leukemic cell proliferation. *MBD3* encodes a member of the methyl-CpG binding domain (MBD) protein family which preferably binds to 5-hydroxymethylcytosine-marked genes, and has been implicated in various cellular processes, including cell differentiation, pluripotency, and cellular reprogramming [56-58]. Moreover, *MBD3* is an essential component of the nucleosome remodeling and deacetylase (NuRD) complex, which is involved in chromatin remodeling and transcriptional regulation[57,58]. Dysregulation of *MBD3* expression or function has been observed in different human cancers, suggesting its involvement in tumorigenesis and cancer progression [59-62]. Further investigation is needed to comprehend the distinct reliance on *MBD3* in *KMT2A*-r ALL as opposed to *KMT2A*-w BCP-ALL. Unfortunately, as is the case for *ARID4B*, no known *MBD3* inhibitors are currently available.

Finally, we found the loss of *BMP2* to be lethal to *KMT2A*-r ALL cells. *BMP2* encodes a member of the bone morphogenetic protein (BMP) receptor family of transmembrane serine/threonine kinases. BMP signaling is activated by binding of TGF-beta superfamily ligands and is involved in various cellular processes, including embryonic development, tissue homeostasis, cell differentiation and hematopoietic stem cell (HSC) renewal

[63-67]. Moreover, the BMP pathway has been implicated in various cancers, including leukemia, by playing a role in tumor progression, invasion, and metastasis in various cancer types and has been recognized as a potential therapeutic strategy for cancer treatment [68]. Apart from ligand binding, activation of BMP2 requires homodimerization or heterodimerization with BMP type 1 receptors such as BMPR1A, BMPR1B, ALK1 and ACVR1, to exert its function [69]. Subsequently, this leads to the activation of intracellular pathways, such as the SMAD signaling pathway, resulting in the regulation of target genes and cellular responses [68,70-72]. Interestingly, we also identified both *ACVR1* and *BMPR1A* to be potential molecular vulnerabilities in *KMT2A-r* ALL (Figure 1D and 1F). Hence, inhibition of BMP signaling may well induce favorable anti-leukemic effects in this aggressive type of leukemia.

In summary, the present study provides novel molecular vulnerabilities of *KMT2A-r* ALL using CRISPR-Cas9 drop-out screens targeting the human epigenome and kinome in various cell line models. While the discoveries are promising, further research and exploration is warranted, particularly in patient samples *in vitro* and *in vivo* using patient-derived xenograft (PDX) mouse models. Moreover, conducting further exploratory experiments involving knockdown (instead of knockout) techniques such as siRNA- or shRNA- mediated RNA interference, might provide valuable insights. Additionally, it would be intriguing to investigate whether the recently identified therapeutic targets are under the influence of the *KMT2A* fusion complex. Furthermore, exploring the potential of MENIN inhibition, which targets the interaction between MENIN and the *KMT2A* fusion complex [73], to effectively counteract these vulnerabilities would be of interest. Taken together, further research and exploration might lead the development of attractive therapeutic strategies to improve clinical outcome for patients diagnosed with *KMT2A-r* ALL.

## **MATERIALS AND METHODS**

### **Cell culture**

The pediatric *KMT2A*-rearranged B-ALL cell lines utilized in this study include SEM (*KMT2A::AFF1*; ACC 546 DSMZ), KOPN-8 (*KMT2A::MLL1*; ACC 552 DSMZ) and ALL-PO [74] (*KMT2A::AFF1*). ALL-PO was kind gift from the lab of Prof. dr. Cazzaniga (University of Milano-Bicocca, Monza, Italy). The *KMT2A* wildtype B-cell precursor (BCP) ALL cell lines utilized include 697 (*TCF3::PBX*; ACC 42 DSMZ) and NALM-6 (carrying translocation t(5;12)(q33.2;p13.2); ACC 128 DSMZ). All leukemia cell lines were cultured in RPMI-1640 medium containing GlutaMAX™ supplemented with 10% fetal calf serum, 100 IU/ml Penicillin and Streptomycin, and 0.125µg/ml Amphotericin B (Life Technologies), at 37°C under a 5% CO<sub>2</sub> containing atmosphere. HEK293T cells (DSMZ; ACC 875) were used for virus production and

maintained in Dulbecco's modified Eagle medium (DMEM, Life Technologies) with similar supplements and cultured under similar conditions. All cell lines were routinely tested for the absence of mycoplasma and DNA fingerprinted to assure cell line authenticity.

Ch1

Ch2

### **Generation of epigenome/kinome CRISPR-sgRNA plasmid libraries and lentivirus production for CRISPR-Cas9 knockout screens**

Ch3

The epigenome and kinome sgRNA libraries were a kind gift from Dr. B. Evers and were previously described in Evers *et al.* [22]. In short, the epigenome sgRNA library consisted of 5130 sgRNAs targeting a total of 446 genes encoding epigenetic regulators, and the kinome sgRNA library consisted of 5860 sgRNAs targeting 504 genes encoding human kinases, with both libraries containing  $\geq 10$  sgRNAs per gene [22,23]. The sgRNA plasmid library was generated by cloning all sgRNAs into lentiCRISPR v2 vectors (Addgene #52961) containing an U6 promoter. A complete list of all gene-specific sgRNAs, as well as positive and negative (non-targeting) controls is provided in Supplementary Table 1. Virus was generated by transfection of HEK293T cells using library plasmid, MD2.G plasmid (Addgene #12259), PAX2 plasmid (Addgene #12260), and X-tremeGENE™ HP DNA Transfection Reagent (Sigma-Aldrich #XTGHPORO). The medium was replaced by Gibco Opti-MEM (ThermoFisher #31985070) the following day. Virus was harvested two days after transfection, filtered through a 0.45 $\mu$ M low protein binding membrane (Millipore #HAWP04700), and concentrated using vivaspin-20 columns (Sigma-Aldrich #Z614653). Concentrated virus was stored in aliquots at -80°C for further use.

Ch4

### ***In vitro* CRISPR-Cas9 knockout screening, sequencing, and analysis**

All cell lines were transduced with lentivirus carrying the sgRNA library via spinfection at a deliberately low Multiplicity of infection (MOI) of  $< 0.3$  to minimize the number of cells with more than one genetic editing event. We aimed to obtain at least 500 sequencing reads per sgRNA by using 1000 cells per sgRNA at the starting point of the screen. Transduction was facilitated using 4 $\mu$ g/ml polybrene (Millipore #TR-1003-G). To find the optimal virus volume for achieving an MOI of  $< 0.3$ , each new cell type and virus lot was tested by a titration, which was assessed by measuring cell viability (i.e., 7AAD staining) on Cytoflex S flow cytometer (Beckman Coulter). 24 hours after transduction, medium was replaced to remove polybrene and puromycin selection (1  $\mu$ g/ml) was initiated one day after. 48 hours after puromycin selection, cells were harvested, representing baseline (Day 0) samples. Remaining surviving cells carrying the sgRNA library were maintained for another 21 days and passaged every three to four days, to harvest cells at day 21. Genomic DNA was isolated using Trizol reagent (Life Technologies) according to manufacturer's instructions. sgRNA sequences were recovered by a first round of PCR (Biorad) by using 5  $\mu$ g genomic DNA to ensure sgRNA pool complexity. PCR primer sequences were forward

5'-ACACTCTTCCCTACACGACGCTCTCCGATCT NNNNNNGGCTTATATATCTTGTGGAAAGGACG-3' with NNNNNN as barcode and reverse 5'-GTGACTGGAGTTCAGACGTGTGCTCTCCGATCTACT-GACGGCACCGGAGCCAATCC-3' as described previously [22,23,75]. Reaction mixtures were combined and purified using a QIAquick PCR Purification Kit (Qiagen) according to manufacturer's instructions. A second PCR was performed to attach Illumina adapters and 6 bp indexing primers to the sgRNA sequences on 2ng of the purified PCR product using forward primer 5' -AATGATACGGCGACCACCGAGATCTAC ACTCTTCCCTACACGACGCTCTCCGATCT-3' and reverse primer 5' -CAAGCAGAAGACGG CATAACGAGATNNNNNNGTGACTGGAGTTCAGACGTGTGCTCTCCGATCT-3' with NNNNNN as illumina indexing read as described previously [22,23,75]. Phusion Hot Start II Polymerase (ThermoFisher #F549S) was used for the PCR reactions according to the manufacturer's manual. The amplicons were purified again and pooled equimolarly. Successful library preparation and correct amplicon length were assessed using the 2100 Bioanalyzer instrument (Agilent). Samples were sequenced on an Illumina HiSeq2500 instrument at the Utrecht Sequencing Facility. Samples that did not pass our quality control criteria due to low read counts were excluded from the analysis. A schematic overview of the CRISPR-Cas9 knockout (KO) screen is depicted in Figure 1A.

Analysis of the data was performed on the web-based analysis platform Galaxy version 0.5.8.4 (usegalaxy.eu), using default parameters. Sequencing reads were analyzed in a Model-based Analysis of Genome-wide CRISPR-Cas9 Knockout (MAGeCK)[76], a publicly available computational tool to identify gene essentiality from the CRISPR-Cas9 knockout screening. sgRNA read counts were normalized to the non-targeting (negative) controls using read mapping files by MAGeCK-count (Galaxy Version 0.5.8.4). We utilized the maximum-likelihood estimations (MLE) module of MAGeCK (Galaxy Version 0.5.8.1), a statistical tool that employs MLE, to determine how essential a gene is to the proliferation and/or viability of the cells, represented by a z-score which quantifies the number of standard deviations by which the normalized read counts for that gene differ from the mean. The difference in z-scores between *KMT2A*-rearranged and wild-type *KMT2A* ALL cell line models were assessed to identify genes specifically essential to either type of ALL.

### **Validation of potential targets by CRISPR-Cas9 knockout competition assays**

Candidate molecular vulnerabilities coming forth from our CRISPR-Cas9 sgRNA library screens were validated by examining cell survival upon gene knockout using a competition assay[43].

The doxycyclin (DOX) inducible pCW-Cas9 vector (Addgene #50661) was utilized to express CAS9. For each target gene, one or two gRNAs were chosen from the CRISPR KO screen sgRNA libraries, complemented with one or two commercially available gRNAs against the genes of interest (Supplementary Table 2, IDT). Each gRNA was cloned into the pLKO5-sgRNA-EFS-GFP vector with the sgRNA under the U6 promoter (Addgene #57822).

The lentivirus containing pCW-Cas9 or pLKO5-sgRNA-EFS-GFP expression vectors were produced, harvested, concentrated, and transduced as described above. The Cas9-expressing cell lines SEM and 697 were established through the transduction of pCW-Cas9 lentivirus, puromycin selection, and testing for Cas9 inducibility by DOX, and then transduced with pLKO5-sgRNA-EFS-GFP lentivirus containing the gRNA of interest. After four days of transduction, the GFP-positive cells were determined, mixed with non-transduced SEM or 697 cells at an equal ratio, and re-analyzed by FACS. This marked day 0 of the CRISPR KO competition assay and was set at 100% of GFP-positivity, as determined using a Beckman Coulter CytoFLEX LX Flow Cytometer with 7AAD viability dye (Biolegend) to discriminate between viable and dead cells. Raw CytoFLEX data were processed using the CytExpert software version 2.3 (Beckman Coulter). The percentage of GFP positive cells, and therefore gRNA-positive cells, were measured at day 3, 7, 14, and 21, and the percentage of GFP positive cells compared to day 0 was calculated. A schematic overview of this competition assay is illustrated in Figure 3E. At day 0 and day 21, cells were harvested, and genomic DNA was isolated using Trizol reagent (Life Technologies) according to the manufacturer's instructions. The percentage of CRISPR KO was determined by performing PCR and Sanger sequencing of the DNA region of interest, followed by Indel quantification of the genomic locus using the Synthego ICE Analysis tool v3.0 (<https://ice.synthego.com>). The primers used are listed in Supplemental table 2.

Ch1

Ch2

Ch3

Ch4

### **Immunoblot analysis**

The levels of protein expression were determined by immunoblot analysis. For this, protein was extracted using RIPA buffer supplemented with protease inhibitors (ThermoScientific), and resolved on precast TGX™ gels and transferred to an 0.2 μm nitrocellulose membrane using a Transblot Turbo Transfer System (Bio-Rad). Blots were then probed with antibodies against MBD3 (#99169S, Cell Signaling Technology), ARID4B (#A302-233A-M Bethyl labs), B-actin (#ab6276 Abcam) or GAPDH (#97166S (Cell Signaling Technology)). The membranes were then probed with infrared-labeled secondary antibodies IRDye 800CW goat-anti-rabbit antibody (#926-32211, LI-COR) and IRDye 680 goat anti-mouse antibody (#926-32220, LI-COR). Proteins were visualized using an Odyssey Infrared Imaging System (LI-COR), and protein expression was quantified using the Odyssey software Image Studio Lite version 4.0.

### **Flowcytometry analysis**

FACS analysis experiments for determination of BMPR2 expressing cells were performed on a CytoFlex Flow Cytometer (Beckman Coulter). Cells were fixed with 1% PFA before blocking with Human TruStain FcX™ (BioLegend) and subsequently labeled with eBioscience™ Fixable Viability Dye eFluor™ 450 (Invitrogen) to select for viable cells. Subsequently the cells were stained with BMPR2 antibody (#ab78422, Abcam) and

PE goat anti mouse IgG as secondary antibody (#405307 BioLegend) according to the manufacturer's recommendation. Raw CytoFLEX data were processed using CytExpert version2.3 (Beckman Coulter).

### **Statistical analysis**

Statistical significance of independent experimental replicates in the graphs were determined using two-sided Student's t-tests as indicated in the figure legends. All statistical analyses were conducted using GraphPad Prism8, version 8.3.4.  $p < 0.05$  was considered statistically significant.

**Supplementary Materials:** The following supporting information can be downloaded at: [www.mdpi.com/xxx/s1](http://www.mdpi.com/xxx/s1), Figure S1: Evaluation of the negative and positive controls; Supplementary Figure 2: Evaluation of the known KMT2A-r ALL vulnerability genes CREBBP. Supplemental table 1: Overview epigenome and kinome sgRNAs ; Supplemental table S2: Overview sequence primers for determining CRISPR KO score.

**Author Contributions:** R.W.S. and P.S. conceived and designed the study; R.W.S. arranged funding; P.S., P.W., S.T.C.J.M.A-P, V.V., F.R.S.A and I.P performed experiments; F.R.S.A and P.W. analyzed data; P.S. processed and analyzed data, and performed statistical analysis; P.S. made figures; P.S and R.W.S. wrote the paper; J.D. and R.P. contributed to review and editing; all authors co-authors performed critical review of the manuscript and gave their final approval; P.S. performed data curation, P.S., and R.W.S. supervised the project.

**Funding:** The present study was financially supported by Foundation KiKa (Stichting Kinderen Kankervrij/Foundation Children Cancer-free), the Netherlands. .

**Institutional Review Board Statement:** Not applicable.

**Informed Consent Statement:** Not applicable.

**Data Availability Statement:** Any information required to reanalyze the data reported in this paper is available from the lead contact upon request.

**Acknowledgments:** We thank the members of the Stam group at the Princess Máxima Center for advice and discussions. We thank Utrecht Sequencing Facility (USEQ) for providing sequencing service and data. Utrecht Sequencing Facility is subsidized by the University Medical Center Utrecht, Hubrecht Institute, Utrecht University and The Netherlands X-omics Initiative (NWO project 184.034.019). We thank Bastiaan Evers for the kind gift of the epigenome and kinome sgRNA libraries.

**Conflicts of Interest:** The authors declare no conflict of interest.

Ch1

Ch2

Ch3

**Ch4**

## REFERENCES

1. Hunger, S.P.; Mullighan, C.G. Acute Lymphoblastic Leukemia in Children. *N Engl J Med* **2015**, *373*, 1541-1552, doi:10.1056/NEJMra1400972.
2. Pieters, R.; De Lorenzo, P.; Ancliffe, P.; Aversa, L.A.; Brethon, B.; Biondi, A.; Campbell, M.; Escherich, G.; Ferster, A.; Gardner, R.A.; et al. Outcome of Infants Younger Than 1 Year With Acute Lymphoblastic Leukemia Treated With the Interfant-06 Protocol: Results From an International Phase III Randomized Study. *J Clin Oncol* **2019**, *37*, 2246-2256, doi:10.1200/JCO.19.00261.
3. Pieters, R.; Schrappe, M.; De Lorenzo, P.; Hann, I.; De Rossi, G.; Felice, M.; Hovi, L.; LeBlanc, T.; Szczepanski, T.; Ferster, A.; et al. A treatment protocol for infants younger than 1 year with acute lymphoblastic leukaemia (Interfant-99): an observational study and a multicentre randomised trial. *Lancet* **2007**, *370*, 240-250, doi:10.1016/S0140-6736(07)61126-X.
4. Meyer, C.; Burmeister, T.; Groger, D.; Tsauro, G.; Fechina, L.; Renneville, A.; Sutton, R.; Venn, N.C.; Emerenciano, M.; Pombo-de-Oliveira, M.S.; et al. The MLL recombinome of acute leukemias in 2017. *Leukemia* **2018**, *32*, 273-284, doi:10.1038/leu.2017.213.
5. Ernst, P.; Wang, J.; Korsmeyer, S.J. The role of MLL in hematopoiesis and leukemia. *Curr Opin Hematol* **2002**, *9*, 282-287, doi:10.1097/00062752-200207000-00004.
6. Krivtsov, A.V.; Armstrong, S.A. MLL translocations, histone modifications and leukaemia stem-cell development. *Nat Rev Cancer* **2007**, *7*, 823-833, doi:10.1038/nrc2253.
7. Ernst, P.; Fisher, J.K.; Avery, W.; Wade, S.; Foy, D.; Korsmeyer, S.J. Definitive hematopoiesis requires the mixed-lineage leukemia gene. *Dev Cell* **2004**, *6*, 437-443, doi:10.1016/s1534-5807(04)00061-9.
8. Yokoyama, A. Molecular mechanisms of MLL-associated leukemia. *Int J Hematol* **2015**, *101*, 352-361, doi:10.1007/s12185-015-1774-4.
9. Bernt, K.M.; Zhu, N.; Sinha, A.U.; Vempati, S.; Faber, J.; Krivtsov, A.V.; Feng, Z.; Punt, N.; Daigle, A.; Bullinger, L.; et al. MLL-rearranged leukemia is dependent on aberrant H3K79 methylation by DOT1L. *Cancer Cell* **2011**, *20*, 66-78, doi:10.1016/j.ccr.2011.06.010.
10. Krivtsov, A.V.; Feng, Z.; Lemieux, M.E.; Faber, J.; Vempati, S.; Sinha, A.U.; Xia, X.; Jesneck, J.; Bracken, A.P.; Silverman, L.B.; et al. H3K79 methylation profiles define murine and human MLL-AF4 leukemias. *Cancer Cell* **2008**, *14*, 355-368, doi:10.1016/j.ccr.2008.10.001.
11. Armstrong, S.A.; Staunton, J.E.; Silverman, L.B.; Pieters, R.; den Boer, M.L.; Minden, M.D.; Sallan, S.E.; Lander, E.S.; Golub, T.R.; Korsmeyer, S.J. MLL translocations specify a distinct gene expression profile that distinguishes a unique leukemia. *Nat Genet* **2002**, *30*, 41-47, doi:10.1038/ng765.
12. Stam, R.W.; Schneider, P.; Hagelstein, J.A.; van der Linden, M.H.; Stumpel, D.J.; de Menezes, R.X.; de Lorenzo, P.; Valsecchi, M.G.; Pieters, R. Gene expression profiling-based dissection of MLL translocated and MLL germline acute lymphoblastic leukemia in infants. *Blood* **2010**, *115*, 2835-2844, doi:10.1182/blood-2009-07-233049.
13. van der Sluis, I.M.; de Lorenzo, P.; Kotecha, R.S.; Attarbaschi, A.; Escherich, G.; Nysom, K.; Stary, J.; Ferster, A.; Brethon, B.; Locatelli, F.; et al. Blinatumomab Added to Chemotherapy in Infant Lymphoblastic Leukemia. *N Engl J Med* **2023**, *388*, 1572-1581, doi:10.1056/NEJMoa221471.
14. Garrido Castro, P.; van Roon, E.H.J.; Pinhancos, S.S.; Trentin, L.; Schneider, P.; Kerstjens, M.; Te Kronnie, G.; Heidenreich, O.; Pieters, R.; Stam, R.W. The HDAC inhibitor panobinostat (LBH589) exerts in vivo anti-leukaemic activity against MLL-rearranged acute lymphoblastic leukaemia



- and involves the RNF20/RNF40/WAC-H2B ubiquitination axis. *Leukemia* **2018**, *32*, 323-331, doi:10.1038/leu.2017.216. Ch1
15. Stumpel, D.J.; Schneider, P.; Seslija, L.; Osaki, H.; Williams, O.; Pieters, R.; Stam, R.W. Connectivity mapping identifies HDAC inhibitors for the treatment of t(4;11)-positive infant acute lymphoblastic leukemia. *Leukemia* **2012**, *26*, 682-692, doi:10.1038/leu.2011.278. Ch2
16. Biersack, B.; Nitzsche, B.; Hopfner, M. Immunomodulatory properties of HDAC6 inhibitors in cancer diseases: New chances for sophisticated drug design and treatment optimization. *Semin Cell Dev Biol* **2022**, doi:10.1016/j.semcdb.2022.09.009. Ch3
17. Waitman, K.; Parise-Filho, R. New kinase and HDAC hybrid inhibitors: recent advances and perspectives. *Future Med Chem* **2022**, *14*, 745-766, doi:10.4155/fmc-2021-0276. Ch4
18. Brown, P.A.; Kairalla, J.A.; Hilden, J.M.; Dreyer, Z.E.; Carroll, A.J.; Heerema, N.A.; Wang, C.; Devidas, M.; Gore, L.; Salzer, W.L.; et al. FLT3 inhibitor lestaurtinib plus chemotherapy for newly diagnosed *KMT2A*-rearranged infant acute lymphoblastic leukemia: Children's Oncology Group trial AALL0631. *Leukemia* **2021**, *35*, 1279-1290, doi:10.1038/s41375-021-01177-6.
19. Hopkins, A.L.; Groom, C.R. The druggable genome. *Nat Rev Drug Discov* **2002**, *1*, 727-730, doi:10.1038/nrd892.
20. Doudna, J.A.; Charpentier, E. Genome editing. The new frontier of genome engineering with CRISPR-Cas9. *Science* **2014**, *346*, 1258096, doi:10.1126/science.1258096.
21. Shalem, O.; Sanjana, N.E.; Hartenian, E.; Shi, X.; Scott, D.A.; Mikkelsen, T.; Heckl, D.; Ebert, B.L.; Root, D.E.; Doench, J.G.; et al. Genome-scale CRISPR-Cas9 knockout screening in human cells. *Science* **2014**, *343*, 84-87, doi:10.1126/science.1247005.
22. Evers, B.; Jastrzebski, K.; Heijmans, J.P.; Grønrum, W.; Beijersbergen, R.L.; Bernards, R. CRISPR knockout screening outperforms shRNA and CRISPRi in identifying essential genes. *Nat Biotechnol* **2016**, *34*, 631-633, doi:10.1038/nbt.3536.
23. Wang, C.; Jin, H.; Gao, D.; Wang, L.; Evers, B.; Xue, Z.; Jin, G.; Lieftink, C.; Beijersbergen, R.L.; Qin, W.; et al. A CRISPR screen identifies CDK7 as a therapeutic target in hepatocellular carcinoma. *Cell Res* **2018**, *28*, 690-692, doi:10.1038/s41422-018-0020-z.
24. Fellmann, C.; Gowen, B.G.; Lin, P.C.; Doudna, J.A.; Corn, J.E. Cornerstones of CRISPR-Cas in drug discovery and therapy. *Nat Rev Drug Discov* **2017**, *16*, 89-100, doi:10.1038/nrd.2016.238.
25. Wilkinson, A.C.; Ballabio, E.; Geng, H.; North, P.; Tapia, M.; Kerry, J.; Biswas, D.; Roeder, R.G.; Allis, C.D.; Melnick, A.; et al. RUNX1 is a key target in t(4;11) leukemias that contributes to gene activation through an AF4-MLL complex interaction. *Cell Rep* **2013**, *3*, 116-127, doi:10.1016/j.celrep.2012.12.016.
26. Zuber, J.; Shi, J.; Wang, E.; Rappaport, A.R.; Herrmann, H.; Sison, E.A.; Magoon, D.; Qi, J.; Blatt, K.; Wunderlich, M.; et al. RNAi screen identifies Brd4 as a therapeutic target in acute myeloid leukaemia. *Nature* **2011**, *478*, 524-528, doi:10.1038/nature10334.
27. Cheung, N.; Chan, L.C.; Thompson, A.; Cleary, M.L.; So, C.W. Protein arginine-methyltransferase-dependent oncogenesis. *Nat Cell Biol* **2007**, *9*, 1208-1215, doi:10.1038/ncb1642.
28. Dou, Y.; Milne, T.A.; Tackett, A.J.; Smith, E.R.; Fukuda, A.; Wysocka, J.; Allis, C.D.; Chait, B.T.; Hess, J.L.; Roeder, R.G. Physical association and coordinate function of the H3 K4 methyltransferase MLL1 and the H4 K16 acetyltransferase MOF. *Cell* **2005**, *121*, 873-885, doi:10.1016/j.cell.2005.04.031.

29. Rozenblatt-Rosen, O.; Rozovskaia, T.; Burakov, D.; Sedkov, Y.; Tillib, S.; Blechman, J.; Nakamura, T.; Croce, C.M.; Mazo, A.; Canaani, E. The C-terminal SET domains of ALL-1 and TRITHORAX interact with the INI1 and SNR1 proteins, components of the SWI/SNF complex. *Proc Natl Acad Sci U S A* **1998**, *95*, 4152-4157, doi:10.1073/pnas.95.8.4152.
30. Nie, Z.; Yan, Z.; Chen, E.H.; Sechi, S.; Ling, C.; Zhou, S.; Xue, Y.; Yang, D.; Murray, D.; Kanakubo, E.; et al. Novel SWI/SNF chromatin-remodeling complexes contain a mixed-lineage leukemia chromosomal translocation partner. *Mol Cell Biol* **2003**, *23*, 2942-2952, doi:10.1128/mcb.23.8.2942-2952.2003.
31. Lillico, R.; Lawrence, C.K.; Lakowski, T.M. Selective DOT1L, LSD1, and HDAC Class I Inhibitors Reduce HOXA9 Expression in MLL-AF9 Rearranged Leukemia Cells, But Dysregulate the Expression of Many Histone-Modifying Enzymes. *J Proteome Res* **2018**, *17*, 2657-2667, doi:10.1021/acs.jproteome.8b00118.
32. Steward, M.M.; Lee, J.S.; O'Donovan, A.; Wyatt, M.; Bernstein, B.E.; Shilatifard, A. Molecular regulation of H3K4 trimethylation by ASH2L, a shared subunit of MLL complexes. *Nat Struct Mol Biol* **2006**, *13*, 852-854, doi:10.1038/nsmb1131.
33. El Ashkar, S.; Schwaller, J.; Pieters, T.; Goossens, S.; Demeulemeester, J.; Christ, F.; Van Belle, S.; Juge, S.; Boeckx, N.; Engelman, A.; et al. LEDGF/p75 is dispensable for hematopoiesis but essential for MLL-rearranged leukemogenesis. *Blood* **2018**, *131*, 95-107, doi:10.1182/blood-2017-05-786962.
34. Milne, T.A. LEDGF: a leukemia-specific target. *Blood* **2018**, *131*, 4-5, doi:10.1182/blood-2017-11-815449.
35. Dutta, R.; Tiu, B.; Sakamoto, K.M. CBP/p300 acetyltransferase activity in hematologic malignancies. *Mol Genet Metab* **2016**, *119*, 37-43, doi:10.1016/j.ymgme.2016.06.013.
36. Armstrong, S.A.; Kung, A.L.; Mabon, M.E.; Silverman, L.B.; Stam, R.W.; Den Boer, M.L.; Pieters, R.; Kersey, J.H.; Sallan, S.E.; Fletcher, J.A.; et al. Inhibition of FLT3 in MLL. Validation of a therapeutic target identified by gene expression based classification. *Cancer Cell* **2003**, *3*, 173-183, doi:10.1016/s1535-6108(03)00003-5.
37. Stam, R.W.; den Boer, M.L.; Schneider, P.; Meier, M.; Beverloo, H.B.; Pieters, R. D-HPLC analysis of the entire FLT3 gene in MLL rearranged and hyperdiploid acute lymphoblastic leukemia. *Haematologica* **2007**, *92*, 1565-1568, doi:10.3324/haematol.11220.
38. Stam, R.W.; den Boer, M.L.; Schneider, P.; Nollau, P.; Horstmann, M.; Beverloo, H.B.; van der Voort, E.; Valsecchi, M.G.; de Lorenzo, P.; Sallan, S.E.; et al. Targeting FLT3 in primary MLL-gene-rearranged infant acute lymphoblastic leukemia. *Blood* **2005**, *106*, 2484-2490, doi:10.1182/blood-2004-09-3667.
39. Stam, R.W.; Schneider, P.; de Lorenzo, P.; Valsecchi, M.G.; den Boer, M.L.; Pieters, R. Prognostic significance of high-level FLT3 expression in MLL-rearranged infant acute lymphoblastic leukemia. *Blood* **2007**, *110*, 2774-2775, doi:10.1182/blood-2007-05-091934.
40. Enserink, J.M.; Chymkowitch, P. Cell Cycle-Dependent Transcription: The Cyclin Dependent Kinase Cdk1 Is a Direct Regulator of Basal Transcription Machinery. *Int J Mol Sci* **2022**, *23*, doi:10.3390/ijms23031293.
41. Enserink, J.M.; Kolodner, R.D. An overview of Cdk1-controlled targets and processes. *Cell Div* **2010**, *5*, 11, doi:10.1186/1747-1028-5-11.
42. Morgan, D.O. Cyclin-dependent kinases: engines, clocks, and microprocessors. *Annu Rev Cell Dev Biol* **1997**, *13*, 261-291, doi:10.1146/annurev.cellbio.13.1.261.

43. Girish, V.; Sheltzer, J.M. A CRISPR Competition Assay to Identify Cancer Genetic Dependencies. *Bio Protoc* **2020**, *10*, e3682, doi:10.21769/BioProtoc.3682. Ch1
44. Shi, J.; Wang, E.; Milazzo, J.P.; Wang, Z.; Kinney, J.B.; Vakoc, C.R. Discovery of cancer drug targets by CRISPR-Cas9 screening of protein domains. *Nat Biotechnol* **2015**, *33*, 661-667, doi:10.1038/nbt.3235. Ch2
45. Tsai, W.C.; Hueng, D.Y.; Nieh, S.; Gao, H.W. ARID4B is a good biomarker to predict tumour behaviour and decide WHO grades in gliomas and meningiomas. *J Clin Pathol* **2017**, *70*, 162-167, doi:10.1136/jclinpath-2016-203804. Ch3
46. Wang, R.; Yu, Z.; Chen, F.; Liao, C.; Wang, Q.; Huang, X. Overexpression of ARID4B predicts poor survival in patients with hepatocellular carcinoma. *Hum Pathol* **2018**, *73*, 114-121, doi:10.1016/j.humpath.2017.12.012. Ch4
47. Winter, S.F.; Lukes, L.; Walker, R.C.; Welch, D.R.; Hunter, K.W. Allelic variation and differential expression of the mSIN3A histone deacetylase complex gene *Arid4b* promote mammary tumor growth and metastasis. *PLoS Genet* **2012**, *8*, e1002735, doi:10.1371/journal.pgen.1002735.
48. G, G.U.; Terz, I.C.N. *Arid4b* alters cell cycle and cell death dynamics during mouse embryonic stem cell differentiation. *Turk J Biol* **2021**, *45*, 56-64, doi:10.3906/biy-2009-6.
49. Lin, C.; Song, W.; Bi, X.; Zhao, J.; Huang, Z.; Li, Z.; Zhou, J.; Cai, J.; Zhao, H. Recent advances in the ARID family: focusing on roles in human cancer. *Onco Targets Ther* **2014**, *7*, 315-324, doi:10.2147/OTT.S57023.
50. Terzi Cizmecioglu, N.; Huang, J.; Keskin, E.G.; Wang, X.; Esen, I.; Chen, F.; Orkin, S.H. ARID4B is critical for mouse embryonic stem cell differentiation towards mesoderm and endoderm, linking epigenetics to pluripotency exit. *J Biol Chem* **2020**, *295*, 17738-17751, doi:10.1074/jbc.RA120.015534.
51. Young, I.C.; Wu, B.; Andricovich, J.; Chuang, S.T.; Li, R.; Tzatsos, A.; Wu, R.C.; Wu, M.Y. Differentiation of fetal hematopoietic stem cells requires ARID4B to restrict autocrine KITLG/KIT-*Src* signaling. *Cell Rep* **2021**, *37*, 110036, doi:10.1016/j.celrep.2021.110036.
52. Luo, S.M.; Tsai, W.C.; Tsai, C.K.; Chen, Y.; Hueng, D.Y. ARID4B Knockdown Suppresses PI3K/AKT Signaling and Induces Apoptosis in Human Glioma Cells. *Onco Targets Ther* **2021**, *14*, 1843-1855, doi:10.2147/OTT.S286837.
53. Wu, R.C.; Young, I.C.; Chen, Y.F.; Chuang, S.T.; Toubaji, A.; Wu, M.Y. Identification of the PTEN-ARID4B-PI3K pathway reveals the dependency on ARID4B by PTEN-deficient prostate cancer. *Nat Commun* **2019**, *10*, 4332, doi:10.1038/s41467-019-12184-8.
54. Fleischer, T.C.; Yun, U.J.; Ayer, D.E. Identification and characterization of three new components of the mSin3A corepressor complex. *Mol Cell Biol* **2003**, *23*, 3456-3467, doi:10.1128/MCB.23.10.3456-3467.2003.
55. Hassig, C.A.; Fleischer, T.C.; Billin, A.N.; Schreiber, S.L.; Ayer, D.E. Histone deacetylase activity is required for full transcriptional repression by mSin3A. *Cell* **1997**, *89*, 341-347, doi:10.1016/s0092-8674(00)80214-7.
56. Loughran, S.J.; Comoglio, F.; Hamey, F.K.; Giustacchini, A.; Errami, Y.; Earp, E.; Gottgens, B.; Jacobsen, S.E.W.; Mead, A.J.; Hendrich, B.; et al. Mbd3/NuRD controls lymphoid cell fate and inhibits tumorigenesis by repressing a B cell transcriptional program. *J Exp Med* **2017**, *214*, 3085-3104, doi:10.1084/jem.20161827.

57. Shimbo, T.; Du, Y.; Grimm, S.A.; Dhasarathy, A.; Mav, D.; Shah, R.R.; Shi, H.; Wade, P.A. MBD3 localizes at promoters, gene bodies and enhancers of active genes. *PLoS Genet* **2013**, *9*, e1004028, doi:10.1371/journal.pgen.1004028.
58. Yildirim, O.; Li, R.; Hung, J.H.; Chen, P.B.; Dong, X.; Ee, L.S.; Weng, Z.; Rando, O.J.; Fazio, T.G. Mbd3/NURD complex regulates expression of 5-hydroxymethylcytosine marked genes in embryonic stem cells. *Cell* **2011**, *147*, 1498-1510, doi:10.1016/j.cell.2011.11.054.
59. Cui, J.; Duan, B.; Zhao, X.; Chen, Y.; Sun, S.; Deng, W.; Zhang, Y.; Du, J.; Chen, Y.; Gu, L. MBD3 mediates epigenetic regulation on EPAS1 promoter in cancer. *Tumour Biol* **2016**, *37*, 13455-13467, doi:10.1007/s13277-016-5237-1.
60. Shimbo, T.; Takaku, M.; Wade, P.A. High-quality ChIP-seq analysis of MBD3 in human breast cancer cells. *Genom Data* **2016**, *7*, 173-174, doi:10.1016/j.gdata.2015.12.029.
61. Yan, W.; Han, Q.; Gong, L.; Zhan, X.; Li, W.; Guo, Z.; Zhao, J.; Li, T.; Bai, Z.; Wu, J.; et al. MBD3 promotes hepatocellular carcinoma progression and metastasis through negative regulation of tumour suppressor TFPI2. *Br J Cancer* **2022**, *127*, 612-623, doi:10.1038/s41416-022-01831-5.
62. Zhu, Y.; Harrison, D.J.; Bader, S.A. Genetic and epigenetic analyses of MBD3 in colon and lung cancer. *Br J Cancer* **2004**, *90*, 1972-1975, doi:10.1038/sj.bjc.6601776.
63. Raymond, A.; Liu, B.; Liang, H.; Wei, C.; Guindani, M.; Lu, Y.; Liang, S.; St John, L.S.; Molldrem, J.; Nagarajan, L. A role for BMP-induced homeobox gene MIXL1 in acute myelogenous leukemia and identification of type I BMP receptor as a potential target for therapy. *Oncotarget* **2014**, *5*, 12675-12693, doi:10.18632/oncotarget.2564.
64. Toofan, P.; Busch, C.; Morrison, H.; O'Brien, S.; Jorgensen, H.; Copland, M.; Wheadon, H. Chronic myeloid leukaemia cells require the bone morphogenic protein pathway for cell cycle progression and self-renewal. *Cell Death Dis* **2018**, *9*, 927, doi:10.1038/s41419-018-0905-2.
65. Toofan, P.; Irvine, D.; Hopcroft, L.; Copland, M.; Wheadon, H. The role of the bone morphogenetic proteins in leukaemic stem cell persistence. *Biochem Soc Trans* **2014**, *42*, 809-815, doi:10.1042/BST20140037.
66. Toofan, P.; Wheadon, H. Role of the bone morphogenic protein pathway in developmental haemopoiesis and leukaemogenesis. *Biochem Soc Trans* **2016**, *44*, 1455-1463, doi:10.1042/BST20160104.
67. Topic, I.; Ikić, M.; Ivcević, S.; Kovacic, N.; Marusic, A.; Kusec, R.; Grcević, D. Bone morphogenetic proteins regulate differentiation of human promyelocytic leukemia cells. *Leuk Res* **2013**, *37*, 705-712, doi:10.1016/j.leukres.2013.03.002.
68. Jiramongkolchai, P.; Owens, P.; Hong, C.C. Emerging roles of the bone morphogenetic protein pathway in cancer: potential therapeutic target for kinase inhibition. *Biochem Soc Trans* **2016**, *44*, 1117-1134, doi:10.1042/BST20160069.
69. Kim, M.J.; Park, S.Y.; Chang, H.R.; Jung, E.Y.; Munkhjargal, A.; Lim, J.S.; Lee, M.S.; Kim, Y. Clinical significance linked to functional defects in bone morphogenetic protein type 2 receptor, BMPR2. *BMB Rep* **2017**, *50*, 308-317, doi:10.5483/bmbrep.2017.50.6.059.
70. Attisano, L.; Wrana, J.L. Signal transduction by the TGF-beta superfamily. *Science* **2002**, *296*, 1646-1647, doi:10.1126/science.1071809.
71. Huang, P.; Chen, A.; He, W.; Li, Z.; Zhang, G.; Liu, Z.; Liu, G.; Liu, X.; He, S.; Xiao, G.; et al. BMP-2

- induces EMT and breast cancer stemness through Rb and CD44. *Cell Death Discov* **2017**, *3*, 17039, doi:10.1038/cddiscovery.2017.39. Ch1
72. Zhang, G.; Huang, P.; Chen, A.; He, W.; Li, Z.; Liu, G.; Wang, J. How BMP-2 induces EMT and breast cancer stemness through Rb and CD44? *Cell Death Dis* **2018**, *9*, 20, doi:10.1038/s41419-017-0037-0. Ch2
73. Issa, G.C.; Aldoss, I.; DiPersio, J.; Cuglievan, B.; Stone, R.; Arellano, M.; Thirman, M.J.; Patel, M.R.; Dickens, D.S.; Shenoy, S.; et al. The menin inhibitor revumenib in *KMT2A*-rearranged or *NPM1*-mutant leukaemia. *Nature* **2023**, *615*, 920-924, doi:10.1038/s41586-023-05812-3. Ch3
74. Gobbi, A.; Di Bernardino, C.; Scanziani, E.; Garofalo, A.; Rivolta, A.; Fontana, G.; Rambaldi, A.; Giavazzi, R.; Biondi, A. A human acute lymphoblastic leukemia line with the T(4;11) translocation as a model of minimal residual disease in SCID mice. *Leuk Res* **1997**, *21*, 1107-1114, doi:10.1016/s0145-2126(97)00092-1. Ch4
75. Joungh, J.; Konermann, S.; Gootenberg, J.S.; Abudayyeh, O.O.; Platt, R.J.; Brigham, M.D.; Sanjana, N.E.; Zhang, F. Genome-scale CRISPR-Cas9 knockout and transcriptional activation screening. *Nat Protoc* **2017**, *12*, 828-863, doi:10.1038/nprot.2017.016.
76. Li, W.; Xu, H.; Xiao, T.; Cong, L.; Love, M.I.; Zhang, F.; Irizarry, R.A.; Liu, J.S.; Brown, M.; Liu, X.S. MAGECK enables robust identification of essential genes from genome-scale CRISPR/Cas9 knockout screens. *Genome Biol* **2014**, *15*, 554, doi:10.1186/s13059-014-0554-4.



# CHAPTER 5

## Identification and characterization of relapse-initiating cells in *MLL*-rearranged infant ALL by single-cell transcriptomics



Tito Candelli<sup>1\*</sup>, Pauline Schneider<sup>1\*</sup>, Patricia Garrido Castro<sup>1</sup>, Luke A. Jones<sup>1</sup>, Eduard Bodewes<sup>1</sup>, Dedeke Rockx-Brouwer<sup>1</sup>, Rob Pieters<sup>1</sup>, Frank C. P. Holstege<sup>1\*</sup>, Thanasis Margaritis<sup>1\*</sup> and Ronald W. Stam<sup>1\*</sup>

<sup>1</sup>*Princess Máxima Center for Pediatric Oncology,  
Heidelberglaan 25, 3584 CS Utrecht, the Netherlands*

\*Both authors contributed equally

Leukemia (2022) 36:58–67

## **ABSTRACT**

Infants with MLL-rearranged infant acute lymphoblastic leukemia (MLL-r iALL) undergo intense therapy to counter a highly aggressive malignancy with survival rates of only 30–40%. The majority of patients initially show therapy response, but in two-thirds of cases the leukemia returns, typically during treatment. The glucocorticoid drug prednisone is established as a major player in the treatment of leukemia and the in vivo response to prednisone monotherapy is currently the best indicator of risk for MLL-r iALL. We used two different single-cell RNA sequencing technologies to analyze the expression of a prednisone-dependent signature, derived from an independent study, in diagnostic bone marrow and peripheral blood biopsies. This allowed us to classify individual leukemic cells as either resistant or sensitive to treatment and show that quantification of these two groups can be used to better predict the occurrence of future relapse in individual patients. This work also sheds light on the nature of the therapy-resistant subpopulation of relapse-initiating cells. Leukemic cells associated with high relapse risk are characterized by basal activation of glucocorticoid response, smaller size, and a quiescent gene expression program with cell stemness properties. These results improve current risk stratification and elucidate leukemic therapy-resistant subpopulations at diagnosis.



## INTRODUCTION

Acute lymphoblastic leukemia (ALL) in infants (i.e., children < 1 year of age) is frequently driven by chromosomal translocations of the *mixed lineage leukemia* (*MLL* or *KMT2A*) gene, which occur in

~80% of the cases. Translocations of the *MLL* gene on chromosome 11q23 lead to fusions of the N-terminus of *MLL* to the C-terminus of one of many known translocation partner genes. The majority of infant ALL patients carry one of three recurrent types of *MLL* translocations in which the *MLL* gene becomes fused to either *AF4* (aka *AFF1*; 49% of the cases), *ENL* (aka *MLLT1*; 22% of the cases), or *AF9* (aka *MLLT3*; 16% of the cases) [1]. *MLL*-rearranged infant ALL (*MLL-r iALL*) represents a rare but highly aggressive type of childhood leukemia that is notoriously characterized by chemotherapy resistance and high relapse rates, leading to a very poor prognosis. Regardless of the type of *MLL* translocation, event-free survival (EFS) rates for *MLL-r iALL* patients remain at 30–40% when treated according to the international collaborative INTERFANT treatment protocol [2, 3], whereas cases without *MLL* translocations fare significantly better at 75–80%.

Despite the massive disparity in EFS, the majority (~95%) of *MLL-r iALL* patients seemingly achieve disease remission after induction therapy. In two-thirds of the cases, however, the leukemia reemerges, typically within the first year from diagnosis and while still on treatment, giving rise to an even more chemotherapy-resistant form.

Relapse occurrence in infant ALL is usually fatal and despite advances in the field its mechanism still needs to be elucidated. Currently, one of the best predictors of future relapse occurrence is the response to a 7-day window of prednisone monotherapy administered prior to induction therapy [2, 3]. This suggests that predisposition to the effects of prednisone at diagnosis might play a pivotal role in the development of relapse. Many hypotheses about relapse emergence also involve cellular heterogeneity [4–10] and a high degree of clonal heterogeneity has been observed in *MLL-r iALL* [11, 12].

To shed light on the interplay between sensitivity to prednisone, cell heterogeneity, and relapse occurrence, we decided to exploit the transformative ability of single-cell RNA sequencing (scRNA-seq) to analyze heterogeneous systems [13–18]. This allowed us to accurately predict which patients were at high risk of leukemia relapse, based on scRNA-seq analyses on diagnostic primary *MLL-r iALL* samples. In addition, we were able to characterize the nature of these relapse-predicting cells.

Ch1

Ch2

Ch3

Ch4

Ch5

## **METHODS**

### **Patient samples**

Bone marrow (BM) biopsies and peripheral blood (PB) samples taken at diagnosis were from infants (<1 year of age) with *MLL*-rearranged ALL and treated according to the international collaborative Interfant-99 and Interfant-06 protocols [2, 3]. We did not distinguish between the two protocols as the treatment differences between the two are minimal and no outcome differences were detected [3]. Samples used were from *MLL*-rearranged pro-B infant ALL patients, carrying either of the two most common *MLL* fusion genes, i.e., *MLL-AF4* or *MLL-ENL* [19], and with cell viability over 65%. Samples were either from patients with at least 7-year relapse-free survival or from patients who experienced relapse within 2 years after diagnosis. Care was taken to spread attributes such as sex and translocation type across the dataset (Table 1). Informed consent was obtained from the parents or legal guardians according to the Helsinki Declaration. BM and PB samples were processed as described [20]. Leukemic blast percentages (Table 1) were determined microscopically using May-Grünwald-Giemsa stained cytopsin preparations.

### **Single-cell RNA sequencing**

Samples were sorted into 384-well plates (SORT-seq, primers shown in Supplementary Table 1) or tubes (10x Genomics) using FACS sorting. The gating strategy employed for sorting is shown in Supplementary Figure 1. See Supplementary Methods for more details.

For SORT-seq, 384-well plates with sorted cells were processed into Illumina sequencing libraries as described [21, 22] and preprocessed as in ref. [23]. Because of their high variation in gene expression, at this stage mitochondrial genes were removed. A minimum transcripts threshold was set to 500 transcripts per cell. The number of detected genes and adequacy of sequencing were evaluated in Supplementary Figure 2a, b.

10x Genomics processed samples were prepared and sequenced according to the manufacturer's protocol using the Illumina NextSeq500 sequencer. Reads were processed with the zUMIs pipeline version 2.2.0 using the same genome and annotation version as in ref. [23]. At this stage, mitochondrial genes were removed and all barcodes with less than 500 transcripts were excluded.

### **scRNA-seq analysis**

For BM samples, further analysis was performed using R version 3.3.4 and the package Seurat [24] version 2.1.0 with default parameters unless stated otherwise. Per-cell transcript counts were normalized to 3500 transcripts. The first 15 principal

components (PCs) of a PC analysis (PCA) were used to generate t-distributed stochastic neighbor embedding plots (Figure 1b, c, Supplementary Figure 2) and perform Louvain clustering [24] (Figure 1c) using a resolution of 1.1. Cluster number 9 consisted of T cells (Supplementary Figure 2c, d) and was excluded from further analyses.

For PB samples, further analysis was performed using R version 3.6.0 and the package Seurat version 3.0.2 with default parameters unless stated otherwise. Normalization was performed using SCTransform [25]. Gene filtering was performed as in ref. [23]. The following genes were removed from all analyses: XIST and TSIX genes as well as all genes on the Y chromosome and hemoglobin genes. The first 30 PCs were used to perform Louvain clustering [24] using a resolution of 1.

### **Gene module scores**

Genes used for the calculation of the sensitivity and resistance module scores were obtained from ref. [26] and are shown in Supplementary Table 2. Calculation of module scores was performed using the Seurat AddModuleScore function with modifications [24]. Briefly, each gene is classified into an expression bin according to its average expression across all cells. To obtain the score, for each cell, each chosen gene's expression is compared to the average of 100 randomly chosen genes from the same expression bin as a control. The difference between each chosen gene's expression and its matching control value is then averaged across all chosen genes, yielding the final module score.

### **Categorization of sensitive and resistant cells**

Cells were categorized as sensitive when their sensitivity score was above the median sensitivity score of the complete dataset and their resistance score was below the median resistance score calculated over the whole dataset. Vice versa, cells were categorized as resistant when their resistance score was above and their sensitivity score was below the corresponding median scores of the dataset.

### **PC score**

The PC score constitutes the first PC of a PCA calculated using the union of sensitivity and resistance module genes on scaled log normalized expression values (see "Gene module scores" section above). As depicted in Supplementary Figure 3, a high PC score corresponds to cells with a predicted high sensitivity to treatment.

### **In vitro prednisolone treatment**

In vitro drug exposures were performed by incubation with 100 µg/mL prednisolone (BUFA, Uitgeest, The Netherlands), the liver-activated form of prednisone, or with vehicle for 3 days. Cells were viably frozen [20] and later thawed for scRNA-seq. All processed samples had at least 90% blasts.

Ch1

Ch2

Ch3

Ch4

Ch5

## **PB differential expression**

To determine genes differentially expressed between sensitive and resistant cells in 15 PB samples processed with SORT-seq, we defined cells as sensitive or resistant depending on their module scores (see the “Methods” section). This yielded 1722 cells in each group. Differential expression was calculated using the FindMarkers function with default arguments. The resulting  $p$  values were Bonferroni multiple-testing corrected. Genes with an adjusted  $p$  value lower than 0.05 and with an average log fold change (natural log) above 0.20 were considered differentially expressed.

Gene Ontology (GO) enrichment GO category enrichment was calculated using the compareCluster function from the clusterProfiler R package [27], see Supplementary Methods for details.

## **RESULTS**

### **Clustering of leukemic cells according to individual patients**

To identify subpopulations of cells potentially associated with relapse, we analyzed leukemic cells derived from BM biopsies taken at diagnosis. These samples were obtained from seven *MLL-r iALL* patients covering the two most recurrent *MLL* translocations, t(4;11) and t(11;19), giving rise to the *MLL* fusion genes *MLL-AF4* and *MLL-ENL*, respectively [1–3, 21]. We processed the samples into scRNA-seq libraries using SORT-seq [21] (Figure 1A), a medium-throughput platform that provides high sensitivity [28] and cytometric data on individual cells. As anticipated, cells clustered largely according to individual patients (Figure 1B, C). This agrees well with the personalized nature of cancer [29] and the substantial patient-to-patient heterogeneity of *MLL-r iALL* [11, 12].

We identified two clusters with contribution from multiple patients. These were revealed to be highly proliferating blasts (Supplementary Figure 2C, F–G) and healthy T cells (Supplementary Figure 2C–E). The latter were removed from further analyses.

Unsupervised clustering did not group leukemic cells by characteristics such as sex, translocation type, or relapse occurrence (Supplementary Figure 2H), underscoring the distinct nature of individual cancers and the challenge of accurately predicting treatment outcome.

### **Single-cell analysis predicts relapse occurrence in *MLL-r iALL* BM biopsies**

The glucocorticoid drug prednisone is one of the cornerstones of the treatment of ALLs [30]. The response to 1 week of prednisone monotherapy is considered a major parameter for current risk stratification and a strong predictor of clinical outcome [2, 3, 30]. The

response to this drug has been studied by a variety of approaches, including bulk mRNA measurements in samples derived from pediatric ALL patients [26].

Rather than interpreting these results as revealing a prednisone gene expression response, we reasoned that apparent up- and downregulation of specific genes might be at least partially driven by a process of Darwinian selection. Gene signatures specific to a preexisting subset of prednisone-resistant cells would emerge as upregulated after treatment by virtue of their higher survival rate even if their expression levels remain constant, while signatures specific to cells sensitive to treatment would appear down-regulated for the opposite reason (Figure 1D). Following this logic, genes upregulated after prednisone exposure mark leukemic cells with a high chance of surviving treatment, while genes with apparent downregulation represent markers of cells sensitive to treatment and therefore preferentially eliminated by prednisone exposure.

To explore this possibility, we took advantage of published differential expression results from the work of Rhein et al. [26] obtained by comparing prednisone-treated samples with matched diagnosis samples. We considered two gene modules consisting of 78 upregulated and 370 downregulated genes (Supplementary Table 2) [26], respectively. Based on the expression of the two gene modules, we classified individual cells as being sensitive or resistant to therapy. The distribution of cells is a continuum from apparent sensitivity to apparent resistance and the two modules strongly anticorrelate with each other (Figure 1E). This strengthens the notion that these are not two independent signatures, but a common set of intrinsic properties that are mutually exclusive. Strikingly, labeling the cells according to future relapse occurrence reveals a significant difference in both modules, implicating the sensitivity and resistance markers in the process of relapse development.

To further test the predictive capability of our data, we examined the single-cell classification in individual patients (Figure 1F). Visual inspection indicates more resistant-predicted cells (Figure 1F, bottom-right quadrants) in patients who eventually relapsed and more sensitive-predicted cells (upper-left quadrants) in patients who remained relapse-free. For quantitative comparison, we calculated the percentage of cells classified as sensitive/ resistant for each diagnostic sample. This yielded a strong distinction between patients with and without relapse (Figure 1G). As a further control and for future ease of comparison with other metrics, we used PCA to assign a singular value to each cell representing the position along the sensitivity-resistance continuum (Figure 1H, see Supplementary Figure 3A–D for how well the first PC embodies the signal from the two modules). As expected, PC score is able to

Ch1

Ch2

Ch3

Ch4

Ch5

**Table 1. Overview of the patient samples used in this study, their characteristics, Interfant risk stratification, and number of sequenced cells.**

Sample ID BM	1977N	1702N	635N	8010R	6806R	4483R	4484R	3595R	6487R	1776R	175R	2009R
Sample ID PB	1978N	1703N	636N	1443N	1966N	888N	8812N	8011R	6807R	4484R	3595R	6487R
Translocation	t (4;11)	t (11;19)	t (4;11)	t (4;11)	t (4;11)	t (11;19)	t (11;19)	t (4;11)	t (4;11)	t (11;19)	t (4;11)	t (4;11)
Gender	Female	Male	Male	Female	Female	Female	Female	Female	Male	Female	Female	Female
Age at diagnosis (months) <sup>1</sup>	6.5	11.1	2.8	10.3	1.9	5.3	10.3	0	11.3	5.3	3.6	11.3
Time to relapse (months) <sup>2</sup>							7.0		10.3	4.8	4.6	13.4
Risk stratification adjusted to <sup>3</sup>	Medium	Medium	High	Medium	Medium	Medium	Medium	Medium	Medium	High	High	Medium
Protocol	Interfant	Interfant	Interfant	Interfant	Interfant	Interfant	Interfant	Interfant	Interfant	Interfant	Interfant	Interfant
Lymphoblasts (%) SCS sample <sup>4</sup>	-99	-99	-99	-99	-99	-99	-06	-06	-06	-06	-06	-99
Lymphoblasts (%) initial sample <sup>5</sup>	92	95	92	70	91	95	100	98	99	98	96	95
White blood cell counts at diagnosis <sup>6</sup>	82	93	94	45	90	95	93	83	86	82	95	90
Count blasts at day 8 <sup>7</sup>	291,000	310,000	571,200	69,900	263,000	226,800	201,000	125,000	75,000	487,400	635,300	348,600
Number of cells BM SORT-seq <sup>8</sup>	102	162	0	623	495	450	99	44	605	1197	782	200
Number of cells PB SORT-seq <sup>9</sup>	109	144	149					187	218	111	162	
Number of cells PB 10xGenomics <sup>10</sup>	188	267	264	410	603	428	641	231	192	260	617	272
	4733	2194	4792					3828	4232	4950		272
												290
												165
												24,729

1. Days after birth divided by 30.

2. No value means no relapse for the duration of follow-up (minimally 7 years).

3. Risk stratification according to Interfant-06. For MLL-r iALL there is only medium and high risk.

4. Lymphoblasts in bone marrow sample used for single-cell sequencing.

5. Percentage leukemic blast cells of the initial sample, at diagnosis.

6. White blood cell counts per microliter of blood at diagnosis in  $\times 10^9/L$ .

7. Leukemic blast cell count per microliter of blood at day 8.

8. Number of analyzed leukemic blast cells of bone marrow samples in SORT-seq.

9. Number of analyzed leukemic blast cells of peripheral blood samples in SORT-seq.

10. Number of analyzed leukemic blast cells of peripheral blood samples in 10x Genomics.

	Good prognostic factors: Age at diagnosis > 6 months; white blood cell counts at diagnosis < 300 × 10 <sup>9</sup> /L; leukemic blast cell count per microliter of blood at day 8 < 1000.	Ch1
	Poor prognostic factors: Age at diagnosis < 6 months; white blood cell counts at diagnosis > 300 × 10 <sup>9</sup> /L; leukemic blast cell count per microliter of blood at day 8 > 1000.	Ch2
Interfant-99	Standard risk (SR): good PRED response, leukemic blast cell count per microliter of blood at day 8 < 1000. High risk (HR): poor PRED response, leukemic blast cell count per microliter of blood at day 8 < 1000.	Ch3 Ch4
Interfant-06	Low risk (LR): <i>KMT2A</i> germline. High risk (HR): presence of a <i>KMT2A</i> -rearrangement and age < 6 months at diagnosis and with WBC count > 300 × 10 <sup>9</sup> /L at diagnosis or a poor prednisone response. Medium risk (MR): comprising all other <i>KMT2A</i> -rearranged patients.	Ch5

differentiate between long-term survivors and relapsing patients. Treatment resistance is an obvious determinant of outcome [31] and taken together, these analyses suggest that such property might already be detectable at diagnosis, possibly owing to a preexisting subpopulation of resistant cells.

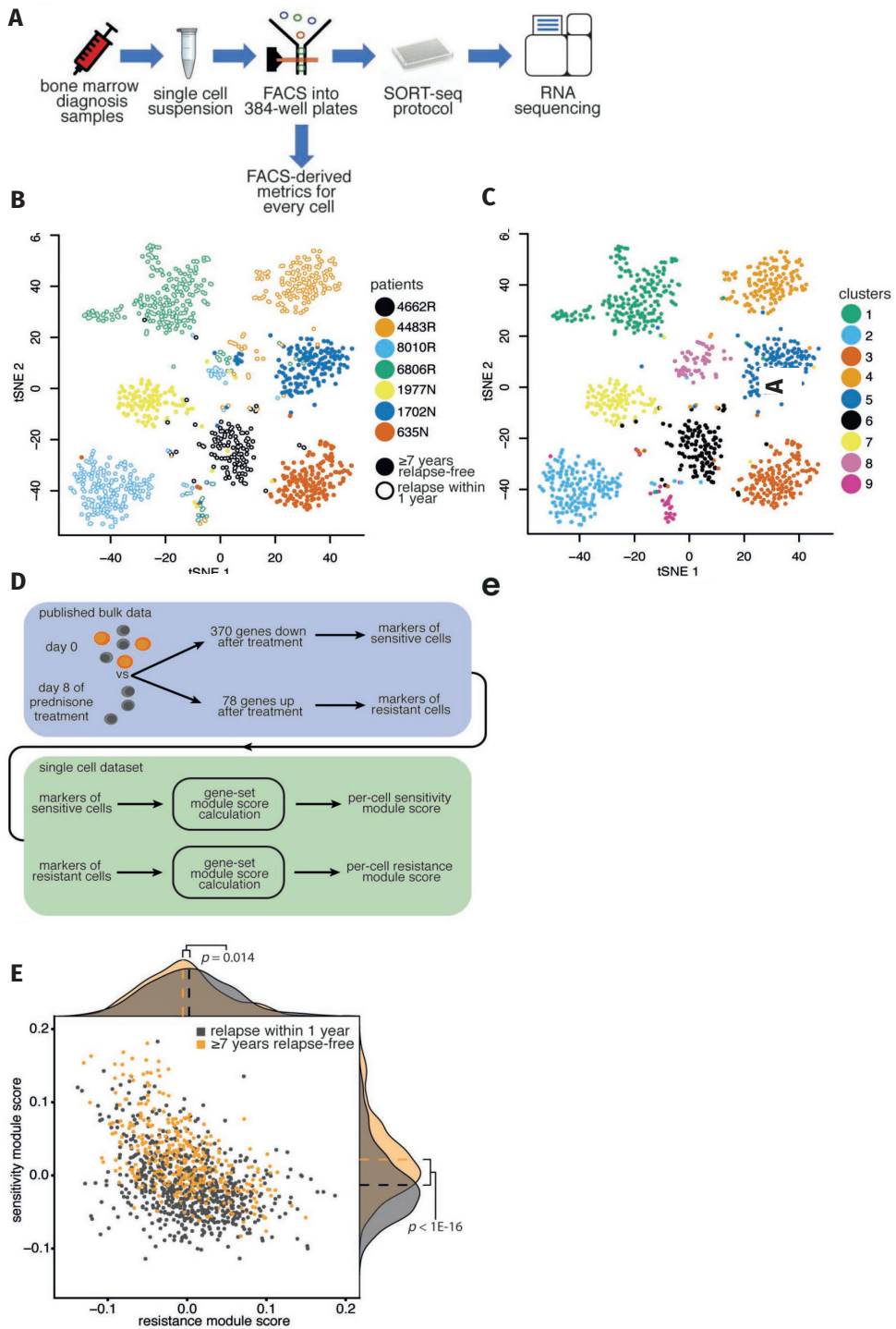
### **In vitro prednisolone treatment enriches for cells classified as resistant**

The single-cell relapse prediction is based on the idea that gene expression response to prednisone [26] reflects survival of treatment-resistant cells (Figure 1D). To further test this, untreated leukemic cells from a diagnosis sample were exposed to prednisolone (the liver-activated form of prednisone) in vitro (Figure 2A). As expected, treated cells are less viable (Figure 2B), consistent with prednisolone activity. Single-cell classification shows that leukemic cells predicted to be resistant are present in a lower proportion in the control sample and become highly enriched after elimination of the sensitive cells by prednisolone (Figure 2C–E). This agrees with our interpretation that the previously published prednisone response genes are indeed markers for treatment sensitivity/resistance (Figure 1D) and is consistent with the two programs been present in the samples before any treatment.

### **Relapse prediction is robust across scRNA-seq technologies and leukemic niches**

Encouraged by our findings in a relatively small cohort of primary *MLL-r* *iALL* BM biopsies, we repeated our analysis on PB samples. This allowed us to greatly increase the number of patients included in this study, and validation of these results in PB could open more avenues for future clinical applications.

In addition, to further validate our findings, we evaluated our PB results using two different techniques, SORT-seq and the industry standard 10x Genomics.





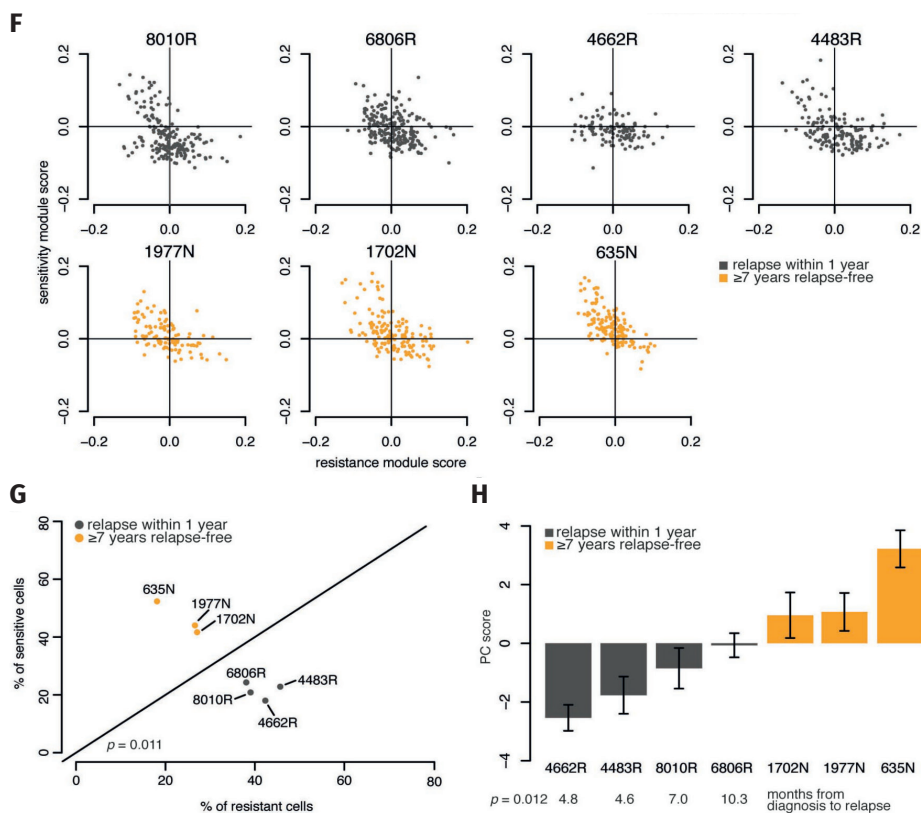


**Figure 1. Single-cell drug-sensitivity classification leads to relapse prediction.**

**A** Experiment design. **B** t-distributed stochastic neighbor embedding (t-SNE) plot of cells labeled according to sample ID, with R indicating patients who suffered relapse and N indicating no relapse. **C** Louvain clustering<sup>24</sup> projected onto the t-SNE plot. **D** Previously published differential expression data obtained comparing naive and prednisone-treated samples<sup>26</sup> were applied as gene modules to classify cells for sensitivity (downregulated genes) and resistance (upregulated genes). **E** Gene module scores (x- and y-axis) for each cell, with cells from patients who later developed relapse labeled gray and cells from relapse-free patients labeled orange. **F** Gene module scores for cells from each patient individually. Cells in the upper-left quadrant are predicted to be more sensitive and in the bottom-right more resistant to treatment. **G** Quantification of the fraction of cells from each patient (from f) predicted to be sensitive (y-axis) or resistant (x-axis). **H** First principal component (PC) calculated using the union of sensitive/resistance module genes for each cell. Bar height represents the mean score per patient. Error bars represent standard error of the mean.

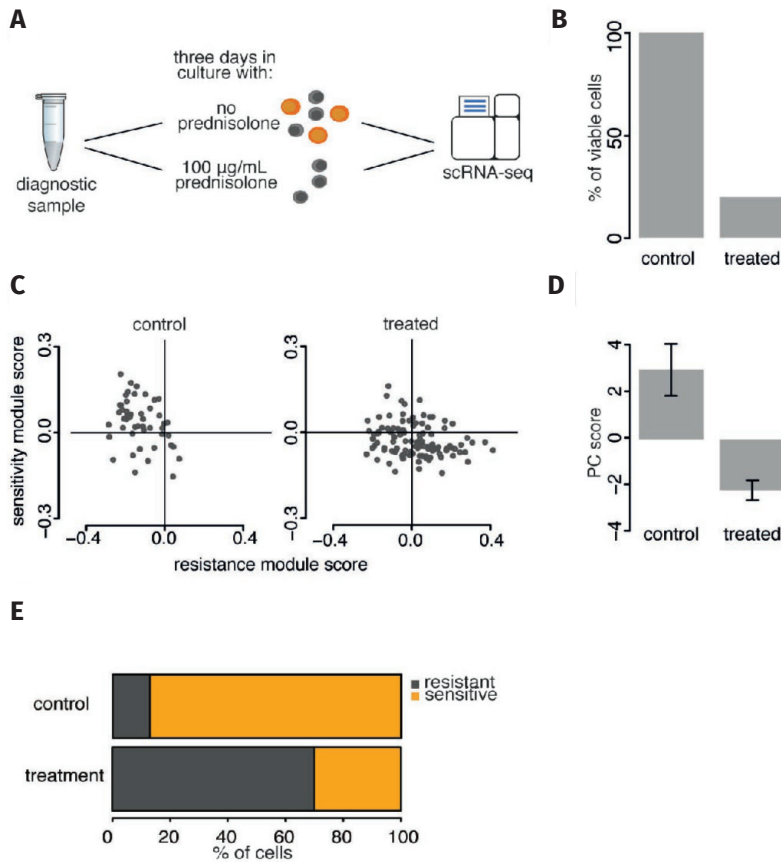


**Figure 2. In vitro treatment enriches for cells classified as resistant.**

**a** Untreated leukemic cells from bone marrow diagnostic biopsy were cultured with and without prednisolone. **B** Cell viability after treatment. **C** scRNA-seq-based sensitivity and resistance module scores of viable cells from control and treated cultures as in Figure 1f. **D** First PC score as in Figure 1h. **E** Fractions of cells classified as sensitive/resistant in control and treated samples.

As an initial pilot we used matched PB samples corresponding to six of the BM samples analyzed above (Table 1, Figure 3A), and processed them with both SORT-seq and 10x Genomics. After exclusion of healthy cells from the analysis (Supplementary Figure 4A), we again detected differences in the expression of the sensitivity and resistance module between long-term survivors and relapsing patients in both technologies (Figure 3B, C), consistent with previous results.

Relapse status classification of these six PB samples was also consistent with earlier findings in BM (10x Genomics: Supplementary Figure 4B, C, SORT-seq: together with

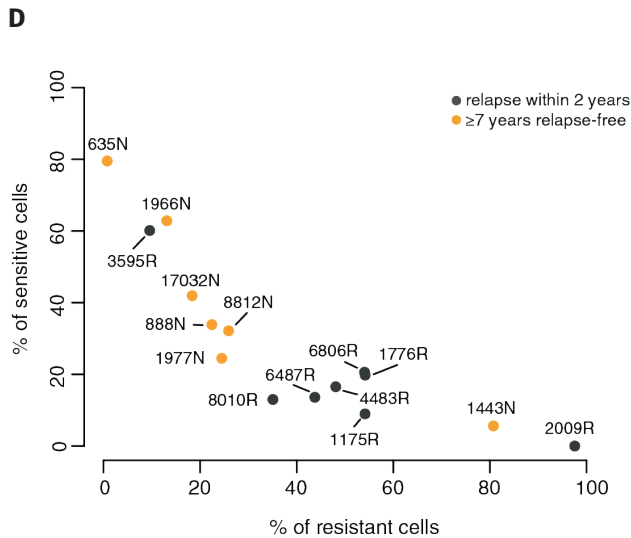
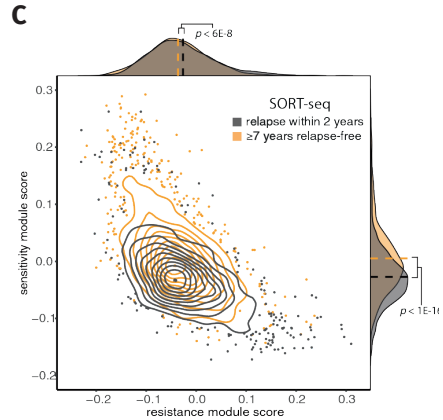
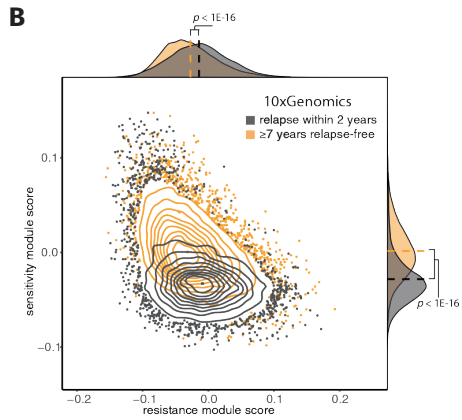
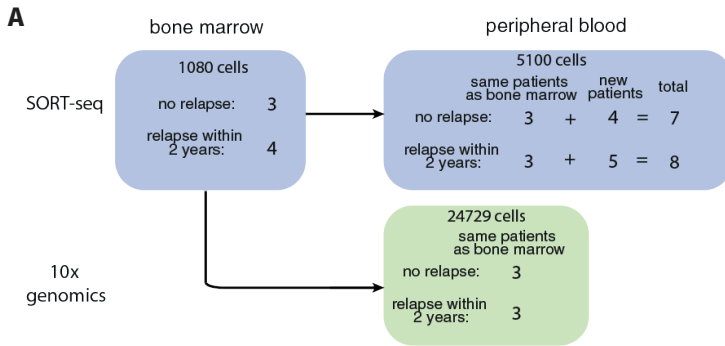
additional samples in Figure 3D, E, Supplementary Figure 4D, E) and did not depend on the technology despite the difference in number of analyzed cells (Figure 3A). Taken together, these results confirm that our classification signature is robust both across scRNA-seq technologies and across leukemic niches (PB and BM), further validating the general applicability of these findings.

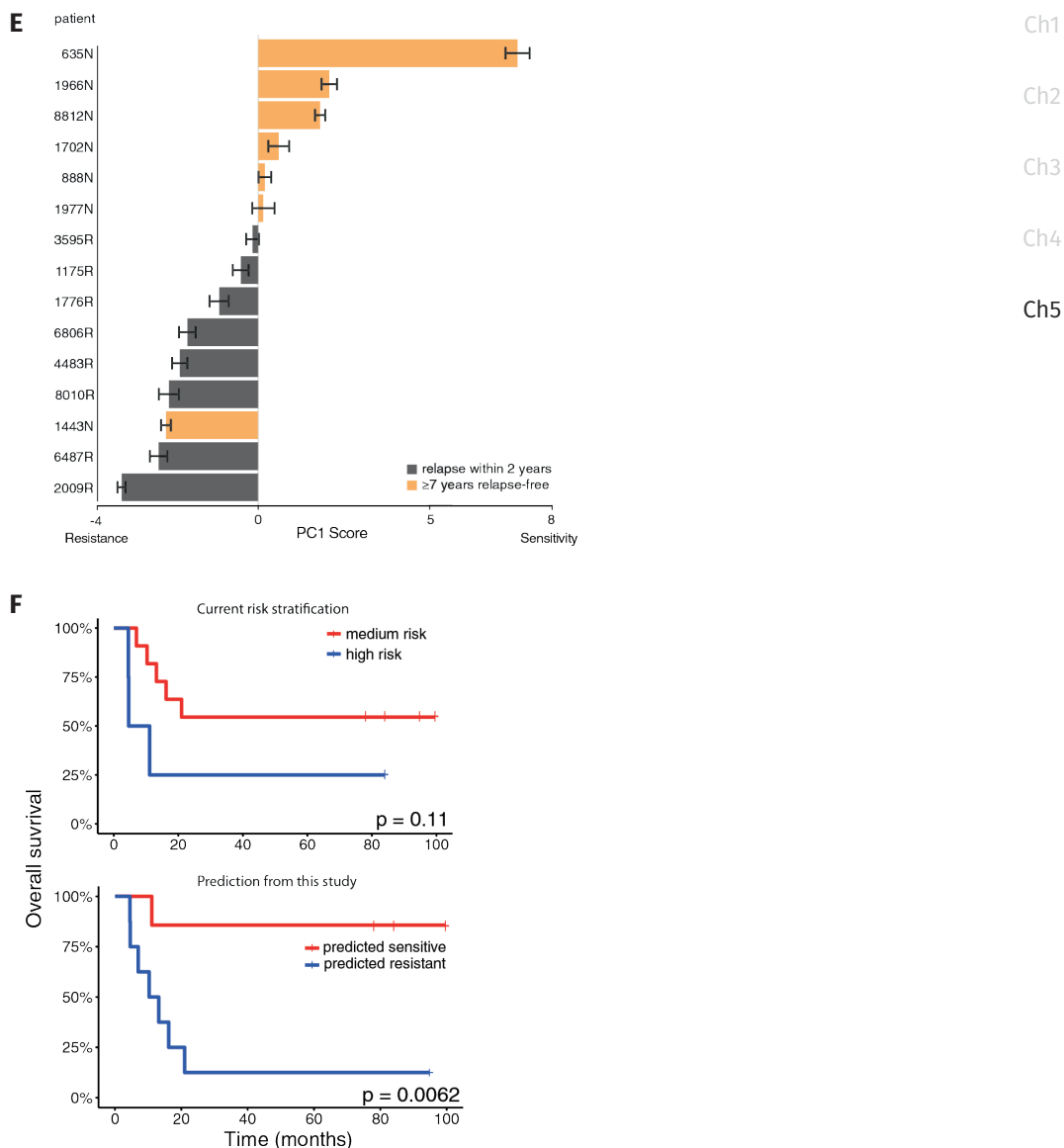
### **Relapse prediction in an extended cohort of *MLL-r* iALL PB samples**

We performed SORT-seq on nine additional primary *MLL-r* iALL PB samples taken at diagnosis (Supplementary Figure 5A–C), resulting in an extended cohort comprising of seven patients who remained relapse-free for at least 7 years, and eight patients who relapsed within the first 2 years from diagnosis. Focusing on this extended cohort, we again asked whether the percentage of therapy-resistant and -sensitive cells present at diagnosis could be indicative of future relapse. Despite 2 out of the 15 samples being misclassified (a long-term survivor and an early relapsing patient), we observed a strong association between the proportion of resistant cells at diagnosis and relapse occurrence (Figure 3D, E, Supplementary Figure 5C). Taken together, these results show that higher proportion of drug-resistant cells in PB blasts strongly correlate with relapse occurrence in an extended cohort of 15 infants with *MLL*-rearranged ALL. Relapse prediction based on this extended dataset is still overall superior to current risk stratification (Figure 3F). Interestingly, current metrics used for risk stratification perform as well as this study when evaluating long-term survivors (6/7 correct predictions in both cases) but fall substantially short when evaluating patients who eventually relapse (3/8 correct predictions, compared to 7/8 correct predictions in this study). This difference highlights the need for improved risk assessment, especially for patients that are most at risk.

### **Characterization of relapse-initiating leukemic cells identified by single-cell analysis**

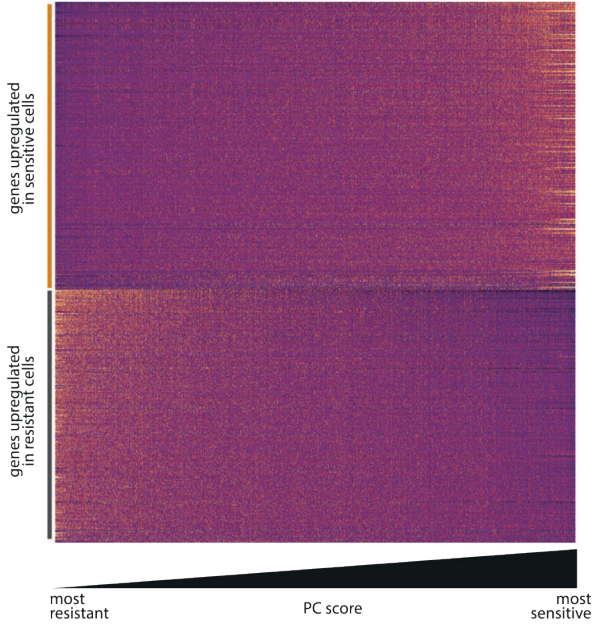
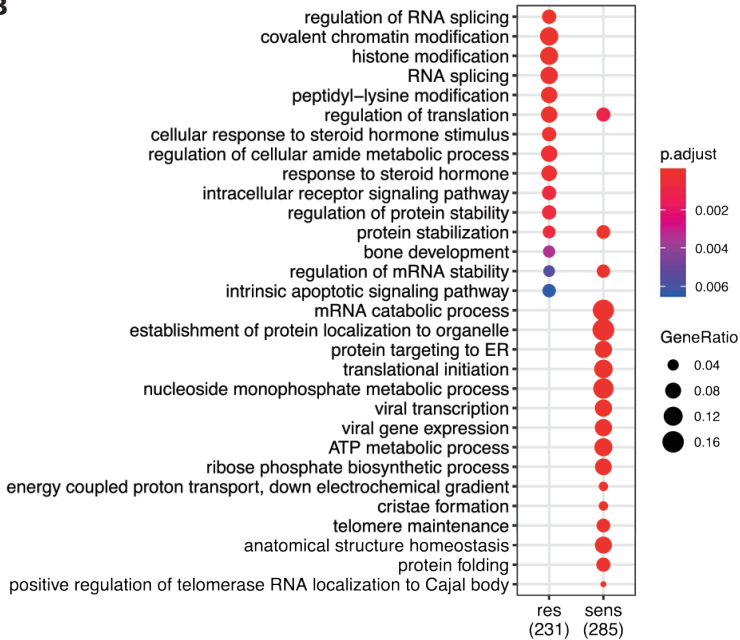
To further characterize sensitive/resistant cells, we first compared them by differential expression analysis (PB: Supplementary Table 3, BM: Supplementary Table 4) and then performed GO enrichment on the resulting markers. As detected for the module scores themselves (Figs. 1E and 3B, C), sensitivity and resistance markers are also expressed as a continuum of characteristics rather than distinct subtypes in both PB (Figure 4A) and BM (Supplementary Figure 5D). GO enrichment indicates that cells with predicted higher sensitivity to treatment are metabolically more active (Figure 4B). This resonates with our findings in BM samples, which revealed that sensitive cells are actively proliferating (Supplementary Figure 5E, F). The anticorrelation of sensitivity and resistance markers expression also emphasizes the converse trend: resistant cells are associated with reduced metabolic (Figure 4B) and cell-cycle activity (Supplementary Figure 5E, F) and appear to represent more quiescent or dormant





**Figure 3 Relapse prediction is confirmed in an expanded cohort of 15 peripheral blood samples.**

**A** Experimental design. **B** Gene module scores distribution for all cells processed with 10x Genomics. Cells from patients who later developed relapse labeled gray and cells from relapse-free patients labeled orange. **C** As b, but for cells processed with SORT-seq. **D** Quantification of the fraction of cells from each patient predicted to be sensitive or resistant. **E** Barplot showing the average PC score for each patient. Error bars represent standard error of the mean. **F** Kaplan–Meier plots showing the performance of current risk stratification versus the classification of this study.

**A****B**

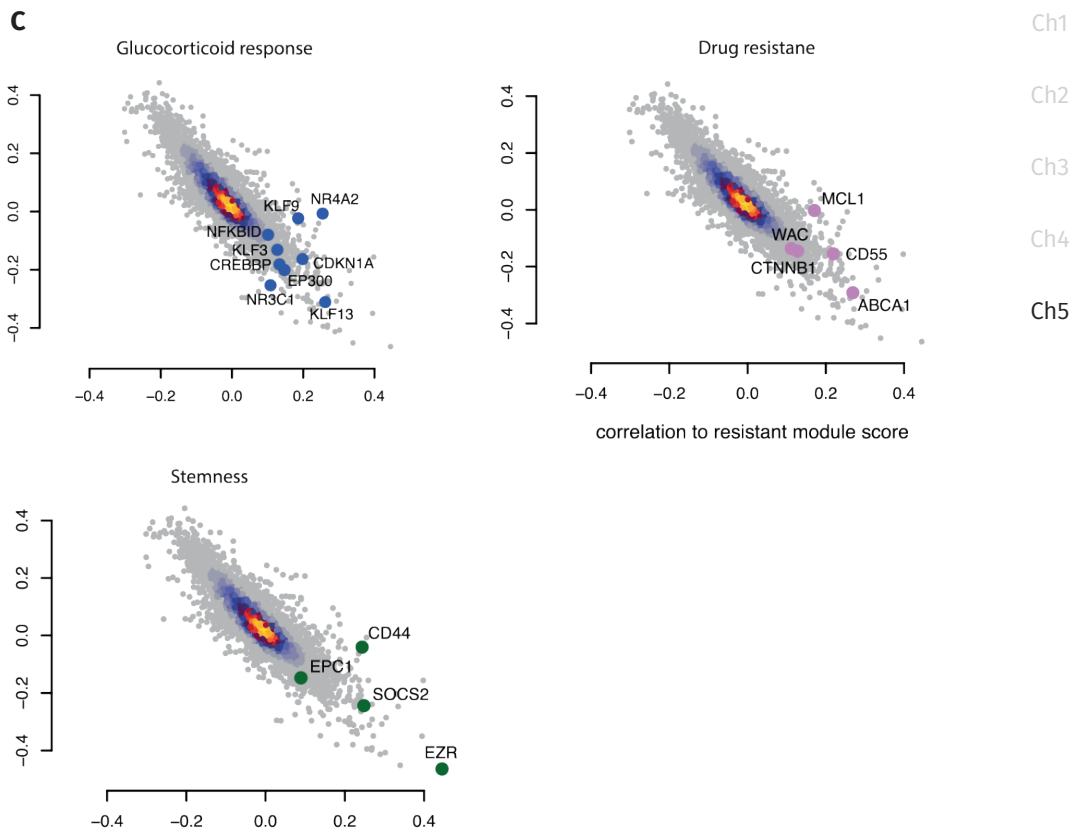


**Figure 4. Cells associated with high relapse risk are quiescent and show activated prednisone response.** **A** Expression heatmap of all differentially expressed genes between cells classified as sensitive and resistant. Cells (columns) are ordered by PC score, reflecting a gradient from resistant to sensitive. **B** Gene Ontology categories enriched in the markers of sensitive and resistant cells. Gene ratio represents the fraction of differentially expressed genes in each category. **C** Spearman correlation of all genes with either sensitivity (y-axis) or resistance (x-axis) module score. Each plot is the same, but different categories of genes are highlighted in each plot.

cells. Therefore, we asked whether resistant cells would appear smaller by virtue of their quiescence and lack of metabolic activity. This trend was consistently observed in BM samples using FACS forward scatter as a proxy for cell size (Supplementary Figure 6A, B). However, further size analysis by both microscopy and FACS on a patient-by-patient basis—while highlighting a significant global trend in both PB and BM when patients were aggregated according to future relapse occurrence (Supplementary Figure 6D-F, aggregate) - was not able to stratify patients as accurately as our gene signature (Supplementary Figure 6C-F).

While quiescence/activity seems to be an important dichotomy characterizing the two ends of the resistance/sensitivity continuum, several interesting GO categories also appear differentially enriched (Figure 4B). Notably, categories comprising steroid hormone response and apoptotic signaling pathway suggest intrinsic differences in the regulation of these processes and might explain the differential treatment sensitivity. In order to relate the expression levels of these genes to the sensitivity/resistance modules that associate with relapse occurrence, we correlated the expression of all genes with said module scores and represented the results as scatterplots (Figure 4C).

We identified several groups of genes with high correlation to the resistance module score, relating to glucocorticoid response, drug resistance, and cell stemness. In the first group, we found *NR3C1*, the gene encoding the glucocorticoid receptor, as well as several of its downstream targets such as the *KLF* family of genes, *CDKN1A*, and *CREBBP* [32–34]. This suggests that therapy-resistant cells already exhibit at least a partially activated glucocorticoid response before treatment and we speculate that this may blunt the effects of subsequent prednisone administrations. We identified several additional genes that may contribute to the survival of resistant cells by mediating drug resistance. *CTNNB1*

[35] and *MCL1* [36, 37] have both been previously implicated in establishing drug resistance in *MLL*-driven leukemic cells and additional death escape mechanisms might be provided by the efflux transporter *ABCA1* and antiapoptotic activity of *CD55* [38].

A number of stemness markers such as *CD44*, *EPC1*, *SET2D*, and *SOCS2* seemed to correlate very well with our resistance module score and may explain how these cells are able to avoid apoptosis while maintaining replicative potential. In particular, *EPC1* has been reported to sustain the oncogenic potential of the leukemic stem cells in *MLL*-rearranged acute myeloid leukemia [39] and *SET2D* has been recently implicated in safeguarding the genomic integrity of *MLL*-rearranged leukemias [40]. Expression



of these factors might provide an *MLL*-rearrangement-specific contribution to the resilience of resistant cells.

Taken together, these results point at a continuum of characteristics present in treatment-naive samples as a determining factor of relapse occurrence, highlighting the role of quiescence, unstimulated glucocorticoid response activation, and apoptosis escape mechanisms.

### **Lower amounts of transcripts in relapse-associated cells hampers classification by bulk mRNA expression analyses**

Beyond indicating the cells from which relapse arises and the potential for improving treatment of these vulnerable patients, this study also reveals why single-cell analyses may in some cases outperform bulk mRNA approaches for patient classification. The smaller cells associated with higher risk of disease relapse have substantially lower numbers of transcripts (Supplementary Figure 7A). This fits with quiescence/dormancy as a means to escape chemotherapy and means that bulk mRNA data will not proportionately represent the relative abundance of such cells. Indeed, applying the gene modules (Figure 1) on previously published bulk mRNA *MLL-r iALL* datasets [12, 41, 42] does not result in a relapse/non-relapse distinction (Supplementary Figure 7b). Bulkifying the BM scRNA-seq data by complete pooling of all transcripts yields a dataset that also does not discriminate well (Supplementary Figure 7C). However, pooling the scRNA-seq data after downsampling so that each cell contributes an equal number of transcripts does yield “bulk” data on which the modules discriminate between patients who do and do not relapse (Supplementary Figure 7d).

## **DISCUSSION**

To date, *MLL-r iALL* remains an aggressive and difficult-to-treat childhood malignancy. Although induction therapy leads to complete remissions in the vast majority of cases (~95%), two-thirds of the patients experience disease relapse within 1 year from diagnosis, while treatment is still ongoing [2, 3]. This suggests that most of the blasts are responsive to treatment, while a small subpopulation of therapy-refractory cells survives to initiate relapse. In this study, we performed scRNA-seq on 15 diagnosis samples from patients with *MLL-r iALL*. We then used an independently generated gene signature to predict future relapse occurrence correctly in 13 out of the 15 cases, substantially improving on the performance of current risk stratification. In addition, we characterized the subpopulation of therapy-refractory cells, finding them associated with small size, quiescent nature, and heightened glucocorticoid response. Clinical outcome seems to be largely correlated with the abundance of such therapy-resistant leukemic cells. Their

Ch1

Ch2

Ch3

Ch4

Ch5

detection and further characterization have tremendous potential to drastically improve risk stratification and guide the development of new drugs [11, 12].

Current risk stratification of *MLL-r iALL* involves categorizing patients into either being medium risk or high risk, based on age at diagnosis, white blood cell counts, and the *in vivo* response to 7 days of prednisone treatment. Although this division does lead to significant differences in clinical outcome (Figure 3f) [2, 3], it is still often inaccurate, especially for patients that have a high risk of relapse. A possible explanation for this may lie in some of the criteria by which patients are currently being categorized. For instance, one of the most important criteria for risk stratification is COunt of BLAsts at day 8 (COBLA8), representing the count of surviving blasts after 7 days of prednisone monotherapy. Although this measurement is certainly associated with future relapse occurrence, it is often inaccurate and possibly influenced by confounding factors such as differences in initial WBC. In our scRNA-seq-based relapse-prediction model, we improved upon the predictive power of COBLA8 by analyzing the gene expression patterns that characterize surviving cells and finding this signature back in naive untreated diagnostic samples. This allowed us to classify cells as either sensitive or resistant to treatment and to show that the relative proportion of resistant cells in a sample is strongly correlated with relapse occurrence. The direct correlation between expression of the resistance signature and treatment outcome suggests that the signature represents general resistance to chemotherapeutics rather than being specific to prednisone. This is not surprising given the well-known association between COBLA8 and relapse occurrence, but it does raise the question of how a prednisone-associated gene expression pattern is able to affect general therapy resistance.

In our analyses, we found that an activity-quiescence continuum is the most prominent feature separating resistant cells from sensitive cells. Although unlikely to be directly associated with prednisone, it reflects the well-documented resilience of quiescent cells to chemotherapy and suggests that the resistance signature might represent not only prednisone resistance but also multiple therapy-escape mechanisms. This view is further supported by several classes of genes we found enriched in resistant cells. Detection of general mediators of drug resistance and efflux transporters argues for broad therapy resistance, while stemness markers typical of leukemic stem cells might help escape drug-induced cell death and maintain replicative potential. Taken together, these results argue for a model where prednisone monotherapy selects for cells that are small, quiescent, and generally resistant to chemotherapy, setting the stage for future research to characterize them more in depth and decode their therapy-resistance mechanisms.

There are several aspects and limitations of this study that will need to be addressed in order to help translate this knowledge to the clinic. scRNA-seq is not yet a routine lab technique and application of bulk RNA-seq to detect the gene signature suffers from quantification problems owing to the smaller RNA content of resistant cells. Identification of an easily detectable hallmark could help offset this problem and simplify the quantification of resistant cells. However, investigation of clonality and mutation analysis might be required to identify DNA-based hallmarks that are not affected by the smaller size of resistant cells. Despite considerable success, two patients in the cohort were misclassified by our method. At this stage we cannot exclude that specific mutations might act as epistatic factors, bypassing the drug escape mechanisms and resulting in relapse development. Finally, validation of this signature on vast numbers of patients—while essential for inclusion in upcoming trials—is problematic both due to the technique and to the rarity of the disease.

Ch1

Ch2

Ch3

Ch4

Ch5

Taken together, these results demonstrate how single-cell sequencing can be used to further our understanding of cancer cell population dynamics and use them for accurate risk assessment. Eventually, elimination of these therapy-resistant cells during early phases of the treatment may well prevent relapse occurrence in a substantial number of cases, leading to increased survival.

## REFERENCES

1. Meyer C, Burmeister T, Groger D, Tsaour G, Fehina L, Renneville A, et al. The MLL recombinome of acute leukemias in 2017. *Leukemia*. 2018;32:273–84.
2. Pieters R, Schrappe M, De Lorenzo P, Hann I, De Rossi G, Felice M, et al. A treatment protocol for infants younger than 1 year with acute lymphoblastic leukaemia (Interfant-99): an observational study and a multicentre randomised trial. *Lancet*. 2007;370:240–50.
3. Pieters R, De Lorenzo P, Ancliffe P, Aversa LA, Brethon B, Biondi A, et al. Outcome of infants younger than 1 year with acute lymphoblastic leukemia treated with the Interfant-06 protocol: results from an international phase III randomized study. *J Clin Oncol*. 2019;37:2246–56.
4. Dick JE. Stem cell concepts renew cancer research. *Blood*. 2008;112:4793–807.
5. Hanahan D, Weinberg RA. Hallmarks of cancer: the next generation. *Cell*. 2011;144:646–74.
6. Hong SP, Chan TE, Lombardo Y, Corleone G, Rotmensz N, Bravaccini S, et al. Single-cell transcriptomics reveals multi-step adaptations to endocrine therapy. *Nat Commun*. 2019;10:3840.
7. Good Z, Sarno J, Jager A, Samusik N, Aghaeepour N, Simonds EF, et al. Single-cell developmental classification of B cell precursor acute lymphoblastic leukemia at diagnosis reveals predictors of relapse. *Nat Med*. 2018;24:474.
8. Shlush LI, Mitchell A, Heister L, Abelson S, Ng SWK, Trotman-Grant A, et al. Tracing the origins of relapse in acute myeloid leukaemia to stem cells. *Nature*. 2017;547:104–8.
9. Battle E, Clevers H. Cancer stem cells revisited. *Nat Med*. 2017;23:1124.
10. Roberts KG, Mullighan CG. Genomics in acute lymphoblastic leukaemia: insights and treatment implications. *Nat Rev Clin Oncol*. 2015;12:344–57.
11. Bardini M, Woll PS, Corral L, Luc S, Wittmann L, Ma Z, et al. Clonal variegation and dynamic competition of leukemia-initiating cells in infant acute lymphoblastic leukemia with MLL rearrangement. *Leukemia*. 2015;29:38–50.
12. Andersson AK, Ma J, Wang J, Chen X, Gedman AL, Dang J, et al. The landscape of somatic mutations in infant MLL-rearranged acute lymphoblastic leukemias. *Nat Genet*. 2015;47:330–7.
13. Suva ML, Tirosh I. Single-cell RNA sequencing in cancer: lessons learned and emerging challenges. *Mol Cell*. 2019;75:7–12.
14. Giladi A, Amit I. Single-cell genomics: a stepping stone for future immunology discoveries. *Cell*. 2018;172:14–21.
15. Tanay A, Regev A. Scaling single-cell genomics from phenomenology to mechanism. *Nature*. 2017;541:331.
16. Gawad C, Koh W, Quake SR. Single-cell genome sequencing: current state of the science. *Nat Rev Genet*. 2016;17:175–88.
17. Stegle O, Teichmann SA, Marioni JC. Computational and analytical challenges in single-cell transcriptomics. *Nat Rev Genet*. 2015;16:133–45.
18. Shapiro E, Biezuner T, Linnarsson S. Single-cell sequencing-based technologies will revolutionize whole-organism science. *Nat Rev Genet*. 2013;14:618–30.
19. Pui CH, Gaynon PS, Boyett JM, Chessells JM, Baruchel A, Kamps W, et al. Outcome of treatment

- in childhood acute lymphoblastic leukaemia with rearrangements of the 11q23 chromosomal region. *Lancet*. 2002;359:1909–15. Ch1
20. Stam RW, den Boer ML, Schneider P, Nollau P, Horstmann M, Beverloo HB, et al. Targeting FLT3 in primary *MLL*-gene-rearranged infant acute lymphoblastic leukemia. *Blood*. 2005;106:2484–90. Ch2
21. Muraro Mauro J, Dharmadhikari G, Grün D, Groen N, Dielen T, Jansen E, et al. A single-cell transcriptome atlas of the human pancreas. *Cell Syst*. 2016;3:385–94.e3. Ch3
22. Hashimshony T, Senderovich N, Avital G, Klochendler A, de Leeuw Y, Anavy L, et al. CEL-Seq2: sensitive highly-multiplexed single-cell RNA-Seq. *Genome Biol*. 2016;17:77. Ch4
23. Calandrini C, Schutgens F, Oka R, Margaritis T, Candelli T, Mathijssen L, et al. An organoid biobank for childhood kidney cancers that captures disease and tissue heterogeneity. *Nat Commun*. 2020;11:1310. Ch5
24. Butler A, Hoffman P, Smibert P, Papalexi E, Satija R. Integrating single-cell transcriptomic data across different conditions, technologies, and species. *Nat Biotechnol*. 2018;36:411–20.
25. Hafemeister C, Satija R. Normalization and variance stabilization of single-cell RNA-seq data using regularized negative binomial regression. *Genome Biol*. 2019;20:296.
26. Rhein P, Scheid S, Rätei R, Hagemeyer C, Seeger K, Kirschner-Schwabe R, et al. Gene expression shift towards normal B cells, decreased proliferative capacity and distinct surface receptors characterize leukemic blasts persisting during induction therapy in childhood acute lymphoblastic leukemia. *Leukemia*. 2007;21:897–905.
27. Yu G, Wang LG, Han Y, He QY. clusterProfiler: an R package for comparing biological themes among gene clusters. *OMICS*. 2012;16:284–7.
28. Ding J, Adiconis X, Simmons SK, Kowalczyk MS, Hession CC, Marjanovic ND, et al. Systematic comparative analysis of single cell RNA-sequencing methods. 2019. <https://doi.org/10.1101/632216>.
29. van 't Veer LJ, Bernards R. Enabling personalized cancer medicine through analysis of gene-expression patterns. *Nature*. 2008;452:564–70.
30. Dördelmann M, Reiter A, Borkhardt A, Ludwig WD, Götz N, Viehmann S, et al. Prednisone response is the strongest predictor of treatment outcome in infant acute lymphoblastic leukemia. *Blood*. 1999;94:1209–17.
31. Den Boer ML, Harms DO, Pieters R, Kazemier KM, Gobel U, Korholz D, et al. Patient stratification based on prednisolone-vincristine-asparaginase resistance profiles in children with acute lymphoblastic leukemia. *J Clin Oncol*. 2003;21:3262–8.
32. Nuñez FJ, Johnstone TB, Corpuz ML, Kazarian AG, Mohajer NN, Tliba O, et al. Glucocorticoids rapidly activate cAMP production via G(αs) to initiate non-genomic signaling that contributes to one-third of their canonical genomic effects. *FASEB J*. 2020;34:2882–95.
33. Gans I, Hartig EI, Zhu S, Tilden AR, Hutchins LN, Maki NJ, et al. Klf9 is a key feedforward regulator of the transcriptomic response to glucocorticoid receptor activity. *Sci Rep*. 2020;10:11415.
34. Cha HH, Cram EJ, Wang EC, Huang AJ, Kasler HG, Firestone GL. Glucocorticoids stimulate p21 gene expression by targeting multiple transcriptional elements within a steroid responsive region of the p21waf1/cip1 promoter in rat hepatoma cells. *J Biol Chem*. 1998;273:1998–2007.

35. Yeung J, Esposito MT, Gandillet A, Zeisig BB, Griessinger E, Bonnet D, et al.  $\beta$ - Catenin mediates the establishment and drug resistance of MLL leukemic stem cells. *Cancer Cell*. 2010;18:606–18.
36. Stam RW, Den Boer ML, Schneider P, de Boer J, Hagelstein J, Valsecchi MG, et al. Association of high-level MCL-1 expression with in vitro and in vivo prednisone resistance in MLL-rearranged infant acute lymphoblastic leukemia. *Blood*. 2010;115:1018–25.
37. Wei G, Twomey D, Lamb J, Schlis K, Agarwal J, Stam RW, et al. Gene expression- based chemical genomics identifies rapamycin as a modulator of MCL1 and glucocorticoid resistance. *Cancer Cell*. 2006;10:331–42.
38. Loeff FC, van Egmond HME, Nijmeijer BA, Falkenburg JHF, Halkes CJ, Jedema I. Complement-dependent cytotoxicity induced by therapeutic antibodies in B-cell acute lymphoblastic leukemia is dictated by target antigen expression levels and augmented by loss of membrane-bound complement inhibitors. *Leuk Lym- phoma*. 2017;58:1–14.
39. Huang X, Spencer GJ, Lynch JT, Ciceri F, Somerville TD, Somervaille TC. Enhancers of polycomb EPC1 and EPC2 sustain the oncogenic potential of MLL leukemia stem cells. *Leukemia*. 2014;28:1081–91.
40. Skucha A, Ebner J, Schmöllerl J, Roth M, Eder T, César-Razquin A, et al. MLL- fusion-driven leukemia requires SETD2 to safeguard genomic integrity. *Nat Commun*. 2018;9:1983.
41. Agraz-Doblas A, Bueno C, Bashford-Rogers R, Roy A, Schneider P, Bardini M, et al. Unraveling the cellular origin and clinical prognostic markers of infant B-cell acute lymphoblastic leukemia using genome-wide analysis. *Haematologica*. 2019;104:1176–88.
42. Stam RW, Schneider P, Hagelstein JA, van der Linden MH, Stumpel DJ, de Menezes RX, et al. Gene expression profiling-based dissection of MLL translocated and MLL germline acute lymphoblastic leukemia in infants. *Blood*. 2010;115:2835–44.

Ch1

Ch2

Ch3

Ch4

Ch5





# CHAPTER 6

## General discussion and implications



## GENERAL DISCUSSION AND IMPLICATIONS

*KMT2A*-rearranged infant acute lymphoblastic leukemia (*KMT2A*-r iALL) is a highly aggressive ALL subtype characterized by abnormal DNA methylation patterns (1-4). Previously, we have shown that demethylating agents, including decitabine, effectively eliminates *KMT2A*-r ALL cells *in vitro* (3-6). In **Chapter 2**, our research focused on the *in vivo* response of a xenograft mouse model of *KMT2A*-r ALL to a clinically relevant low-dose of decitabine. Unfortunately, we observed only a slight delay in leukemia progression, suggesting limited efficacy as a single drug. Given the potential of decitabine as a chemosensitizer in various cancer types (7-9), we explored whether it could enhance the sensitivity of *KMT2A*-r ALL to conventional chemotherapeutics as well as other epigenetic-based compounds, and antineoplastic agents. However, prolonged pre-treatment with low-dose decitabine only moderately improved the sensitivity of *KMT2A*-r ALL cell lines *in vitro*. Consequently, we concluded that decitabine treatment, alone or in combination with other agents, may not provide sufficient benefits for *KMT2A*-r iALL patients. As a result, we decided not to pursue further investigations of decitabine efficacy in patient-derived xenograft (PDX) mouse models of *KMT2A*-r iALL.

In contrast to our observations, a recent study by Cheung *et al.* demonstrated a significant improvement in event-free survival (EFS) through the administration of decitabine as a single agent in *KMT2A*-r infant ALL xenografts (10). This discrepancy could potentially be attributed to the differences in administration of this drug. The previous study used higher dosages of decitabine (0.5 mg/kg once daily for five consecutive days), while our approach involved a clinically relevant low dose of decitabine (0.1 mg/kg) co-administered with tetrahydourine (THU) three times a week to extend its half-life and increase decitabine plasma levels by 10-fold. This raises the question whether the actual plasma levels of decitabine in the two studies varied, potentially explaining the discrepant results. Moreover, Cheung's study utilized in infant *KMT2A*-r ALL PDX models which may also have contributed to the observed differences in response compared to our study which employed a mouse xenograft a *KMT2A*-r ALL cell line model derived from a 5-year-old child in relapse. In addition, in the aforementioned study, researchers also investigated the effects of another DNA demethylating agent, i.e., azacytidine, which has shown efficacy in acute myeloid leukemia (AML) (10). Furthermore, a recent Children's Oncology Group (COG) trial, AALL15P1, showed that azacytidine in addition to Interfant-06 standard chemotherapy in infants with newly diagnosed *KMT2A*-r ALL was well tolerated (11). However, despite this favorable tolerance, the event-free survival (EFS) rates observed in that study remained similar to the low survival rates seen in historical outcomes. This indicates that demethylating agents such as azacytidine and decitabine in combination with current treatment protocols will not improve the outcome of infants with *KMT2A*-r ALL.

Interestingly, further findings by Cheung *et al.*(10) demonstrated that the combination of azacytidine with the BCL-2 inhibitor venetoclax significantly EFS survival in PDX models of *KMT2A-r* iALL. Moreover, the current standard of care for patients with AML who are not eligible for intensive chemotherapy is the combination of venetoclax and azacitidine (12). In our study, we found that venetoclax synergized with decitabine treatment in the *KMT2A-r* iALL cell line KOPN8 *in vitro*. Collectively this suggests that combination therapies involving DNA demethylating agents and venetoclax hold promise for improving outcomes in patients diagnosed with *KMT2A-r* iALL (13). Further research and clinical trials are warranted to validate this and explore the optimal dosage, timing, and patient selection criteria for combination therapy. These studies will provide additional insights into the efficacy and safety of demethylating agents in conjunction with venetoclax, thus paving the way for more effective and tailored treatment approaches for *KMT2A-r* iALL patients.

Ch1

Ch2

Ch3

Ch4

Ch5

Ch6

**Chapter 3** focused on acquired resistance to DOT1L inhibition, another class of epigenetic drugs targeting the molecular pathobiology of *KMT2A-r* acute leukemias. A cell line model of acquired resistance to the first-in-line DOT1L inhibitor pinometostat was established and extensively characterized. This model provided valuable insights into the adaptive capacity of *KMT2A-r* ALL cells, allowing them to evade the effects of DOT1L inhibitors by adopting myeloid-associated characteristics and/or exhibiting cellular plasticity.

Understanding the mechanisms behind acquired pinometostat resistance is not only important for the development of novel and more effective DOT1L inhibitors but is also essential for comprehending the efficacy of other compounds designed to target oncogenic protein complexes containing *KMT2A* fusion proteins, such as *MENIN* inhibitors. In addition to pinometostat, we also induced acquired resistance to the *MENIN* inhibitor, revumenib, which is currently being evaluated in clinical trials for *KMT2A-r* ALL as well as *KMT2A-r* AML (14). Interestingly, we observed similar effects to those observed after acquiring resistance to DOT1L inhibition, suggesting the existence of a common “escape” pathway for both epigenetic drugs that target crucial epigenetic regulators in *KMT2A-r* ALL. We found severe CD133/*PROM1* downregulation and upregulation of both CD33 and *LILRB4/CD85k* in *KMT2A-r* ALL cells with acquired resistance to DOT1L as well as *MENIN* inhibition, indicating a switch towards, or selection of myeloid-like characteristics. Hypothetically, blocking this transition may represent a potential strategy to re-sensitize *KMT2A-r* iALL cells to pinometostat and revumenib treatment, or even effectively eradicate these cells.

*LILRB4/CD85k* was the most prominently upregulated protein in *KMT2A-r* ALL cells upon acquiring pinometostat and revumenib resistance. Interestingly, recent evidence

has shown the effectiveness of LILRB4-targeting immunotherapy in preventing lineage switches from ALL to AML in *KMT2A-r* ALL patients (15). This finding elegantly underscores the potential of myeloid directed immunotherapeutic approaches in managing *KMT2A-r* ALL. Furthermore, our pinometostat-resistant cells exhibited increased sensitivity to the BCL-2 inhibitor venetoclax, a promising drug currently undergoing evaluation in various clinical trials, including those involving *KMT2A-r* ALL patients (16, 17). This observation emphasizes the potential of venetoclax as a promising drug for the treatment of *KMT2A-r* ALL.

Our observation that *KMT2A-r* ALL cells can overcome their dependency on DOT1L, a crucial oncogenic property of this type of leukemia, raises the question whether there are other specific epigenetic vulnerabilities in these cells. To address this question, in **chapter 4** we focused on identifying additional epigenetic regulators as well as kinases that are specifically essential to *KMT2A-r* ALL cells. We employed epigenome and kinome RNA-guided CRISPR-Cas9 knock-out screens *in vitro* and discovered the epigenetic regulators *ARID4B* and *MBD3*, as well as the receptor kinase *BMP2R*, as novel molecular vulnerabilities in this form of leukemia. These findings highlight potential therapeutic targets beyond DOT1L and MENIN and may lead to a deeper understanding of the underlying molecular mechanisms driving *KMT2A-r* ALL. The identification of *ARID4B*, *MBD3*, and *BMP2R* as critical factors in this malignancy potentially represent exciting possibilities for the development of novel treatment strategies.

*ARID4B* encodes a chromatin remodeling protein that is essential for differentiation of fetal hematopoietic cells (18-20). This feature could be particularly relevant to *KMT2A-r* ALL since this type of leukemia likely originates from a hematopoietic progenitor in the fetal liver (21). In other words, this suggests a connection between the developmental processes occurring in the fetal hematopoietic system and the development of *KMT2A-r* ALL. Given that *ARID4B* is essential for fetal hematopoietic cell differentiation, its involvement in *KMT2A-r* ALL could potentially contribute to disturbed differentiation and the accumulation of very immature hematopoietic cells, i.e., leukemogenesis.

Moreover, aberrant up-regulation of *HOXA9* expression is considered to be one of the hallmarks of *KMT2A-r* ALL in particular (22-24). The dysregulation of *HOXA9* plays a significant role in leukemogenesis and is often associated with poor prognosis in patients diagnosed with *KMT2A-r* ALL. Remarkably, a study involving siRNA-mediated knockdown of *ARID4B* in a prostate cancer cell line revealed that the loss of *ARID4B* expression resulted in severe down-regulation of *HOXA9* expression (25). This raises the question whether *HOXA9* expression may be regulated by *ARID4B* in *KMT2A-r* ALL. Moreover, our findings in **chapter 3** indicate that the proposed and widely accepted relationship between DOT1L and *HOXA* genes is not fully conclusive, in spite of clear binding of *KMT2A::AFF1* to the

*HOXA* gene locus. Despite the loss of dependency on DOT1L mediated H3K79 methylation, *HOXA9* expression remained largely unaffected in pinometostat-resistant *KMT2A-r* ALL cells, and knockdown of *HOXA9* did result in the induction of leukemic cell death. Collectively this may suggest that in *KMT2A-r* ALL cells *HOXA9* (and other *HOXA* genes) may not necessarily be controlled by DOT1L but rather by an alternative regulator such as, for instance, *ARID4B*, which in turn may possibly be influenced by the *KMT2A* fusion. This could explain why vulnerability to the loss of *ARID4B* is selectively observed in *KMT2A-r* ALL but not in BCP-ALL without *KMT2A* translocations. This is supported by the fact that we indeed found binding of *KMT2A* as well as *AFF1* at the *ARID4B* promoter locus in SEM cells (data not shown). Nevertheless, further experimental evidence is necessary to establish these interesting connections conclusively.

Ch1  
Ch2  
Ch3  
Ch4  
Ch5  
Ch6

In contrast to *ARID4B*, we further revealed in **chapter 4** that the loss of *MBD3* rather effectively and specifically inhibited leukemic cell proliferation instead of being lethal to *KMT2A-r* ALL cells. *MBD3* encodes a member of the methyl-CpG binding domain (MBD) protein family which preferably binds to 5-hydroxymethylcytosine-marked genes, and is an essential component of the nucleosome remodeling and deacetylase (NuRD) complex, which is involved in chromatin remodeling and transcriptional regulation (26, 27). Recent studies have demonstrated direct interactions between the NuRD complex and *KMT2A* fusion proteins in *KMT2A-r* acute leukemia, contributing to aberrant epigenetic changes observed in these leukemias (28, 29). This interaction leads to recruitment of the NuRD complex to target genes of *KMT2A* fusion proteins, causing chromatin compaction and transcriptional repression, which significantly impacts the development and progression of *KMT2A-r* acute leukemias. Additionally, the NuRD complex is a dynamic assembly of several subunits and can exist in different compositions, leading to variable and sometimes opposing effects (30, 31). Many of the subunits of the NuRD complex have functions beyond the complex, such as essential mammalian genes, like *HDAC1/2* and *RBBP4/7* and isoforms of *MBD2*. (31, 32). Notably, subunits *MBD2* and *MBD3* have distinct functions and are mutually exclusive within the NuRD complex (32), indicating that the NuRD complex can exert context-specific effects by utilizing different combinations of its subunits. Moreover, its multifaceted effects may be influenced by interactions with tissue-specific transcription and coregulatory factors not considered core NuRD components. Given the intricate compositions and interactions, exploring configurations involving *MBD3* in the NuRD complex offers potential for targeted therapy in *KMT2A-r* ALL. Further investigation into these unique combinations and their impact on this leukemia subtype, as well as understanding the interplay between the NuRD complex and *KMT2A* fusion proteins provides insights into the molecular mechanisms underlying *KMT2A-r* acute leukemia and may facilitate the development of novel therapeutic strategies targeting this protein complex.

With our kinome CRISPR-Cas9 KO screen we identified BMP type 2 receptor *BMPR2*, as well as BMP type 1 receptors *BMPR1A* and *ACVR1*, all involved in bone morphogenic protein (BMP) signaling, as kinases specifically essential to *KMT2A-r* ALL. Receptor kinase *BMPR2* is a component of the BMP pathway which is often deregulated in human cancers, including for example acute megakaryoblastic leukemia (AMKL) (33). Hence, inhibition of BMP signaling may well induce favorable anti-leukemic effects in *KMT2A-r* iALL. Its function in this context relies on its role in the renewal of hematopoietic stem cells, and the induction of epithelial-to-mesenchymal transition (EMT) (34). Furthermore, *BMPR2* activates the SMAD signaling pathway, which is responsible for regulating cell proliferation and differentiation (35). The dysregulation of such a pathway likely leads to disruption of cellular differentiation, which may contribute to the development of leukemia.

Understanding the role of *ARID4B*, *MBD3* and *BMPR2* in the context of *KMT2A-r* ALL could provide valuable insights into unexplored and unknown mechanisms involved in leukemogenesis and/or leukemia maintenance. It may shed light on the specific molecular events that contribute to the transformation of fetal hematopoietic cells into leukemic cells. Such knowledge could have implications for the development of targeted therapies that aim to restore proper differentiation and halt the progression of *KMT2A-r* ALL. While understanding how *KMT2A-r* ALL cells exploit the epigenetic machinery to drive leukemogenesis and identifying counteractive therapeutic strategies remains a crucial objective, it is equally imperative to comprehend the mechanisms underlying leukemia relapse within the current treatment regimens. To address this, we conducted single-cell RNA sequencing (scRNA-seq) on diagnostic samples from infants with *KMT2A-r* ALL in **chapter 5**, providing valuable insights into the complex biology of relapse in this aggressive type of leukemia.

The glucocorticoid prednisone plays a critical role in ALL treatment, and the response to 7 days of prednisone monotherapy prior to induction therapy serves as a key indicator of clinical outcome in *KMT2A-r* iALL. In our study, we employed scRNA-seq technologies to analyze the expression of a prednisone-dependent signature, derived from an independent study, in diagnostic bone marrow and peripheral blood samples. By examining the expression profiles at the single-cell level, we were able to classify individual leukemic cells as either resistant or sensitive to treatment. This classification improved our ability to predict the likelihood of relapse in individual patients. Moreover, our research shed light on the characteristics of the therapy-resistant subpopulation of cells that initiate relapse. We observed that these cells had a smaller size as compared to the remaining population of leukemic cells, and that these cells exhibit a gene expression program that is compatible with quiescence and stemness properties.

Targeting and eliminating these relapse-initiating cells during the early stages of treatment holds significant potential to prevent relapse. An important aspect in this regard is the identification of biomarkers associated with these relapse-initiating cells. By identifying specific biomarkers, such as CD markers, upfront risk assessment can be performed through routine diagnostic procedures, eliminating the need for expensive scRNA-seq experiments to determine patient prognosis. To accomplish this, we are currently employing the Cellular Indexing of Transcriptomes and Epitopes by Sequencing (CITE)-Seq technique, which allows us to determine CD marker expression at the protein and single-cell level in the cells of interest alongside with scRNAseq. This approach, along with the potential of utilizing a rapid FACS experiment, shows promise for improving risk assessment. Furthermore, the possibility of selecting the relapse-initiating cells through a specific set of CD markers would enable us to selectively target and extensively study these cells. By focusing on these critical cells, we can potentially prevent relapse occurrence and improve patient outcomes and increased chances of long-term remission.

Ch1  
Ch2  
Ch3  
Ch4  
Ch5  
Ch6

It is important to note that the original study by Rhein et al. (36), which formed the foundation of our scRNA-seq findings, involved a cohort of 18 ALL patients comprising various different subtypes of ALL. Among the patients included, there was only one individual with *KMT2A-r* ALL who was 16 years of age, and no samples from infants (<1 year of age) with ALL were included. Hence, it is reasonable to consider that our findings in *KMT2A-r* iALL may have broader implications and relevance for other types of ALL as well.

In conclusion, there remains a pressing need for improved treatment strategies in *KMT2A-r* ALL. Although van der Sluijs et al. (37) recently reported promising results with blinatumomab, an immunotherapeutic agent targeting CD19 on top of intensive chemotherapy, the discoveries made in this thesis hold significant importance. The findings of this thesis have uncovered novel targets, leads, and mechanisms related to relapse and therapy resistance, which might be considered for treatment *KMT2A-r* infant ALL patients. Focusing on these specific vulnerabilities and exploring innovative treatment approaches holds the potential to enhance overall outcomes and prognosis for patients with *KMT2A-r* infant ALL. Ongoing research and evaluation in these areas are vital for advancing our understanding and developing more effective treatment strategies.

## REFERENCES

1. Schafer E, Irizarry R, Negi S, McIntyre E, Small D, Figueroa ME, et al. Promoter hypermethylation in MLL-r infant acute lymphoblastic leukemia: biology and therapeutic targeting. *Blood*. 2010;115(23):4798-809.
2. Stumpel DJ, Schneider P, van Roon EH, Boer JM, de Lorenzo P, Valsecchi MG, et al. Specific promoter methylation identifies different subgroups of MLL-rearranged infant acute lymphoblastic leukemia, influences clinical outcome, and provides therapeutic options. *Blood*. 2009;114(27):5490-8.
3. Stumpel DJ, Schneider P, van Roon EH, Pieters R, Stam RW. Absence of global hypomethylation in promoter hypermethylated Mixed Lineage Leukaemia-rearranged infant acute lymphoblastic leukaemia. *Eur J Cancer*. 2013;49(1):175-84.
4. Stumpel DJ, Schotte D, Lange-Turenhout EA, Schneider P, Seslija L, de Menezes RX, et al. Hypermethylation of specific microRNA genes in MLL-rearranged infant acute lymphoblastic leukemia: major matters at a micro scale. *Leukemia*. 2011;25(3):429-39.
5. Zhang Y, Chen A, Yan XM, Huang G. Disordered epigenetic regulation in MLL-related leukemia. *Int J Hematol*. 2012;96(4):428-37.
6. Brown P, Pieters R, Biondi A. How I treat infant leukemia. *Blood*. 2019;133(3):205-14.
7. Fang F, Zuo Q, Pilrose J, Wang Y, Shen C, Li M, et al. Decitabine reactivated pathways in platinum resistant ovarian cancer. *Oncotarget*. 2014;5(11):3579-89.
8. Serravalle S, Bertuccio SN, Astolfi A, Melchionda F, Pession A. Synergistic Cytotoxic Effect of L-Asparaginase Combined with Decitabine as a Demethylating Agent in Pediatric T-ALL, with Specific Epigenetic Signature. *Biomed Res Int*. 2016;2016:1985750.
9. Gore L, Triche TJ, Jr., Farrar JE, Wai D, Legendre C, Gooden GC, et al. A multicenter, randomized study of decitabine as epigenetic priming with induction chemotherapy in children with AML. *Clin Epigenetics*. 2017;9:108.
10. Cheung LC, Aya-Bonilla C, Cruickshank MN, Chiu SK, Kuek V, Anderson D, et al. Preclinical efficacy of azacitidine and venetoclax for infant KMT2A-rearranged acute lymphoblastic leukemia reveals a new therapeutic strategy. *Leukemia*. 2023;37(1):61-71.
11. Erin Guest JK, Meenakshi Devidas, Emily Hibbitts, Andrew J. Carroll, Nyla A. Heerema, Holly Kubaney, Amanda August, Melinda Pauly, Daniel Wechsler, Rodney R. Miles, Joel M. Reid, Cynthia Kihei, Lia Gore, Elizabeth A. Raetz, Stephen P. Hunger, Mignon L. Loh, Patrick A. Brown. A Pilot Study of Azacitidine As Epigenetic Priming for Chemotherapy in Infants Less Than 1 Year of Age with KMT2A-Rearranged Acute Lymphoblastic Leukemia (ALL); Results from the Children's Oncology Group (COG) Trial AALL15P1. *ASH2022: Blood*; 2022. p. 3256-7.
12. Gutman JA, Winters A, Kent A, Amaya M, McMahon C, Smith C, et al. Higher-dose venetoclax with measurable residual disease-guided azacitidine discontinuation in newly diagnosed acute myeloid leukemia. *Haematologica*. 2023.
13. Frismantas V, Dobay MP, Rinaldi A, Tchinda J, Dunn SH, Kunz J, et al. Ex vivo drug response profiling detects recurrent sensitivity patterns in drug-resistant acute lymphoblastic leukemia. *Blood*. 2017;129(11):e26-e37.
14. Issa GC, Aldoss I, DiPersio J, Cuglievan B, Stone R, Arellano M, et al. The menin inhibitor revumenib in KMT2A-rearranged or NPM1-mutant leukaemia. *Nature*. 2023;615(7954):920-4.
15. Smith C HR, Xie J, Liu X, He Y, Ludwig K, Klesse L, Zhang C, John S. LILRB4 Is a Novel Target for KMT2A Rearranged Acute Leukemia. *Blood*2022. p. 7423-4.



16. Gibson A, Trabal A, McCall D, Khazal S, Toepfer L, Bell DH, et al. Venetoclax for Children and Adolescents with Acute Lymphoblastic Leukemia and Lymphoblastic Lymphoma. *Cancers (Basel)*. 2021;14(1). Ch1
17. Pullarkat VA, Lacayo NJ, Jabbour E, Rubnitz JE, Bajel A, Laetsch TW, et al. Venetoclax and Navitoclax in Combination with Chemotherapy in Patients with Relapsed or Refractory Acute Lymphoblastic Leukemia and Lymphoblastic Lymphoma. *Cancer Discov*. 2021;11(6):1440-53. Ch2
18. G GU, Terz ICN. Arid4b alters cell cycle and cell death dynamics during mouse embryonic stem cell differentiation. *Turk J Biol*. 2021;45(1):56-64. Ch3
19. Terzi Cizmecioglu N, Huang J, Keskin EG, Wang X, Esen I, Chen F, et al. ARID4B is critical for mouse embryonic stem cell differentiation towards mesoderm and endoderm, linking epigenetics to pluripotency exit. *J Biol Chem*. 2020;295(51):17738-51. Ch4
20. Young IC, Wu B, Andricovich J, Chuang ST, Li R, Tzatsos A, et al. Differentiation of fetal hematopoietic stem cells requires ARID4B to restrict autocrine KITLG/KIT-*Src* signaling. *Cell Rep*. 2021;37(8):110036. Ch5
21. Malouf C, Ottersbach K. The fetal liver lymphoid-primed multipotent progenitor provides the prerequisites for the initiation of t(4;11) MLL-AF4 infant leukemia. *Haematologica*. 2018;103(12):e571-e4. Ch6
22. Ernst P, Wang J, Korsmeyer SJ. The role of MLL in hematopoiesis and leukemia. *Curr Opin Hematol*. 2002;9(4):282-7.
23. Hu YL, Fong S, Ferrell C, Largman C, Shen WF. HOXA9 modulates its oncogenic partner Meis1 to influence normal hematopoiesis. *Mol Cell Biol*. 2009;29(18):5181-92.
24. Adamaki M, Lambrou GI, Athanasiadou A, Vlahopoulos S, Papavassiliou AG, Moschovi M. HOXA9 and MEIS1 gene overexpression in the diagnosis of childhood acute leukemias: Significant correlation with relapse and overall survival. *Leuk Res*. 2015;39(8):874-82.
25. Wu RC, Young IC, Chen YF, Chuang ST, Toubaji A, Wu MY. Identification of the PTEN-ARID4B-PI3K pathway reveals the dependency on ARID4B by PTEN-deficient prostate cancer. *Nat Commun*. 2019;10(1):4332.
26. Shimbo T, Du Y, Grimm SA, Dhasarathy A, Mav D, Shah RR, et al. MBD3 localizes at promoters, gene bodies and enhancers of active genes. *PLoS Genet*. 2013;9(12):e1004028.
27. Yildirim O, Li R, Hung JH, Chen PB, Dong X, Ee LS, et al. Mbd3/NURD complex regulates expression of 5-hydroxymethylcytosine marked genes in embryonic stem cells. *Cell*. 2011;147(7):1498-510.
28. Harman JR, Thorne R, Jamilly M, Tapia M, Crump NT, Rice S, et al. A KMT2A-AFF1 gene regulatory network highlights the role of core transcription factors and reveals the regulatory logic of key downstream target genes. *Genome Res*. 2021;31(7):1159-73.
29. Kerry J, Godfrey L, Repapi E, Tapia M, Blackledge NP, Ma H, et al. MLL-AF4 Spreading Identifies Binding Sites that Are Distinct from Super-Enhancers and that Govern Sensitivity to DOT1L Inhibition in Leukemia. *Cell Rep*. 2017;18(2):482-95.
30. Torchy MP, Hamiche A, Klaholz BP. Structure and function insights into the NuRD chromatin remodeling complex. *Cell Mol Life Sci*. 2015;72(13):2491-507.
31. Lai AY, Wade PA. Cancer biology and NuRD: a multifaceted chromatin remodelling complex. *Nat Rev Cancer*. 2011;11(8):588-96.
32. Wood KH, Zhou Z. Emerging Molecular and Biological Functions of MBD2, a Reader of DNA Methylation. *Front Genet*. 2016;7:93.

33. Jiramongkolchai P, Owens P, Hong CC. Emerging roles of the bone morphogenetic protein pathway in cancer: potential therapeutic target for kinase inhibition. *Biochem Soc Trans.* 2016;44(4):1117-34.
34. Toofan P, Wheadon H. Role of the bone morphogenic protein pathway in developmental haemopoiesis and leukaemogenesis. *Biochem Soc Trans.* 2016;44(5):1455-63.
35. Jiao G, Guo W, Ren T, Lu Q, Sun Y, Liang W, et al. BMP2 inhibition induced apoptosis and autophagy via destabilization of XIAP in human chondrosarcoma cells. *Cell Death Dis.* 2014;5(12):e1571.
36. Rhein P, Scheid S, Ratei R, Hagemeyer C, Seeger K, Kirschner-Schwabe R, et al. Gene expression shift towards normal B cells, decreased proliferative capacity and distinct surface receptors characterize leukemic blasts persisting during induction therapy in childhood acute lymphoblastic leukemia. *Leukemia.* 2007;21(5):897-905.
37. van der Sluis IM, de Lorenzo P, Kotecha RS, Attarbaschi A, Escherich G, Nysom K, et al. Blinatumomab Added to Chemotherapy in Infant Lymphoblastic Leukemia. *N Engl J Med.* 2023;388(17):1572-81.

Ch1

Ch2

Ch3

Ch4

Ch5

**Ch6**



# CHAPTER 7

## Nederlandse wetenschappelijke samenvatting



## **NEDERLANDSE WETENSCHAPPELIJKE SAMENVATTING**

### **Kanker**

Kanker is een ziekte die al duizenden jaren bestaat en is een van de meest uitdagende en complexe ziekten om te doorgronden en te behandelen. Ondanks de immense vooruitgang die in de loop van de eeuwen is geboekt op het gebied van onderzoek en behandeling, blijft kanker een van de belangrijkste doodsoorzaken wereldwijd. Volgens de Wereldgezondheidsorganisatie zorgt kanker jaarlijks voor ongeveer 9,6 miljoen sterfgevallen, wat neerkomt op ongeveer één op de zes sterfgevallen wereldwijd. De incidentie van kanker zal naar verwachting met meer dan 50% toenemen in de komende twee decennia, met naar schatting 24 miljoen nieuwe gevallen per jaar tegen 2035.

### **Kinderkanker**

Met wereldwijd naar schatting jaarlijks 400.000 kankerpatiënten tussen 0 en 19 jaar, is kinderkanker een zeldzame ziekte. Desondanks blijft het de belangrijkste doodsoorzaak door ziekte bij kinderen en adolescenten. De meest voorkomende soorten kinderkanker zijn leukemieën, hersentumoren, lymfomen en solide tumoren zoals neuroblastoma (ontstaan uit zenuwcellen) en Wilms-tumoren (een nierkanker die voornamelijk kinderen treft).

Ondanks dat kinderkanker in vergelijking met kanker bij volwassenen een zeldzame ziekte is, vereist het aandacht en gespecialiseerde zorg. De unieke aard van kinderkanker onderscheidt zich van die van volwassenen. Bij kinderkanker zijn er over het algemeen minder genetische mutaties aanwezig en is de associatie met levensstijl- of omgevingsrisicofactoren veel minder sterk. Deze verschillen vereisen een aparte aanpak in de behandeling van kinderkanker. Bovendien is het bij de behandeling van kinderkanker cruciaal om rekening te houden met de mogelijke langetermijneffecten op kinderen. Anders dan bij volwassenen, waar de focus vaak ligt op het balanceren van korte-termijn complicaties met de voordelen van de behandeling, moeten de langetermijngevolgen van therapieën en interventies bij kinderen zorgvuldig worden overwogen.

### **Acute lymfatische leukemie bij kinderen**

Acute lymfatische leukemie (ALL) is de meest voorkomende maligniteit bij kinderen. Het vertegenwoordigt ongeveer 30% van alle gevallen van kinderkanker, met jaarlijks ongeveer 125 nieuwe gevallen in Nederland. Leukemie is een hematologische maligniteit die ontstaat in het beenmerg. Het wordt gekenmerkt door de accumulatie en ongecontroleerde groei van abnormale witte bloedcellen, de lymfoblasten, in het beenmerg. In een gezond proces van bloedvorming, ook wel hematopoëse genoemd, worden de functionele bloedcellen gevormd in het beenmerg, waarna ze differentiëren en vrijkomen in de bloedbaan om hun functies te bewerkstelligen. Bij leukemie is er een ongecontroleerde groei van

onrijpe lymfoblasten, waardoor de normale bloedcelvorming wordt onderdrukt. Het grote aantal van deze niet-functionele lymfoblasten in het beenmerg en hun circulatie in de bloedbaan veroorzaken typische symptomen en complicaties, zoals verdringing van gezonde bloedcellen met als gevolg infecties, bloedarmoede, bloedingen, botpijn en infiltratie van vitale organen zoals de milt, hersenen, lever en andere organen. Het begrijpen van de mechanismen en gevolgen van de abnormale groei en verspreiding van lymfoblasten is cruciaal voor de diagnose en behandeling van leukemie bij kinderen.

Ch1

Ch2

Ch3

Ch4

### **ALL bij zuigelingen**

Ch5

De behandeling van pediatrische ALL heeft de afgelopen decennia aanzienlijke vooruitgang geboekt, met opmerkelijke verbeteringen in de overlevingskansen, resulterend in een huidige 5-jaarsoverleving van boven de 90%. Echter, zuigelingen (kinderen jonger dan 1 jaar) met ALL vormen ongeveer 5% van alle gevallen van kinderleukemie en hebben een lagere overlevingskans van ongeveer 50%. ALL vertoont bij zuigelingen vaak meer agressieve kenmerken in vergelijking met oudere kinderen. Zuigelingen presenteren zich vaak met hogere tumorcel aantallen en vaker met infiltratie van het centrale zenuwstelsel, wat de aanwezigheid van leukemische cellen in de hersenen en het ruggenmerg betekent. Ondanks succesvolle initiële behandeling is het risico op terugval bij deze jonge patiënten hoog, vaak zelfs tijdens de behandelingsperiode. Dit hoge recidiepercentage geeft aan dat de bestaande behandelingen niet volledig effectief zijn bij het voorkomen van een terugval bij zuigelingen met ALL. Daarom is er een dringende behoefte aan verbeterde behandelstrategieën om het risico op terugval te verminderen en de lange termijn uitkomsten voor deze patiënten te verbeteren.

Ch6

Ch7

### **De unieke biologie van *KMT2A*-herschikte ALL**

ALL bij zuigelingen wordt gekenmerkt door een hoge frequentie (80%) chromosomale afwijkingen in het Lysine Methyltransferase 2A (*KMT2A*) gen, voorheen bekend als het *Mixed Lineage Leukemia (MLL)* gen. Deze *KMT2A*-herschikte ALL komt bij oudere kinderen met ALL slechts bij ongeveer 5% van de gevallen voor. Helaas vertegenwoordigt deze *KMT2A*-herschikte ALL bij zuigelingen een zeer agressieve vorm van kinderleukemie met een unieke biologie. De behandeling van deze patiënten volgens de huidige behandelprotocollen resulteert in een overleving van ongeveer 40% na 6 jaar, in vergelijking met bijna 75% bij zuigelingen met ALL zonder afwijkingen in het *KMT2A* gen (wildtype *KMT2A*) en 90% bij oudere kinderen met ALL.

In een gezonde situatie speelt het *KMT2A*-gen een cruciale rol bij de vorming van bloedcellen door 'epigenetische' regulatie van bepaalde genen. Epigenetica omvat verschillende mechanismen die genen kunnen reguleren zonder wijzigingen aan te brengen in de DNA-sequentie zelf. Epigenetica is bijvoorbeeld de reden waarom een cel

in de hersenen verschilt van een cel in de huid. Het DNA in de cel is hetzelfde, maar verschillende genen worden “aan” en “uit” geschakeld, oftewel de genexpressie is per celtype verschillend, hetgeen resulteert in cellen met volledig verschillende functies. Het epigenoom omvat onder andere de methylering van het DNA, modificaties in de histonen (eiwitten waaromheen het DNA gewonden is) en niet-coderende RNA-moleculen. Deze modificaties kunnen invloed hebben op de structuur van het DNA en de toegankelijkheid van genen voor transcriptie, wat leidt tot veranderingen in genexpressie.

Bij *KMT2A*-herschikte leukemie vindt er een fusie plaats tussen het *KMT2A* gen en een ander gen, resulterend in de vorming van een nieuw eiwit dat abnormale groei en proliferatie van leukemiecellen veroorzaakt. De meest voorkomende genen waarmee *KMT2A* bij zuigelingen-ALL fuseert zijn het *AFF1* gen (*AF4*), het *MLLT3* gen (*AF9*) en het *MLLT1* gen (*ENL*). Deze genen coderen allemaal voor eiwitten die deel uitmaken van complexen die verantwoordelijk zijn voor de regulatie van epigenetische mechanismen. Deze fusie eiwitten verstoren activiteiten van deze regulerende complexen. Als gevolg hiervan wordt *KMT2A*-herschikte ALL gekenmerkt door een abnormaal epigenoom, wat tot uiting komt in afwijkende patronen van DNA-methylering en histon modificaties die de genexpressie van de cel veranderen. Aangezien er naast de afwijking in het *KMT2A* gen nauwelijks verder afwijkingen worden geconstateerd, wordt deze vorm van leukemie als een epigenetische ziekte gezien.

### **Demethyleerder medicijn decitabine**

Eerder is aangetoond door ons en anderen dat *KMT2A*-herschikte ALL gekenmerkt wordt door afwijkende methylering patronen van het DNA. Dit heeft geleid tot de evaluatie van zogenaamde demethyleerende medicijnen, die de methylering van het DNA remmen, zoals decitabine en zebularine. Hoewel de cytotoxiciteit tegen *KMT2A*-herschikte ALL-cellen in gekweekte leukemiecellen buiten het lichaam is waargenomen, ontbraken gegevens over de effectiviteit van demethyleerende middelen in muismodellen. Daarom hebben we in **hoofdstuk 2** het anti-leukemische effect van lage en klinisch relevante doseringen van het demethyleerende middel decitabine geëvalueerd in een muismodel voor humaan *KMT2A*-herschikte ALL. Helaas hebben we slechts een lichte vertraging in de progressie van leukemie waargenomen, wat wijst op beperkte werkzaamheid van decitabine. Aangezien demethyleerende middelen bij andere soorten kanker vaak als middel gebruikt wordt om de gevoeligheid voor andere medicijnen te verhogen, hebben we onderzocht of dit wellicht ook het geval is bij *KMT2A*-herschikte ALL. Een recent klinisch onderzoek bij zuigelingen met *KMT2A*-herschikte ALL toonde aan dat een ander demethyleerend middel, azacytidine, in combinatie met de huidige standaard chemotherapie voor deze patiënten goed verdragen werd. Helaas bleven ondanks deze gunstige verdraagbaarheid de overlevingskansen van de patiënten in de studie



vergelijkbaar met de lage overlevingspercentages die te zien zijn in historische resultaten. Dit geeft aan dat demethylatie-agents zoals azacitidine en decitabine in combinatie met huidige behandelingsprotocollen de uitkomst van zuigelingen met *KMT2A*-herschikte ALL waarschijnlijk niet zullen verbeteren.

Ch1

Ch2

Ch3

### **Verworven drug resistentie tegen DOT1L inhibitie**

Zoals hierboven beschreven ontstaan *KMT2A*-herschikte leukemieën door een fusie tussen het *KMT2A* gen en een ander gen, wat resulteert in de vorming van abnormale *KMT2A*-fusie-eiwitten. Deze fusie-eiwitten trekken het eiwit DOT1L aan. DOT1L is verantwoordelijk voor het toevoegen van een methylgroep aan histonen, de eiwitten waar het DNA omheen is gewikkeld in onze cellen. Door deze methylering vindt er abnormale genregulatie plaats wat leidt tot de ontwikkeling van leukemie.

Ch4

Ch5

Ch6

Ch7

Pinometostat is een geneesmiddel dat behoort tot de klasse van DOT1L-remmers en remt specifiek de werking van DOT1L. Hoewel veelbelovende resultaten zijn behaald met pinometostat in laboratoriumtesten bij *KMT2A*-herschikte leukemieën, hebben klinische onderzoeken bij volwassen patiënten met deze vorm van leukemie aangetoond dat de ziekteprogressie als gevolg van verworven resistentie tegen pinometostat onvermijdelijk is. Het begrijpen van de mechanismen die ten grondslag liggen aan deze verworven resistentie kan helpen bij het identificeren van manieren om deze resistentie te omzeilen of kan helpen om alternatieve mechanismen te ontdekken waardoor *KMT2A*-fusie-eiwitten hun kankerverwekkende functies kunnen uitoefenen, onafhankelijk van DOT1L. Om deze reden hebben we ons in **hoofdstuk 3** gericht op het onderzoeken van de mechanismen van verworven resistentie tegen pinometostat. Dit hebben we gedaan door het opzetten en uitgebreid karakteriseren van een cellijnmodel waarin verworven resistentie tegen DOT1L-remming is geïnduceerd bij *KMT2A*-herschikte ALL. Dit model heeft belangrijke inzichten opgeleverd over het aanpassingsvermogen van leukemische cellen aan DOT1L-remmers.

Opmerkelijk genoeg bleek de expressie van het gen *CD133/PROM1* verminderd was in de onderzochte leukemische cellen. *CD133/PROM1* wordt beschouwd als een marker die vaak aanwezig is op stamcellen, pluripotente cellen met het vermogen tot zelfvernieuwing en differentiatie naar diverse celtypes. De verminderde expressie van *CD133/PROM1* suggereert dat deze leukemische cellen mogelijk hun stamcelkenmerken verliezen of verminderen. Dit kan wijzen op een verandering in de ontwikkelingsstatus van de cellen en kan gevolgen hebben voor hun fenotype en respons op behandelingen. Daarnaast zagen we dat deze cellen het vermogen vertonen om myeloïde kenmerken aan te nemen, wat verwijst naar eigenschappen en functies die typisch zijn voor myeloïde cellen, een ander subtype van witte bloedcellen. De verhoogde expressie van myeloïde markers CD33

en LILRB4/cd85k na verworven resistentie voor pinometostat duiden op een overgang of selectie naar myeloïde-achtige kenmerken. Het blokkeren van deze overgang of selectie naar myeloïde-achtige eigenschappen kan een mogelijke strategie zijn om *KMT2A*-herschikte ALL te genezen.

Deze opmerkelijke veranderingen na verworven resistentie tegen pinometostat toont de cellulaire plasticiteit van *KMT2A*-herschikte ALL, wat betekent dat ze flexibel zijn en in staat zijn om verschillende celtypes te worden of verschillende functies aan te nemen.

### **Identificatie van nieuwe moleculaire kwetsbaarheden *ARID4B*, *MBD3* en *BMPR2***

Vervolgens hebben we ons afgevraagd in **hoofdstuk 4** of er andere en nog onbekende epigenetische kwetsbaarheden bestaan die specifiek zijn voor *KMT2A*-herschikte ALL-cellen. Om deze vraag te beantwoorden, hebben we gebruik gemaakt van de CRISPR-Cas9 technologie. Met behulp van deze technologie is het mogelijk om bepaalde genen uit te schakelen om zo te onderzoeken of deze genen van belang zijn voor de overleving van de *KMT2A*-herschikte ALL cellen. Dit heeft inderdaad geleid tot de identificatie van nieuwe moleculaire afhankelijkheden en potentiële therapeutische doelwitten, waaronder *ARID4B*, *MBD3* en *BMPR2*, voor dit type leukemie. Momenteel wordt onderzocht wat de exacte rol van *ARID4B*, *MBD3* en *BMPR2* is in de context van *KMT2A*-herschikte ALL en hoe dit gebruikt kan worden voor de behandeling.

### **Identificatie van recidief initiërende cellen**

In **hoofdstuk 5** hebben we gebruikgemaakt van de single-cell RNA-sequencing (scRNA-seq) techniek om de genexpressie in individuele leukemiecellen te analyseren. We hebben diagnostische monsters van *KMT2A*-herschikte infant ALL-patiënten die vroege recidieven hadden vergeleken met monsters van patiënten die een langdurige overleving hadden. Dit stelde ons in staat om individuele leukemische cellen te classificeren als 'resistent' of 'gevoelig' voor behandeling, we toonden aan dat subpopulaties van de meest therapieresistente cellen bij diagnose nauwkeurig de kans op toekomstige recidieven bij individuele patiënten kan voorspellen. De identificatie en karakterisering van deze cellen die recidief voorspellen of initiëren, vormt een cruciale stap in ons begrip van het mechanisme achter het terugkeren van leukemie tijdens de behandeling en draagt bij aan het ontwikkelen van preventieve maatregelen. Het onderzoek heeft inzicht gegeven in de complexe biologie van een recidief.

### **Perspectieven**

Er is een dringende behoefte aan verbeterde behandelingsstrategieën voor *KMT2A*-herschikte infant ALL patiënten. De bevindingen in dit proefschrift bieden nieuwe inzichten die kunnen bijdragen aan de verbetering van de prognose voor deze patiënten.

Momenteel worden de recidief-initiërende cellen verder onderzocht om ze vroeg in de behandeling te identificeren en te elimineren, om zo het terugkeren van de leukemie later te voorkomen en de overlevingskansen van de zuigelingen te verbeteren.

Ch1

Ch2

Tevens onderzoeken we momenteel of er overeenkomsten zijn in de mechanismen achter de verworven resistentie tegen de DOT1L-remmers en verworven resistentie tegen MENIN-remmers. MENIN-remmers zijn, net als de DOT1L-remmers, gericht op het tegengaan van de oncogene effecten van de KMT2A-fusie-eiwitten en worden momenteel geëvalueerd in klinische onderzoeken bij kinderen met *KMT2A*-herschikte leukemie. Interessant genoeg hebben we inderdaad vergelijkbare effecten waargenomen na het ontstaan van resistentie tegen MENIN-remmers als eerder gezien bij resistentie tegen DOT1L-remming, wat suggereert dat er een gemeenschappelijk “ontsnappingsmechanisme” bestaat voor beide epigenetische medicijnen. Dit zal de komende tijd verder onderzocht worden.

Ch3

Ch4

Ch5

Ch6

Ch7

Daarnaast wordt er verder onderzoek gedaan naar de rol van de nieuwe geïdentificeerde moleculaire kwetsbaarheden *ARID4B*, *MBD3* en *BMPR2* in de context van *KMT2A*-herschikte ALL om mogelijke aanknopingspunten te vinden voor innovatieve therapieën.



# ABOUT THE AUTHOR

**Curriculum Vitae**

**List of Publications**

**Dankwoord/Acknowledgments**



## ABOUT THE AUTHOR / CURRICULUM VITAE

Pauline Schneider was born on the 16<sup>th</sup> of August 1977 in Alkmaar. She attended high school (VWO) at the Jan Arentsz in Alkmaar, the Netherlands, where she graduated in 1995.

She began her studies in Medical Biology at Vrije Universiteit in Amsterdam. After two years, she switched to the Medical Biology program at Amsterdam University of Applied Sciences. During this period, she completed an internship at the Netherlands Cancer Institute (NKI) within the tumor research group led by John Hilkens. Her project had a specific focus on insertional mutagenesis for the identification of genes associated with metastasis in mammary cancer. Pauline obtained her bachelor's degree in 2000 and continued working within the tumor research group for several months before embarking on a six-month journey to India, Nepal, and Tibet.



Upon her return, she joined Galapagos, a pharmaceutical research company where her work aligned with her interests in cancer research, focusing on the discovery of novel targets for the treatment of metastasis. After switching to several not-cancer related projects, which included the production of lentiviral knockout libraries and target validations, she returned to academia in 2003 to continue working in the field of cancer research. She became a research technician in the Pediatric Oncology/Hematology department led by Rob Pieters and Monique den Boer at Erasmus MC/Sophia Children's Hospital. In 2007, she started the position of labmanager, where she supervised a team of research technicians in the pediatric oncology research laboratory, led by Monique den Boer. Simultaneously, she continued her research activities within the infant acute lymphoblastic leukemia group, led by Ronald Stam. Over the years, she provided valuable assistance to numerous Ph.D. students in their projects, played a pivotal role in setting up new research projects, and concurrently pursued her own research projects, including investigating the role of extracellular vesicles, and CNS involvement in *MLL*-rearranged infant acute lymphoblastic leukemia. After setting up several research projects and guiding other phd students, in 2016 she took the opportunity to realize her own PhD project.

In 2016, she started her PhD research in Ronald Stam's group, which had transitioned to the Princess Maxima Center for Pediatric Oncology. Her research focused on epigenetic drugs, cellular resistance, and epigenetic plasticity in *MLL*-rearranged acute lymphoblastic

leukemia. The results of this research are detailed in this thesis. Currently, she is working as a postdoc in the Stam group on the follow-up of the thesis results within the 'Cure2MLL' project, funded by Fight Kids Cancer. This project is a collaborative initiative involving a large international team of scientists.

Pauline lives in Zeist with her sons Quinn (2007), Yannick (2009), and Ayden (2011).

Ch1

Ch2

Ch3

Ch4

Ch5

Ch6

Ch7

AA

## LIST OF PUBLICATIONS

Kerstjens M, Pinhancos SS, Castro PG, **Schneider P**, Wander P, Pieters R, Stam RW. Trametinib inhibits RAS-mutant MLL-rearranged acute lymphoblastic leukemia at specific niche sites and reduces ERK phosphorylation in vivo. *Haematologica*. 2018

Hyrenius-Wittsten A, Pilheden M, Falqués-Costa A, Eriksson M, Stuesson H, **Schneider P**, Wander P, Garcia-Ruiz C, Liu J, Ågerstam H, Hultquist A, Lilljebjörn H, Stam RW, Järås M, Hagström-Andersson AK.

FLT3N676K drives acute myeloid leukemia in a xenograft model of KMT2A-MLL3 leukemogenesis. *Leukemia*, 2019

Agraz-Doblas A, Bueno C, Bashford-Rogers R, Roy A, **Schneider P**, Bardini M, Ballerini P, Cazzaniga G, Moreno T, Revilla C, Gut M, Valsecchi MG, Roberts I, Pieters R, De Lorenzo P, Varela I, Menendez P, Stam RW.

Unraveling the cellular origin and clinical prognostic markers of infant B-cell acute lymphoblastic leukemia using genome-wide analysis. *Haematologica*, 2019

**Pauline Schneider\***, Patricia Garrido Castro\*, Sandra M. Pinhancos, Mark Kerstjens, Eddy H. van Roon, Anke H.W. Essing, M. Emmy M. Dolman, Jan J. Molenaar, Rob Pieters, Ronald W. Stam.

Decitabine mildly attenuates MLL-rearranged acute lymphoblastic leukemia in vivo, and represents a poor chemo-sensitizer. *eJHaem* 2020

Wander P, Cheung LC, Pinhancos SS, Jones L, Kerstjens M, Arentsen-Peters STCJM, Singh S, Chua GA, Castro PG, **Schneider P**, Dolman MEM, Koopmans B, Molenaar JJ, Pieters R, Zwaan CM, Kotecha RS, Stam RW.

Preclinical efficacy of gemcitabine in MLL-rearranged infant acute lymphoblastic leukemia. *Leukemia*. 2020

Juan Ramón Tejedor, Clara Bueno, Meritxell Vinyoles, Paolo Petazzi, Antonio AgrazDoblas, Isabel Cobo, Raúl Torres-Ruiz, Gustavo F Bayón, Raúl F Perez, Sara LópezTamargo, Francisco Gutierrez-Agüera, Pablo Santamarina-Ojeda, Manuel Ramírez-Orellana, Michela Bardini, Gianni Cazzaniga, Paola Ballerini, **Pauline Schneider**, Ronald W Stam, Ignacio Varela, Mario F Fraga, Agustín F Fernández1, Pablo Menéndez.

Integrative methylome-transcriptome analysis unravels cancer-cell vulnerabilities in infant MLL-rearranged B-cell acute lymphoblastic leukemia. *J Clin Invest*. 2021

Priscilla Wander, Susan T.C.J.M. Arentsen-Peters, Sandra S. Pinhancos, Bianca Koopmans, M.Emmy M. Dolman, Rijndert Ariese, Frank L. Bos, Patricia Garrido Castro, Luke Jones,



- Pauline Schneider**, Miriam Guillen Navarro, Jan J. Molenaar, Anne C. Rios, C. Michel Zwaan, Ronald W. Stam, Ch1  
 High-throughput drug screening reveals Pyrvinium pamoate as effective candidate Ch2  
 against pediatric MLL-rearranged acute myeloid leukemia, *Translational Oncology* 2021 Ch3
- Kerstjens, M.; Garrido Castro, P.; Pinhanços, S.S.; **Schneider, P.**; Wander, P.; Pieters, R.; Stam, Ch4  
 R.W. Irinotecan Induces Disease Remission in Xenograft Mouse Models of Pediatric MLL- Ch4  
 Rearranged Acute Lymphoblastic Leukemia. *Biomedicines* 2021.
- Wander P, Arentsen-Peters STCJM, Vrenken KS, Pinhanços SM, Koopmans B, Dolman Ch5  
 MEM, Jones L, Garrido Castro P, **Schneider P**, Kerstjens M, Molenaar JJ, Pieters R, Zwaan Ch6  
 CM, Stam RW.
- High-Throughput Drug Library Screening in Primary KMT2A-Rearranged Infant ALL Cells Ch7  
 Favors the Identification of Drug Candidates That Activate P53 Signaling. *Biomedicines*, 2022
- Morris V, Wang D, Li Z, Marion W, Hughes T, Sousa P, Harada T, Sui SH, Naumenko S, Kalfon AA  
 J, Sensharma P, Falchetti M, Vinicius da Silva R, Candelli T, **Schneider P**, Margaritis T,  
 Holstege FCP, Pikman Y, Harris M, Stam RW, Orkin SH, Koehler AN, Shalek AK, North TE,  
 Pimkin M, Daley GQ, Lummertz da Rocha E, Rowe RG. Hypoxic, glycolytic metabolism is a  
 vulnerability of B-acute lymphoblastic leukemia-initiating cells. *Cell Rep*, 2022
- Candelli T, **Schneider P**, Garrido Castro P, Jones LA, Bodewes E, Rockx-Brouwer D, Pieters  
 R, Holstege FCP, Margaritis T, Stam RW.  
 Identification and characterization of relapse-initiating cells in MLL-rearranged infant ALL  
 by single-cell transcriptomics. *Leukemia* 2022
- Schneider, P.**; Wander, P.; Arentsen-Peters, S.T.C.J.M.; Vrenken, K.S.; Rockx-Brouwer, D.;  
 Adriaanse, F.R.S.; Hoeve, V.; Paassen, I.; Drost, J.; Pieters, R.; et al. CRISPR-Cas9 Library  
 Screening Identifies Novel Molecular Vulnerabilities in KMT2A-Rearranged Acute  
 Lymphoblastic Leukemia. *Int. J. Mol. Sci*, 2023.
- Schneider, P.**, Crump, N.T., Arentsen-Peters, S.T. et al. Modelling acquired resistance to  
 DOT1L inhibition exhibits the adaptive potential of KMT2A-rearranged acute lymphoblastic  
 leukemia. *Exp Hematol Oncol*, 2023

## **DANKWOORD / ACKNOWLEDGMENTS**

Daar ligt hij dan, mijn eigen gouden boekje, mijn proefschrift, het eind van een lange weg met dit mooie resultaat. En daar ben ik best een beetje trots op.

Het begon allemaal in 2003 toen ik aangenomen werd als research analist bij de research kinderoncologie in het Erasmus MC/Sophia kinderziekenhuis. Mede daarom beperkt mijn dankwoord zich niet tot alleen de periode van mijn PhD, maar beslaat dit ook de periode in aanloop hiernaartoe.

Het afronden van dit proefschrift betekent het einde van een lange en spannende reis, en ik realiseer me goed dat ik deze reis niet alleen heb gemaakt. Veel mensen hebben een bijdrage geleverd aan het succesvol voltooien van dit onderzoek, en ik wil dan ook graag mijn oprechte dank uitspreken aan iedereen die me heeft gesteund, begeleid en aangemoedigd.

Allereerst wil ik graag alle zuigelingen met leukemie en hun ouders bedanken voor het doneren van materiaal ten behoeve van het onderzoek. Dit patiënten materiaal heeft een cruciale rol gespeeld in het onderzoek in dit proefschrift en is tevens van onschatbare waarde voor verder onderzoek. Ik hoop van harte dat de resultaten van dit onderzoek zullen bijdragen aan een verbetering van de overlevingskansen bij zuigelingen met leukemie.

Mijn dank gaat eveneens uit naar Stichting Kinderen Kankervrij (KiKa) voor hun financiële steun aan dit onderzoek. Mijn waardering gaat uit naar iedereen die betrokken is bij en zich inzet voor KiKa, want jullie inzet maakt een verschil in de strijd tegen deze oneerlijke ziekte. Laten we samen streven naar genezing voor iedere patiënt.

Dank aan mijn promotor prof. Dr. R. Pieters. Beste Rob, we kennen elkaar al sinds 2003, toen ik begon als research analist in het laboratorium voor kinderoncologie. Tijdens vergaderingen met Ronald, je PhD student op dat moment, en later met de PhD-studenten onder de leiding van Ronald, zag ik hoe je begeleiding eruitzag. Het was echter een heel andere ervaring toen ik zelf een PhD-student werd en de besprekingen ineens over mijn eigen onderzoek gingen. In je drukke schema wist je altijd tijd vrij te maken voor overleg, en op jouw karakteristieke, ontspannen manier gaf je waardevolle feedback. Jouw ervaring en visie waren tijdens onze ontmoetingen van onschatbare waarde om het grotere plaatje in het onderzoek niet uit het oog te verliezen. Hartelijk dank voor jouw begeleiding.

En natuurlijk grote dank aan mijn co-promotor Dr. R.W. Stam. Beste Ronald, waar zal ik beginnen? Toen ik begon als research analist in het lab, was er al snel een klik tussen ons. Telkens weer werden nieuwe ideeën met veel enthousiasme uitgewerkt. In eerste

instantie als research analist tijdens jouw AIO-periode en later toen je begon als groepsleider, had ik altijd de vrijheid om naast het ondersteunen van de PhD-studenten mijn eigen onderzoek te doen. Dit heeft mijn verlangen aangewakkerd om mijn eigen onderzoek af te ronden, en die kans heb je me geboden. Daar ben ik je enorm dankbaar voor. Fijn om nu als postdoc in je groep aan het vervolg van de onderwerpen uit dit proefschrift verder te werken. Ik ben benieuwd naar welke interessante ontwikkelingen daaruit zullen voortvloeien.

Ch1

Ch2

Ch3

Ch4

Verder gaat mijn dank uit naar de leescommissie. Prof. Dr. Monique den Boer, Prof. dr. O.T. Heidenreich, Dr. E. Hulleman, Prof. dr. G.J. Kaspers en Prof. dr. R.P. Kuiper, bedankt voor het beoordelen van mijn proefschrift.

Ch5

Ch6

Beste Monique, wij gaan al heel wat jaren terug. Ik heb de tijd in Rotterdam als erg prettig ervaren. Ik kan me dan ook geen betere opponent bedenken voor mijn promotie.

Ch7

Dear Olaf, thank you for your insightful input and fruitful comments during our work discussions. Your sense of humor is always engaging.

AA

Beste Esther, ook wij kennen elkaar al vanuit Rotterdam, maar ook na je vertrek daar, hebben we samengewerkt in het lab aan de VU. Bedankt voor je betrokkenheid bij de voortgang van mijn PhD project. Het is prettig om je als opponent in de commissie te hebben.

Beste Gertjan, fijn dat je als kinderoncoloog en expert op het gebied van kinderleukemie in de commissie wil plaats nemen.

Beste Roland, het is een genoegen dat je als deskundige op het gebied van Moleculaire Genetica deel uitmaakt van de promotiecommissie.

Hartelijk dank aan mijn paranimfen, Susan en Kirsten. Wat een eer dat jullie naast me staan bij deze plechtigheid!

Susan, in 2003 starten we tegelijk als research analist bij de kinderoncologie lab van het Erasmus MC voor ondersteuning van de PhD studenten en opwerken van het patiënten materiaal. Na al die jaren als collega's op verschillende manieren, is het leuk om jou naast me te hebben als paranimf.

Kirsten, een paar jaar geleden voegde je je bij de Stam groep als startende postdoc. Altijd bereid om te helpen met onderzoek en kritisch te kijken naar de geschreven stukken. Een aanwinst voor de groep. Bedankt voor je hulp en fijn dat je naast me staat als paranimf. Thanks to all the members of the Stam group, recent or previous, for their expertise, input, help and 'gezelligheid'.

Fabienne, bedankt voor de fijne samenwerking bij de verschillende projecten. Succes met de laatste loodjes van je PhD, en wens je een prachtige reis door Vietnam! Benieuwd wat de toekomst je zal brengen, wellicht worden we in de toekomst weer collega's.

Tamara, onze trip naar de ASH in New Orleans was erg goed geslaagd, leuk om je zo beter te leren kennen. Succes met het afmaken van je PhD en veel geluk met je kersverse gezinnetje.

Ana, it is great to have you as a student in the lab. I love your enthusiasm, dedication, and commitment. I genuinely hope you will continue as a PhD student in the Princess Maxima Center and develop to become a brilliant researcher. I think now is a good time to open the bottle of port...

Priscilla, bedankt voor de fijne samenwerking, gezelligheid op het lab, en niet te vergeten de uitjes naar de escaperooms. Het was fijn je als collega te hebben met als hoogtepunt de AACR meeting in Chicago. Fijn dat je je plek hebt gevonden bij de HOVON in Rotterdam.

Sandra, also for you it was a huge change when we moved to Utrecht as a group. Thank you for all your help in the lab. Your honesty and hard work is highly appreciated. It loved all the years working with you and sharing the office space. All the best to you as a PhD in Portugal.

Patricia, I appreciate all the collaborations, valuable discussions, and insights, as well as the enjoyable lunch breaks, dinners, social gatherings and of course working on the decitabine project together. Your wealth of knowledge on various topics has always been engaging and entertaining to hear. All the best in your career and it would be nice to catch up in Zeist.

Dedeke, bedankt voor je hulp bij de verschillende projecten. Jou ervaring als analist is van grote waarde. Jammer dat je niet meer bij ons werkt, maar fijn dat je je plek hebt gevonden bij het UMC.

Aida, Luke, Miriam, and Sanne, thank you for the input and contributions you've made during our time working together. Your insights, discussions, and helping hands are much appreciated. All the best in your careers.

Stagiaires, Elise, Romy, Veerle, bedankt voor jullie bijdrage aan de verschillende projecten van mijn proefschrift en Noud, Sietske, Daniel, Carmen, Hannah, Jezabel, en alle andere studenten, hartelijk dank voor jullie bijdrage aan het onderzoek van de Stam groep. Ik wens jullie het allerbeste voor het verder ontwikkelen van jullie carrières.

Also, thanks to the members of the Infant group at the Erasmus MC, the previous Stam group, for their contributions during my time before becoming a PhD student. Eddy, Mark, Merel, Adrian, Emma, Robin, Marieke, Lidija, Jill, Dominique, and all the others, I really enjoyed working together.

Oud-analisten Karin, Jessica, Monique, Susan en Mathilde - de research analisten van het begin van mijn tijd bij het Erasmus MC, die een sterke basis hebben gelegd. Bedankt voor

de gezellige goede oude tijd. Daar denk ik met plezier aan terug. Dat we nog maar lang elk jaar een uitje organiseren om bij te kletsen.

Ook hartelijk dank aan de collega's van de afdeling Kindergeneeskunde van het Erasmus MC in Rotterdam, voor de fijne tijd daar en het leggen van de basis voor mijn PhD-periode. Ik heb besloten maar geen namen te noemen, veel te veel om allemaal hier te vermelden. Maar wel ik graag Marcel bedanken voor zijn inzet, altijd fijn om je als collega gehad te hebben. En Wilco, fijn dat je weer terug bent op het lab kindergeneeskunde. Bedankt voor je bereidheid om altijd ergens mee te helpen. Veel succes allemaal met jullie inzet voor de kindergeneeskunde.

Daarnaast ook dank aan de samenwerkingen met de kinderoncologen, zowel uit de periode van het Erasmus MC als ook bij Het Prinses Maxima Centrum, zoals Michel Zwaan, Marry van den Heuvel, Max van Noesel, Auke Beishuizen, Peter Hoogebrugge, Bianca Goemans, Janine Stutterheim, Inge van der Sluis, en natuurlijk alle andere kinderoncologen. Fijn om samen te werken, informatie uit te wisselen en de kloof tussen research en kliniek te verkleinen.

Collega's van het specieel lab van het Erasmus MC, het SKION, en het diagnostisch lab van het Prinses Maxima Centrum, hartelijk dank voor jullie inzet. Met name Rolinda en Henk, hartelijk dank. Ik heb de samenwerking altijd erg gewaardeerd.

Hartelijk dank aan Jules Meijerink. Beste Jules, je inzichten, input en visie heb ik altijd erg gewaardeerd. Het was prettig samenwerken zowel bij het ErasmusMC als bij het Prinses Maxima Centrum. Ik wens je het allerbeste in het vervolg van je carrière bij Acerta Pharma/AstraZenica.

Dan de werknemers van het begin van het Prinses Maxima Centrum in het Hubrecht instituut, waar ik de kamer deelde met Eric, Sabine, Esmé, Sandra en Kirsten. Bedankt voor de prettige gesprekken en goede discussies. En ja Sabine, je komt in het dankwoord. Je had altijd wel een gezellig praatje. Esmé, leuk om je musical verhalen mee te krijgen. Ik ben benieuwd hoe het nu gaat met je als Klinisch Geneticus. Kirsten, veel geluk in het lab van Frank Staal. Eric, je missie is geslaagd, wanneer het kan ga ik nu met de fiets naar het werk.

Many thanks for the collaborators within the Princess Máxima Center for their expertise and helping hands.

Collega's van de Drost-groep, met name Jarno, Irene en Lars, hartelijk bedankt voor jullie hulp bij het CRISPR-project. Jules en Rico, dank jullie wel voor de vruchtbare discussies en analyses in het DOT1L-project. Daarnaast wil ik ook mijn collega's van alle andere groepen waarmee ik heb samengewerkt, van harte bedanken voor de prettige samenwerking, het

meedenken en de gezelligheid in het lab, zoals de collega's van de Drost-groep, Holstege-groep, Rios-groep, Molenaar-groep, van Leeuwen groep, Kuiper-groep, den Boer-groep, Heidenreich-groep, Hulleman-groep, van Boxtel-groep, Nierkens-groep, Clevers-groep, Imaging Facility, FACS Facility, High-throughput Screening Facility, Single-Cell Genomics Facility en alle andere groepen. Bianca, Anke en Emmy, bedankt voor jullie hulp bij de drug library screenings in het Stratenum. Cesca en Judith, altijd fijn om nog even bij te kletsen met collega's uit Rotterdam en hulp te vragen of bieden. Dennis en Thomas, dank voor het delen van jullie expertise over p53 mutaties. Frank, Laurens, Dorette, Gawin, Jessica en Trisha, het is fijn om jullie als collega's te hebben en samen te werken op het gebied van leukemie, informatie te delen en elkaar hulp te kunnen vragen en bieden.

Graag wil ik Prof. Dr. Frank Holstege bedanken. Beste Frank, onze samenwerking in het single cell sequencing project heb ik enorm gewaardeerd. Jou manier van werken vind ik erg prettig, doortastend, duidelijk, eerlijk en direct, een inspiratie voor velen. Bedankt voor je fijne voorbeeld.

Thanasis and Tito, thank you for the very pleasant collaboration on the single-cell project. Thanasis, I truly enjoy and appreciate your insights and perspective on the experiments. It is a great pleasure to have you as opponent in the dissertation committee. Tito, it's very interesting to see your biostatistician viewpoint. It was great working on the paper together. Miriam and Evelyn, thank you for your recent and highly valuable contributions to the continuation of the single-cell sequencing project.

Also, many thanks to our international collaborators for their expertise. I'd like to thank Thomas Milne, Nicholas Crump, Alastair Smith and Vassilena Sharlandjjeva from the MRC Weatherall Institute of Molecular Medicine, University of Oxford, UK, for their collaboration. Tom, Nick and Alastair, your help in the DOT1L resistance project is greatly appreciated. Vassi, I'm truly excited to collaborate on the MENIN resistance experiments.

To the members of The Fight Kids Cancer Cure2MLL group, including Pablo Menendez, Clara Bueno, Maribel Parra and Oriol de Barrios at the Josep Carreras Leukemia Research Institute in Barcelona, Spain; Anindita Roy and Thomas Milne at the University of Oxford, UK; Giovanni Cazzaniga and Michela Bardini at the University of Milan Bicocca, Italy; and Katrin Ottersbach at the University of Edinburgh, UK, it is an honor to work together to enhance the survival of infant ALL patients.

En dan natuurlijk mijn vrienden, Janna en Johan, Irene, Franciska, Jeroen, Els, Roland, Ellen, Anouk en Jetteke. Bedankt voor de nodige afleiding en jullie vriendschap, op naar nog vele gezellige momenten samen.

Lieve ma, wat was het fijn geweest als je dit zelf had kunnen lezen. Lieve pa, lieve ma, bedankt voor alles.

Lieve Eric, lieve Marieke, lieve Marleen, lieve familie, fijn dat jullie er zijn! We zijn niet de familie die dit soort dingen vaak uitspreken, maar hoe fijn is het om te weten dat we op elkaar kunnen rekenen.

Marien, ook al is het anders gelopen dan we voorzien hadden, het leven gaat zoals het gaat, bedankt voor alle steun en natuurlijk de opvoeding van de mannen, zeker ook als ik druk was met mijn werk. Je bijdrage aan dit proefschrift wordt zeer gewaardeerd.

John, ik denk dat we ons er allebei prettiger bij voelen als ik dit stukje lekker voor ons houd. Maar, waar je niet onderuit komt..... ik wil je toch bedanken voor je warme steun en alle suggesties (ja echt!).

Lieve Quinn, Yannick en Ayden, mijn mannen, bedankt vooral voor de afleiding van het promoveren en het relativeren van wat belangrijk is in het leven. Trots op hoe jullie je ontwikkelen ondanks de uitdagingen die er soms zijn!

Dit proefschrift is het resultaat van de inzet en samenwerking van velen, en ik ben dankbaar voor de steun die ik heb ontvangen gedurende deze reis. Het is een voorrecht geweest om dit onderzoek uit te mogen voeren en ik kijk ernaar uit om bij te dragen aan mijn vakgebied in de toekomst.

**Met oprechte dankbaarheid,**

A handwritten signature in black ink that reads "Pauline". The signature is written in a cursive style with a long, sweeping underline that extends to the right.





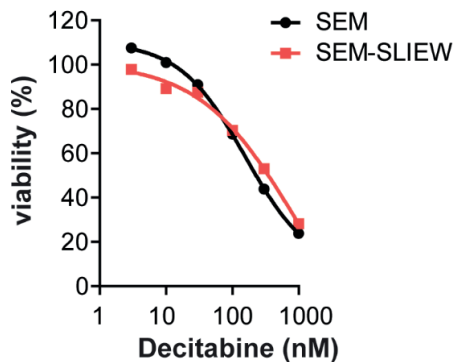
# APPENDIX

## supplementals



## SUPPLEMENTALS CHAPTER 2

### Supplementary Figure



**Supplementary Figure 1. Dose response curve of SEM-SLIEW and the parental cell line SEM for decitabine.** The MLL-rearranged ALL cell line SEM and its offspring, SEM-SLIEW, which has been modified to express eGFP and luciferase, were exposed for 4 days to a concentration range of decitabine. Viability was determined using MTS assay.

### Supplementary Tables

**Supplementary Table 1.** List of compounds tested by high-throughput drug screening.

**Supplementary Table 2.** Results of compounds tested by high-throughput drug screening

The supplementary tables can be downloaded at <https://doi.org/10.1002/jha2.81>

## SUPPLEMENTALS CHAPTER 3

### **Supplementary methods**

#### **Cell line culturing conditions**

All cell lines, including the generated pinometostat-resistant daughter lines were cultured in RPMI-1640 medium containing GlutaMAX™ supplemented with 10% fetal calf serum, 100 IU/ml Penicillin and Streptomycin, and 0.125µg/ml Amphotericin B (LifeTechnologies), at 37°C under a 5% CO<sub>2</sub> containing atmosphere. Cell lines passed every 3-4 days and routinely tested for the absence of mycoplasma and DNA fingerprinted to assure cell line authenticity.

#### **Immunoblotting**

For the presence of histone modifications, protein was isolated by using the flow-through of RNA isolation using the RNeasy Mini Kit (Qiagen), as described previously.<sup>1</sup> For the expression levels of other proteins, protein was extracted using RIPA buffer supplemented with protease inhibitors (ThermoScientific). Protein extractions were resolved on precast TGX™ gels and transferred to an 0.2 µm nitrocellulose membrane using a Transblot Turbo Transfer System (Bio-Rad). Blots were then probed with antibodies against H3K79Me<sub>2</sub>, H3K79Ac, H4K20Ac (cat. nrs. 39143, 39565, 61531, Active Motif), H3K79Me<sub>3</sub> (cat.nr. 4260, Cell signaling), H1K25Me<sub>3</sub> (cat.nr. 68370, Epigentek), H3K122A, total H3 (cat. nrs. ab33309, ab10799, Abcam), CD133 (PROM1), or GAPDH (cat. nrs. 64326S, 97166S, Cell Signaling). Proteins were visualized using an Odyssey Infrared Imaging System (LI-COR), and protein expression was quantified using the Odyssey software Image Studio Lite ver 4.0.

#### **RNA sequencing (RNA-seq)**

RNA was isolated from leukemic cells using the RNeasy Mini Kit (Qiagen) and RNA samples were sequenced in quadruplicate on a NextSeq® 500 System (Illumina®). QC was performed with fastQC (<http://www.bioinformatics.babraham.ac.uk/projects/fastqc>) and reads were aligned against the human genome assembly (hg19) with STAR.<sup>2</sup> Gene expression levels were quantified using the featureCounts function of the Subread package<sup>3</sup> and read counts were used to identify differential gene expression using DESeq2 (v3.12).<sup>4</sup> Genes were considered differentially expressed between sample groups at a false discovery rate (FDR) adjusted *p*-values of <0.05. Read counts were used for Gene Set Enrichment Analysis (GSEA) using the GSEA version 4.1.0 software with the Hallmarks gene set database<sup>5</sup>. The heatmap of genes with the most differential GSEA scores was created using the GenePattern software using the Heat Map Image Module<sup>6</sup>, and Venn diagrams were created using the interactive Venny tool.<sup>7</sup>

Ch1

Ch2

Ch3

Ch4

Ch5

Ch6

Ch7

AA

A

## **Chromatin Immunoprecipitation sequencing (ChIP-seq)**

Up to 20 million leukemic cells were crosslinked and lysed using the SimpleChIP kit (Cell Signaling Technology®) according to the manufacturer's recommendations and subsequently sonicated using a Bioruptor sonicator (Diagenode) to generate 150-300 bp fragment size. Next, immunoprecipitation and antibody-protein-DNA precipitation were performed according to the guidelines of the manufacturer.

Antibodies against KMT2A (Bethyl labs; cat.nr. A300-086-A), AFF1 (Abcam; cat.nr. ab31812), H3K4Me3, H3K27Ac and H3K79Me2 (Diagenode; cat. nrs. pAB-003-050, C15410196 and C15410051) were used. ChIP-seq DNA libraries were generated using the NEB Next Ultra DNA library preparation kit for Illumina (New England Biolabs) according to the manufacturer's recommendations and sequenced paired-end on a NextSeq® 500 System (Illumina®). Following QC analysis by fastQC (<https://www.bioinformatics.babraham.ac.uk/projects/fastqc/>), reads were trimmed using trim\_galore ([https://www.bioinformatics.babraham.ac.uk/projects/trim\\_galore/](https://www.bioinformatics.babraham.ac.uk/projects/trim_galore/)). Reads were then aligned to the human genome, hg19, with bowtie2.<sup>8</sup> Duplicate reads were removed using DeepTools alignmentSieve, with the flag –ignore duplicates.<sup>9</sup> BigWigs were generated using the DeepTools bamCoverage command, with the flags –extendReads –normalize using RPKM, and visualized in the UCSC genome browser.<sup>10</sup>

Peaks were called using the Homer tool findPeaks,<sup>11</sup> with the input track provided for background correction, using the –style histone flag. KMT2A::AFF1 peaks were generated from the overlap of KMT2A and AFF1 peaks, after which overlapping peaks closer than 5 kb were stitched together. Heatmaps were generated using DeepTools.

## **Assay for Transposase-Accessible Chromatin sequencing (ATAC-seq)**

100.000 SEM cells or SEMPINO\_RES cells were viable sent in duplicate and further processed by Active Motif. Samples were sequenced on a NextSeq® 500 System (Illumina®) and analyzed as for ChIP-seq, except that duplicate read removal with DeepTools alignmentSieve included the –ATAC shift flag to correct for adapter insertion.

## **Flow cytometry (FACS) analysis**

All FACS analysis experiments were performed on a CytoFlex Flow Cytometer (BeckmanCoulter). For flow cytometric assays determining the protein expression cells were blocked with Human TruStain FcX™ (BioLegend) and subsequently labeled with ViaKrome 808 (Beckman Coulter) to select for viable cells, as well as with CD133(PROM1)-FITC, CD33-APC (BD Biosciences, cat. nrs. 567029, 551378) or CD85k(LILRB4)-PE (BioLegend, cat. nr. 333008) according to the manufacturer's recommendation. Raw CytoFLEX data were processed using the CytExpert software version2.3 (Beckman Coulter) or FlowJo™ software version7.6.5 (BD Biosciences).

## RNA interference

Electroporation was performed in 400  $\mu$ L culture medium without antibiotics containing  $4 \times 10^6$ /mL cells in 4 mm cuvettes at 350 V for 10 milliseconds using a Gene Pulser Xcell™ Electroporation System (Bio-Rad) in the presence of 10 nM siRNAs directed against *DOT1L*, *HOXA9* (siGENOME SMARTpool Dharmacon™/Horizon), *KMT2A::AFF1* (named siMA6) targeting the *KMT2A* exon 9–*AFF1* exon 4 *KMT2A::AFF1* fusion site characteristic for SEM cells<sup>12</sup> or AML1-MTG8 fusion gene (named siAGF1), not present in *KMT2A*-rearranged acute leukemias, as non-targeting control.<sup>13</sup>

## Quantitative reverse-transcription PCR analysis

RNA, isolated using the RNeasy Mini Kit (QIAGEN), was reverse transcribed and the obtained cDNA was used for quantitative reverse-transcription PCR (qRT-PCR) analysis as described previously,<sup>14</sup> and is described in the supplemental methods. The sequences of the used primers were designed to detect the target genes *KMT2A::AFF1* (forward: 5'-ACAGAAAAAGTGG CTCCCG-3'; reverse: 5'-TATTGCTGTCAAAGGAGGCGG-3'),<sup>1</sup> *DOT1L* (forward 5'-GGCCAGATGATTGATGAGA-3'; reverse 5'- CATTTCATCCACTTCTGAACTC-3'), *HOXA9* (forward 5'-GCGCCTTCTGAAAAC-3'; reverse 5'- TGCTCGGTCTTT GTTGA), and the references genes *B2M* (forward 5'- ATGCGGCATCTTCAA-3'; reverse 5'-GGAGCATTGACTTGTCTT-3'), and *GUS* (forward: 5'-GCGCCGACTT CTCTG-3'; reverse: 5'-CTCCGGCAGGATCAC-3').

## Mod Spec® mass spectrometry

The quantification of >80 different histone post-translational modifications (PTMs) by Mod Spec® mass spectrometry was outsourced to Active Motif (Mod Spec® Service: <https://www.activemotif.com/catalog/1235/mod-spec>). For this, histones were acid extracted, derivatized via propionylation and digested with trypsin. Newly formed N-termini were propionylated as previously described,<sup>15</sup> and measured 3 separate times using the Thermo Scientific TSQ Quantum Ultra mass spectrometer coupled with an UltiMate 3000 Dionex nano-liquid chromatography system. The data was quantified using Skyline,<sup>16</sup> and represents the percent of each modification within the total pool of that amino acid residue.

## High-throughput drug screening

For high-throughput drug screening, leukemic cells were semi-automatically seeded in 384-well plates at 10.000 cells/well (Corning) using a Multidrop™ dispenser (Thermo Fisher Scientific). Drugs were added using a SciClone ALH3000 liquid handling robot (Caliper Life Sciences) to a final concentration of 1 nM, 10 nM, 100 nM, or 1000 nM. All tested drugs came from commercially available drug libraries, including the EnzoSCREEN-WELL® epigenetics library (BML-2836, 41 compounds; Enzo Life Sciences), the Cayman epigenetics library (11076, 64 compounds; Cayman Chemical), the Sequoia

FDA approved anti-neoplastic drug library (165 compounds Sequoia Research Products), the MCE Cell Cycle/DNA Damage Compound Library (HY-L0043; 387 compounds; MedChem Express) and an additional 22 compounds of interest (purchased from Selleckchem). All compounds tested are listed in Supplementary Table 1. Cell viability upon drug exposure was assessed by 4-day thiazolyl blue tetrazolium bromide (MTT; Sigma-Aldrich) assays as previously described,<sup>17</sup> and normalized against DMSO (i.e., no drug) controls. Normalized cell viabilities at the various concentrations of each compound were used to calculate IC50 values using GraphPad Prism8, version 8.3.4.

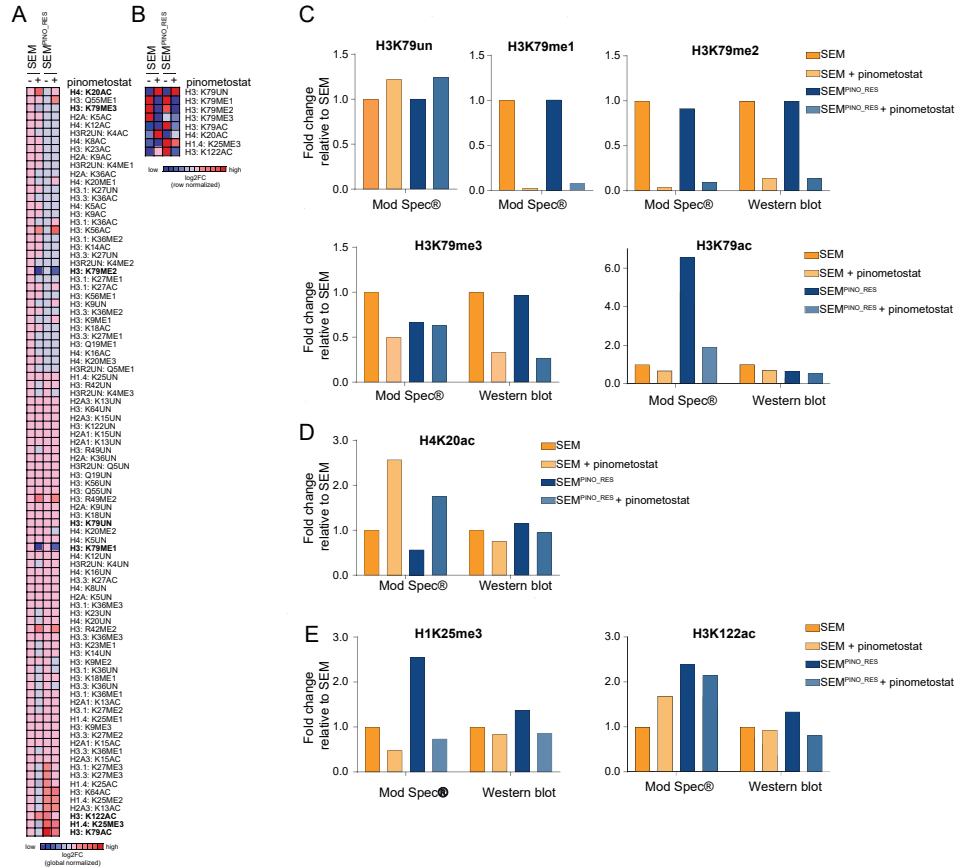
### **Cell viability assays**

For the validation of the hits from the high-throughput drug screening as well as evaluation of the chemotherapeutic agents currently used in the treatment of *KMT2A*-rearranged infant ALL cell viability assays were performed using flow cytometry with the 7-AAD viability dye (BioLegend) to discriminate between viable and dead cells. Expanded dose response curves were made using the Tecan D300 Digital Dispenser (Tecan) to dispense venetoclax, prednisolone, dexamethasone, vincristine, daunorubicin, cladribine, cytarabine (all purchased from Selleckchem), and L-asparaginase (Oncospar).

## References

- |     |   |     |
|-----|---|-----|
| 1.  | Gessner A, Thomas M, Castro PG, et al. Leukemic fusion genes MLL/AF4 and AML1/MTG8 support leukemic self-renewal by controlling expression of the telomerase subunit TERT. <i>Leukemia</i> . 2010;24(10):1751-1759.                           | Ch1 |
| 2.  | Dobin A, Davis CA, Schlesinger F, et al. STAR: ultrafast universal RNA-seq aligner. <i>Bioinformatics</i> . 2013;29(1):15-21.   | Ch2 |
| 3.  | Liao Y, Smyth GK, Shi W. The Subread aligner: fast, accurate and scalable read mapping by seed-and-vote. <i>Nucleic Acids Res</i> . 2013;41(10):e108.   | Ch3 |
| 4.  | Love MI, Huber W, Anders S. Moderated estimation of fold change and dispersion for RNA-seq data with DESeq2. <i>Genome Biol</i> . 2014;15(12):550.  | Ch4 |
| 5.  | Subramanian A, Tamayo P, Mootha VK, et al. Gene set enrichment analysis: a knowledge-based approach for interpreting genome-wide expression profiles. <i>Proc Natl Acad Sci U S A</i> . 2005;102(43):15545-15550.                             | Ch5 |
| 6.  | Reich M, Liefeld T, Gould J, Lerner J, Tamayo P, Mesirov JP. GenePattern 2.0. <i>Nat Genet</i> . 2006;38(5):500-501.  | Ch6 |
| 7.  | Venny. An interactive tool for comparing lists with Venn's diagrams. <a href="https://bioinfogp.cnb.csic.es/tools/venny/index.html">https://bioinfogp.cnb.csic.es/tools/venny/index.html</a> [computer program]. (2007-2015).                 | Ch7 |
| 8.  | Langmead B, Trapnell C, Pop M, Salzberg SL. Ultrafast and memory-efficient alignment of short DNA sequences to the human genome. <i>Genome Biol</i> . 2009;10(3):R25.   | AA  |
| 9.  | Ramirez F, Ryan DP, Gruning B, et al. deepTools2: a next generation web server for deep sequencing data analysis. <i>Nucleic Acids Res</i> . 2016;44(W1):W160-165.  | A   |
| 10. | Kent WJ, Sugnet CW, Furey TS, et al. The human genome browser at UCSC. <i>Genome Res</i> . 2002;12(6):996-1006.   |     |
| 11. | Heinz S, Benner C, Spann N, et al. Simple combinations of lineage-determining transcription factors prime cis-regulatory elements required for macrophage and B cell identities. <i>Mol Cell</i> . 2010;38(4):576-589.                        |     |
| 12. | Thomas M, Gessner A, Vornlocher HP, Hadwiger P, Greil J, Heidenreich O. Targeting MLL-AF4 with short interfering RNAs inhibits clonogenicity and engraftment of t(4;11)-positive human leukemic cells. <i>Blood</i> . 2005;106(10):3559-3566. |     |
| 13. | Heidenreich O, Krauter J, Riehle H, et al. AML1/MTG8 oncogene suppression by small interfering RNAs supports myeloid differentiation of t(8;21)-positive leukemic cells. <i>Blood</i> . 2003;101(8):3157-3163.                                |     |
| 14. | Spijkers-Hagelstein JA, Pinhancos SS, Schneider P, Pieters R, Stam RW. Chemical genomic screening identifies LY294002 as a modulator of glucocorticoid resistance in MLL-rearranged infant ALL. <i>Leukemia</i> . 2014;28(4):761-769.         |     |
| 15. | Garcia BA, Mollah S, Ueberheide BM, et al. Chemical derivatization of histones for facilitated analysis by mass spectrometry. <i>Nat Protoc</i> . 2007;2(4):933-938.  |     |
| 16. | MacLean B, Tomazela DM, Shulman N, et al. Skyline: an open source document editor for creating and analyzing targeted proteomics experiments. <i>Bioinformatics</i> . 2010;26(7):966-968.   |     |
| 17. | Pieters R, Loonen AH, Huismans DR, et al. In vitro drug sensitivity of cells from children with leukemia using the MTT assay with improved culture conditions. <i>Blood</i> . 1990;76(11):2327-2336.  |     |

## Supplementary Figures

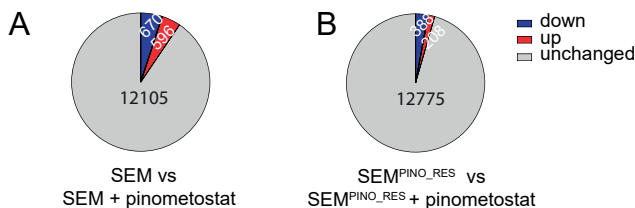


### Supplementary Figure 1: Global histone modification differences assessment. Related to Figure 1

Mod Spec®, a mass spectrometry-based measurement for the relative abundance of over 80 distinct histone marks, was performed on SEM and SEM<sup>PINO\_RES</sup> in the presence and absence of pinometostat.

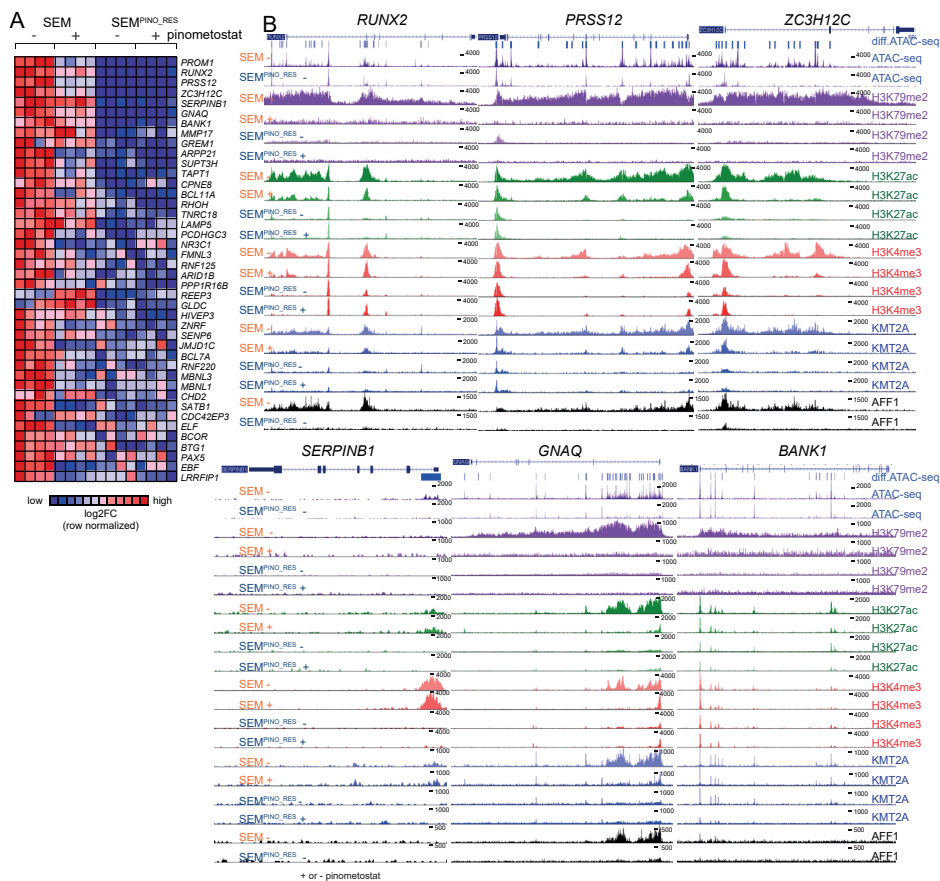
**A.** Heatmap showing the log<sub>2</sub> fold change (log<sub>2</sub>FC) comparisons of histone modification level of SEM + 7 days 50µM pinometostat, SEM<sup>PINO\_RES</sup> or SEM<sup>PINO\_RES</sup> + 7 days 50µM pinometostat relative to SEM, based on the percentages of each histone mark modification within the total pool of modifications measured by Mod Spec® at a specific amino acid residue, ranked from lowest to highest log<sub>2</sub>FC with global normalization. This analysis confirmed no differences in the levels of H3K79 mono-, di-, and tri-methylation (i.e., H3K79me1, H3K79me2, and H3K79me3, respectively) between SEM and SEM<sup>PINO\_RES</sup> and showed equal reduction of these histone marks upon pinometostat exposure in both cell lines. In addition, some histone modifications appeared to be present at differential levels between SEM and SEM<sup>PINO\_RES</sup>, including higher levels of histone 4 lysine 20 acetylation (H4K20ac) in SEM, and higher levels of histone 1 lysine 25 tri-methylation (H1K25me3) and histone 3 lysine 122 acetylation (H3K122ac) in SEM<sup>PINO\_RES</sup>. **B.** Heatmap showing the log<sub>2</sub>FC comparisons of all H3K79 histone modifications measured by Mod Spec® of SEM + 7 days 50µM pinometostat, SEM<sup>PINO\_RES</sup> or SEM<sup>PINO\_RES</sup> + 7 days 50µM pinometostat relative to SEM, as well as the histone modifications showing the highest log<sub>2</sub>FC, H4K20ac, H1K25me3 and H3K122ac, with row normalization. **C.** Fold change of histone modification level of SEM + 7 days 50µM pinometostat, SEM<sup>PINO\_RES</sup> or SEM<sup>PINO\_RES</sup> + 7 days 50µM pinometostat relative to the level in SEM, measured by Mod Spec® or by immunoblot analysis for all H3K79 histone modifications. **D.** fold change of histone modification level of SEM + 7 days 50µM pinometostat, SEM<sup>PINO\_RES</sup> or SEM<sup>PINO\_RES</sup> + 7 days 50µM pinometostat compared to the level in SEM, measured by mass spec or by immunoblot analysis for histone modification most reduced in SEM<sup>PINO\_RES</sup> H4K20ac. **E.** fold change of histone modification level of SEM + 7 days 50µM pinometostat, SEM<sup>PINO\_RES</sup> or SEM<sup>PINO\_RES</sup> + 7 days 50µM pinometostat compared to the level in SEM, measured by mass spec or by immunoblot analysis for the histone modifications most enhanced in SEM<sup>PINO\_RES</sup>, H1K25me3 and H3K122ac. This reveals that the differences found for H4K20ac, H1K25me3 and H3K122ac could not be validated by immunoblot analyses. Moreover, these data demonstrated that the global landscape of histone modifications between SEM cells and SEM<sup>PINO\_RES</sup> largely remained similar. The only histone modification that is downregulated in response to pinometostat exposure appeared to be H3K79 methylation, demonstrating the specificity of this agent.





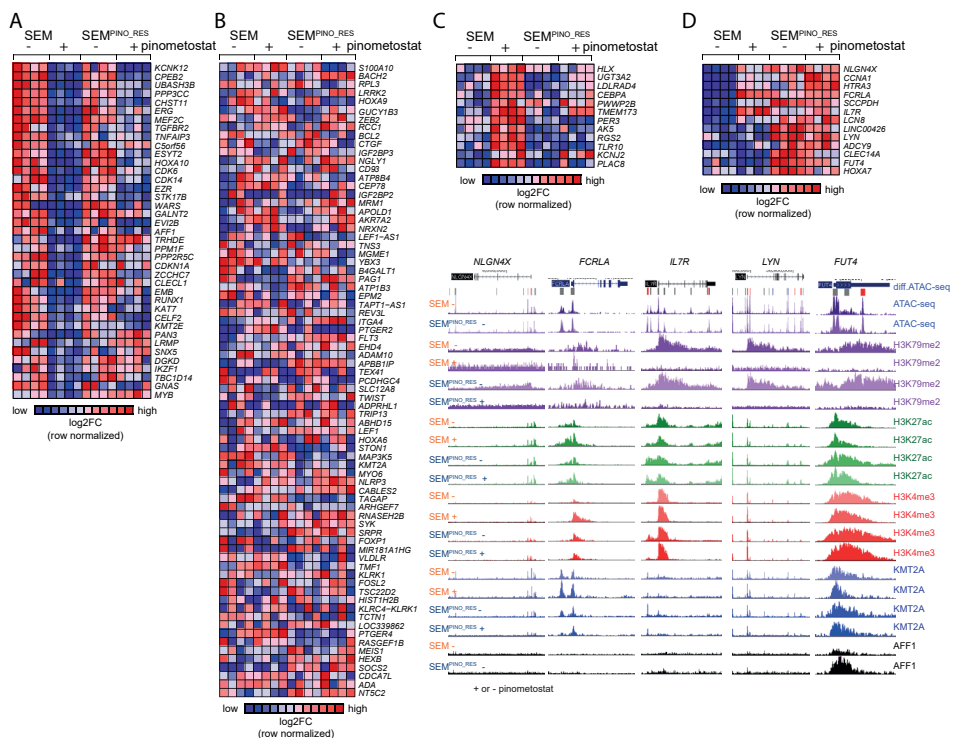
### Supplementary Figure 2: Gene expression comparisons of SEM and SEM<sup>PINO\_RES</sup> treated with pinometostat compared to untreated cells. Related to Figure 2.

A-B. Pie charts showing the number of genes that are significantly downregulated (blue), upregulated (red), or remain unchanged (gray) between **A** SEM and SEM treated for 7 days with 50  $\mu$ M pinometostat and **B** between SEM and SEM<sup>PINO\_RES</sup> treated for 7 days with 50  $\mu$ M pinometostat, 4 biological replicates each.



### Supplementary Figure 3: RNA expression in SEM<sup>PINO\_RES</sup> of genes previously associated with KMT2A-rearranged leukemias and/or high levels of H3K79Me2 reduced in SEM<sup>PINO\_RES</sup>. Related to Figure 3

**A** Heatmap of RNA expression of putative KMT2A fusion target genes downregulated in SEM<sup>PINO\_RES</sup> compared to SEM cells. Normalized counts of RNAseq shown of SEM and SEM<sup>PINO\_RES</sup>, both untreated or treated 7 days with 50  $\mu$ M pinometostat, 4 biological replicates each, mean with standard deviation (SD). **B** ATACseq differences between untreated SEM and SEM<sup>PINO\_RES</sup> cells at *PRSS12*, *ZCH12C*, *SERPINB1*, *GNAQ* and *BANK1*. Blue lines indicate significant decrease of chromatin accessibility in SEM<sup>PINO\_RES</sup> cells compared to SEM, grey lines indicate equal chromatin accessibility in both cell lines. 2 biological replicates; ChIPseq tracks showing H3K79me2, H3K27ac, H3K4me3, KMT2A in SEM and SEM<sup>PINO\_RES</sup> cells after 7 days treatment + or - 50  $\mu$ M pinometostat and AFF1 in untreated SEM and SEM<sup>PINO\_RES</sup> cells at genes *PRSS12*, *ZCH12C*, *SERPINB1*, *GNAQ* and *BANK1*

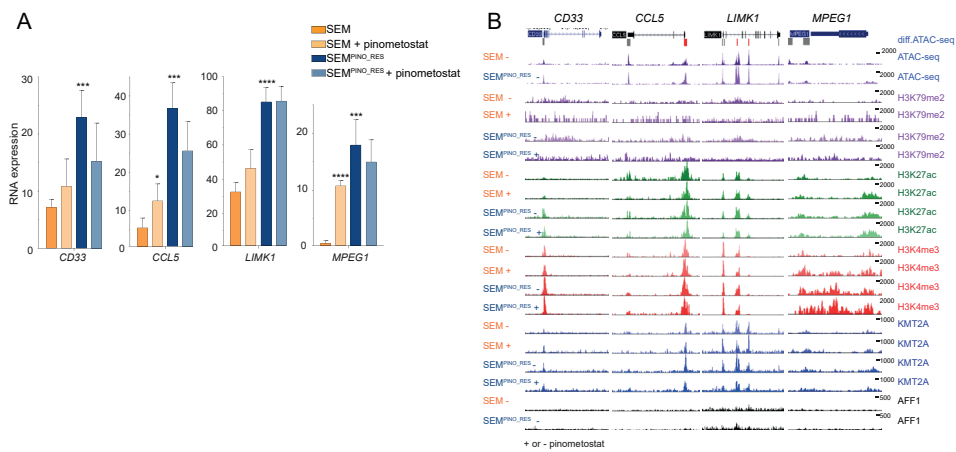


**Supplementary Figure 4: Putative KMT2A fusion target genes with no transcriptional changes or upregulated in SEM<sup>PINO\_RES</sup> compared to SEM. Related to Figure 4.**

**A-D** Normalized counts of RNAseq shown of SEM and SEM<sup>PINO\_RES</sup>, both untreated or treated 7 days with 50µM pinometostat, 4 biological replicates each.

**A.** Heatmap of RNA expression of putative KMT2A fusion target genes with no transcriptional changes between SEM and SEM<sup>PINO\_RES</sup>, yet downregulated in SEM treated with pinometostat compared to untreated SEM cells. **B.** Heatmap of RNA expression of putative KMT2A fusion target genes with no transcriptional changes between SEM and SEM<sup>PINO\_RES</sup> and no differences in SEM treated with pinometostat compared to untreated SEM cells. **C.** Heatmap of RNA expression of putative KMT2A fusion target genes with no transcriptional changes between SEM and SEM<sup>PINO\_RES</sup>, yet upregulated in SEM treated with pinometostat compared to untreated SEM cells. **D.** Heatmap of RNA expression of putative KMT2A fusion target genes upregulated in SEM<sup>PINO\_RES</sup> compared to SEM cells.

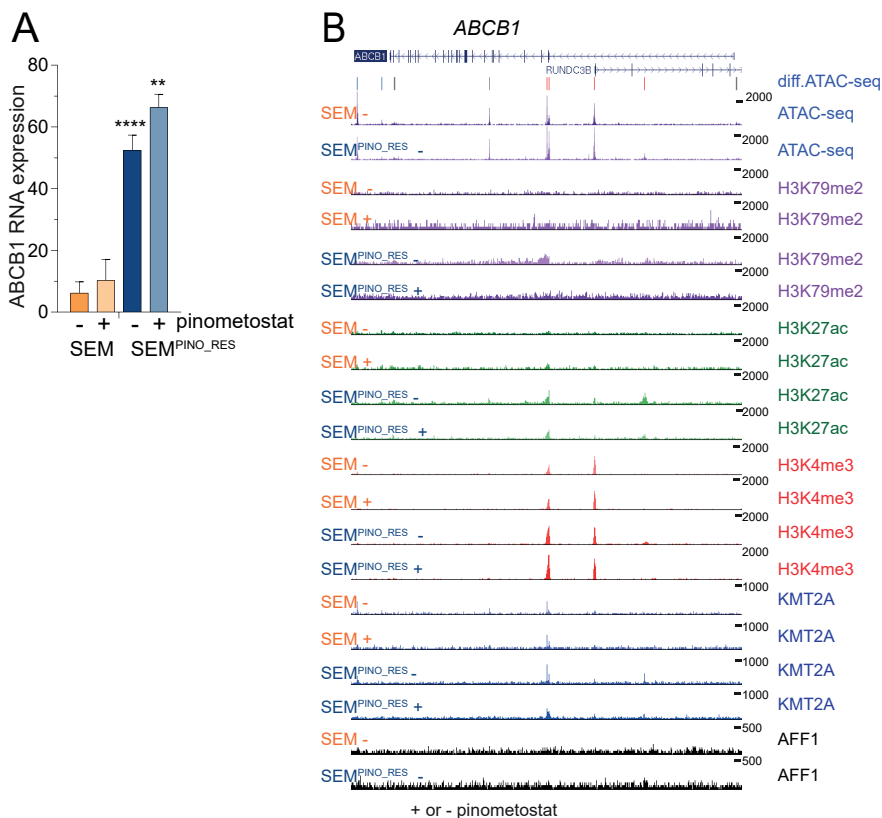
**E.** ATACseq and ChIPseq tracks of SEM and SEM<sup>PINO\_RES</sup> cells for the putative KMT2A fusion target genes significantly upregulated in SEM<sup>PINO\_RES</sup> compared to SEM cells. Blue lines of the ATACseq indicate significant more open chromatin access in SEM compared to SEM<sup>PINO\_RES</sup> cells. 2 biological replicates; ChIPseq tracks show H3K79me2, H3K27ac, H3K4me3, KMT2A in SEM and SEM<sup>PINO\_RES</sup> cells after 7 days treatment + or - 50µM pinometostat and AFF1 in untreated SEM and SEM<sup>PINO\_RES</sup> cells at the putative KMT2A fusion target genes significantly upregulated in SEM<sup>PINO\_RES</sup> compared to SEM cells.



**Supplementary Figure 5: Myeloid associated genes upregulated in SEM<sup>PINO\_RES</sup> compared to SEM. Related to Figure 5.**

**A** *CD33*, *CCL5*, *LIMK1* and *MPEG1* RNA expression of SEM and SEM<sup>PINO\_RES</sup> after 7 days treatment + or - 50µM pinometostat. Mean of normalized counts of RNAseq data with SD depicted, 4 biological replicates each. *p* values calculated with unpaired t-test, \* *p*<0.05, \* *p*<0.05, \*\* *p*<0.005, \*\*\* *p*<0.0005, \*\*\*\* *p*<0.00001.

**B** ATACseq differences between untreated SEM and SEM<sup>PINO\_RES</sup> cells at *CD33*, *CCL5*, *LIMK1* and *MPEG1*. Red lines indicate significant increase of chromatin accessibility in SEM<sup>PINO\_RES</sup> cells compared to SEM, grey lines indicate equal chromatin accessibility in both cell lines. 2 biological replicates; ChIPseq tracks showing H3K79me2, H3K27ac, H3K4me3, KMT2A in SEM and SEM<sup>PINO\_RES</sup> cells after 7 days treatment + or - 50µM pinometostat and AFF1 in untreated SEM and SEM<sup>PINO\_RES</sup> cells at genes *CD33*, *CCL5*, *LIMK1* and *MPEG1*.



**Supplementary Figure 6: Validation of sensitizing hits nimustine, carmustine and BIX01294 reveals cell line specificity. Related to Figure 6.**

**Figure S6: Validation of sensitizing hits nimustine, carmustine and BIX01294 reveals cell line specificity. Related to Figure 6**

**A.** *ABCB1* expression of SEM and SEM<sup>PINO\_RES</sup> after 7 days treatment + or - 50µM pinometostat. Mean of normalized counts of RNAseq data with SD depicted, 4 biological replicates each. *p* values calculated with unpaired t-test, \* *p*<0.05, \* *p*<0.05, \*\* *p*<0.005, \*\*\* *p*<0.0005, \*\*\*\* *p*<0.0001. **B.** ATACseq differences between untreated SEM and SEM<sup>PINO\_RES</sup> cells at *ABCB1*. Red lines indicate significant increase of chromatin accessibility in SEM<sup>PINO\_RES</sup> cells compared to SEM, grey lines indicate equal chromatin accessibility in both cell lines. 2 biological replicates; ChIPseq tracks showing H3K79me2, H3K27ac, H3K4me3, KMT2A in SEM and SEM<sup>PINO\_RES</sup> cells after 7 days treatment + or - 50µM pinometostat and AFF1 in untreated SEM and SEM<sup>PINO\_RES</sup> cells at genes *ABCB1*.

## Supplementary Tables

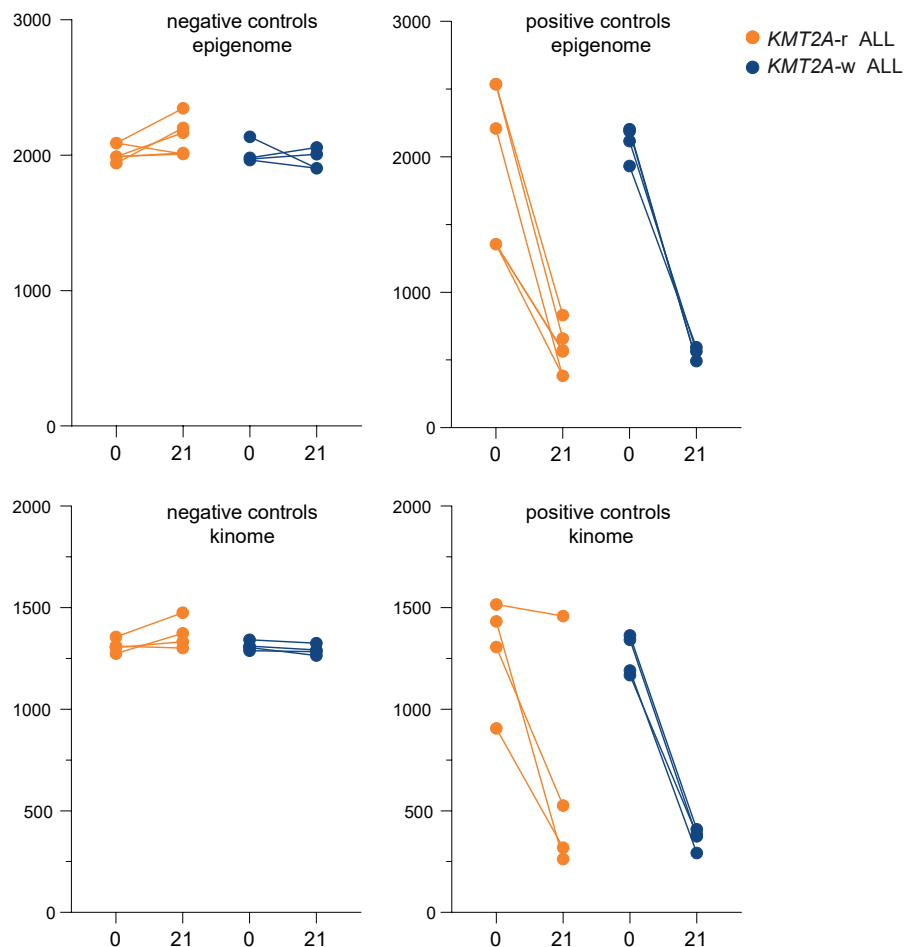
**Supplementary Table 1.** List of genes Venn diagrams.

**Supplementary Table 2.** Normalized cell viability of the various concentrations of each compound.

The supplementary tables can be downloaded at <https://doi.org/10.1002/jha2.81>

## SUPPLEMENTALS CHAPTER 4

## Supplementary Figures



**Supplementary Figure 1.** Evaluation of the negative and positive controls Read counts of negative sgRNA controls, represented by 50 non-targeting control guides, and positive sgRNA controls, represented by 5 sgRNAs targeting 10 different genes essential for human cells namely COPB1, KPNB1, NUP98, PSMB2, PSMC4, PSMD6, PSMD11, RPS13, RPL3, RPL11 that were present in the CRISPR-Cas9 library screening, measured at day 0 and day 21. Each line represents a summary of the sgRNA controls of a single cell line, in orange for the *KMT2A-r* ALL cell lines and in blue for the *KMT2A-w* ALL cell lines.

Ch1

Ch2

Ch3

Ch4

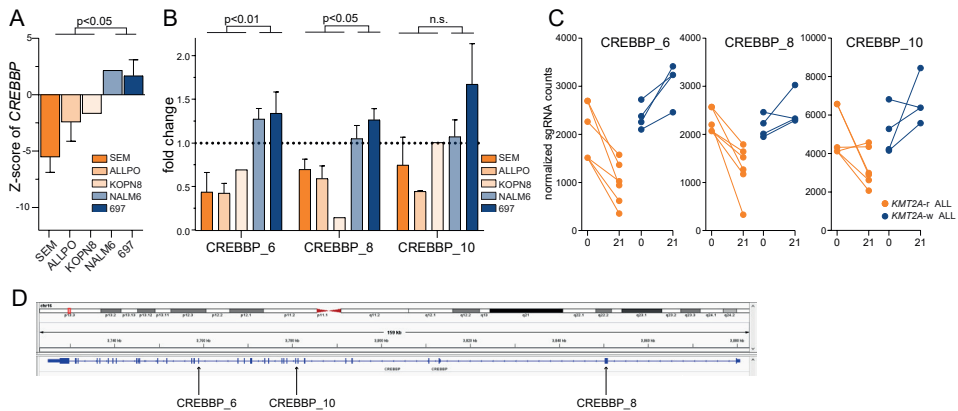
Ch5

Ch6

Ch7

AA

A



**Supplementary Figure 2: Evaluation of the known KMT2A-r ALL vulnerability genes CREBBP. Related to Figure 2.**

**A** Z-scores of the individual cell lines for CREBBP knockout. **B** Fold change at day 21 compared to day 0 of normalized read counts of sgRNAs CREBBP\_6, CREBBP\_8 and CREBBP\_10 from the CRISPR KO screen. n=2, mean ± SEM. **C** Normalized read counts at day 0 and day 21 of sgRNAs CREBBP\_6, CREBBP\_8 and CREBBP\_10 from the CRISPR KO screen. n=2, mean ± SEM. **D** overview sgRNA locations on the CREBBP gene

**Supplementary Tables**

**Supplementary Table 1.** Overview epigenome and kinome sgRNAs.

The supplementary tables can be downloaded at <https://doi.org/10.1186/s40164-023-00445-810.3390/ijms241713207>

## SUPPLEMENTALS CHAPTER 5

### **Supplementary methods**

#### **Fluorescence-activated cell sorting (FACS)**

Samples were thawed and resuspended in 1xPBS, 2mM EDTA, 0.5%BSA and a viability stain (2.5 µg/mL 7AAD or 5 µg/mL DAPI (BD Biosciences, San Jose, CA, USA)) in a concentration of approximately 1 million cells/mL. Viable single cells were sorted based on forward/side scatter properties and 7AAD/DAPI staining using FACS (FACSAria III, BD Biosciences for BM samples; MoFlo Astrios Cell Sorter, Beckman Coulter for PB samples). SORT-seq samples were sorted into 384-well plates (Bio-Rad, Veenendaal, The Netherlands) containing 10 µL mineral oil (Sigma-Aldrich, Zwijndrecht, The Netherlands) and 50 nL of barcoded reverse transcription primers as described (26) (Supplementary Table 1). 10xGenomics samples were sorted into tubes. Data was acquired using FACSDiva version 8.0.1 for the FacsAria sorter or Summit version 6.3.1 for the Astrios sorter, the gating strategy employed for sorting is shown in Supplementary Figure 1.

#### **FACS metrics**

Index sorting files containing cytometric data for each sorted cell were recovered for BM samples plates. This allowed association between transcriptomic data and forward scatter area values as depicted in Supplementary Figure 6. To obtain forward scatter area values for larger populations of cells, Flow Cytometry Standard (FCS) files for each of the samples were analysed. These samples were gated by the same strategy used for sorting into plates (Supplementary Figure 1), yielding cytometric data on a minimum of 4224 cells (sample 635N) and maximum of 170866 cells (sample 8010R). When comparing forward scatter area values across groups of patients (Supplementary Figure 6d, aggregate) an identical number of cells (n=4224) were taken from each patient to ensure equal representation.

#### **Module Score Calculation**

Module score calculation was performed with the following modification: when sampling control genes, the same gene can be selected multiple times. This ensures that the distribution of values is centred around zero and eliminates biases due to uneven number of genes when two modules are compared.

#### **Gene Ontology Enrichment**

Arguments and databases used to calculate gene ontology enrichment were: the org.Hs.eg.db annotation database (OrgDb = "org.Hs.eg.db", version 3.5.0), the biological process ontology (ont="BP"), a p-value and q-value cut-off of 0.01 and 0.05 respectively

Ch1

Ch2

Ch3

Ch4

Ch5

Ch6

Ch7

AA

A

(pvalueCutoff = 0.01, qvalueCutoff = 0.05) and a minimum gene set size of 15 (minGSSize = 15). Results were subsequently simplified using the simplify function.

### **T-B similarity score**

To compute the T-, B-cell similarity score (Supplementary Figure 2d-e), two module scores were calculated as described, using markers of T and B cells respectively. T-cell markers were: CD3E, CD3D, CD3G, CD8A, CD7, CD4, TRBC1. B-cell markers were: CD19, CD79A, MS4A1, CD22. The scores were rescaled so that the values for each module is between 0 and 1 and then the B-cell module score was subtracted from the T-cell module score for each cell. The resulting similarity score ranges between -1 and +1, with the highest values representing high similarity to T-cells and the lowest values high similarity to B-cells.

### **Cell-cycle analysis**

Cell-cycle phase (Supplementary Figures 2G, 5F) was determined for each cell using the Seurat (1) (version 2.1.0) CellCycleScoring function with default parameters. The list of marker genes for S and G2M phase are as described (2).

### **Survival analysis**

To obtain the Kaplan-Meier curves for current risk stratification and this study's prediction we used the function "survfit" from the R package "Survival" version 3.2-7 and "ggsurvplot" from the R package "Survminer" version 0.4.8. P-values were calculated using chi-squared test for comparison of categorical variables.

### **Bone Marrow Differential expression**

To find markers of the cell clusters depicted in Figure 1C, differentially expressed genes were determined with the FindAllMarkers function in Seurat (1). Differential expression was assessed using the bimodal test (argument test.use = "bimod", only.pos = TRUE). The resulting p-values were Bonferroni multiple-testing corrected. Genes with an adjusted p-value lower than 0.05 and with an average log fold-change (natural log) above 0.20 were considered differentially expressed. This resulted in 389 cluster-8 specific genes and 428 cluster-9 specific genes. To determine genes differentially expressed between sensitive and resistant cells (Supplementary Figure 5a), two groups were composed consisting of the 15 cells with the lowest PC score from each patient (resistant cells) and the 15 cells with the highest PC score from each patient (sensitive cells). These two groups were compared using the function FindMarkers with the same arguments as above. To eliminate the effect of patient-specific gene expression, we excluded all genes to which a single patient contributed more than 40% of the total number of cells expressing that gene. Genes exceeding the thresholds described above were considered differentially expressed (Supplementary Table 4).



### **removal of healthy cells from Peripheral blood samples**

Clusters detected for both 10x and sort-seq performed on peripheral blood samples were analyzed with SingleR version 1.0.1 with default parameters. clusters classified as pro-B were kept as tumor, while clusters classified as B-cell, monocytes, T-cells, NK cells, or erythroblasts were removed from subsequent analyses.

### **Gene correlation with module scores.**

Expression of all genes in the dataset were correlated to the sensitivity and resistance module score using Spearman correlation. The resulting coordinates were plotted in figure 4C.

### **Cell size determination by microscopy**

Images of May-Grünwald Giemsa stained cytospin slides were made using the DM200 LED microscope (Leica, Amsterdam, The Netherlands) and utilized to create outlines of the cells to determine cell size using ImageJ software (3). Briefly: RGB colour photos were converted into 32-bit pictures and the “threshold” function with the black and white (B&W) setting was used to outline the cells. The outlines were filled by using the ImageJ features “fill holes”, converted using “convert to mask”, and separated using “watershed”. Small outlines with an area below 120 pixel<sup>2</sup> were ignored. Finally, only the leukemic blast cells were used for analysis as shown in Supplementary Figure 6C.

### **Bulk mRNA data analyses**

The bulk mRNA datasets used for the classifications depicted in Supplementary Figure 7b are DNA microarray(4) and RNA-seq datasets (5, 6) from infant ALL patients at diagnosis. The microarray data was processed as described (4). For the RNA-seq data, paired-end reads were mapped with STAR (7) version 2.6.1 and read assignment was performed with featureCounts 1.6.4 (8), using genome and annotation versions as described in the scRNA-seq section above.

To resemble as close as possible the scRNA-seq analysis, reads were assigned to features according to the hierarchical structure described previously (9). Reads were converted to Transcripts Per Million (TPM) and normalized to 1 million transcripts. Sensitivity and resistance module scores were calculated as described above (Gene module score section) on the matrix of bulk mRNA datasets.

### **scRNA-seq bulkification**

For each scRNA-seq dataset, contributions from all cells were pooled by summing all transcripts for each gene. The resulting values were then normalized to 1 million transcripts (Supplementary Figure 7C, top panel). To obtain bulkified scRNA-seq with

Ch1

Ch2

Ch3

Ch4

Ch5

Ch6

Ch7

AA

A

equal contribution from each cell (Supplementary Figure 7d), the number of transcripts from each cell was down- or up-sampled to 1500 according to the original distribution of transcripts in that cell. Datasets were subsequently bulkified as above. In order to estimate sampling errors, the procedure was repeated 30 times.

### **Box plots**

When box plots are used to summarize distributions, the central line represents the median. The lower and upper limits of the box represent the 25th and 75th percentile respectively. The dashed lines extend to 1.5 times the Interquartile Range (IQR) of the distribution. Data points lying beyond this limit are represented as individual dots (outliers). In Supplementary Figure 6D-F these outliers were omitted due to space limitations.

### **Statistical tests**

Distributions of sensitivity and resistance module scores in cells from early relapse patients (n=678 cells) and long-term relapse-free survivors (n=402 cells, Figure 1e) were compared using a two-tailed Welch's two sample t-test. The same test was used to compare PB early relapse and relapse-free survivors in figure 3B-C (figure B: n=719 relapse-free cells, n=683 early relapse cells; figure c: n=11719 relapse-free cells, n=13010 early relapse cells)

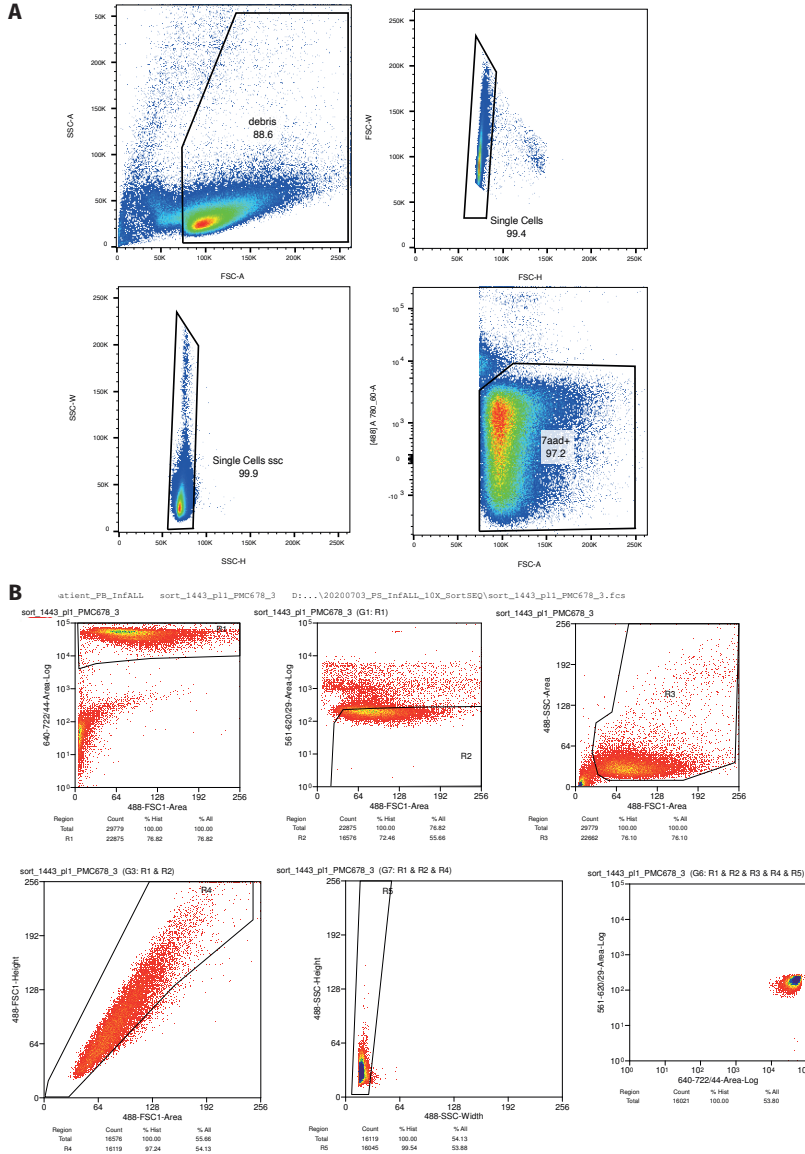
The significance of the separation between early relapse and long-term relapse-free survivors in Figure 1g was assessed by first calculating the best linear fit using all points and then projecting them onto the resulting regression line. This ensures that the points are arrayed along a single dimension and that the variance of the overall distribution is maximized. A two-tailed Welch's two sample t-test was then performed between the two groups containing n=3 relapse-free survivors and n=4 early relapse patients.

Spearman's correlation between gene expression and module score in figure 4C and between PC score and forward scatter area in Supplementary Figure 6B was calculated using the R "cor" function using method = "spearman" as an argument. Pearson's correlation between PC score and sensitivity/resistance module scores (Supplementary Figure 3a-d) were calculated as above but using method = "pearson" as argument. Aggregate distribution depicted in Supplementary Figure 6D-E were compared using two-tailed Welch's two sample t-test. For Supplementary Figure 6D, n=12672 cells for the sensitive category, and n=16896 for the resistant category. For Supplementary Figure 6E, n=288 cells for the sensitive category and n=428 for the resistant category. Survival curves in figure 3F were compared with a log-rank test.

## References

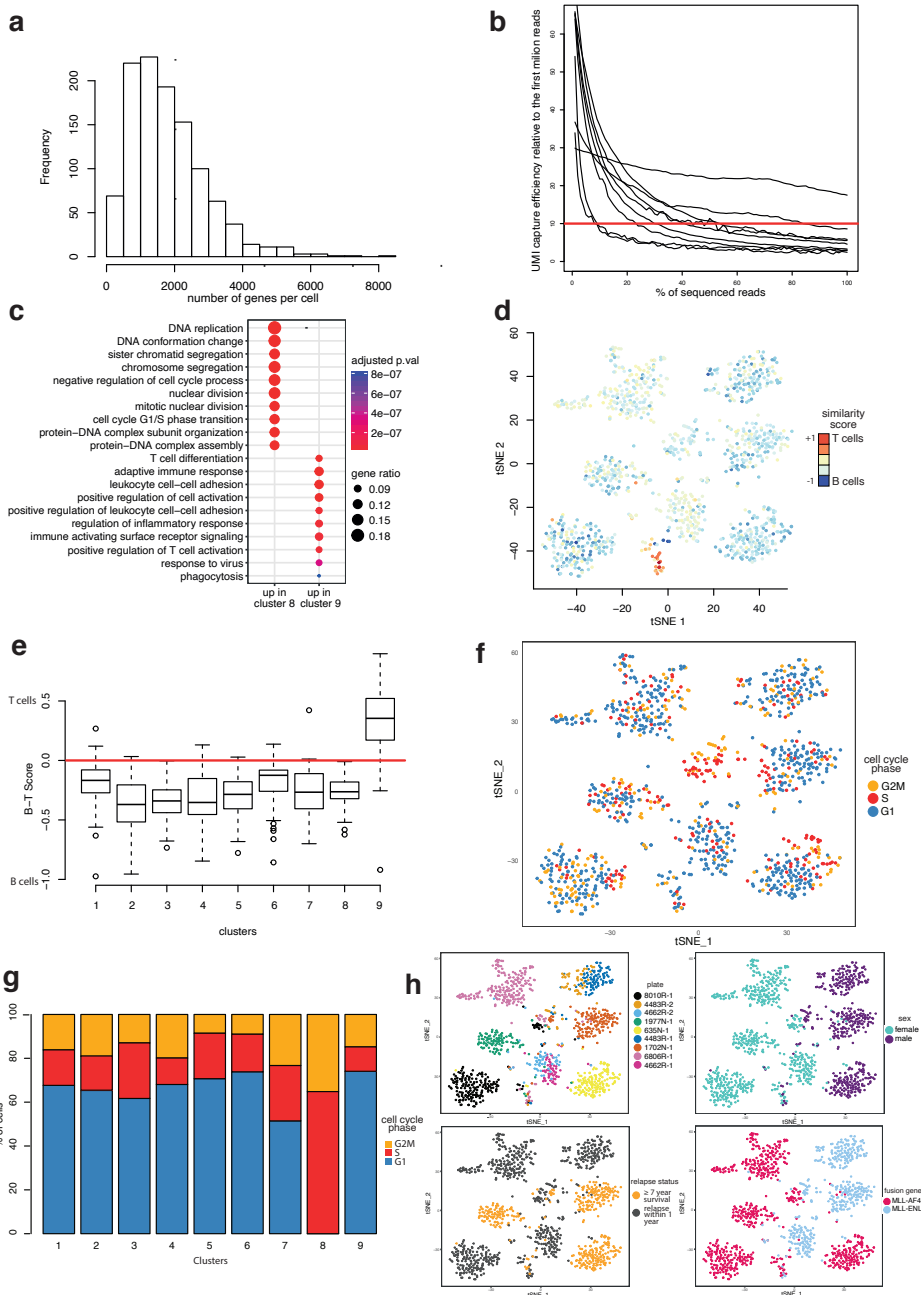
1. Butler A, Hoffman P, Smibert P, Papalexi E, Satija R. Integrating single-cell transcriptomic data across different conditions, technologies, and species. *Nat Biotechnol.* 2018;36(5):411-20. Ch1
2. Tirosh I, Izar B, Prakadan SM, Wadsworth MH, 2nd, Treacy D, Trombetta JJ, et al. Dissecting the multicellular ecosystem of metastatic melanoma by single-cell RNA-seq. *Science.* 2016;352(6282):189-96. Ch2
3. Schneider CA, Rasband WS, Eliceiri KW. NIH Image to ImageJ: 25 years of image analysis. *Nat Methods.* 2012;9(7):671-5. Ch3
4. Stam RW, Schneider P, Hagelstein JA, van der Linden MH, Stumpel DJ, de Menezes RX, et al. Gene expression profiling-based dissection of MLL translocated and MLL germline acute lymphoblastic leukemia in infants. *Blood.* 2010;115(14):2835-44. Ch4
5. Agraz-Doblas A, Bueno C, Bashford-Rogers R, Roy A, Schneider P, Bardini M, et al. Unraveling the cellular origin and clinical prognostic markers of infant B-cell acute lymphoblastic leukemia using genome-wide analysis. *Haematologica.* 2019;104(6):1176-88. Ch5
6. Andersson AK, Ma J, Wang J, Chen X, Gedman AL, Dang J, et al. The landscape of somatic mutations in infant MLL-rearranged acute lymphoblastic leukemias. *Nat Genet.* 2015;47(4):330-7. Ch6
7. Dobin A, Davis CA, Schlesinger F, Drenkow J, Zaleski C, Jha S, et al. STAR: ultrafast universal RNA-seq aligner. *Bioinformatics.* 2013;29(1):15-21. Ch7
8. Liao Y, Smyth GK, Shi W. The Subread aligner: fast, accurate and scalable read mapping by seed-and-vote. *Nucleic Acids Res.* 2013;41(10):e108. AA
9. Candelli T, Lijnzaad P, Muraro MJ, Kerstens H, Kemmeren P, van Oudenaarden A, et al. Sharq, A versatile preprocessing and QC pipeline for Single Cell RNA-seq. *bioRxiv.* 2018:250811. A

## Supplementary Figure



### Supplementary Figure 1. FACS gating strategy.

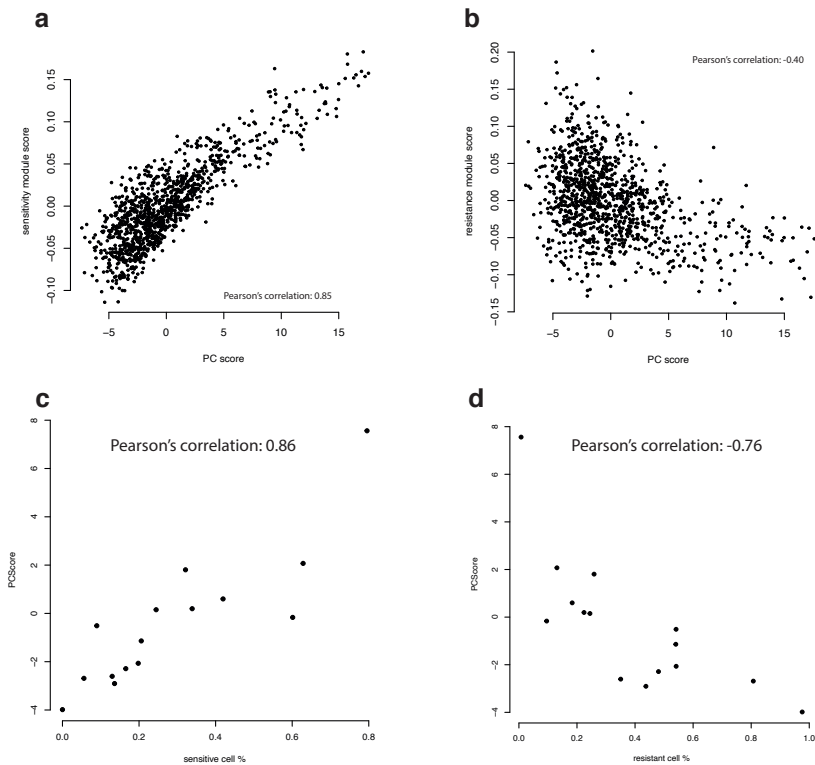
Gating strategy used to sort all samples described in this study. **A**, gating strategy for the FACSaria III **B**, gating strategy for the MoFlo Astrios.



Supplementary Figure 2.

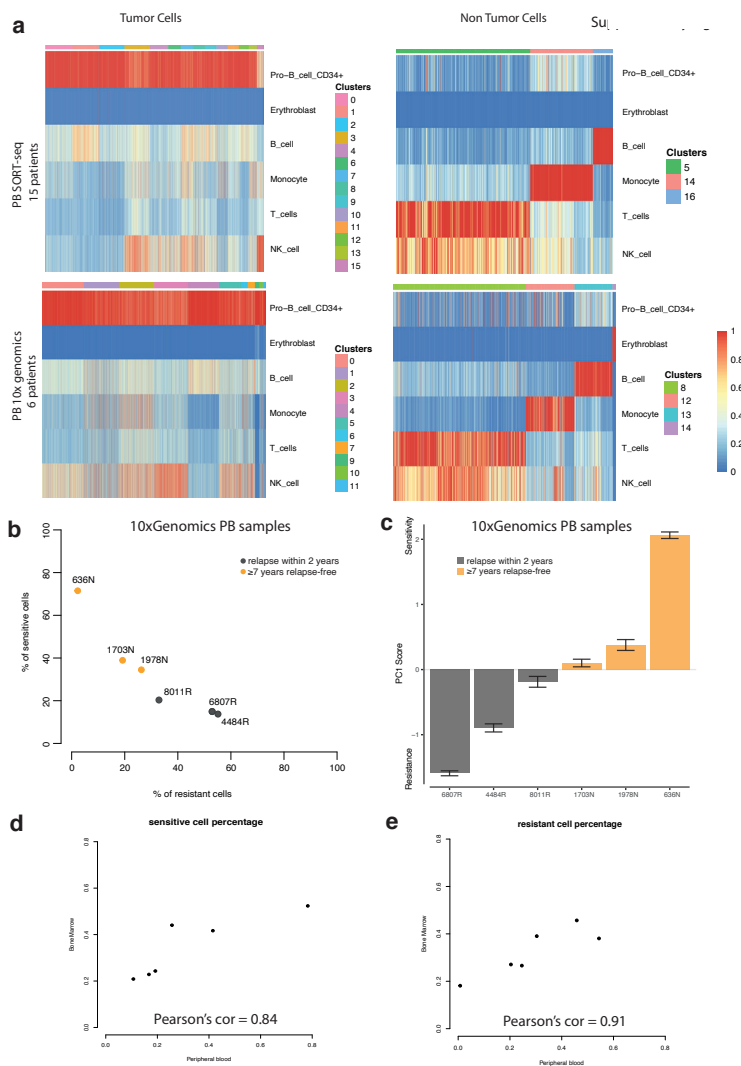
### Supplementary Figure 2. Leukemic cells group largely according to patient.

**a**, histogram showing the frequency of the number of genes detected per cell. **b**, UMI capture efficiency shown as a function of the percentage of sequenced reads (see sup methods). A final efficiency of 10 implies that only 10% of the total complexity of the dataset is left unsequenced. **c**, Gene Ontology enrichment based on cluster 8- and 9-specific genes indicates a high degree of actively dividing cells in cluster 8 and indicates that cluster 9 represents T-cells. **d**, Similarity score based on expression of T- and B-cell markers projected on a t-SNE plot. **e**, boxplot showing the distribution of the B-T similarity score for each cluster. **f**, Distribution of cell cycle phase on the t-SNE plot indicates a high degree of actively dividing cells in cluster 8 (fig 1c). **g**, For each cluster (Figure 1c), the fraction of cells assigned to the different cell cycle phases shows that cluster 8 consists entirely of cycling cells (G2M and S). **h**, t-SNE plots with cells labelled by FACS plate, sex, relapse status, or fusion partner indicate absence of batch effects.



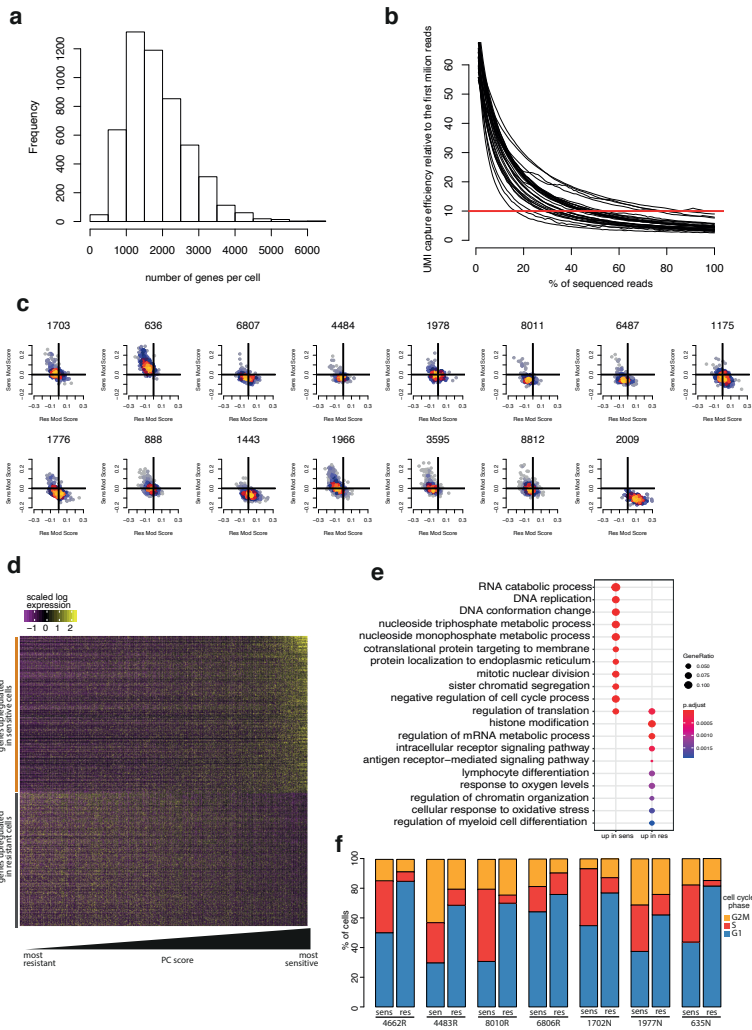
### Supplementary Figure 3. Principal component versus gene module scores.

**a**, PC score correlation with the sensitivity module score and **b**, anti-correlation with the resistance module score in individual cells. This indicates that signals from both sensitivity and resistance modules are captured within the first PC and that the contribution from the sensitivity module is stronger, likely also because it had more genes. **c-d**, average PC score per patient correlated with the % of sensitive or resistant cells, respectively.



### Supplementary Figure 4.

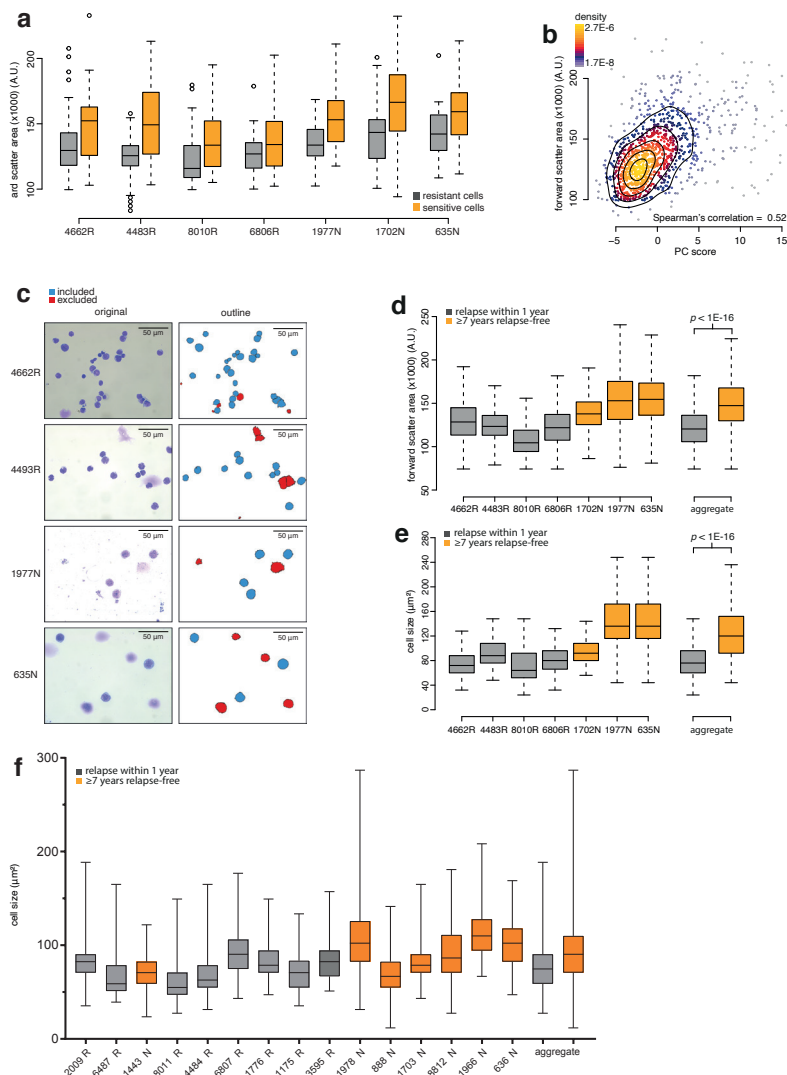
**a**, SingleR heatmap showing correlations between cells (columns) and cell types (rows) for peripheral blood samples. Cells are split by tumor or non-tumor and processed with SORT-seq or 10xGenomics. **b**, quantitation of the proportion of sensitive and resistant cells in six PB samples processed with 10xGenomics. **c**, PC score calculated on the PB samples processed with 10xGenomics. **d-e**, correlation of sensitive and resistant cell percentage between BM and PB samples from the same patients.



## Supplementary Figure 5. Characterization of sensitive and resistant cells in bone marrow samples.

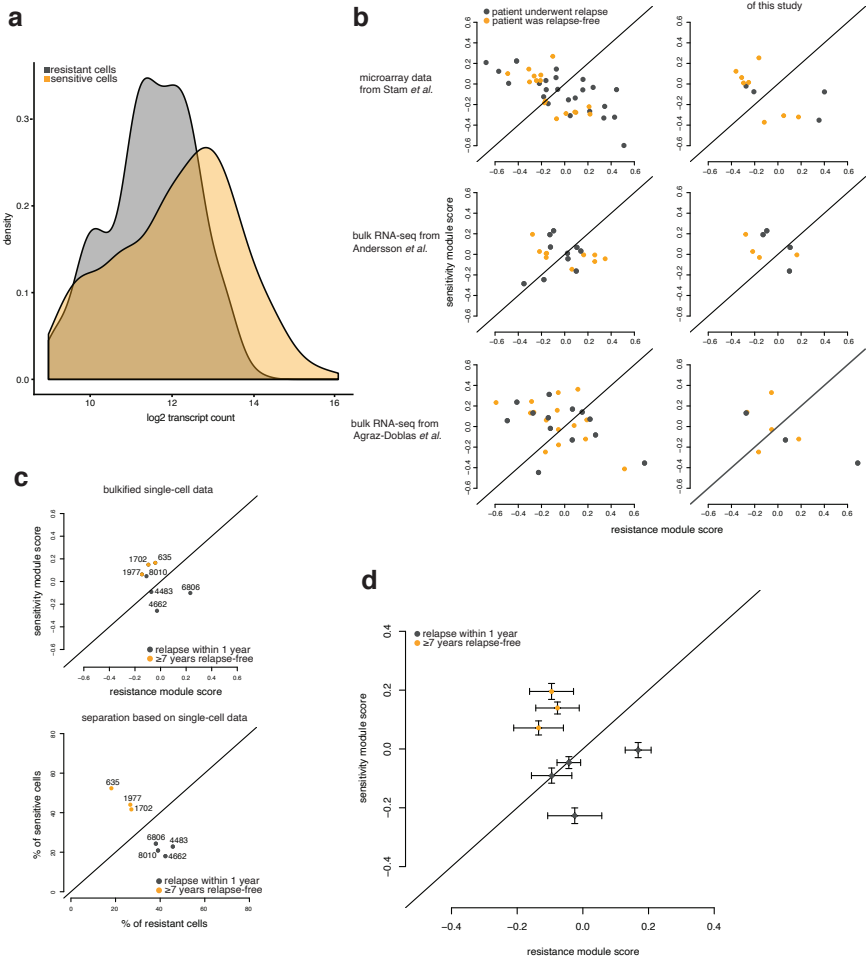
**a**, Frequency distribution of genes per cell in all SORT-seq processed PB samples. **b**, UMI capture efficiency shown as a function of the percentage of sequenced reads (see sup methods). A final efficiency of 10 implies that only 10% of the total complexity of the dataset is left unsequenced. **c**, resistance and sensitivity module scores (x- and y-axis) plotted over all cells for each patient's SORT-seq PB sample. **d**, Expression heatmap of all differentially expressed genes between cells classified as sensitive and resistant. cells (columns) are ordered by PC score, reflecting a gradient from resistant to sensitive. **e**, Gene Ontology categories enriched in the upregulated genes in sensitive and resistant cells. Gene ratio represents the fraction of differentially expressed genes in each category **f**, Cell cycle analysis of cells predicted to be sensitive or resistant in the different samples.





### Supplementary Figure 6. Evaluation of size as an indicator of sensitivity/resistance.

**a**, Boxplots showing the distribution of FACS forward scatter area values for cells classified as sensitive and resistant in individual bone marrow samples. **b**, Correlation between FACS forward scatter area and the first PC score of individual bone marrow cells analysed by scRNA-seq. **c**, Examples of Cytopsin images and their digitally outlined counterparts with excluded objects in red, as used for cell size analysis. **d**, Distribution of forward scatter area values of all cells from individual bone marrow samples shown as box plots. Each sample's contribution to the aggregates is equal. **e**, Distribution of cell sizes as detected by microscopy of all cells from individual bone marrow samples shown as boxplots. Each sample's contribution to the aggregates is equal. **f**, Distribution of cell sizes as detected by microscopy of all cells from individual peripheral blood samples shown as boxplots. Each sample's contribution to the aggregates is equal.



**Supplementary Figure 7. Lower amounts of transcripts in relapse-associated cells hampers classification through bulk expression analyses.**

**a**, Distribution of transcript counts for cells classified as sensitive or resistant. Resistant cells have approximately half as many transcripts as sensitive cells (0.52 ratio,  $p = 8E-10$ ). Note the log2 scale and the skewed distribution of high transcript abundance in sensitive cells. **b**, Sensitivity and resistance module score plots for three bulk datasets. Plots on the left include all infants with B-cell ALL in each study while plots on the right include only patients that are closest to our bone marrow study cohort (bone marrow samples, t(4;11) and t(11;19), relapse within 1 year or at least 7 years relapse-free survival). **c**, Sensitivity/resistance module score plot calculated for bulkified single cell RNA-sequencing datasets (top) compared with classification based on single cells (bottom, identical to Figure 1g). **d**, Sensitivity/resistance module score plot calculated for bulkified single-cell RNA-sequencing datasets where each cell contributes equally to the dataset. Error bars represent the standard error of the mean from 30 samplings.

**Supplementary Tables****Supplementary Table 1.** Single-cell RNA-seq primers.**Supplementary Table 2.** List of sensitivity and resistance module genes obtained from Rhein et al.**Supplementary Table 3.** List of all genes differentially expressed between cells predicted to be sensitive or resistant in PB samples .**Supplementary Table 4.** List of all genes differentially expressed between cells predicted to be sensitive or resistant in BM samples .

*The supplementary tables can be downloaded at <https://doi.org/10.1186/s40164-023-00445-8> and <https://doi.org/10.1186/s41375-021-01341-y>*

Ch1

Ch2

Ch3

Ch4

Ch5

Ch6

Ch7

AA

A









